ENABLEH2

PUBLIC REPORT

Test Report on Hydrogen Flammability, Ignition and Release

Deliverable number :	D4.2 (comprises D4.2a and D4.2b)
Grant Agreement :	769241
Call identifier:	H2020-MG-2016-2017/H2020-MG-2017-Two-Stages
Project full name:	ENABLing cryogEnic Hydrogen-based CO2-free air transport
Project start:	01.09.2018
Project duration:	51 months

This project has received funding from the European Union's Horizon 2020 research and innovation programme under grant agreement no 769241

Grant Agreement: 769241

Call identifier: H2020-MG-2016-2017/H2020-MG-2017-Two-Stages

Project full title: ENABLEH2 – ENABLing cryogEnic Hydrogen-based CO2-free air transport

ENABLEH2

D4.2a - Test report on hydrogen flammability and ignition under altitude conditions

Deliverable lead beneficiary: London South Bank University
Authors: James Ingram, Claire Benson, Paul Battersby

Test report on hydrogen flammability and ignition under altitude conditions.

1. Introduction

Safety assessments of the use of hydrogen for civil aviation have most focused on accident scenarios involving large releases e.g. hazards from pool fires, which have compared favourably and sometimes better than a comparable Jet A release. However, even small leaks into an enclosed part on an aircraft could pose a serious hazard. There are important differences between ignition of unconfined hydrogen/air mixtures and those inside an enclosure. In the first case, to produce damaging overpressures, there needs to be acceleration to fast flame speeds (e.g. as a result of turbulence from flow over obstacles). In the second case the confining walls (in essence as the contents are heated) are subjected to an overpressure irrespective of flame acceleration, for a 30%(v/v) H2/air mixture at RTP this would be around 8 bara (for an unvented vessel).

When considering explosion hazards arising onboard aircraft, with Jet A, concerns are to a very large extent related to the formation of flammable atmospheres within the headspace of a fuel tank. This is not the case for hydrogen. Jet A is a relatively high flash point fuel. At RTP the flash point is specified to be above 38°C (values are generally higher with a median value around 53 °C) and represents the temperature at which the vapour pressure of the liquid results in sufficient hydrocarbon in a headspace above it to be flammable (i.e. equal the LFL). Thus, at RTP, (unless in the form of a fine mist) spills of jet fuel in a confined space rarely create an explosion hazard. At altitude the situation is more complicated as the 'flash point' will depend on the fuel tank temperature and atmospheric pressure. The end result is that there will be a relatively small fraction of a flight profile where a fuel tank ullage will potentially be explosive. For many years such risks were manged by using ignition source control. However, incidents such as the TWA flight 800 crash in 1996 revealed a need for further research on ignition. As a result of new requirements imposed by the FAA in 2008 fuel tanks are now often inerted. This is discussed in much more detail in Reference 1. For the most part leaks of fuel from other parts of the system aren't going to create an explosion hazard and pools are not so readily ignited (as they need a mechanism to heat the pool unless it is already above the flash point or possibly formed a fine mist).

The situation with LH_2 is very different. Flammability inside tanks is not an issue since in effect air is excluded by virtue of pressurisation. If due to say very high liquid take off, traces of air drawn in would freeze. This in itself would be a potential safety issue and the possibility would need to be excluded. It is therefore, absent of a major catastrophic failure, not credible that such a condition could arise. However, any leakage of LH2 , from e.g. a pipe joint or pump, would rapidly evaporate (being exposed to an environment considerably above its boiling point). At

RTP 1 L of LH2 would flash off to give around 780 L of gaseous hydrogen. The lower flammability limit of hydrogen at RTP is 4% (v/v) which equates to only 50 ml of LH2 in a m^3 of air. It is therefore easy to postulate situations were even small leaks into poorly ventilated enclosed volume within an aircraft structure could lead to the formation of explosive atmospheres. In addition, flammable hydrogen/air mixtures are more easily ignited with minimum ignition energies for discharge sparks being an order of magnitude lower than hydrocarbon fuels.

Safe integration of LH2 hydrogen systems into an airframe is very different to Jet fuel. The nature of the hazard, where it might arise and necessary safety measures will change. It is also a different proposition to space systems, needing to operate reliably for many years and not just a single mission. Every pipe connection, valve, and pump is a potential leak point. Steps can obviously be taken to minimise the risk. Typically, in industrial settings, such measures would include providing ventilation to keep hydrogen concentrations below the flammable limit often combined with control of ignition sources, explosions can be vented to limit pressures to safe levels, enclosures can be made sufficiently strong either to not fail catastrophically or not be damaged at all or enclosures can be inerted. LH2 storage tanks would not be placed inside typical buildings. It is simply not possible to apply standard codes of practice to aircraft (see e.g. Reference [1])

Whilst at RTP relevant combustion parameters such as LFL, MOC, MIE, K_G and burning velocity (see section 2 for definitions) are well characterised at RTP there is very limited data at reduced atmospheric pressures and low temperatures. This data is needed to enable optimal design of protection measures. Based on limited existing data and knowledge it is reasonably expected that in some respects the explosion risk at cruise altitude might be very much reduced. Peak overpressure can be estimated by, assuming adiabatic complete combustion in a constant volume reducing from around 7 bar at RTP to ca. 1.4 bar at cruise for a stoichiometric mixture. Similarly ignition energy is reported as being sensitive to initial pressure. For methane it was reported as being proportional to $1/P^2$. Other parameters such as the burning velocity probably will be lessened to some degree.

2. Background literature – combustion parameter testing

As noted above there are a range of combustion parameters that are necessary for the design and specification of explosion prevention and protection systems/measures. To date while these are known at RTP, data at sub atmospheric or low temperatures is limited. There are no studies to date that have obtained actual data at simulated altitude. A few have looked at either pressure or temperature, but there is no guarantee that the effects in isolation with be additive. Determination of such data under simulated altitude will remove uncertainly and underpin the design of safety measures/systems. The various parameters are considered in more detail below.

2.1. Flammability limits and LOC

These are the minimum concentrations (usually quoted by volume) at which a hydrogen/air mixture will support sustained flame propagation. They are also commonly referred to as explosion limits (though occasionally a distinction is made). In Europe these are usually determined in either a bomb or tube type apparatus. The limits are to a small degree apparatus dependent, thus the bomb and tube method give slightly differing results. Additionally, the criteria for determining if ignition has occurred vary (it is not a case of absolute yes/no but whether an ignition source has caused sufficient propagation). This needs to be borne in mind when comparing test data but in reality it is not usually a practical issue as near limit hydrogen/air mixtures burn slowly and combustion is incomplete such that the pressures generated are often of no consequence. At RTP measured the flammability limits range from around 3.6%(v/v) to around 6%(v/v) with 4%(v/v) being generally regarded as the accepted value. The limits are known to be affected by temperature and pressure variations. Small variations from RTP can generally be ignored. However, the much reduced pressures and temperatures encountered at altitude are likely to be significant. Near the upper flammable limit there is a very much more rapid transition from non flammable to rapid combustion and differences between upwards and downwards flammable propagation are minimal.

A key reason for the difference relates to the type of apparatus and the combustion characteristics of near LFL limit mixtures. Where flammability limits are determined in a flame tube type apparatus significantly different values are obtained if the ignition source is positioned at the top or bottom of the tube. Standard practice assumes the ignition source is at the bottom, for which a value of around 4% is observed, however, if ignition is attempted at the top of the tube then a value of around 9% is found (called the downwards LFL). For horizontal propagation around 6% is required. The 9% limit in effect defines when combustion will always be fast and complete. The difference is particularly pronounced with hydrogen. For most fuels the upwards flammability limit corresponds to an adiabatic flame temperature of around 1000°C and the concentration is typically around 50% of the stoichiometric concentration [3]. In the case of hydrogen however the theoretical adiabatic flame temp of a 4% (v/v) mixture is only 350°C and the concentration is 14% of stoichiometric. The reason for this is related to the high diffusivity of hydrogen in comparison to oxygen. Preferential diffusion occurs and the flame becomes unstable and breaks into cells. The hydrogen concentration at the convex flame cells increases and hence the localised flame temperatures, in excess of the calculated adiabatic flame temperature, are generated at the flame fronts. This instability facilitates combustion at lower concentrations than would otherwise be possible. Near upwards $LFL_{(U)}$ mixtures of hydrogen/air are therefore less “explosive” than most other fuels (smaller temperature/pressure rises, slower flame velocities and incomplete combustion). It is also therefore not surprising that bomb methods, relying on pressure rise criteria as opposed to propagation distance up a vertical tube, typically result in higher values for the LFL. This is illustrated by the results obtained by Cashdollar [4] reporting an LFL of 6%(v/v) dropping to 4% with initial turbulence.

While a number of studies have considered the effect of elevated temperatures on flammability limits [5] few appear to have investigated the flammability limits at low temperatures [6,7] and none considering the combined effect of low pressures and temperatures. Figure 1 produced from data from Wierzba et al [6] gives the results of one such study.

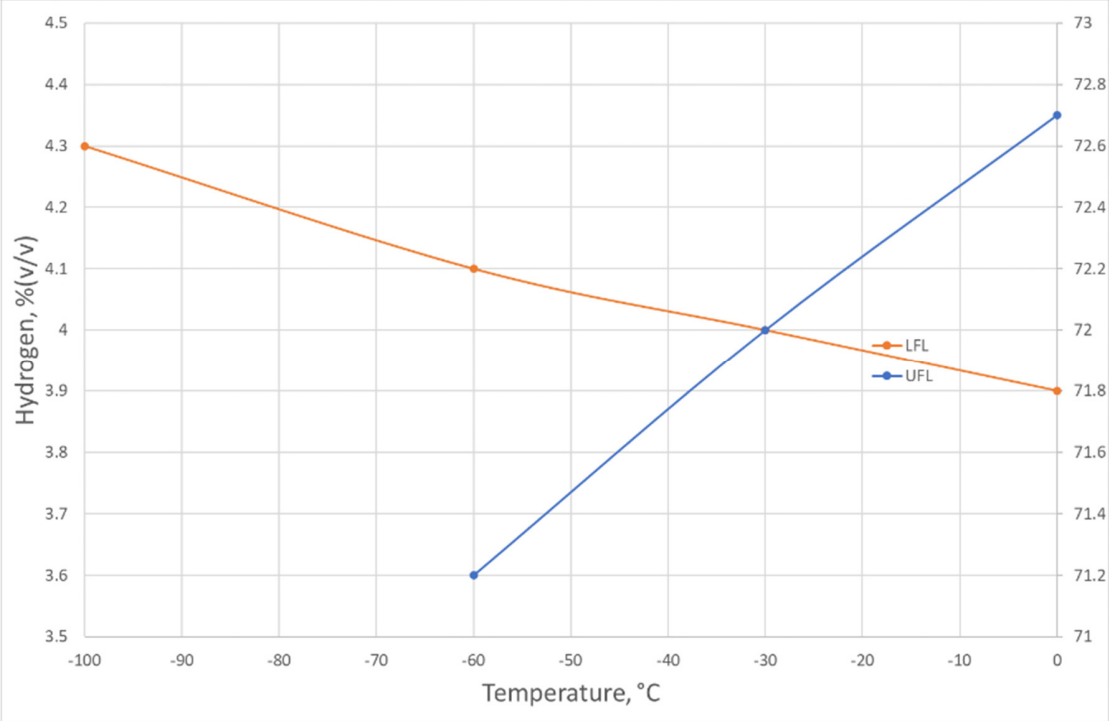

Figure 1 Effect of temperature on LFL from data in Reference [6]

It can be seen from the results of this study that reducing the temperature would be expected to have the effect of narrowing the flammability limits. This study was conducted in a flame tube type apparatus. The values obtained were compared by Wierzba against those obtained using the Burgess-Wheeler law and found to be in reasonable agreement.

$$\frac{LFL_T}{LFL_{T_R}} = 1 - 0.000721(T - T_R) \qquad \text{Equation 1}$$

$$\frac{UFL_T}{UFL_{T_R}} = 1 + 0.000721(T - T_R) \qquad \text{Equation 2}$$

Similarly, few studies have investigated the effect of reduced initial pressures on the lower flammability limit of hydrogen [8,9,10]. The results of these studies are given in Figure 2 below.

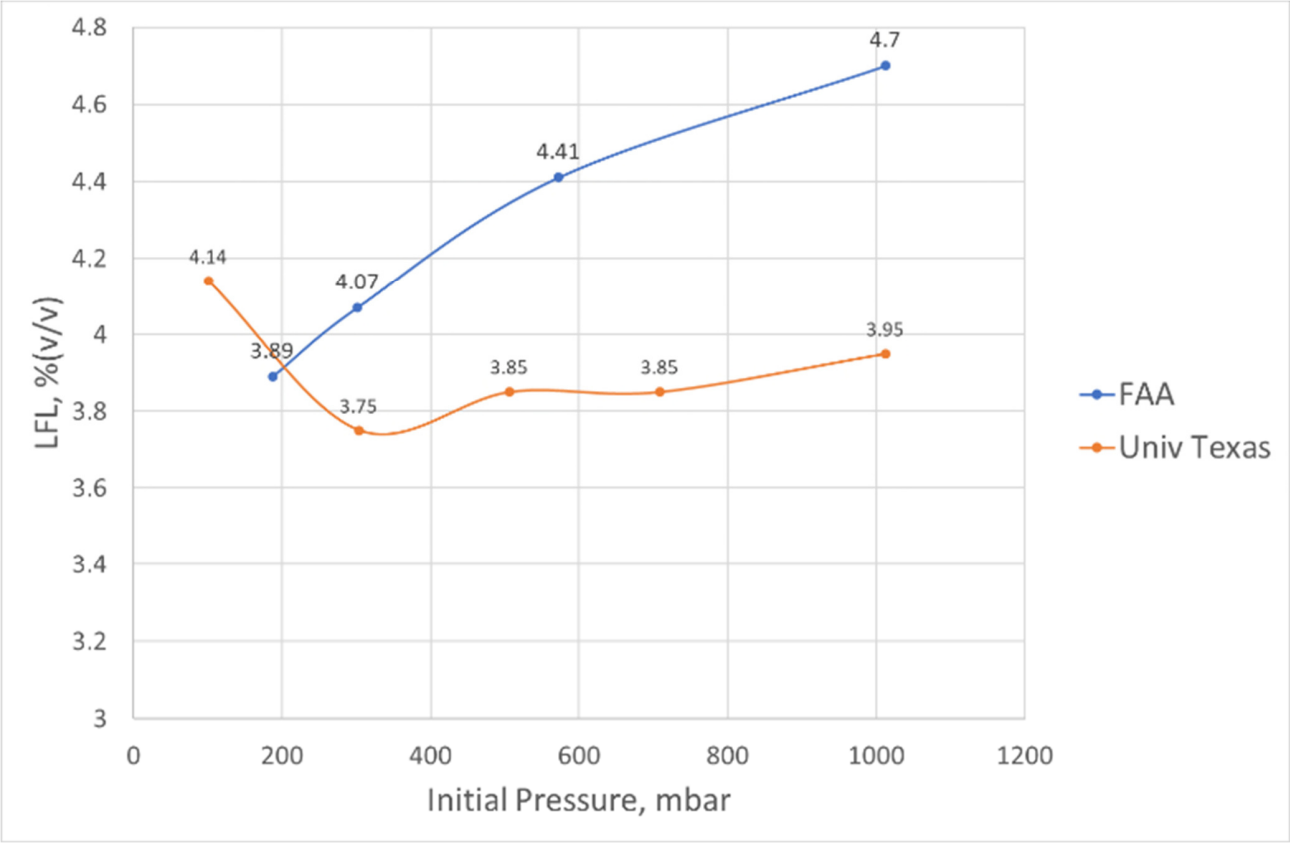

Figure 2 Comparison of FAA and University of texas LFL data for reduced initial pressure

In contrast to most fuels both studies show the flammability limits decreasing (i.e. widenening) as pressures are reduced below atmospheric. However, there is significant difference in the rate of decrease. An obvious difference between the studies is that the Texas University study used a flamability tube, whereas the one in the FAA report used a bomb type apparatus (3% pressure rise criteria). It is also intersting to note that the Texas Univ study observed an increase in the LFL at 100 mbar. Unfortunately there is no comparable test in the FAA dataset. Reference [4] suggests the decrease from 100 to 300 mbar is a result of the increased pressure and hence reactants/free radicals causing an increase in the overall combustion rate. Above 300 mbar it is suggested that increased importance of three body chain termination reactions (particularly $H + O2 + M \rightarrow HO2 + M$) as the pressure increases results in a reduction in the overall rate of reaction and a narrowing of the flammability limits which continues up to around 15 bar. With further initial pressure increases, the amount of reactants and the concentration of free radicals increase. This higher density of reactants and free radicals leads to an increase of the overall reaction rate which results in the promotion of the combustion process and the widening of the flammability range.

As noted by the FAA [10] for hydrogen to be used in aviation the combustion properties need to be investigated in a wide range of conditions that can be applied to the aviation industry. While there is data on the effect of both low temperature and low pressure on flammability limits independently, it is not entirely clear how the effects will combine. This is likely to be the situation encountered in practice since at altitude low temperatures go hand in hand with low pressures. Additionally, leaks from liquid hydrogen systems could well depress gaseous temperatures, if released into the environment. The effects may well cancel out to some degree, but it is difficult to predict particularly given the complexity of the relationship with pressure around 0.1 bara (noting that decreasing temperatures effectively increase fuel density). One of the aims of this project is therefore to determine flammability limits over a range of typical combinations of reduced temperature and pressure.

It is also worth mentioning that there also a pressure limit (depending to a degree on ignition source) below which all mixtures become non-flammable. In work reported by Kuznetsov et al. [11] it was observed that the limit was around 50mbar for a glow plug igniter and 100 m bar for a spark igniter. However, these pressures would correspond to altitudes above which passenger aircraft would fly. Interestingly, in contrast to the spark igniter, with a glow plug the UFL initially increased as pressure was reduced from atmospheric (from 75 to nearly 80% in range 200-500 mbar).

Closely related to the upper and lower flammability limits is the Minimum Oxidant Concentration (MOC). This refers to the minimum concentration of oxidant (usually oxygen and often termed the Limiting Oxygen Concentration) that must be present for a fuel/inert gas mixture to become flammable. This parameter is primarily of interest for the design of inerting systems. It is determined using the same apparatus as flammability limits, however there is less published data on the effect of temperature and pressure. No datasets for the effect of reduced temperature have been found. However, reduced pressure was investigated in the FAA study [10].

Much of the above discussion applies equally to the MOC and the effect of combined reduced pressures and temperatures on the MOC will also be investigated.

2.2. Fundamental Burning Velocity and Rate of Pressure rise

Laminar flame speed or fundamental burning velocity is defined by the rate at which a laminar pre-mixed flame will propagate into an unburned mixture. The laminar flame speed is an important fundamental parameter, that can be related to other properties and appears in a number of numerical and analytical models. In the context of safety it often appears in explosion models, venting equations, estimations of run up distances for detonations and can be related to flame thickness and quenching distances.

There are a number of techniques that have been used to experimentally determine laminar flame speeds over the years using both stationary and non- stationary flames [12]. The two most commonly now used are burner-nozzle methods and bomb type apparatus, measuring spherical flame expansion. It is also possible to estimate laminar burning velocities in bomb type apparatus from rates of initial pressure rise.

As noted above, the aim of this study is to determine a range of combustion parameters under simulated altitude conditions. Since it would be more challenging (although perhaps possible) to utilise a burner method, it was decided to opt for measurement of spherical flame expansion and thus the focus of the discussion. The standard definition of laminar burning velocity relates to an idealised scenario of a one-dimensional free adiabatic flame propagating into an infinite domain. This is good for simulation and provides a consistent definition, but is practically impossible to reproduce in the real world due to factors such as non-quiescent unburned gas due to thermal expansion, wall effects, buoyancy, etc. Thus, regardless of the method used experimental observations of laminar flame speed usually have a small correction applied.

In terms of spherical expanding flames in a bomb type vessel, the effects of unsteady flame propagation, flow field variations, require correction for flame stretch.

A spherical flame propagates into the quiescent combustible mixture. Local flame properties of expanding spherical flame are affected by unsteady flame propagation, non-uniform flow field, variation in flame curvature and diffusional effects. These effects are summarized as flame stretch and they significantly affect the flame propagation speed of the fuel-air mixture.

The maximum rate of pressure rise $\left(\frac{dP}{dt}\right)_{max}$ in a vessel of volume V is related to the factor K_G, defined as:

$$K_G = V^{1/3}\left(\frac{dP}{dt}\right)_{max}$$

where the units of K_G are usually quoted as $bar\ m\ s^{-1}$. The factor is essentially the maximum rate of pressure rise in a vessel of volume $1\ m^3$.

2.5. References for chapter 2

1. DOT/FAA/AR-98/26, A Review of the Flammability Hazard of Jet A Fuel Vapor in Civil Transport Aircraft Fuel Tanks, U.S. Department of Transportation Federal Aviation Administration, June 1998

2.EIGA, SAFETY IN STORAGE, HANDLING AND DISTRIBUTION OF LIQUID HYDROGEN, DOC 06/02/E

3. Bodurtha F.T., “Industrial explosion prevention and protection”,McGraw Hill, New York, 1980

4 K. L. Cashdollar, I. A. Zlochower, G. M. Green, R. A. Thomas and M. Hertzberg, "Flammability of methane, propane, and hydrogen gases," *Journal of Loss Prevention in the Process Industries,* vol. 13, pp. 327-340, 2000.

5 Hustad J.E., Sonju O.K., "Experimental studies of lower flammability limits of gases and mixtures of gases at elevated temperatures", Combustion and Flame, 71, 283-294, 1988

6. Wierzba, I., Harris, K., Karim, G. A. (1992) Effect of low temperature on the rich flammability limits in air of hydrogen and some fuel mixtures containing hydrogen, International Journal of Hydrogen Energy, vol. 17 (2), pp. 149-152.

7.Karim G. A., Wierzba, I., Boon, S. (1984) The lean flammability limits in air of methane, hydrogen and carbon monoxide at low temperatures, Cryogenics: 24, pp. 305-308.

8. THUY MINH HAI LE, “Flammability Characteristics Of Hydrogen And Its Mixtures With Light Hydrocarbons At Atmospheric And Sub-Atmospheric Pressures” A Dissertation by Submitted to the Office of Graduate Studies of Texas A&M University in partial fulfillment of the requirements for the degree of DOCTOR OF PHILOSOPHY, August 2013

9. Le, Y.Liu, M. S. Mannan, “Lower Flammability Limits of Hydrogen and Light Hydrocarbons in Air at Subatmospheric Pressures” by H., 2013. Industrial & Engineering Chemistry Research, 52(3), 1372-1378.

10. Rehn, S.J., DOT/FAA/TC-TT14/36, Technical Thesis “Flammability of Hydrogen at Sub-Atmospheric Pressures and Reduced Oxygen Concentrations”, Federal Aviation Administration, William J. Hughes Technical Center, Aviation Research Division, Atlantic City International Airport, New Jersey 08405, October 2014

11 M. Kuznetsov, S. Kobelt, J. Grune, T. Jordan, Flammability limits and laminar flame speed of hydrogen–air mixtures at sub-atmospheric pressures, International Journal of Hydrogen Energy, Volume 37, Issue 22, 2012,

12. Alexander A. Konnov, Akram Mohammad, Velamati Ratna Kishore, NamIl Kim, Chockalingam Prathap, Sudarshan Kumar, A comprehensive review of measurements and data analysis of laminar burning velocities for various fuel + air mixtures, Progress in Energy and Combustion Science, 68, (2018), 197-267

3. LSBU Combustion Parameter Testing at Simulated Altitude

3.1. Apparatus

The apparatus, developed and constructed by LSBU for ENABLEH2, consists of a number of core components, consistent over the range of parameters, with adaptions/specific components i.e. ignition source, electrodes, imaging depending on the testing being undertaken.

3.1.1. Core components

The base configuration of the apparatus is shown in Figure 3 and can be broken down into the following:

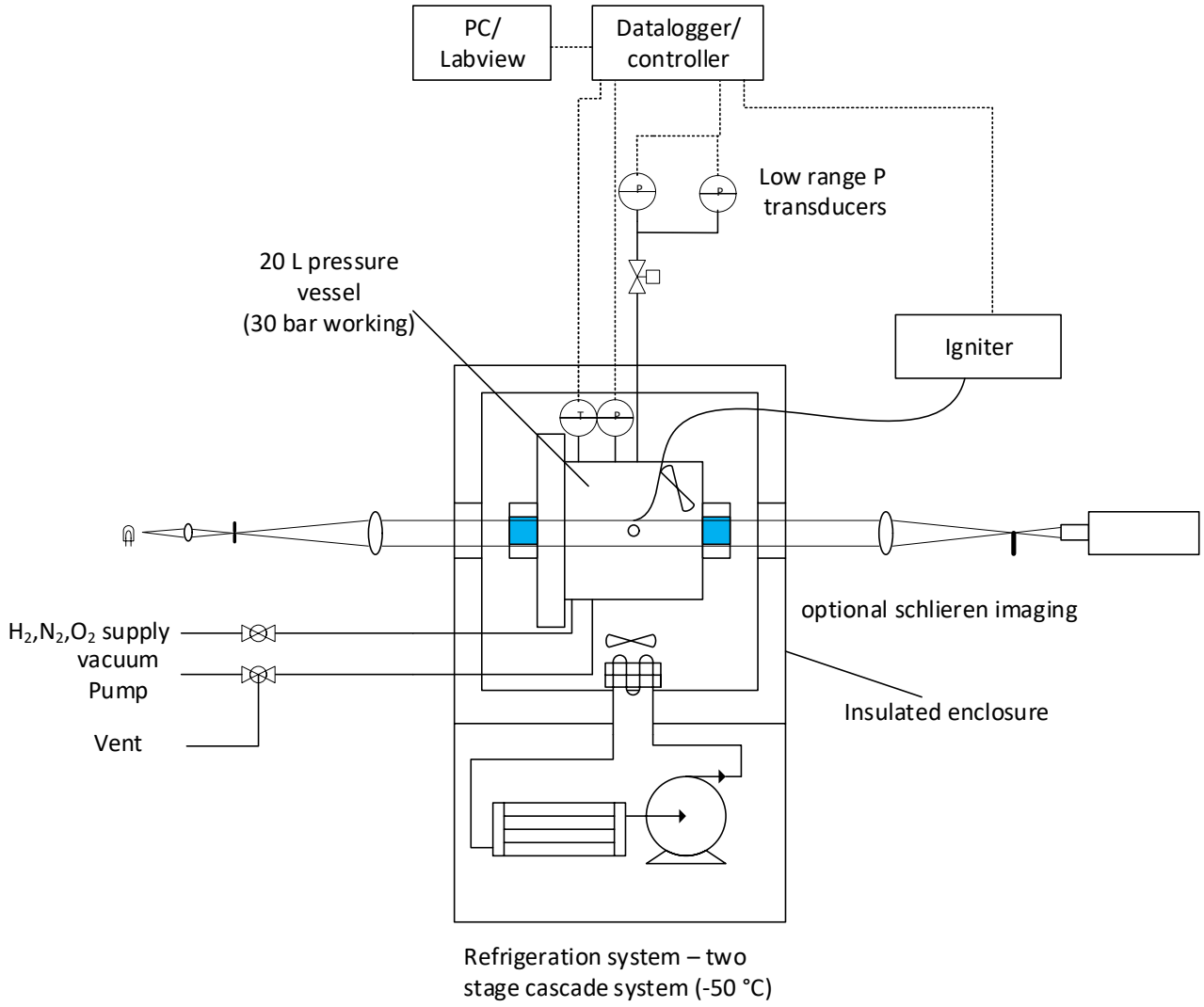

Figure 3 Schematic of LSBU high altitude combustion parameter test apparatus

3.1.2. Pressure vessel

The main component of the apparatus is the pressure vessel as shown in the Figure 4 below.

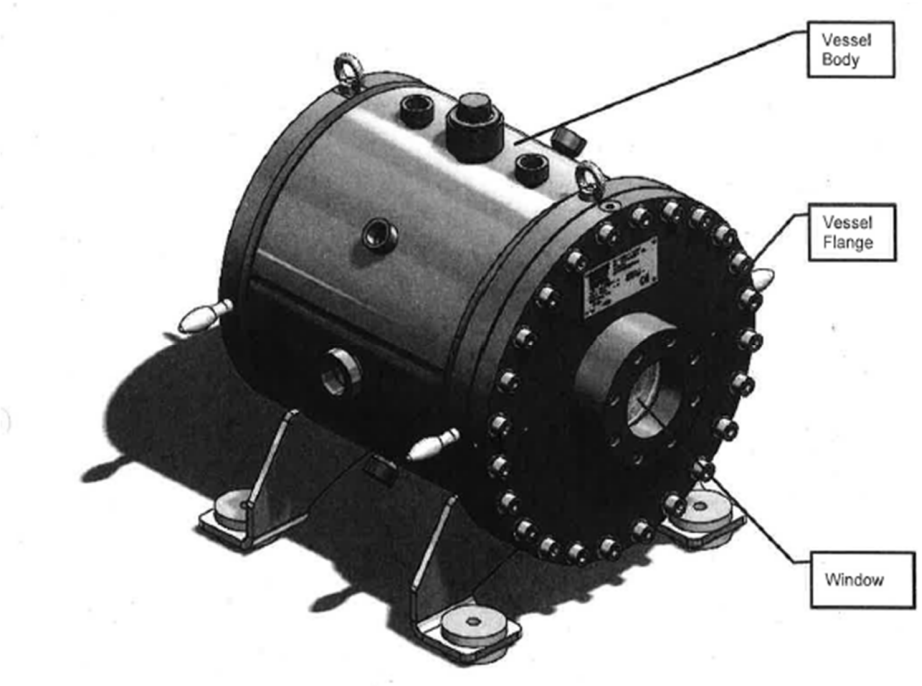

Figure 4 Windowed pressure vessel

The vessel and removable end flange are manufactured from 304 stainless steel. The internal dimensions are 0.30 m Ø and 0.30 m long giving an internal volume of 22.5 L. The custom vessel, supplied by KW Designed Solutions, Chorley, UK, was designed and constructed to "Intent of PD5500:2018 +A1: 2018 Category2" and certified/tested (HTP 47 bar) in accordance with the Pressurised Equipment Directive 2014/68/EU. The vessel has a Maximum Allowable Working Pressure of 30 barg and operational temperature from-50 to +50 °C. The diameter of the end flange is 350 mm. The vessel incorporates two 25 mm thick glass viewing windows, with an unobstructed clear diameter of 78 mm. The overall length across the window flanges is 460 mm. The overall height including mounting is 410 mm.

The vessel body incorporates 8 off ½" NPT located symmetrically around the vessel as illustrated by Figure 4, Two 1" NPT ports located centrally at half height on opposing sides of the vessel and a M36 x 1.5 port on the top of the vessel that could, if required, be used to mount e.g. a mechanical stirrer shaft. The two 1" ports were used to mount ignition electrodes and the ½" ports were used for gas connections, pressure sensor and feed throughs for temperature sensors and electrical connections. The total weight of the vessel is 78 kg and the end flange 29

kg. There is little clearance between the vessel and cabinet. To facilitate removal of the vessel a length of U channel, with spacers to make it level and apertures to accommodate fittings, was bolted to the top of the vessel. The vessel could then be safely lifted out using a manual straddle forklift (SFH1025A Straddle Stacker from Midland Pallet Trucks).

It should also be noted that there is no pressure relief device fitted to the vessel itself. The vessel is specified to withstand the effects of an internal deflagration without deformation. The deflagration over pressure of stoichiometric hydrogen/air mixtures will be maximum of around 8 times the initial absolute pressure. If the initial pressure inside the vessel is sufficiently high it could be taken outside its working limits triggering a need for inspection/testing of at very high pressures damage. The rates of pressure rise would be such that a vent fitted to the vessel is not a practical option due to a) the size it would need to be and b) it would need to vent external to the surrounding enclosure to avoid over pressurising the freezer cabinet. As can be seen from the section below, the system has been designed to limit the fill line pressures, such that a hazardous fill pressure inside the vessel cannot be physically attained even under rare fault conditions. In particular, the pressure in the hydrogen fill line is limited by both by the maximum setting of the cylinder regulator and an inline pressure relief valve to 2 bara. Even if the vessel was filled with pure hydrogen to 2 bara and topped off to a pressure of 8 barg (the maximum lab air supply pressure), this would produce an overpressure of just in excess of the 30 bar MAWP and considerably less than the hydrostatic test pressure. For the experiments planned the initial fills should be a maximum of 1 bara. The initiation of a detonation inside the vessel, would require higher energy ignition sources than those used but might be credible with pure Oxygen instead of air, assuming a dynamic load factor of 2 and a reflected CJ pressure of 30 bar would indicate an equivalent static load of around 60 bar from a 1 bara fill. This in itself would not result in catastrophic vessel failure, clearly additional precautions might be need if pure oxygen was used in place of air. Since the pressure reliefs provide protection for the vessel itself, they were also listed under the Written Scheme of Examination for the system.

The vessel was originally supplied with EPDM O-ring seals. These proved to be unsuitable, leaking below around -40°C. At around this temperature all readily available O-ring materials transform from an elastic to a plastic state and temperature cycling/differential expansion resulted in the O-rings temporarily taking a fixed shape and becoming ‘loose’. This issue was ultimately resolved by sourcing some cryogenic rate ‘Astra’ seals. These utilise a flat spiral stainless-steel spring inside a polymer tube. Specialist polymers would likely also have worked but would have required, in effect, paying for a production run and for small quantities the Astra seals are more cost effective.

3.1.3. Refrigeration system

The refrigeration system and cabinet were custom built by Fisher Refrigeration, Landbeach, Cambridge. The unit re-purposes a Gallenkamp oven coupled to a custom built two stage refrigeration system. A picture of the cabinet is given in Figure 5 and Figure 6. The inside of the

oven has been modified to incorporate the evaporator and two axial fans to direct cooled air directly on to the vessel mounted above the fans. The effective useable dimensions of the enclosure are 0.8m (w) x 0.6m (d) and 0.5 m (h). The unit uses R508B and R410A refrigerants. The cooling power was not stated, however, the unit draws a maximum of 18 amps at 240 V (4kW) with both stages running and is capable of taking the vessel from room temperature to -50 °C in approximately 1.5 hours. The manufacturers estimated that system would be capable of bring the vessel down to around -70°C. The temperature controller for the freezer utilised a PT100 probe that could be located as desired.

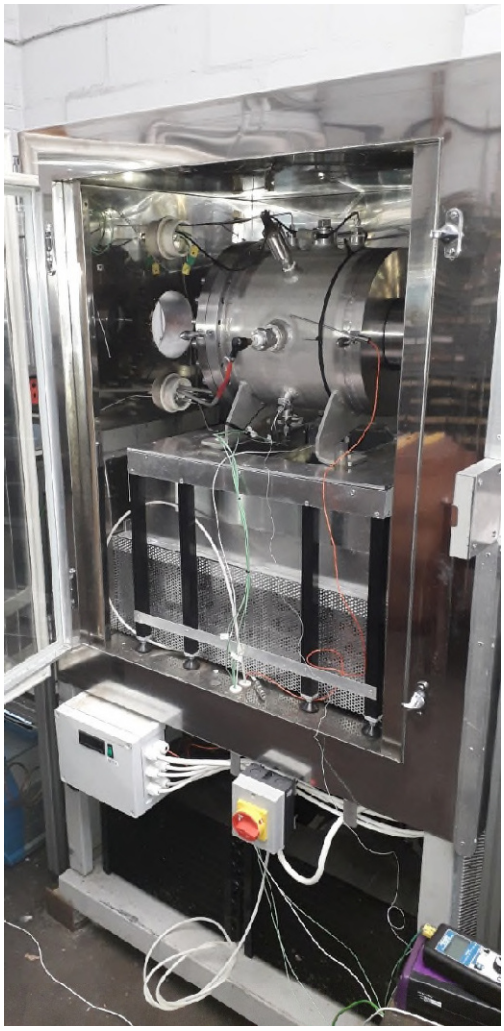

Figure 5: Photo of the cabinet with the door open, showing the vessel inside

Figure 6: Photo of the cabinet with the door closed and the rest of the apparatus

3.1.4. Gas Supply System

A schematic of the gas supply system is shown in Figure 7. Due to low temperatures the control valves and some of the pressure transducers are mounted outside the freezer cabinet.

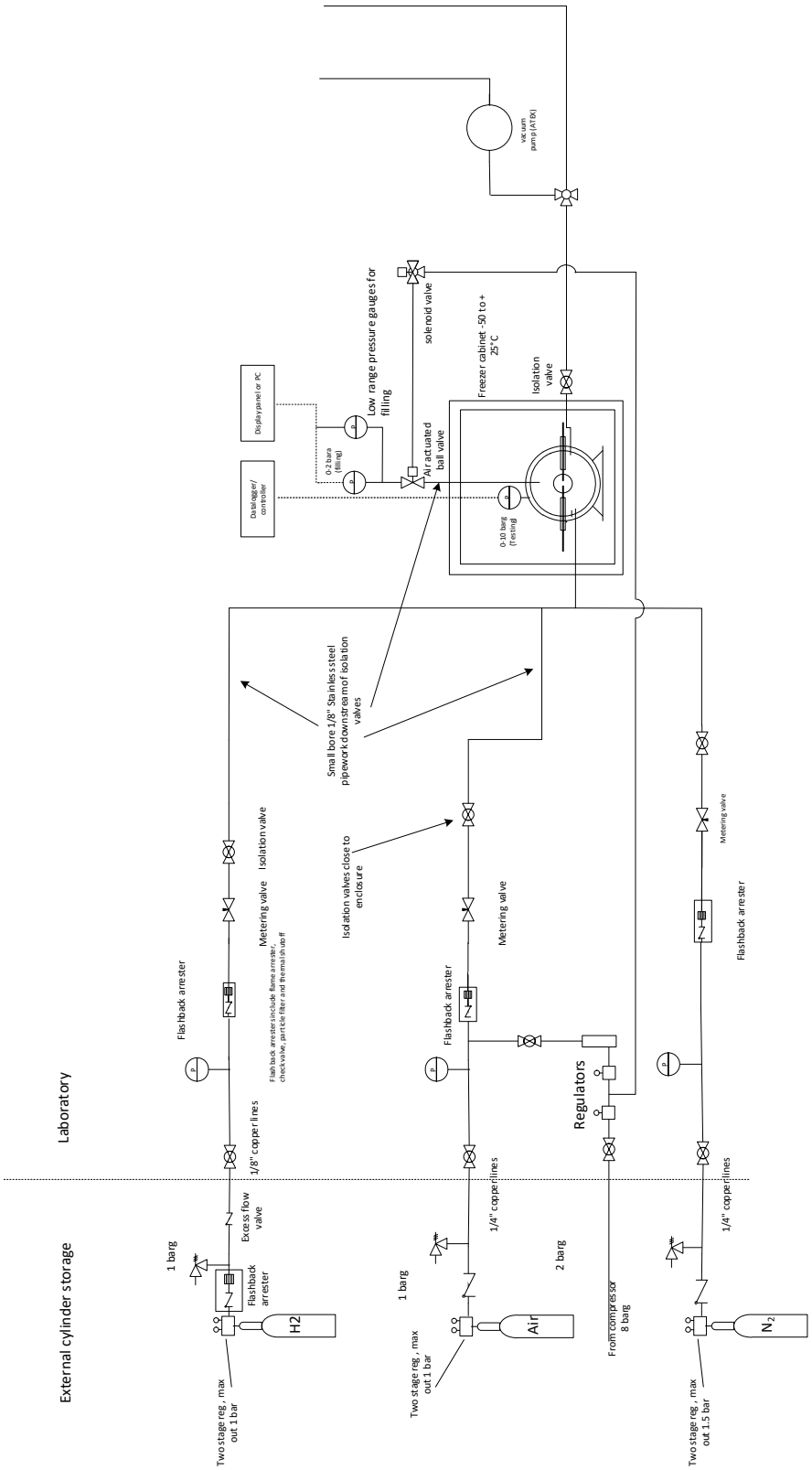

Figure 7 Gas supply system

To minimise the dead volume most of the connections to the vessel are made in 1/8” SS tubing. The exception being the line to the vent/vacuum pump which is run in ¼”. Hydrogen (>99.99% purity) & Nitrogen (>99.998% purity) are supplied to the rig from gas cylinder mounted under weather protection external to the laboratory. For most experiments the air supply to the lab was utilised after drying, but synthetic air from a gas cylinder could also be used. A DRIERITE drying unit was used, capable of drying air to a dew point of -73°C. As noted above in relation to the pressure vessel, the fill lines from the bank of gas cylinders incorporate pressure relief valves mounted external to the building (above the height of the door and away from openings). The valves in the air and hydrogen lines opened at 1 barg (Circle Seal Controls 5598-3M-14.5) and the nitrogen line 3 barg (Circle Seal Controls 5598-3M-14.5). The lines to the rig incorporated flashback arresters (combined flames arrester/check valve) and check valves to protect against backfilling or flashbacks. The pressure transducers external to the cabinet were isolated using an air actuated ball valve, which could be controlled from Labview, so as to prevent accidental over-pressurisation when testing

Except for hydrogen, the lines to the rig were run in ¼” tubing, Hydrogen was run in 1/8” copper tubing, which has a safety benefit in a) restricting leak rate if disconnected and b) being too small for propagation of a detonation. It should be noted that the rig is sited in a 5 x 7 x 6 m high laboratory with roofline ventilation, such that even the maximum possible flow of hydrogen (e.g. if a fitting left disconnected) would not be sufficient to form a hazardous flammable volume in the laboratory.

3.1.5. Instrumentation

Most of the data acquisition and control was accomplished using a National Instruments USB 6212 Bus-Powered M Series Multifunction DAQ device. The device offers eight 16 bit differential analogue inputs with, a sampling rate of up to 400kS/s, and 32 digital input/output connections. The rig utilised 3 pressure transducers. To record explosion pressures, a high range 0 – 10 bara transducer (Omega PXM6000MC6 – 010BARA5T) was mounted directly to the pressure vessel. A key requirement was therefore the ability to operate at -50°C as the transducer would be inside the freezer cabinet. While the transducer was rated to operate at these temperatures there was significant sensitivity to temperature. The data sheet suggested a sensitivity of ±0.05% full scale/°C (5 mbar/°C) for both span and zero offset, however, in practice while the zero offset did vary to this extent, the effect on the span was smaller (appear to be around 0.02% FS). The change in span is small enough to be ignored, however the zero offset, particularly at low pressures is significant, amounting to difference of 0.3 bar between ambient and -50°C, and needed correction. To charge the vessel with a gas mixture prior to test a partial pressure method was employed. For this purpose two pressure transducers an Omega PX409-030A5V 0-30 psia and an Omega PX409-005A5V 0-5 psia. These, for accuracy, need to be mounted external to the freezer and as noted above with reliable isolation to prevent damage from higher explosion pressures. All the pressure transducers gave a 0-5V output which were be directly connected to differential analogue inputs on the DAQ device without any additional filtering or amplification. The isolation valve for the pressure transducers was operated pneumatically utilising air

pressure controlled from 240V solenoid valve switched using a DAQ digital output via switch a solid-state relay.

A small mixing fan is located inside the vessel. Whilst the vessel has a suitable aperture for mounting a shaft for a mixing fan, due to likely additional issues with vessel sealing and other practical considerations the decision was taken to utilise an internal electric fan. A small brushless 12V axial fan had been utilised in earlier combustion testing undertaken at LSBU without causing ignition or sustaining damage, and so one was selected for this purpose. The fan could be turned on/off using a DAQ digital output.

The vessel incorporated four 0.5 mm diameter SS sheathed K type thermocouples and a PT100 probe. An additional thermocouple was also located inside the freezer cabinet. The cabinet temperature and thermocouple closest to the electrode gap were connected to the DAQ. The remaining thermocouples and PT100 were monitored/recorded using a Datataker DT85 logger (which could accommodate up to 16 thermocouple or PT100 inputs).

The rig was controlled and explosion data logged through control of the DAQ using LabView.

3.1.6. Apparatus for Flammability Limit Testing

The specific components required for the flammability limit tests relate to the ignited and ignition electrodes. In essence the electrode configuration was two central pointed electrodes, ground to an angle of 60° as defined in BS EN 1839. The mounting of the electrodes is a shown in Figure 8. Sealing at low temperatures proved problematic due to a combination of differential expansion and transition of O-ring seals from elastic to plastic. Although based on a Swagelok fitting, a ferrule cannot be relied on to keep the Delrin electrode holder in place.

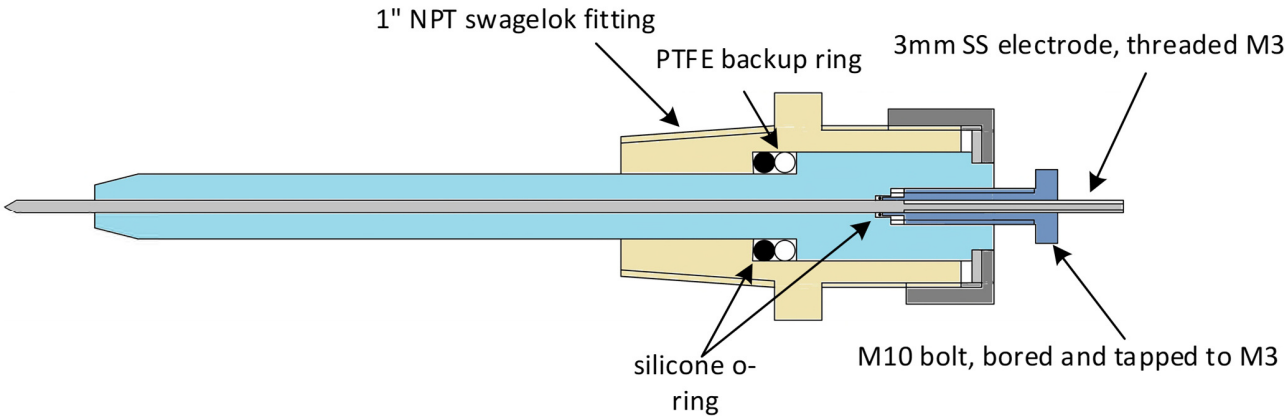

Figure 8 Electrode Mounting

For most of the testing a centre tapped 2 x 6kV rms 20 mA ignition transformer giving an open circuit potential across the electrodes of 12kV was used. The arcing was switched on/off using an opto-isolated dual relay module connected to a DAQ digital output and controlled by Labview. Some tests were also carried out using a 2 x 8kV rms open circuit source produced by connecting the secondary outputs of two single sided 8kV 30 mA transformers in series.

A separate study was conducted to characterise the igniter energy. A high voltage probe (Tektronix P6015A) and current probe (Tektronix A621) were used to measure the instantaneous voltage and current, connected to an Agilent MSOX3014A oscilloscope. The voltage probe needed to measure relative to ground thus recording half the total voltage across both transformer outputs. The waveforms were exported to excel for analysis. Examples of the waveforms obtained for the two igniters are given in Figure 9 and Figure 10 below.

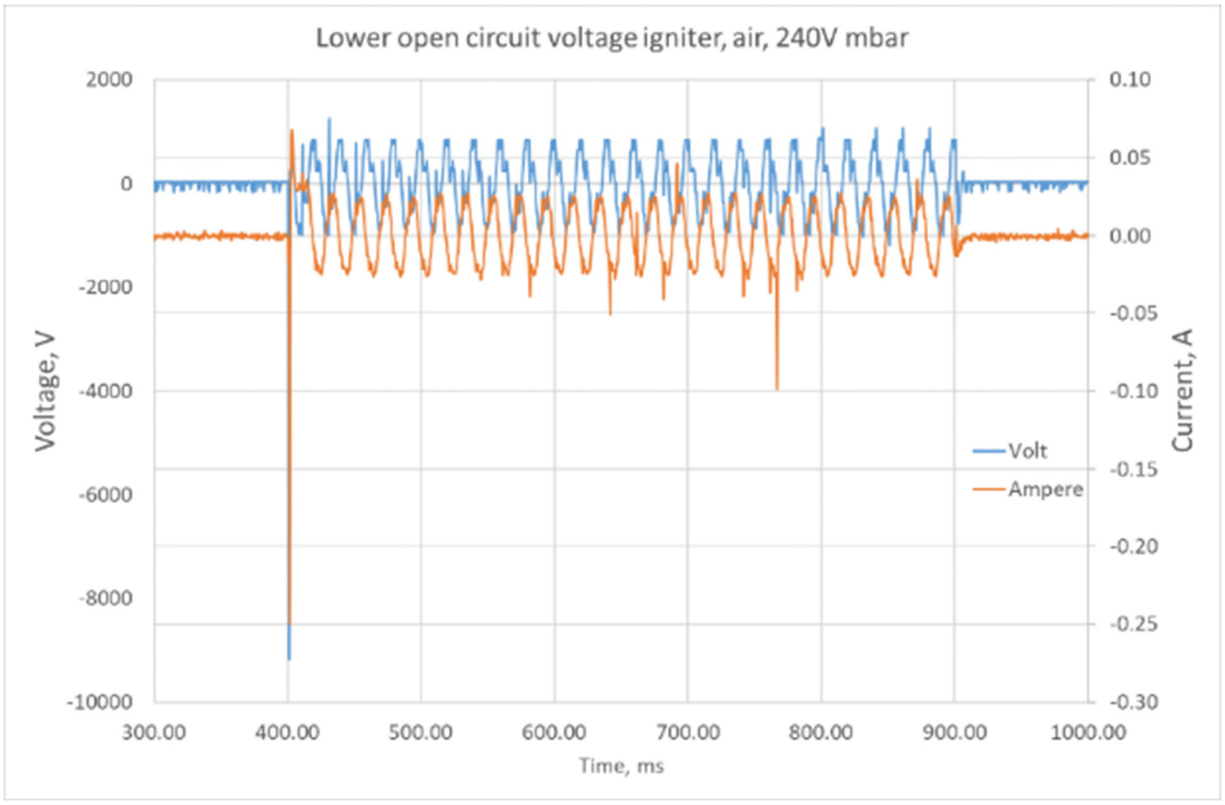

Figure 9 Low open circuit voltage igniter waveform

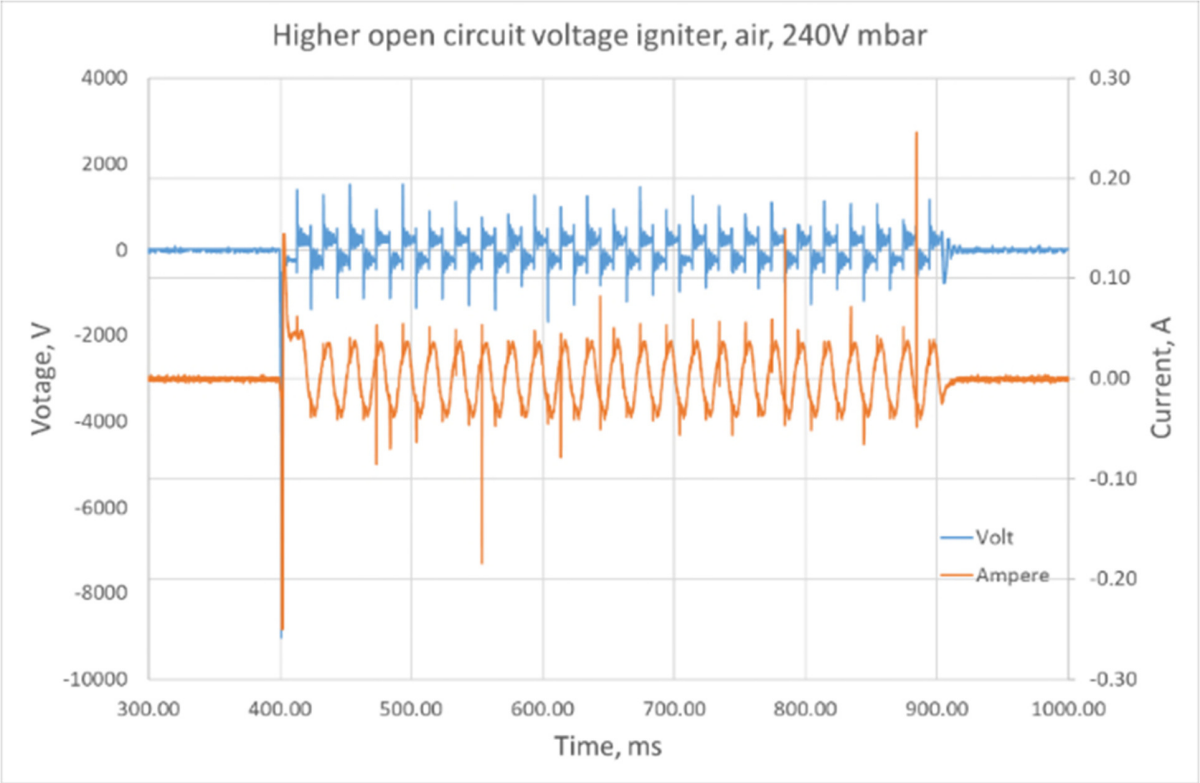

Figure 10 High open circuit voltage igniter waveform

Figure 9 shows two waveforms that are approximately sinusoidal in shape with the current lagging the voltage by around 90°. There is an initial high voltage spike as the arc is initiated that settles down to a stable waveform. The power of the high voltage spike peaks at between a few hundred watts to in some cases a few kV before stabilising to much lower values of between 15 to 45 watts. Figure 10 shows a sinusoidal waveform for the current for the higher voltage rated igniter, but the voltage now appears to be almost square, this probably relates to a combination of more rapid rise and earlier breakdown of the gas (due to high open circuit voltage) and the current limiting protection of the transformers.

Tests were conducted at 3 pressures and some with/without hydrogen added. For both igniters the energy dissipated during arcing decreased with decreasing pressure. For the 2x6kV igniter the energy dissipated averaged 7.6, 4.7 and 3.4 J for pressures of 1013, 572 and 240 mbar respectively. Addition of hydrogen resulted in values of 5.9, 4.3 and 3.0 J. The reduction in energy, given that the ignition transformer has current limiting protection, to enable it to run short circuited, suggests a reduction is the resistance across the spark gap as pressure is decrease and probably a function of the reduced mass of material within the arc gap. Hence replacement of air with H_2 also reduced the energy dissipation The results using the 2x8kV igniter were a little unexpected. Even though it had a high open circuit voltage and would initiate an arc over a much wider gap the steady voltage was consistently lower by around 250 V rms (measured from one side of secondary output to centre tap). Measured currents were similar or slightly lower.

However, the different shape of the voltage curve resulted in comparable power dissipations of 6.1, 5.0 and 3.7 J for air at 1013, 572 and 240 mbar.

3.2. Methodology

3.2.1. Flammability limit Testing

The test methodology applied for LFL, UFL and LOC testing was essentially the same. As detailed in discussions of earlier work in Section 2, to determine the flammability limit for a given condition in a bomb type apparatus requires a series of ignition tests at compositions traversing the limit. The flammability limit is specified by the composition that achieves a particular percentage pressure rise above the initial baseline pressure. The pressure produced by the igniter alone was very small, around 0.3 mbar for a 200 ms arc in air at atmospheric pressure, and was neglected. The limit was then obtained by interpolation from a plot of percentage pressure rise vs hydrogen concentration (or O_2 in the case of LOC determination). Prior to testing the freezer set-point was set to the desired temperature. Once at the desired setpoint the gas supplies were turned on. Before each test the vessel was repeatedly filled with air and evacuated to ensure that residual hydrogen (or oxygen in the case of the LOC tests was <0.01% (v/v)). Following the final evacuation, the residual pressure and temperature was noted. For the purposes of calculating gas composition the residual gas is assumed to be air. The desired mixture composition was achieved by the addition of partial pressures of each gas using the needle valves to achieve the required composition. After each addition the partial pressure and gas temperature was recorded. It was necessary to record the temperature since the addition of warm (relative to the vessel) gases as well as thermal cycling of freezer temperature about the set point meant it was not possible to keep the vessel at a precisely fixed temperature. The partial pressures were adjusted for temperature when calculating the final mixture composition. Gases were added in the order of hydrogen first then nitrogen (if needed) and then air up to the test pressure (i.e. 240, 572 or 1013 mbara corresponding to 35,000 ft, 15,000 ft or sea level respectively).

The mixing fan inside the vessel was run for a period of 3 minutes and the vessel temperatures and pressures recorded. The firing sequence and data acquisition was automated using Labview. On triggering the test, the mixing fan was turned off and the isolation valve for the external pressure transducers closed (for some tests where it was known that the pressure rise would be small the valve was left open, to provide an additional record of the pressure). After a delay of 60s the igniter was triggered to produce (selected prior to test) an arc of either 200 or 500 ms duration. Simultaneously data from the pressure transducers and the vessel temperature was logged and saved to a file. The duration and frequency of data logging could be varied. A duration of 2s was sufficient to capture the peak pressure in all but a few tests and a sampling rate of 5k reading/s was usually used. After the data acquisition the fan was restarted. If no ignition had occurred the firing could be repeated with a longer duration arc. The initial purging cycle was then repeated prior to filling for the next test.

3.3 Results

3.3.1. Flammability limits

This section describes the behaviour of hydrogen firstly in terms of its lower flammable limits and subsequently in terms of its upper flammable limits.

3.3.1.1. Lower flammability limit

Figure 11 below shows a typical pressure time curve for an LFL test. Every test generated curves of this general form.

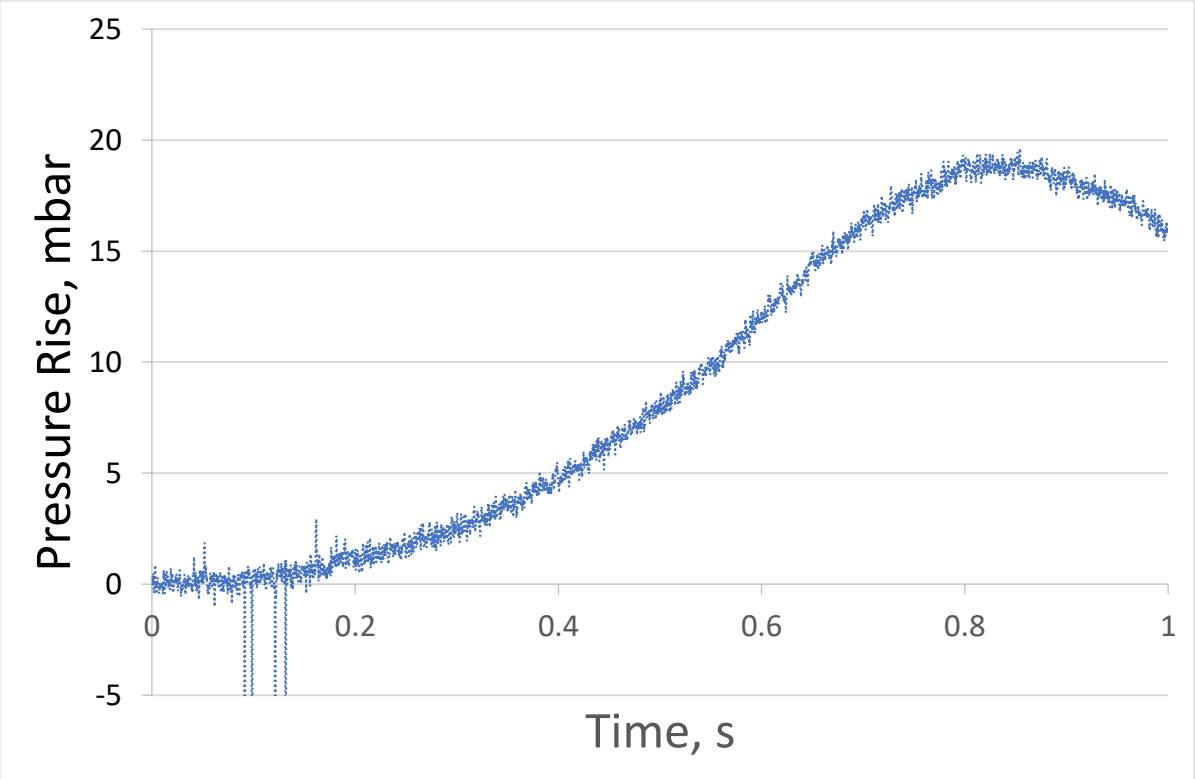

Figure 11 Pressure rise trace from lower flammability limit test (ambient temperature, 1013 mbar and 5.5% (v/v) hydrogen in air)

The igniter operates for the first 200 ms of the trace. Flame propagation continues and pressure inside the vessel rises to maximum before decaying. It should be noted that near the LFL flame propagation is weak and thus the pressure rise is much lower than calculated by assuming AICC and only a small fraction of the hydrogen available is burned. The pressure rise obtained above

the initial fill pressure is then divided by the fill pressure to give a percentage pressure rise and recorded. As discussed earlier the criteria for flammability (in this type of apparatus) is somewhat arbitrary. In keeping with the FAA work a value of 3%(v/v) has been used as the flammable/non-flammable criteria. Obviously, a higher value will result in a slightly higher LFL and conversely a lower one a lower LFL. Test were conducted for hydrogen concentrations from 4 to 6.5%, for initial pressures of 240, 572 and 1013 mbar. This was undertaken for temperatures of ambient, -15 and -50 °C.

The plots obtained are given in Figure 12 below for each of the three temperatures.

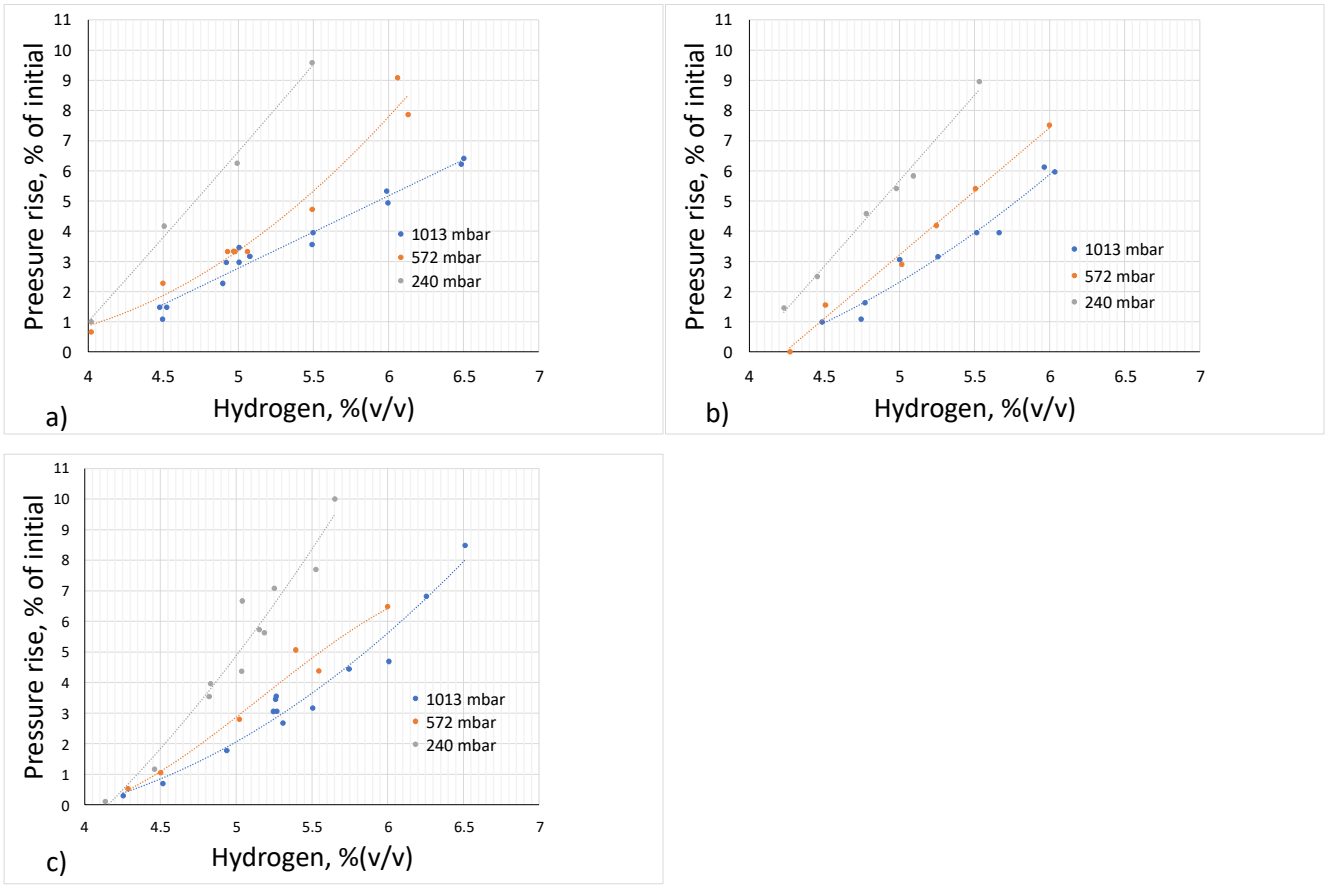

Figure 12 Pressure rise plots for a) Ambient, b) -15°C and c) -50°C

It can be seen from these plots that even for several percent hydrogen above the LFL combustion is still weak and incomplete (i.e. by comparison with the theoretical AICC pressure). Using a criteria of 3% these give rise to the following Lower flammability limits (

Table *1*) for the different combinations of temperature and pressure:

Table 1 Lower flammability limits (%(v/v)

	Ambient (20°C)	-15°C	-50°C
240 mbar	4.35	4.5	4.7
572 mbar	4.9	4.95	5.0
1013 mbar	5.1	5.2	5.3

Figure 13 below gives a plot of LFL vs pressure for the three temperatures and Figure 14 a 3D representation of the data. It can be seen that the LFL increases with increasing pressure and decreases with increasing temperature. Thus the effects are opposing. Both effects are relatively weak, but in relation to air temperatures expected for a given altitude (i.e. -50°C at 35,000 ft and 20°C at sea level) the effect of the pressure dominates and the effect of reduced temperature is insufficient to compensate for the widening due to decreased pressure. The magnitude of the reduction in LFL with pressure at ambient (ca. 0.7 %(v/v)) is reasonably consistent with that reported in Reference [1] (ca. 0.8 % (v/v)), for a similar bomb type testing apparatus, decreasing temperature to -50°C has approximately halved the decrease.

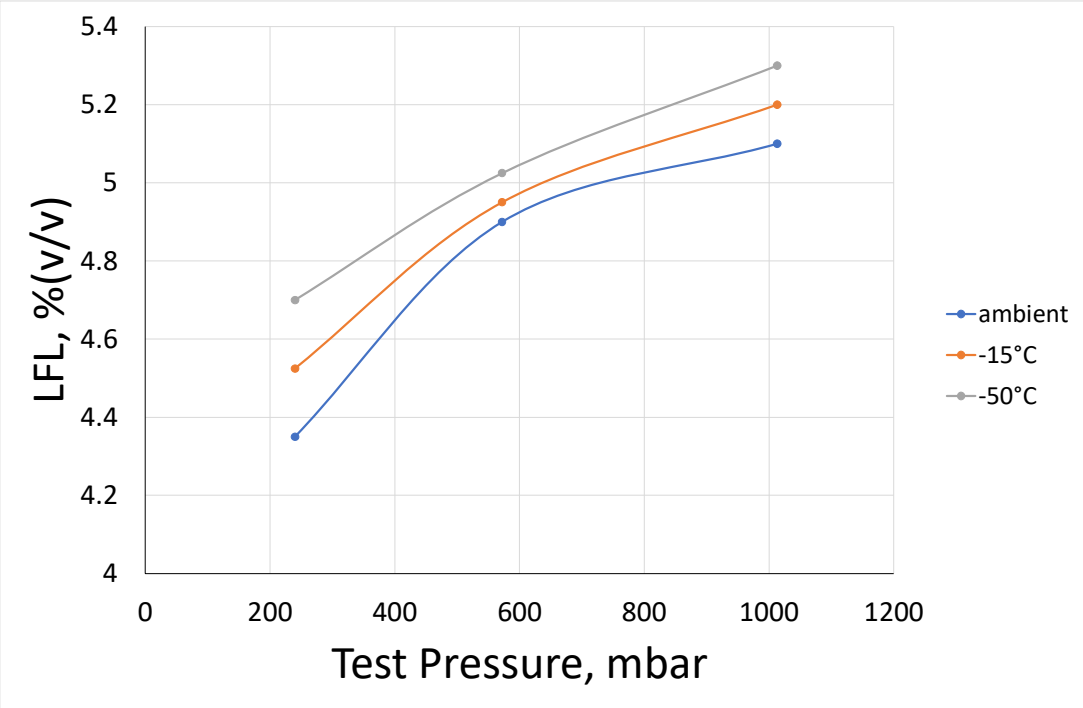

Figure 13 Plot of LFL versus initial pressure

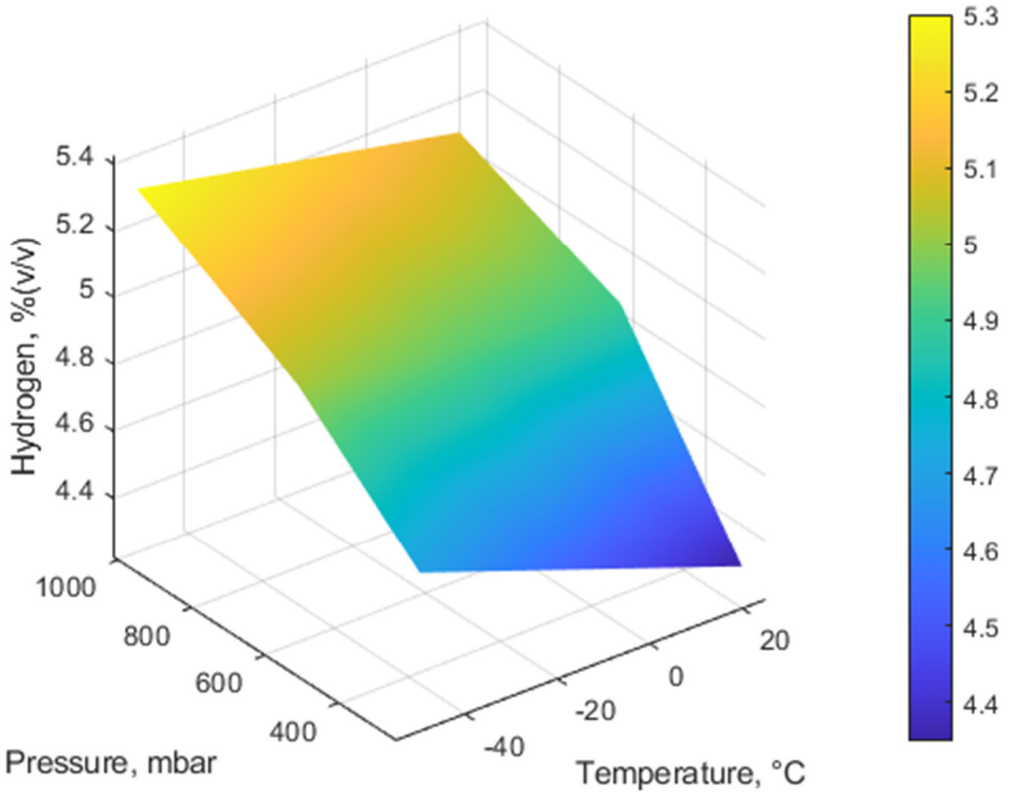

Figure 14 3D representation of LFL data

An additional series of tests was conducted using the 8kV x 2 igniter for atmospheric pressure and ambient temperature. It was found that flammability limit was not altered significantly. Subsequent investigation of the power dissipated by the arc (see section 2.1.2.) showed that although the open circuit voltage of the igniter was significantly greater, in practice the power dissipated during arcing was similar, so this result is perhaps not surprising. A comparison of the pressure rise vs hydrogen concentration for the two igniters is given in Figure 15 below.

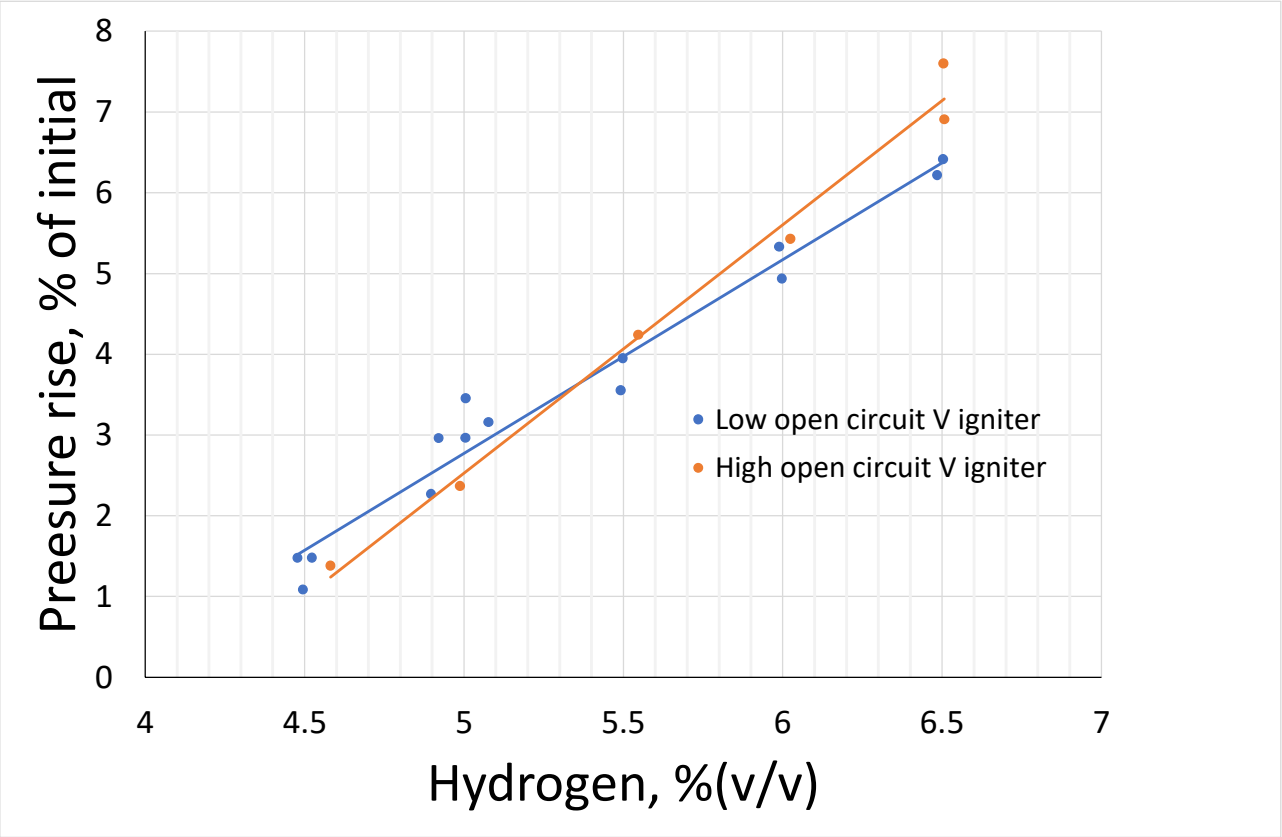

Figure 15 Pressure rise plots obtained for ambient and 1013 mbara using 6kVx2 and 8kVx2 igniters

3.3.1.2. Upper Flammability Limit

A typical pressure time trace for a UFL test is given in Figure 16. The trace is much the same as for the LFL tests. However, the transition from non-flammable to flammable occurred over a very narrow concentration, resulting in a cliff edge between no pressure rise at all and quite large over pressures. Close to the limit ignition would often occur on the second attempt with a 500 ms spark duration. Sometimes a long delay occurred (several hundred ms) between the arcing and the onset of rapid combustion.

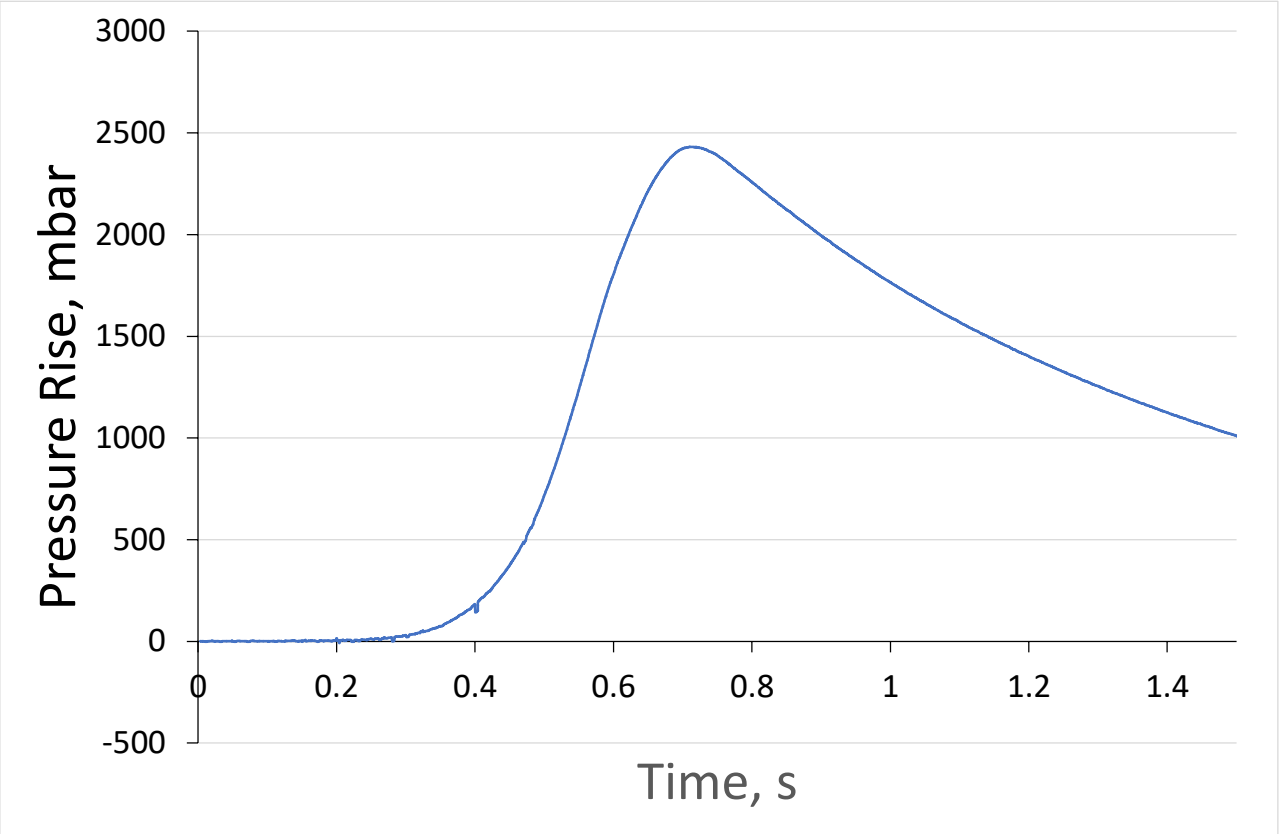

Figure 16: Pressure rise trace from upper flammability tests (ambient temperature, 1013 mbar and 76.2% (v/v) hydrogen in air)

As for the lower flammability limits tests the pressure rise data is used to produce plots of percentage pressure rise above initial vs concentration from which the flammability limit is determined. Test were again for a range of hydrogen concentrations traversing the UFL for initial pressures of 240, 572 and 1013 mbar. This was undertaken for temperatures of ambient, -15 and -50 °C.

The plots obtained are given in Figure 17 below for each of the three temperatures.

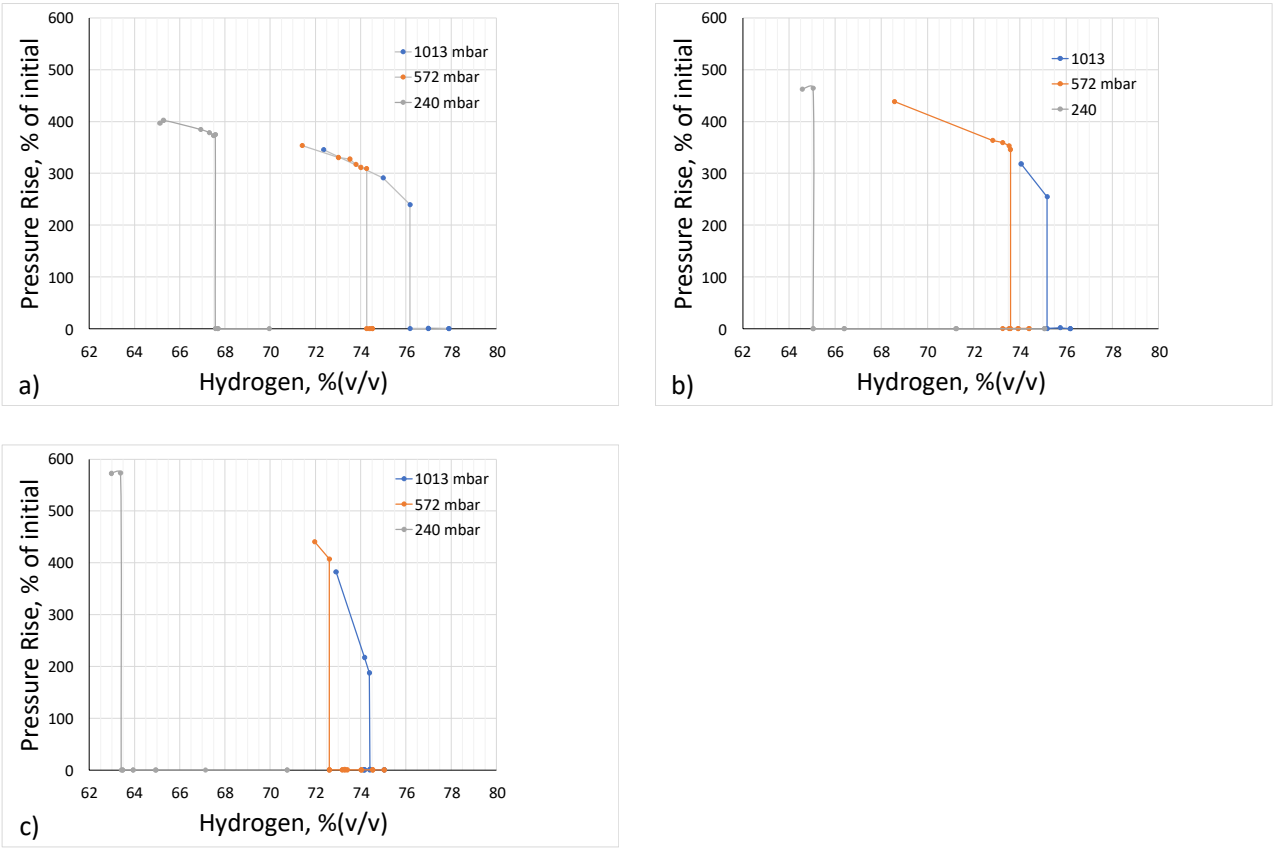

Figure 17 Pressure rise plots for a) Ambient, b) -15°C and c) -50°C

It can be seen from the above plots, that in contrast to the LFL, the transition from no ignition to rapid complete combustion occurs very rapidly in a fraction of a percent. Using a criteria of 3% these produced the following Upper flammability limits (Table 2) for the different combinations of temperature and pressure:

Table 2 Upper flammability limits (%(v/v))

	Ambient (20°C)	-15°C	-50°C
240 mbar	67.6	65.05	63.4
572 mbar	74.3	73.6	72.6
1013 mbar	76.2	75.2	74.4

Figure 18 below gives a plot of UFL vs pressure for the three temperatures and Figure 19 a 3D representation of the data.

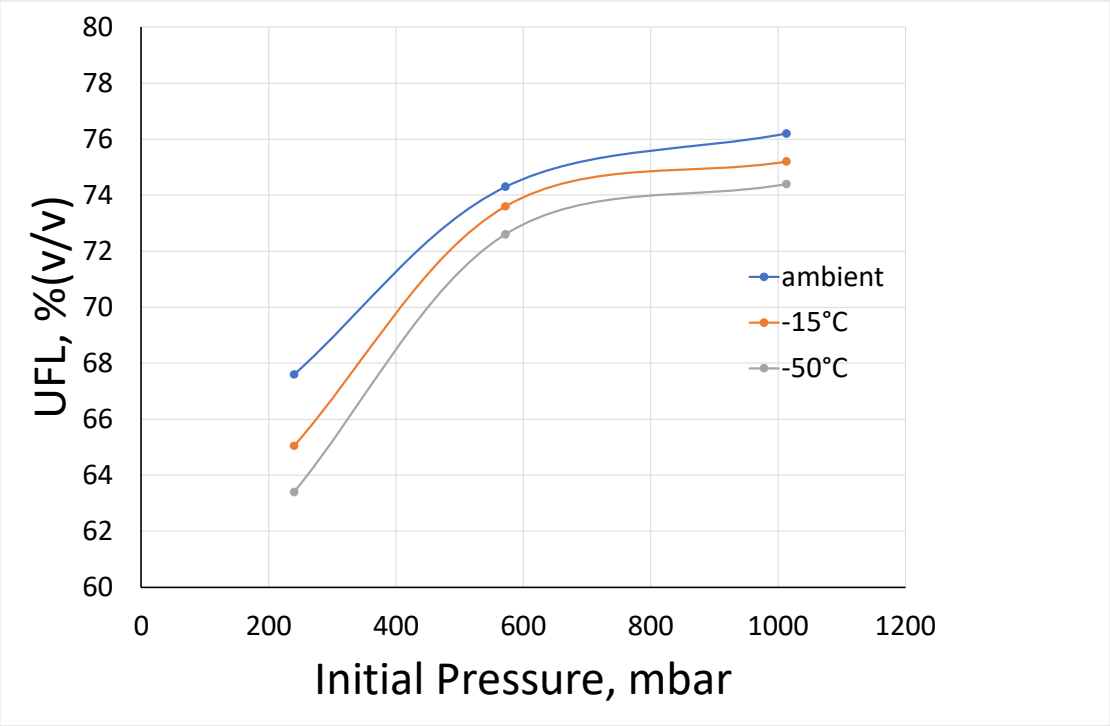

Figure 18 Plot of UFL vs initial pressure.

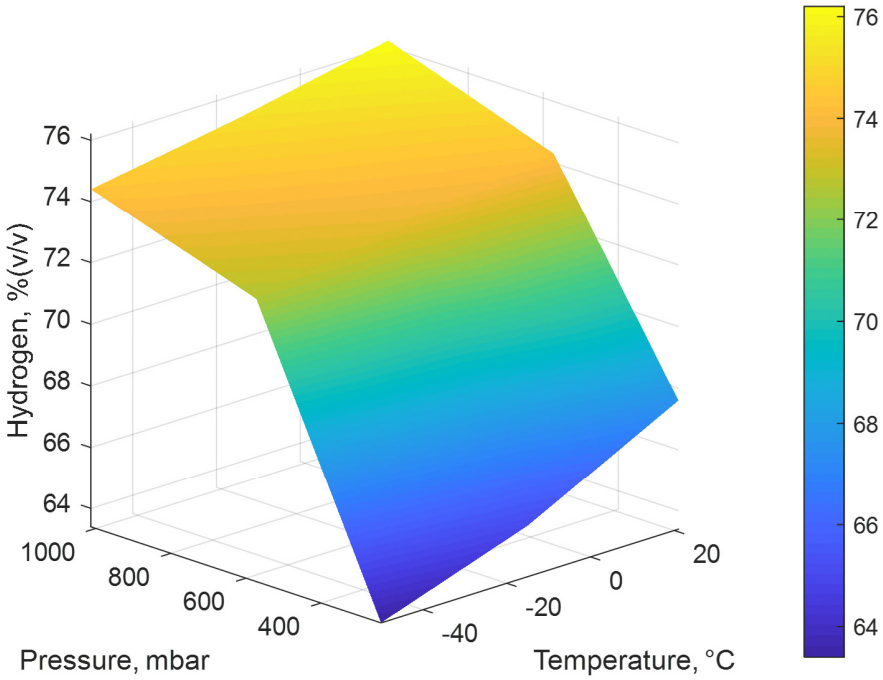

Figure 19 3D representation of UFL data

It can be seen from Figure 18 & Figure 19 that reduction in pressure has resulted in a significant decrease in the UFL of 8 to 10 % H_2. There is a significant non-linearity indicated and increased effect at lower pressures, but more data points are needed to accurately define the curve. The temperature effect can be also seen to decrease the UFL, but is weaker, resulting in a drop of between 2 to 4% H_2 between ambient and – 50°C. The temperature effect also seemed to be greater at low initial pressures.

3.3.1.3 Limiting Oxygen Concentration

Determination of the LOC is a little more complex. As illustrated by the example plot given in BS EN1839, the minimum oxygen concentration does not necessarily occur at the nose of a triangular flammability plot but may occur at a higher concentration on the UFL boundary. To enable a triangular flammability diagram to be drawn tests were carried out at hydrogen concentrations of both 6% (v/v) and 25% (v/v)

Explosion tests were conducted for a range of oxygen concentrations (added as air), with a fixed amount of hydrogen and a variable amount of nitrogen to traverse the boundary between flammable and non-flammable for initial pressures of 240, 572 and 1013 mbar. This was undertaken for temperatures of ambient, -15 and -50 °C for each hydrogen concentration. The pressure time traces are essentially the same in general appearance as those described earlier. Tests with 25%(v/v) hydrogen produced a sudden step change and higher overpressures similar to the UFL tests, whereas those with 6% (v/v) were more typical of the LFL pressure rise plots.

The plots obtained are given in Figure 20 below for each of the three temperatures and two hydrogen concentrations.

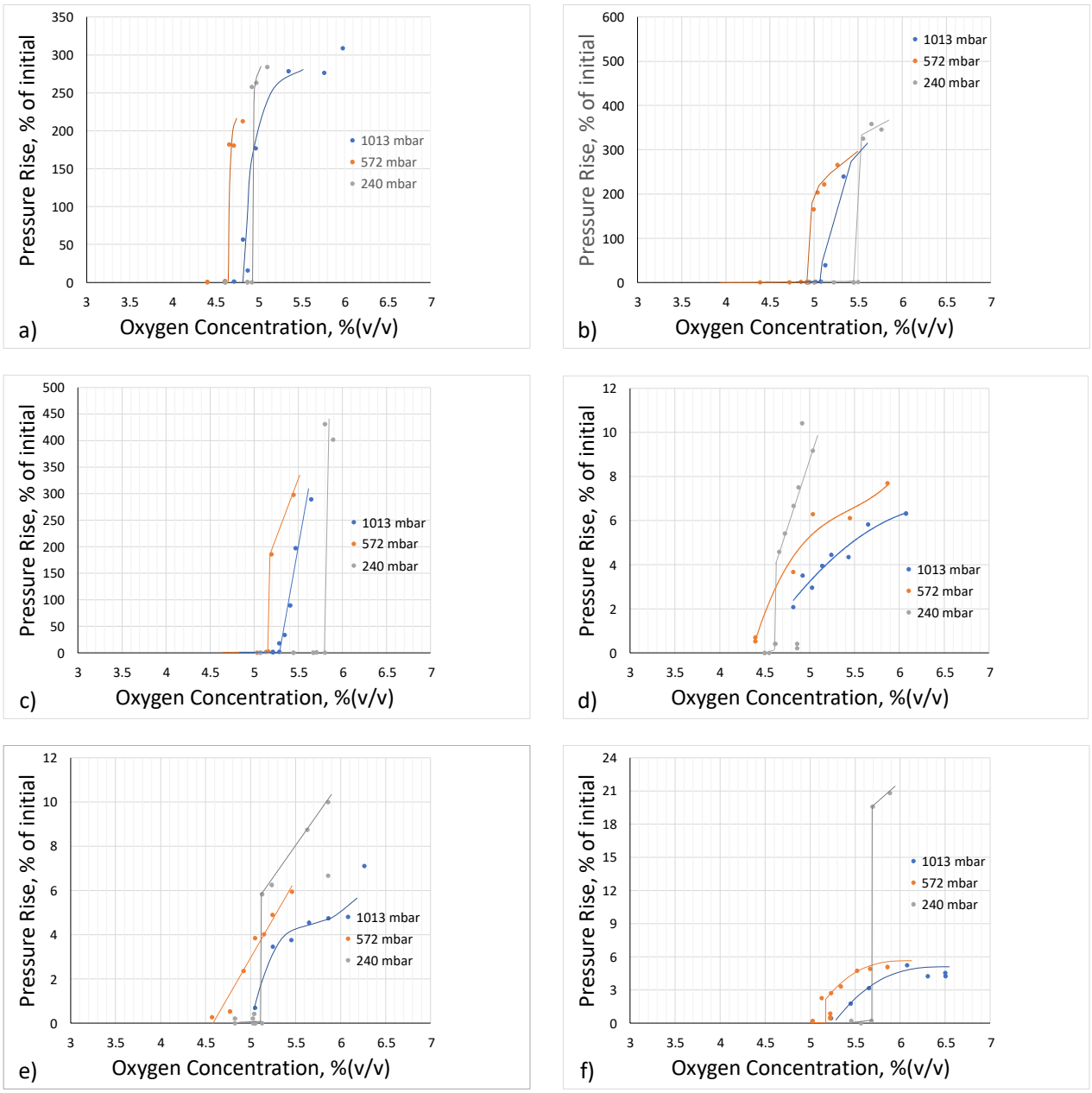

Figure 20 Pressure rise plots for a) Ambient, b) -15°C and c) -50°C with 25%(v/v) hydrogen and d) Ambient, e) -15°C and f) -50°C with 6%(v/v) hydrogen.

Using the criteria of 3% above initial these produced the following limits (Table 3) for the different combinations of temperature and pressure at the two hydrogen concentrations tested:

	6%(v/v) hydrogen			25%(v/v) hydrogen		
	Ambient (20°C)	-15°C	-50°C	Ambient (20°C)	-15°C	-50°C
240 mbar	4.7	5.1	5.7	4.95	5.45	5.8
572 mbar	4.6	5	5.3	4.65	4.9	5.15
1013 mbar	4.95	5.25	5.6	4.8	5.1	5.3

Table 3 LOC data for 6% and 25% hydrogen at 240, 572 and 1013 mbara

The overall LOC at a given temperature was taken as the minimum value from the two datasets (highlighted in red), and as indicated on the triangular flammability diagrams in section 4.1.4 below.

Figure 21 below gives a plots of LOC data vs pressure for the three temperatures and Figure 19 gives 3D representations of the data for each hydrogen concentration.

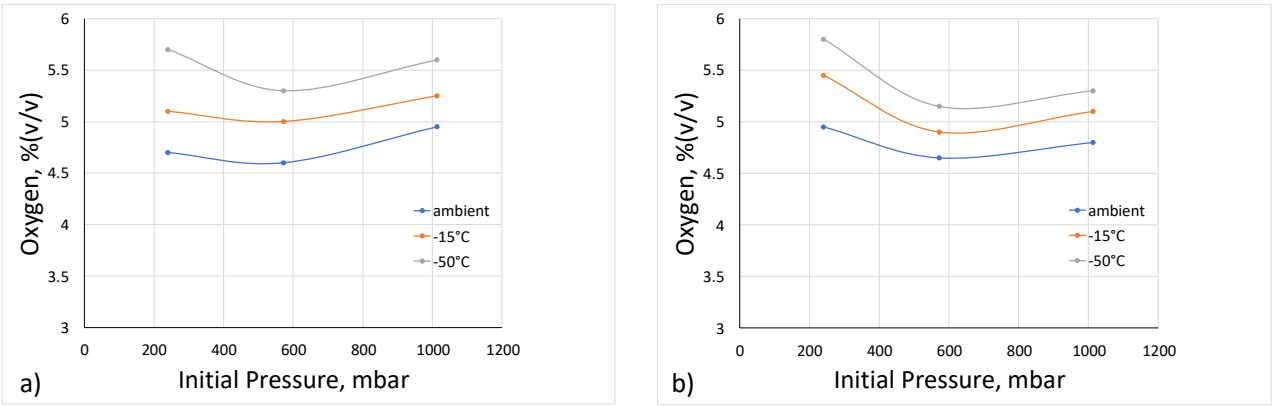

Figure 21 Plot of oxygen concentration vs initial pressure a)6% H_2 & b)25%H_2

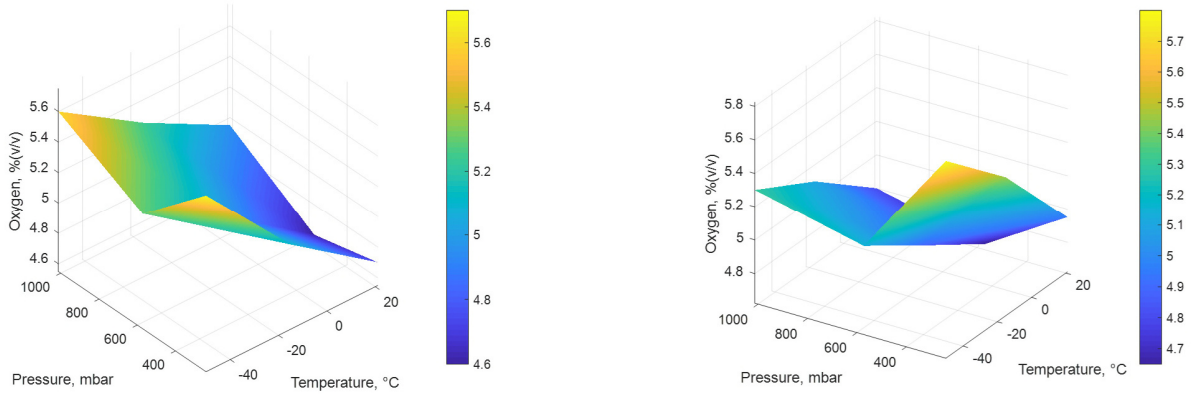

Figure 22 3D representation of LOC data a) 6%H_2 & b)25%H_2

The effect of pressure decrease seems to be quite complex. Initially, from 1013 to 572, bara there is a slight decrease in the oxygen concentration, the flammable range widening slightly. However, as pressure is further reduced to 240mbara the oxygen concentration increases and flammable range narrows. Temperature reduction consistently increases the oxygen limit by around 0.5 to 1% (v/v), there effect being greater at lower temperatures.

3.3.1.4. Triangular flammability limit diagram

The LFL, UFL and LOC data have been combined to produce a series of ternary flammability limit diagrams given in Figure 23 to Figure 29. The area bounded by the line and the hydrogen axis defines the compositions that were found to be flammable and those outside the bounded area to be non-flammable.

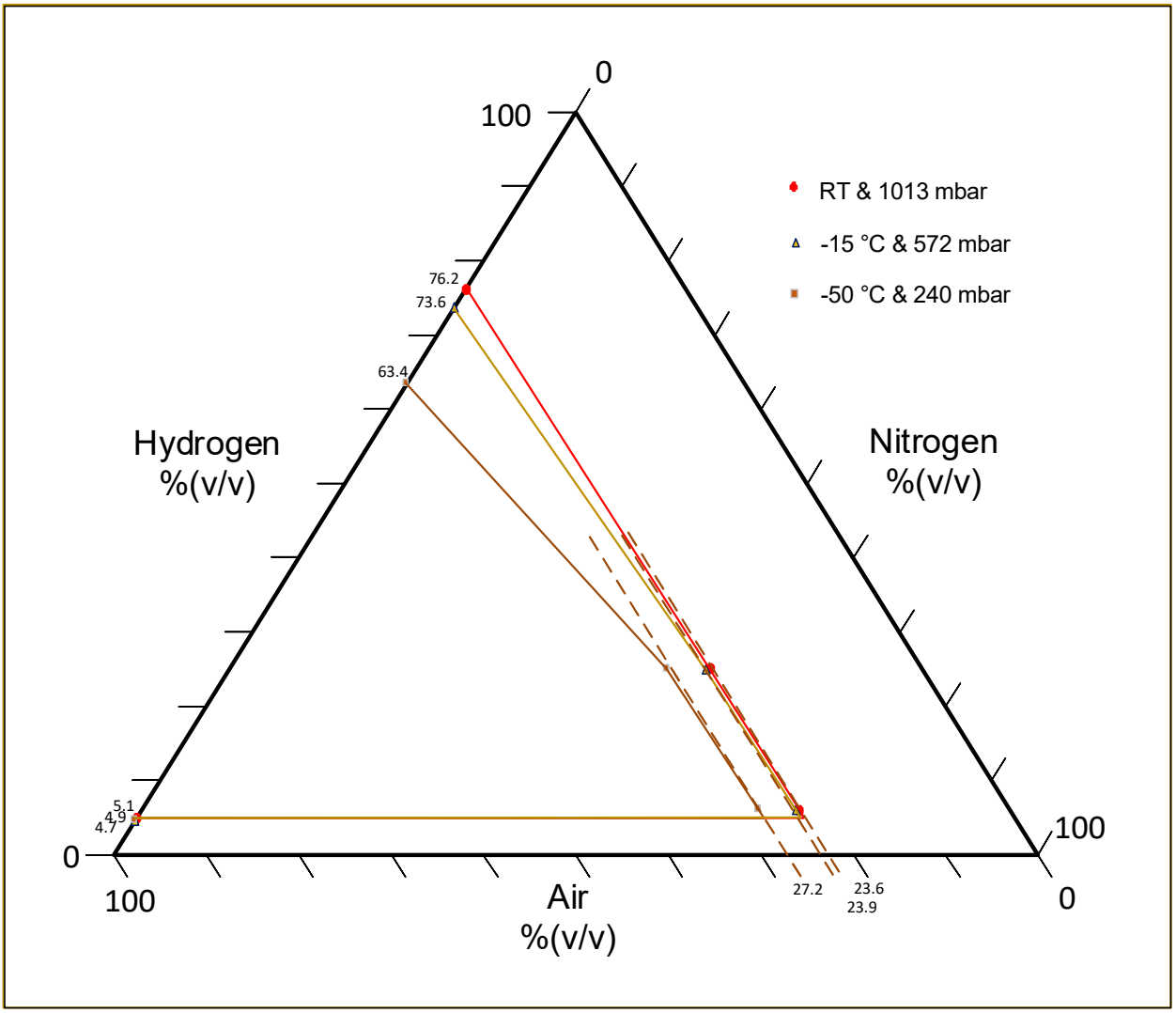

Figure 23 Triangular flammability limit plot for simulated altitude (sea level (RT & 1 atm), 15k ft (-15°C & 572 mbara) & 35k ft (-50°C & 240 mbara).

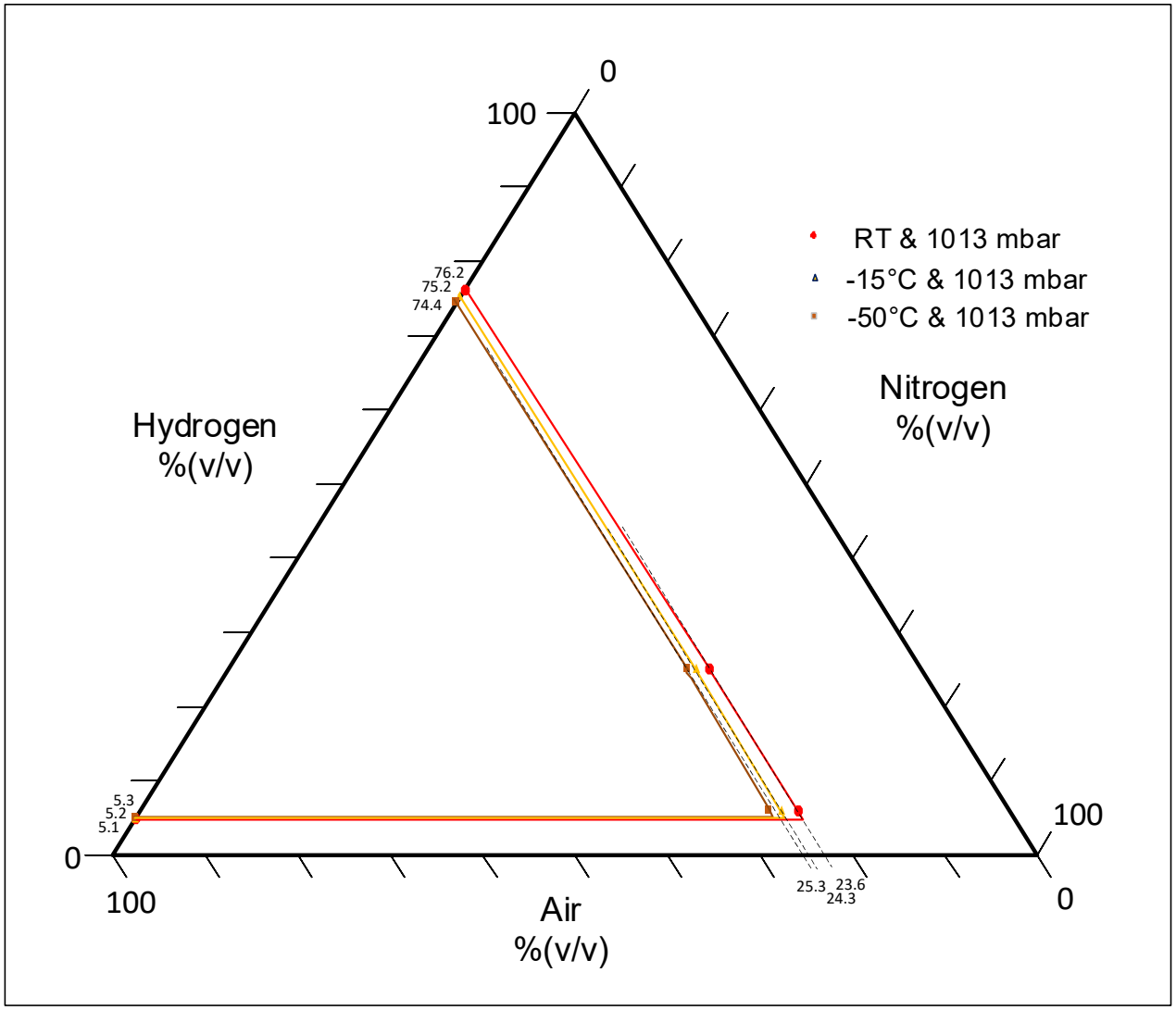

Figure 24 Triangular flammability limit plot for1013 mbara at ambient, -15°C & -50°C.

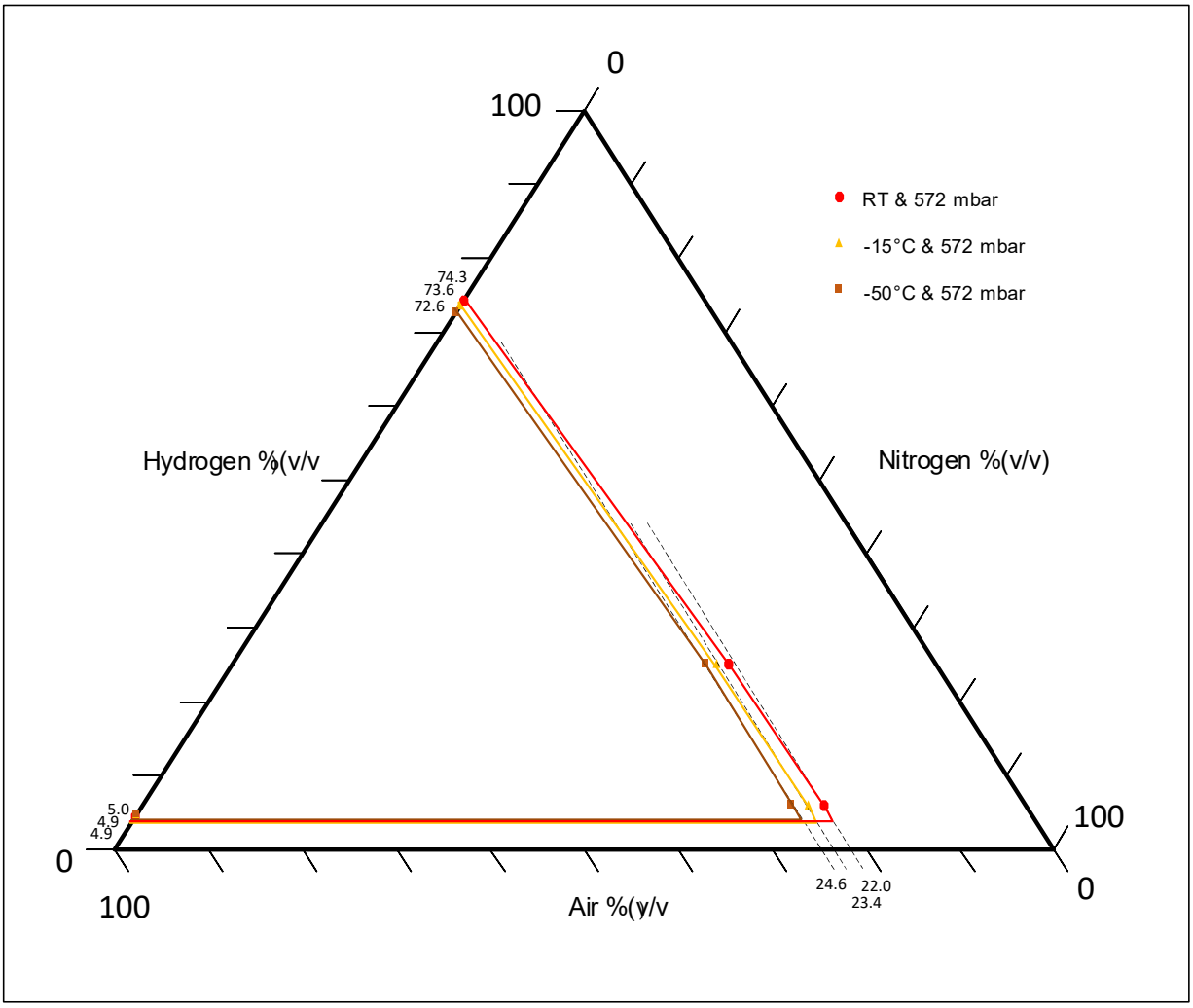

Figure 25 Triangular flammability limit plot for 572 mbar at ambient, -15°C & -50°C.

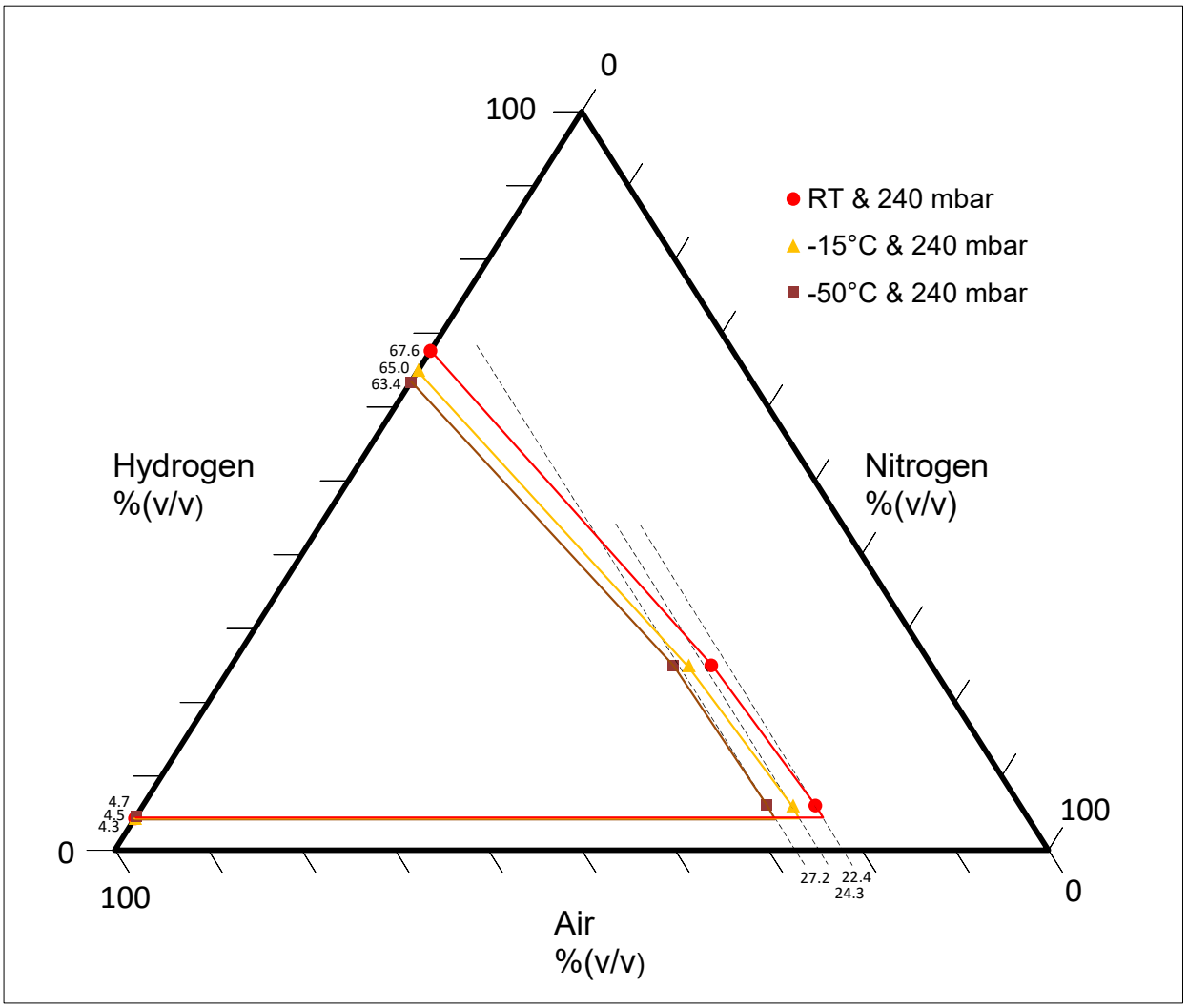

Figure 26 Triangular flammability limit plot for 240 mbara at ambient, -15°C & -50°C.

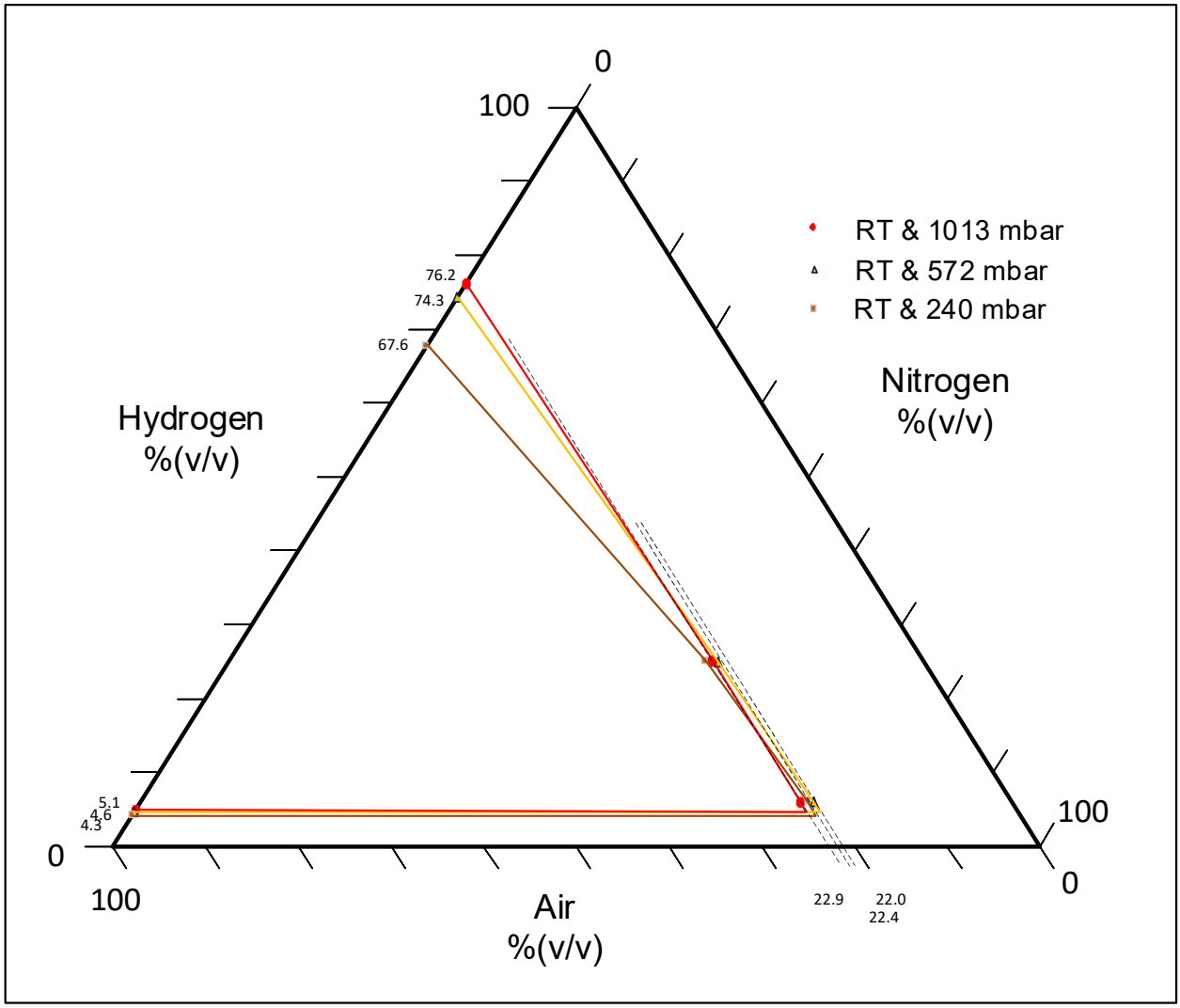

Figure 27 Triangular flammability limit plot for ambient temperature at 1013, 572 and 240 mbara.

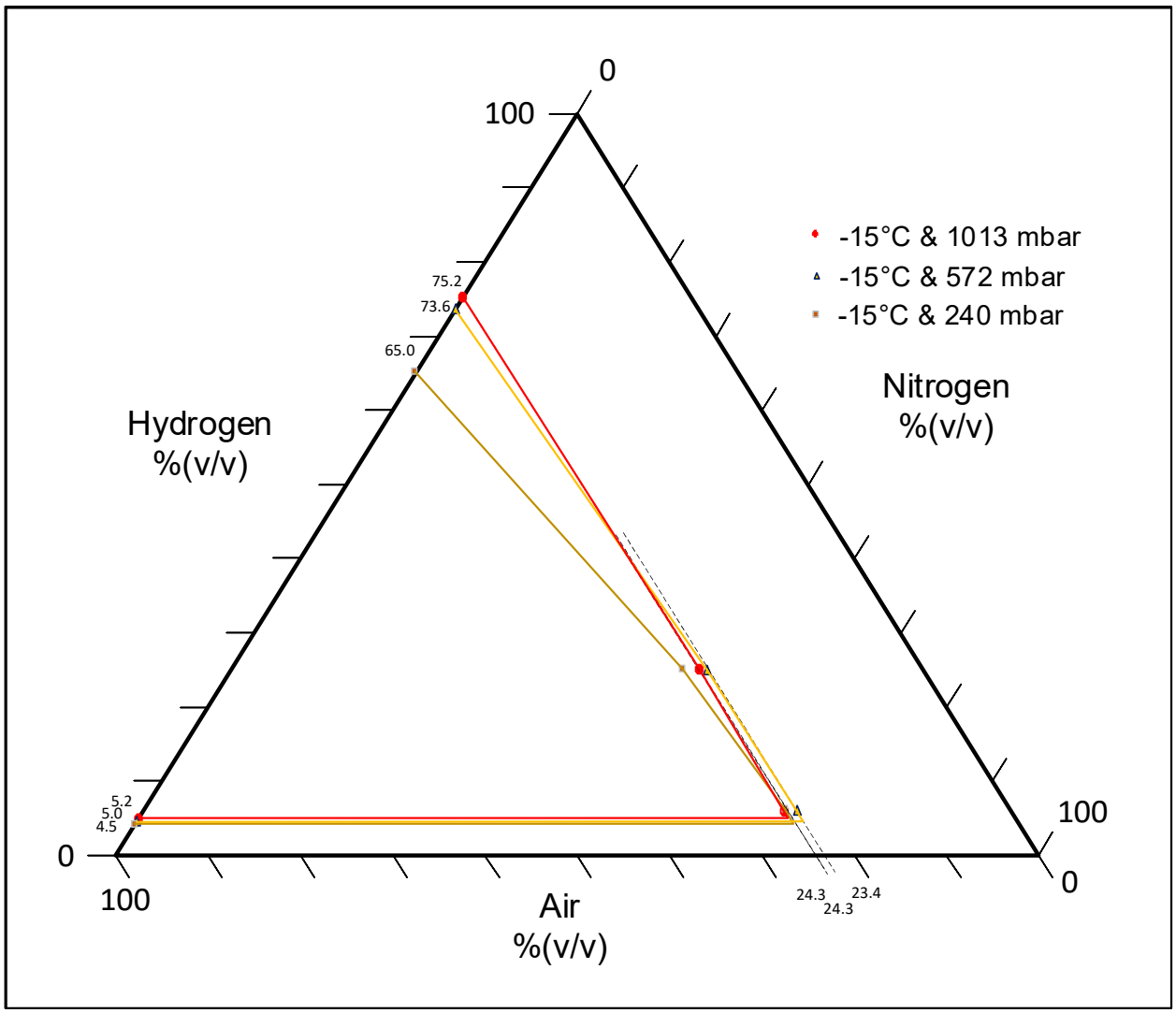

Figure 28 Triangular flammability limit plot for -15°C at 1013, 572 and 240 mbara.

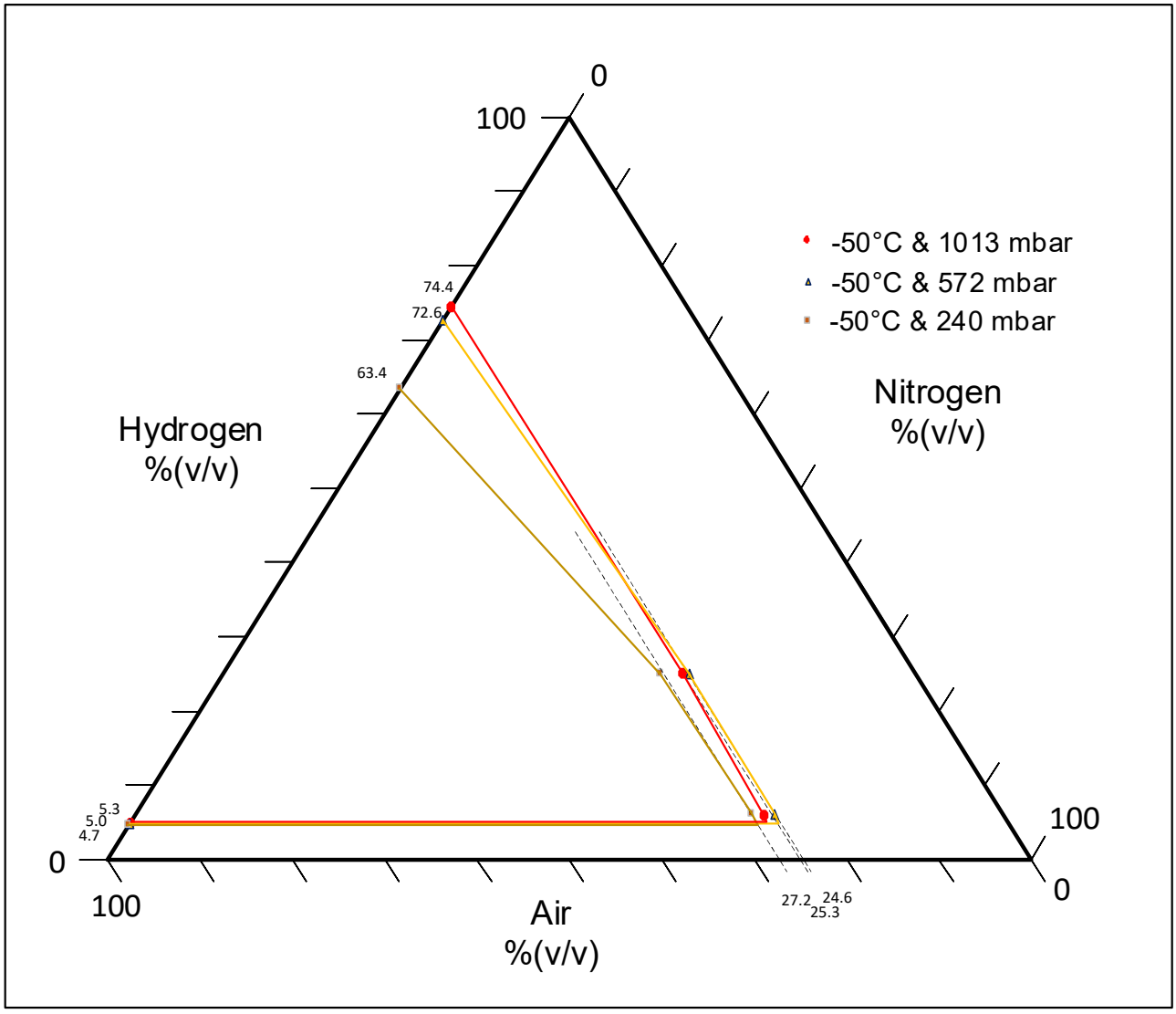

Figure 29 Triangular flammability limit plot for -50°C at 1013, 572 and 240 mbara.

3.4. Discussion of combustion parameter testing results

3.4.1. Flammability limits

As discussed in section 2.1. previous studies have looked at the effect of temperature on flammability limits or the effect of pressure on flammability limits but not the combined effect. The value for the LFL at ambient temperature and 1 atm (5.1%(v/v)) is comparable to the values obtained for other bomb type testing apparatus. For reasons noted earlier this is higher than the normally quoted value of 4%(v/v) determined in flame tube apparatus, but this is expected. The magnitude of the decrease (0.75 % (v/v)) from 1013 to 240 mbara at ambient temperature compares very closely with that obtained by Rehn [chapter 2, reference 10]. Similarly, the magnitude of the increase in LFL with decreasing temperature, for mixtures initially at atmospheric pressure, 0.3%(v/v) is consistent with that predicted from Equation 1. At 572 mbara it has decreased slightly to around 0.2%(v/v), however at 240 mbara the temperature seems to be having a slightly more significant effect at around 0.4 %(v/v). Overall the effect of combined temperature and pressure on the LFL has not revealed anything particularly significant and in practical terms, given that both the effect of pressure and temperature are weak) the sum of the individual effects of temperature and pressure gives a reasonable estimate of the total effect, down to the initial pressures studied.

However, as indicated by the results presented in Reference 11 (chapter 2), at a sufficiently low pressure the LFL stops decreasing and starts to rapidly increase and by around 100 mbara (with a spark igniter at atmospheric pressure) all mixture compositions were non-flammable. Since the effect of temperature is to raise the LFL (and decrease the UFL), it would be expected that the onset of the narrowing and the pressure limit would also increase. A pressure of 240 mbara would appear from Reference 11 (chapter 2) to be around the very start of the narrowing. If temperature were decreased below -50°C at 240 mbar it is possible that a point would be reached where the limit would rapidly increase. This is possibly worth further exploration, as much lower flammable mixture temperatures might be attained in the event of a large LH2 leak. This is illustrated by below comparing the LSBU and Kuznetsov data. It should be noted that the Kuznetsov lines are estimated from markers relating to individual ignition tests whereas the LSBU values are derived from a series of tests as described above. It is possible the Kuznetsov work lacked the resolution to detect the decrease in the LFL.

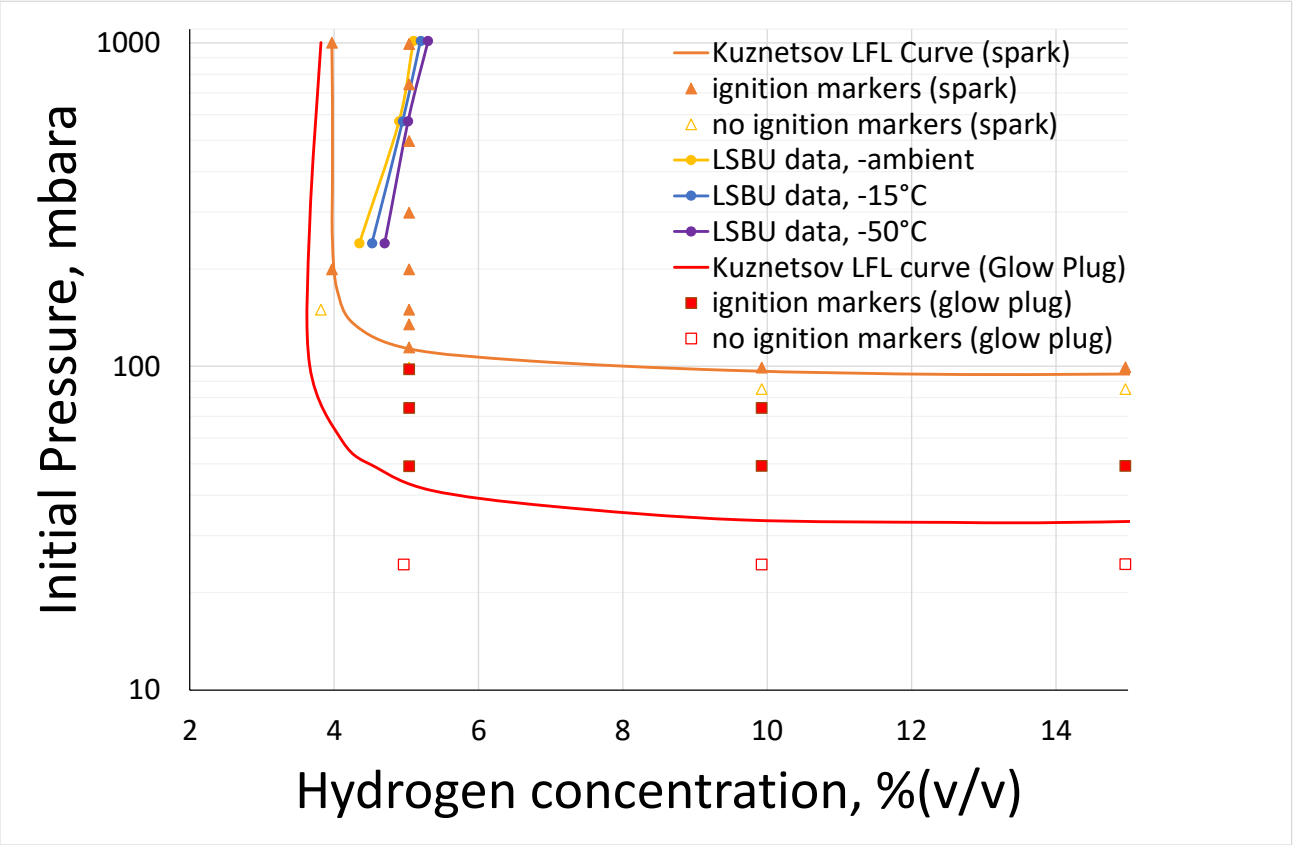

Figure 30 Comparison of LSBU and Kuznetsov data near the LFL

Another interesting feature of the Kuznetsov study is the effect of using a glow plug vs spark igniter. This possibly reflects mixtures at low pressure requiring more energy for ignition.

In practical terms, the effect of altitudes up to the cruise altitudes of current jet aircraft for civil aviation is clearly going to be small. The slight reduction is in any case partially offset as the gas temperatures into which a release occurs will typically be lower and in the case of a liquid hydrogen release the gas vapour mixing with air will also reduce the temperature. Additionally, due to the weak burning nature of near LFL mixtures (i.e. a relatively large margin between just flammable and a mixture capable of causing significant overpressure) there is in reality unlikely to be significant benefit/need to apply a correction and a pragmatic approach would be to simply use the commonly accepted value of 4%(v/v) at RTP to cover all conditions down to 200 mbara and -50°C. The magnitude of the variation is in any case actually less than the variation between types of testing apparatus (i.e. flame tube vs bomb).

The UFL varies a lot more significantly with pressure than the LFL, but the situation is further complicated by sensitivity to the energy and possibly the nature of the ignition source. Figure 31 below show a comparison of the UFL data obtained by LSBU, Kuznetsov and Rehn. With a

spark ignition source, it can be seen that there is very good agreement between the data obtained by Kuznetsov and LSBU at ambient conditions with a UFL of around 76%(v/v) at 1 atm that then decreases quite rapidly as the pressure is decreased. However, the tests by Rehn indicate both a higher UFL at atmospheric conditions (78%(v/v)) and then as the pressure is decreased to 571 mbara the UFL increases further to around 79%(v/v). As the pressure is further reduced the LFL decreases. In his report Rehn suggests the reduction could be due to an insufficiently energetic ignition source that is responsible for the sudden step change in the pressure rise. i.e. if we consider Figure 17a, for example, it is suggested that increased ignition source strength would in effect extrapolate the pressure rise such that it would approach the hydrogen axis at higher concentrations (thus producing a higher UFL), avoiding the 'cliff edge'. Considering the Kuznetsov glow plug igniter data the UFL at 1 atm would seem to be possibly a little lower than that obtained by Rehn, and as the initial pressure is decreased, the UFL again increases. At an initial pressure of 200 mbara the UFL is now slightly higher than that obtained by Rehn suggesting that the glow plug has become a relatively stronger ignition source at the reduced pressure.

This is potentially an area worth further investigation. While at atmospheric pressure the difference between the results is less than 5%(v/v), at an initial pressure of 200 mbara this has increased to over 10%(v/v). From a pessimistic or bounding safety case perspective the higher values would be adopted, though the question remains as to how energetic an ignition source would be required. This could be explored using LSBU's high power capacitive discharge igniter that would allow the spark energy to be readily varied, but would impart energy to the gas mixture over a shorter timescale. As discussed in 3.1.6. Apparatus for Flammability Limit Testing the energy dissipated by the arcing is in any case less at reduced pressures (although gas density is reduced) which might be a factor in the apparent need for higher power ignition sources at reduced pressure.

There is then also the question of how energetic an ignition source could actually be present. Even without ignition source control high voltage arcs probably wouldn't be routinely present so there could be scenarios where a lower limit might be appropriate or a much lower probability of ignition justifiable.

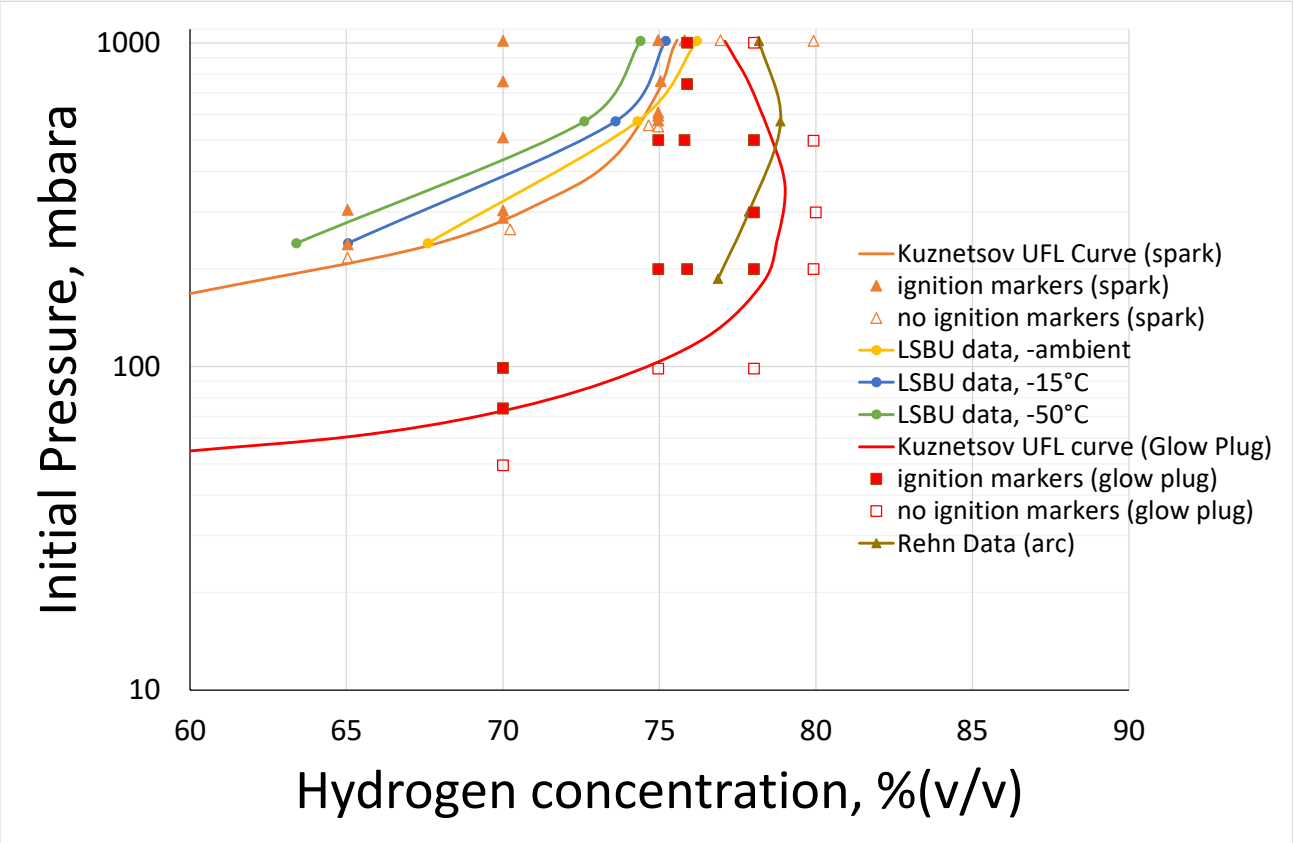

Figure 31 Comparison of LSBU, Rehn (FAA) and Kuznetsov data near the UFL

A key aim of this study is to investigate the combined effect of reduced pressure and temperature. As can be seen from Figure 19 the effect of lowering temperature is to narrow the flammable range, decreasing the UFL. The rate of decrease with temperature is linear. At 1013 mbara initial pressure that rate of decrease (0.0257%°C) is very similar to that observed by Wiezba [chapter 2, ref. 6] (0.0250%/°C), amounting to a 1.8% reduction from ambient to -50°C. The rate of decrease is roughly half of that predicted by Wheelers correlation (Equation 2). A similar rate of decrease is observed at 572 mbara initial pressure. However, at 240 mbara the effect of temperature on the UFL appears to be greater at 0.06 %/°C which is slightly greater than the rate of decrease predicted from Equation 2. This amounts to a decrease of 4.2%(v/v) from ambient to -50°C. Looking at Figure 31 it seems likely that the larger rate of decrease reflects the transition from the mixture being limited by concentration (oxygen concentration since H_2 is in excess) to being limited by initial pressure, thus maintaining a fairly consistent margin on the UFL curve obtained by Kuznetsov for a spark igniter. Had a more energetic igniter been used it is questionable whether the increase in the rate of decrease would have been observed.

Given the potential for a sudden transition from negligible to pressures of several bara over fractions of a percent change in hydrogen concentration, it would be prudent to use the lower rate of decrease with temperature, unless the potential ignition source is well characterised.

The effect of pressure on the LOC also appears complex. As can be seen from Figure 20 the 'cliff edge' jump in pressure rise is also observed for all tests with 25% H_2 and the tests with 6% H_2 at 240 mbara initial pressure. It can be seen from Figure 32 below that, in common with the Rehn data [ch.2, ref. 10] a reduction in the initial pressure initially decreases the LOC (widening the flammable range), the rate of decrease is similar for the two datasets. However, below 572 mbara initial pressure the LSBU data starts to show an increase in the LOC whereas the Rehn data continues to decrease. This behaviour is also likely explained by the effectiveness of the ignition source. Both the UFL and LOC are oxygen limited condition. However, at the LOC a substantial fraction of the hydrogen has been replaced with nitrogen. The ignition process (particularly near limits) will not be adiabatic and heat will be lost to the surrounding cool gas. For ignition to occur the heat generated by combustion (exponential with temperature) needs to exceed the losses (linear) at which point runaway occurs. The thermal properties of hydrogen, e.g. thermal diffusivity, (relative to nitrogen) will enhance the heat loss from the initial flame kernel making ignition more difficult at the UFL. Additionally, as noted in section "3.1.6. Apparatus for Flammability Limit Testing", high hydrogen concentrations reduced the power dissipated by the igniter arc.

The value of the LOC for hydrogen at RTP is typically quoted as 5%(v/v), which is in agreement with the LSBU data and a little higher than the Rehn data. Again, as with the UFL a cautionary approach may be advisable assuming that the LOC will continue to decrease with pressure below 572 mbara unless the potential ignition source is well characterised. Lowering the temperature consistently raises the LOC by around 0.5%(v/v) between ambient and -50°C (0.007 to 0.008 %/°C) for tests at 1013 and 572 mbara. At 240 mbara a larger difference is observed but this is again is likely due to a transition from a concentration limit to a pressure limit, as seemed to be the case for the UFL. Considering the typical atmospheric temperatures associated with a given altitude it can be seen from Figure 32 that the temperature effect is of sufficient magnitude to almost entirely cancel the decrease in the LOC due to reduced pressure (noting that the greater effect at 240 mbara is probably down to ignition energy).

The effect of reduced atmospheric pressures and typical atmospheric temperature on the overall flammable range, as measured in the LSBU apparatus, is shown in Figure 23. It can be seen that the effect on the LFL is almost negligible amounting to less than 0.5%(v/v).

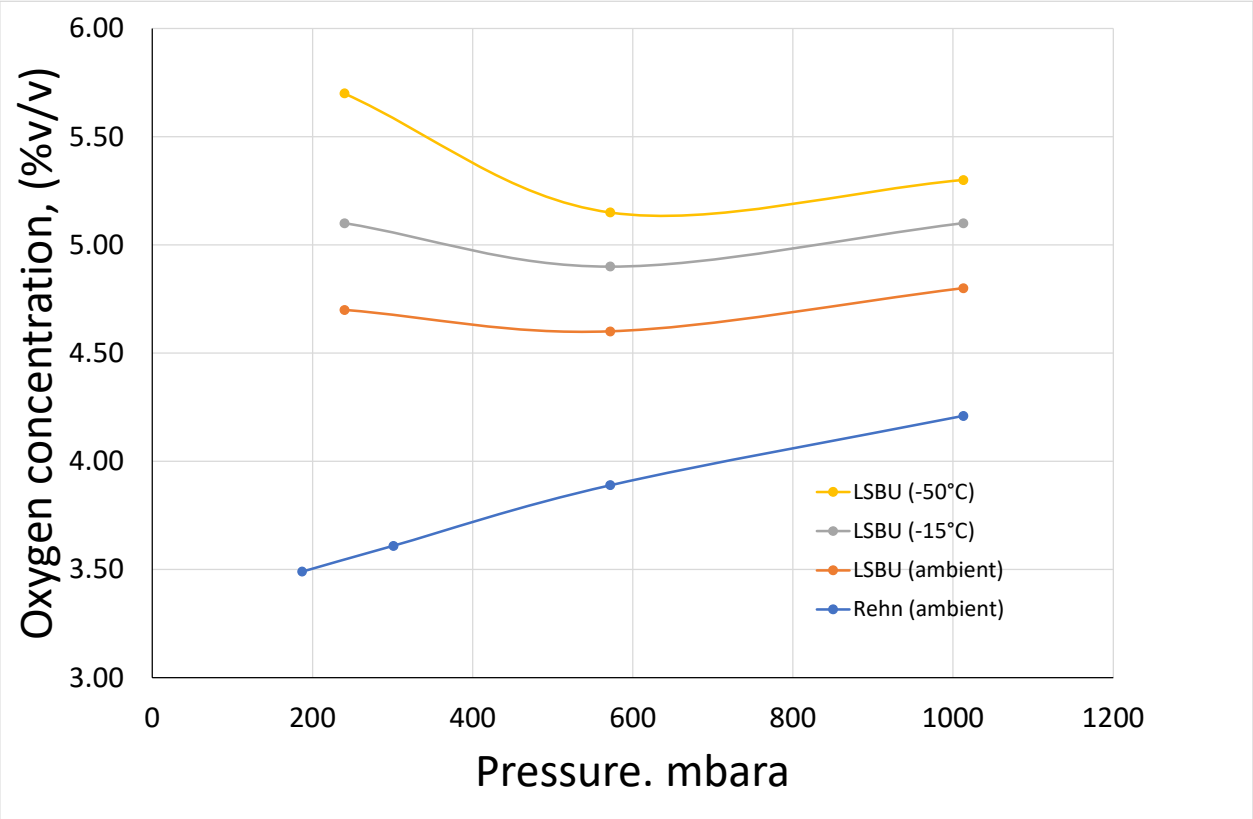

Figure 32 Comparison of LSBU and Rehn [FAA] LOC data

4. Review of hydrogen detection and visualisation

4.1. Introduction

The presence of hydrogen is a potential hazard in many aviation processes and operations. Unless a surrounding enclosure is inerted, whenever a release of hydrogen occurs there is a potential to form a flammable atmosphere. It is necessary to know the extent of a flammable area formed to be able to assess any hazard to airport/ aircraft operation and those nearby. It is also necessary for hazardous zoning in compliance with DSEAR.

The hazards posed from the formation of a flammable atmosphere must be assessed in many different scenarios, including large scale production and storage of hydrogen gas, liquefaction and largescale storage of cryogenic liquid hydrogen, aircraft refuelling activities, airport processes at, and leaks from on-board systems. A range of different hydrogen detection systems will likely be needed for these varied contexts.

The aim of this chapter is to examine the state-of-the-art in relation to hydrogen sensing and visualisation, reviewing techniques that can give a rapid (i.e., essentially real time) indication of hydrogen dispersion and, therefore, the possibility of the formation of a flammable atmosphere. This report details the various technologies available, their advantages and disadvantages however the operating conditions, accuracy and sensitivity of each individual sensor vary from manufacturer to manufacturer.

4.1.1 Environmental conditions

One of the most challenging aspects for sensors and other equipment operating on aircraft is the wide range of pressures and temperatures required. Parts of the aircraft outside the pressurised main fuselage compartment will be subject to very low pressures at altitude (approx. 23 kPa). Aircraft specifications from the FAA and EASA require that some equipment be able to withstand a temperature range of about -55°C to 70°C due to varied nature of airports and the conditions at altitude. The Department of energy has specified target working conditions for sensors for use in the hydrogen economy. This includes temperature ranges for safety and fuel cells systems of -30 to 80 °C and -70 to 150 °C, respectively [1] matching the requirements for many aircraft, but a pressure range of 80-110 kPa, which is well below that required at altitude. At present multiple sensors will be required to cover the widest reaches of these ranges. The sensors would also have to be exceptionally robust to handle the regular turbulence, and take-off/landing conditions that aircraft are subject to.

The widest published review of available sensors [2] does not specify the majority of working temperatures, and many manufacturers do not state this on their websites or in technical information. Thus, although in the following sections example temperatures of operation are given, based on available information from manufacturers, these may not represent the entire class.

4.2. Design and operation of hydrogen measurement instrumentation/apparatus

Generally, a detection system/apparatus, from the smallest handheld instruments to large distributed fixed systems, will be comprised of the elements as detailed in the diagram below. All the components on the diagram taken together describe the “system (or apparatus)” and (in some cases) the sample preparation, the detector, electronics and readout taken collectively are usually referred to as the “instrumentation (or equipment).”

Starting with the sample collection system, if it is unable to deliver a representative sample of the atmosphere to the detector the results will be inaccurate no matter how accurate the detector is. Where detectors are mounted in-situ they are often designed so that transfer of gases to the detector is limited by diffusion through a membrane or metal sinter and, other than blockage, sampling problems are unlikely to occur. In contrast the use of sample lines can present several problems which should not be underestimated. It may be necessary to return the gases to the vessel after analysis, the sampling system may have to integrate with existing ventilation pipework or sampling lines and in many cases instrument response will be sensitive to sample pressure, temperature etc. Sensitivity to sample pressure, temperature etc. might be overcome by sample conditioning or by the use of a correction factors but there is still plenty scope for sample to be lost through leakage or diluted by in-leakage. Additionally, long sampling lines can introduce significant time delays between initial sampling and detection. Factors affecting the ideal location of sampling points or in-situ detectors are likely to be similar but physical limitations could be different.

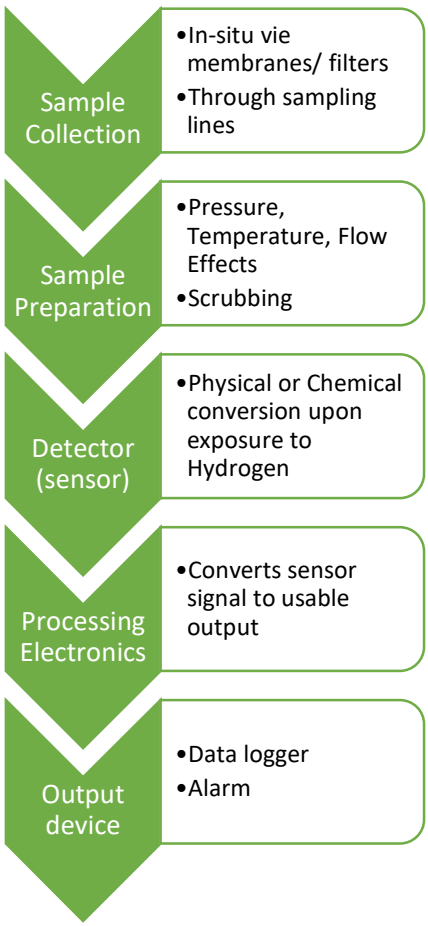

Figure 33 Schematic of a hydrogen measurement system

Almost all systems incorporate some sample conditioning/sample preparation. With portable instruments this might be limited to a filter or membrane incorporated into the detector itself. For larger/fixed installations it might consist of a separate unit, capable of removing compounds to which the detector is cross sensitive or it could be damaged/poisoned/contaminated by and supplying the sample to the detector at the required temperature, pressure and flow rate. The sample conditioning required will mainly depend on the atmosphere being sampled (composition, plant conditions – temp, humidity, etc), the type of detector and the required accuracy (i.e., is the effect of pressure changes, cross sensitive compounds etc. significant). For example, variation in say, sample gas temperature of a few degrees would be unlikely to be significant if using a thermal conductivity detector to measure concentrations to an accuracy of +/- a few %(v/v). However, if trying to measure down to a few hundred ppm the required accuracy is very much greater (i.e. quoting a reading of 300+/-30,000ppm is of limited use) and sampling conditioning (as well as the instrument) would need to be exceptionally good. In addition to possible effects on instrument response sample conditioning to remove poisons/contaminants might be justified in terms of extending detector life which should be as long as possible (to reduce waste & dose uptake).

The detector produces an electrical signal as a result of chemical reaction and/or physical changes in proportion to the concentration of hydrogen to which it is exposed. Types of detector are detailed in the next section. There are advantages and disadvantages to each technique, and there is no universal off the shelf solution. Detectors may measure in ppm or LFL %(v/v) concentrations depending on the context, but it is possible there will be situations where two types of detectors (or instruments) will be required. In addition, many detectors capable of measuring low levels are adversely affected by exposure to high concentration (e.g. physical damage, long time for reading to return to normal levels once exposure to high conc. has stopped, zero offset, etc.), it might be necessary to incorporate measures in the design to protect the lower range detector from high concentrations. Statements made by manufactures for the performance of their products, under idealised laboratory conditions, should be subjected to scrutiny for use in more industrial environments.

Hydrogen instrumentation performs some form of safety function (i.e. used trigger trips or alarms). This raises a number of addition questions/criteria. There can be difficulties in achieving the required Safety Integrity Level (SIL) (particularly if instrumentation is microprocessor controlled). It may occasionally be preferable to use two similar systems rather than two diverse systems if it meant using a system that was poorly suited to the task. There may also be a need to perform FMEA analysis, which may in effect prohibit the use of new and novel technologies. Detectors/instruments ideally need to fail safe and give an indication that they are approaching the end of their life. A detector that could fail to an unsafe condition with no-prior warning would not be suitable for use in a safety instrument. Lastly detectors/instruments/systems will require periodic testing and periodic calibration to demonstrate performance which is unlikely to be straight forward. In-situ detectors may require removal. Where sampling systems are used it may be straightforward to test/calibrate the instrument but this would not detect any faults with the sampling system itself.

An ideal flow visualisation system will not just allow the flow of gases to be visualised but also give quantitative information regarding the hydrogen concentration. This is made more difficult in the case of hydrogen, as hydrogen does not itself absorb radiation in the UV, Visible or IR spectrum, which is a problem for hydrogen detection in general. Many wide area flammable gas detectors for instance make use of IR absorption and can monitor a relatively large area compared to existing detectors for hydrogen which are essentially point measurements. Absorption in the IR region is associated with vibrational and rotation transitions. Unfortunately hydrogen is a simple diatomic molecule with no permanent dipole moment (unless distorted in an electric field) and does not therefore absorb infra-red radiation. UV/Visible spectroscopy is also not directly applicable as the principal electronic transitions occur in the vacuum ultraviolet region which coincides with absorption of UV by air.

Because of these issues the most recent system being explored, the HyWAM system [3] , is an array of point sensors, and it is highly likely that any system for an external location will need to follow this format.

4.3. Hydrogen detection and measurement technologies

With the development of the hydrogen economy powering buildings and vehicles, and from spin offs of space programmes, there has been significant and ongoing research into hydrogen detectors. This section is divided into two parts, firstly covering the commercially available and commonly used sensors, and secondly covering more recent developments and sensor types that are not yet widely commercialised.

The typical specifications given for the various types of detectors/instruments are for rough guidance only. It should be noted that the measurement range simply defines the concentration range over which it is designed to operate. It does not imply any degree of accuracy. No instrument is capable of measuring a concentration of zero (or any other value) with exactly 100% accuracy.

4.3.1 Catalytic flammable gas detectors.

These are the most common type of flammable gas detector, and one of the most popular types available for hydrogen sensing. They are used in portable flammable gas detectors and have also been used in fixed monitoring systems. These types of devices have been available for many decades, with the original developed by Oliver W. Johnson in 1927. The technique was refined resulting in the development of pellistors which consist of a small bead of catalyst (usually palladium) encapsulating a platinum wire filament. Current is passed through the filament causing it to reach the required temperature for mass transfer limited oxidation of the flammable gas to occur (around 450-550°C).

The detectors are mounted so that the rate of oxidation is limited by diffusion to the surface of the catalyst. When the detector is exposed to flammable gas the temperature increases which causes an increase in the electrical resistance of the filament. The change in resistance (normally a matched non-catalytically active sensor is used as a reference) is utilised to give an instrument output, usually in %LFL. Traditionally sensors have been mounted in a Wheatstone bridge circuit as shown below.

Fixed systems detectors are usually mounted inside a flameproof enclosure (see explosion protection requirements below) incorporating a metal sinter through which gases can diffuse. Portable instruments sometimes incorporate a small pump to draw gas through the flameproof enclosure (again with metal sinters used as flame arresters).

Indicative Specifications:

Measurement Range	0 to 100% LFL
Resolution	1% LFL
Accuracy	+/- 3 % to +/- 5 % depending on %LFL range [4]
Temperature range	These vary dramatically but can be -55°C to 125°C [5]
Expected life	2 – 3 years
Response time	T_{90} typically of the order of 20-50s [4], [6]
Possible poisons	Hydrogen sulphide, Halogenated hydrocarbons, heavy metals, gases containing silicone, sulphur or polymerisable substances. Depending on the poison and pellistor concerned response could be significantly reduced by ppm levels of poisons in a few hours.

Figure 34 Example of a wheatstone bridge circuit

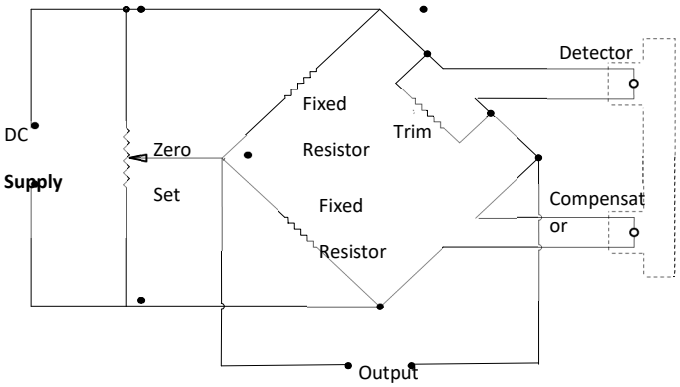

Figure 35 Example sensor mounting arrangements

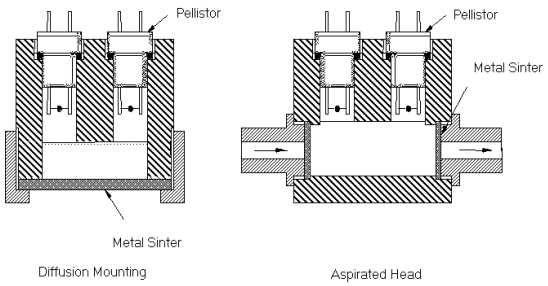

Disadvantages

- Require regular testing and maintenance to ensure reliability.
- Can become poisoned by a variety of species, particularly silicone oils.
- The lifetime of detectors is typically a couple of years.
- No easy means of determining detector poisoning, other than re-calibration
- Can only be used under conditions where there is >10% oxygen present.
- Typically response is limited to the LFL range (0 to 4% (v/v) although it is possible to increase sensitivity (for operation in the ppm range) by variation of the pellistor design.
- Cannot be used for measurement of concentrations exceeding stoichiometric (insufficient oxygen for complete combustion) unless some form of air dilution is used.
- In some cases exposure to high concentrations (above the LFL) can cause the pellistor to become so hot that it becomes cracked or damaged or loses sensitivity due vaporisation of the catalyst.

Advantages

- This type of detector is that it will respond to any flammable gases present (though there is a fall-off in response (per %LFL) as the molecular weight of the flammable species increases (the effect is largely that of the reduction in diffusivity of the flammable species as the molecular weight increases) [7]. The heat of combustion per %LEL is approximately constant for most fuels, hydrogen being an exception. There is therefore a fundamental link between the instrument response and flammability. Although, unless the exact composition of the flammable component of a sample is known, the %LFL reading is unlikely to be accurate, it is sufficient to detect low levels of any flammable gas mixture and indicate that the %LFL lies within a particular range (i.e. if the instrument was to read 5% LFL, for most pellistors, you would know that the true %LFL would be between 1 and 25%).

4.3.2. Electrochemical detectors

These types of detectors measure electrical current flow through an electrolyte exposed to the sample gas (usually via a gas permeable membrane), as described below. Increases in ambient temperature significantly increase the response (i.e. drift). They also exhibit significant cross sensitivity to other gases. For these detectors to function correctly a small amount of oxygen in the atmosphere is normally required. A typical design of electrochemical detector is given the figure below. Other designs sometimes utilise only two electrodes (i.e. no reference electrode).

Indicative Specification

Range Typically 0-2000 ppm (0 to 0.2%(v/v), however up to 20,000ppm readily available. [2]

Temperature range N/A

Lifetime 1 to 3 years. (very dependant on hydrogen levels)

Response time T_{90}: Wide range from 20 – 90 s

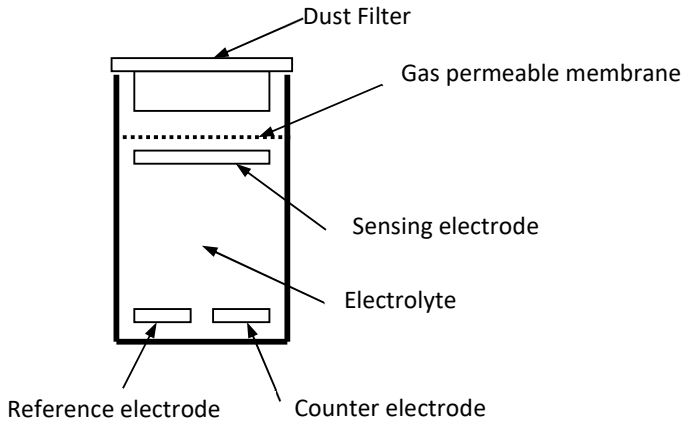

Ambient air diffuses through the permeable membrane into the electrolyte. A potentiostat circuit maintains a constant voltage between the reference and sensing electrode. Hydrogen from the ambient air is oxidised at the sensing electrode ($H_2 \rightarrow 2H^+ + 2e^-$) to form hydrogen ions whilst at the same time the reaction on the counter electrode balances the reaction by reducing oxygen from the ambient air to water ($1/2O_2 + 2H^+ + 2e^- \rightarrow H_2O$). The flow of electrons (current) produced by the reaction gives a measure of the hydrogen concentration.

Figure 36 Typical electrochemical hydrogen detector

Advantages

- Capable of detection of ppm levels.
- Compact.
- Require little power.
- Good linearity and repeatability.

Disadvantages

- Relatively short detector lifetime (compared to say thermal conductivity detectors)
- Typically, significant cross sensitivity to many other compounds such as ethene, methanol, CO
- Require some oxygen to be present for operation
- Not suitable for measurement of high (%(v/v) range) concentrations.
- Exposure to high concentrations will cause saturation of the detector. Sensor can be slow to recover. May suffer irreversible effects e.g. failure to return to zero or change in sensitivity.

4.3.3. Thermal conductivity (TC) detectors

These detectors operate by comparing the thermal conductivity of the sample gas with that of a reference gas (usually air). A heated sensor is mounted so that it is exposed to the sample gas whilst a matched reference sensor (also heated) is enclosed in a sealed compartment full of the reference gas. If the sample has a higher thermal conductivity than the reference gas, heat is lost from the exposed element and its temperature decreases, whilst if the thermal conductivity is lower than that of the reference, the sensor heats up. The temperature changes are normally monitored by electrical resistance changes in the sensing element (typically using a wheatstone bridge circuit similar to that used for pellistors described above). The technique is often used to measure hydrogen, helium, methane, neon or carbon dioxide. Thermal conductivity sensors are available for both fixed and portable instruments. The technique is not suitable for measuring extremely low (low ppm) levels of hydrogen. There is considerable variation in the design and performance of thermal conductivity detectors ranging from little more than a couple of matched filaments, as found in portable gas detectors, through to more sophisticated devices utilising for example silicon sensors. The correct operation of the devices relies upon thermal equilibrium being established in the sample (and reference) cells. Instruments may therefore be sensitive to changes in external and sample temperatures and depending on the accuracy required detectors are often thermostatically controlled. Sample conditioning is often required to remove other gases such as water vapour that would interfere with the response. Thermal conductivity detectors are particularly good for hydrogen measurement due to the large difference in thermal conductivity between hydrogen (0.18 W/mK at 300 K) and air/nitrogen (0.026 W/mK at 300 K) [8]. Table 4 shows thermal conductivities relative to air for common gases.

Indicative Specification:

Measurement range: Typically, 0 to 100%(v/v) (typical gas detectors) however there is wide variation with some sensors reading 0.5ppm, up to 2%- 50%.

Temperature range -40 to 95 °C [9]

Response Time T_{90}: 1.8-2 s [6]

Many dedicated analysers will have in-built temperature, flow, pressure control and good sample conditioning and will be largely unaffected by atmospheric conditions.

Advantages

- Ability to measure hydrogen concentrations in atmospheres without any oxygen present (for example where using nitrogen inerting; note the thermal conductivities of air and nitrogen are very similar). Both pellistor and electrochemical detectors require the presence of oxygen for operation and are thus not suitable.
- These detectors are reasonably cheap and are reported to have a fast response time and wide measurement range.
- High reliability (no chemicals to deplete, not subject to poisoning, no moving parts to wear out), long working lives and maintain calibration reasonably well.
- Maintenance limited to routine calibration and where required the servicing/replacement of any sample conditioning equipment (e.g. for removal of water vapour). They will often last an order of magnitude longer than other types of hydrogen detector.
- Unlike some of the other techniques e.g. electrochemical detectors or pellistors they can be used to measure hydrogen concentrations up to 100% (v/v).

Table 4 Thermal conductivities relative to air.

Gas	Thermal Conductivity	
	0°C	100°C
Air	1.00	1.00
Nitrogen	0.99	0.99
Oxygen	1.01	1.01
Carbon Monoxide	0.96	0.97
Carbon Dioxide	0.69	0.70
Methane	1.25	1.45
Ethane	0.75	0.90
Propane	0.58	0.70
Butane	0.55	0.66
Pentane	0.52	0.58
Hexane	0.45	0.58
Acetylene	0.77	0.85
Ethylene	0.68	0.78
Ammonia	0.90	1.06
Hydrogen	7.0	6.8
Helium	5.9	5.5
Argon	0.65	0.70
Neon	1.92	1.87
Water	0.66	0.74

Disadvantages

- Unlike pellistors, there is no fundamental link between the response and flammability
- The instrument response will be affected by the presence of other components such as water and carbon dioxide. Fortunately, the relative thermal conductivities of nitrogen and oxygen are similar and consequently the variation in response between hydrogen/air and hydrogen/nitrogen mixtures will be small.
- They can really only be used for binary mixtures, they would not be suitable for say a H_2/CO_2/Air mixture (unless the CO_2/Air ratio was fixed and used as the reference gas).
- Not suited to determining low (i.e. ppm levels).
- Will be cross sensitive to any other components in the sample gas i.e. if calibrated for H_2/Air (air a the reference gas) it will not give the correct reading for say a H_2/Air/Ar mixture. From Table 1 it can be seen that the addition of Argon would in fact result in a reduced response.

4.3.4. Resistive semi-conductor detectors

Broadly speaking these types of detector are based on changes in electronic conductivity induced by gas (i.e. hydrogen) on metal oxide semiconductors. A diagram of a semi-conductor detector is given below. The semiconducting material is heated to a few hundred degrees Celsius. When the semi-conducting (metal oxide) material is exposed to gases other than air, resistance changes can be detected across the two electrodes. These types of detectors may be used for detection of hydrogen over a range of concentrations. They are particularly sensitive to hydrogen and may be used to detect ppm levels. Unfortunately, other characteristics such as poor linearity of response, sensitivity to a wide range of other gases (i.e. poor selectivity), poor recovery of response after exposure to gases in excess of the measuring range, poor reproducibility between detector of the same type has restricted their use to apparatus for leak detection or alarm only apparatus. Variation in oxygen concentration, temperature and humidity also significantly affect the sensitivity of such devices. Poisoning is also an issue (similar compounds as those that affect pellistors). If such devices are to be used for hydrogen measurement/detection the gas samples composition must be known and advice sought from the detector manufacturers. They are however reported to be useful where species such as chlorinated hydrocarbons or ammonia are present.

Indicative Specification

Range Typically 0-2000 ppm (0 to 0.2%(v/v), however up to 20,000ppm readily available. [2]

Temperature range -20 °C to 80 °C [1]

Lifetime 1 to 3 years. (very dependent on hydrogen levels)

Response time T_{90}: 2-16 s [6]

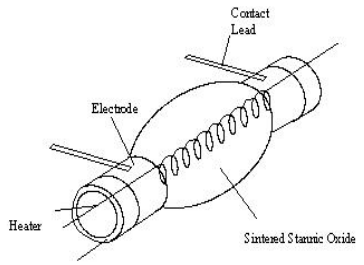

Figure 37 Typical semi-conductor detector

4.3.5. Resistive thin film hydrogen detectors

A significant amount of recent work has been directed towards various forms of solid-state detectors which promise low cost, reliable hydrogen detection. The commercially available solid-state detectors generally take the form of Pd/Ni thin film detectors. Further details on other varieties appear in the recent development section.

These sensors comprise a thin film of generally palladium-based alloy. Hydrogen dissociation is catalysed by the palladium and the hydrogen then adsorbs on to the surface of the metal, diffusing into the layer, and into interstitial sites. This changes the electrical and optical properties, increasing electron scattering and increasing the electrical resistance of the film. A phase change of palladium at high hydrogen concentrations is solved by alloying with Nickel [10] [11]. Thus, the sensors are generally Pd/Ni thin film based. However, other alloys and techniques are also being explored.

A great deal of research and development work is being done on Palladium-based thin film detection sensors. Elsevier's ScienceDirect site lists over 4000 papers from 2018-2021 with "Pd", "thin film" and "hydrogen" in the title. The EU H2Sense (2014) project produced a database [2] of sensors and list only one company supplying commercially available tests (then Applied Nanotech Inc, now H2Scan) and this appears to still be the only example commercially available. This appears to have been developed with Sandia National Laboratories. The sensor uses a lattice of Pd/Ni thin films.

Indicative Specification [1]

Range 0.1 to 4 %

Temperature range -15 °C to 50 °C

Lifetime 1 to 3 years. (very dependant on hydrogen levels)

Response time T_{90}: <60 s

Advantages

- Can cover a wide range from 0.5-100 vol%
- High reliability and ease of use as solid state and no moving parts.
- Intrinsically safe, meeting a number of ATEX, CE and UL certifications

Disadvantages

- Limited to use around 1 atm
- Poisoning of the sensor s possible (manufacturers claim sensor coating/ condition will protect from a certain level of CO and H2S)
- Subject to issues related to pressure fluctuations so can be paired with a pressure transducer

4.3.6. Schottky- Diode hydrogen detectors

These detectors were developed by the NASA Lewis Research Center in collaboration with Case Western Reserve University. The thrust of the program was to develop very sensitive gas detectors using Schottky diode detector structures. The detector developed is reported to be able to detect hydrogen concentrations from 1 to 4000 ppm (0.0001 to 0.4% (v/v)) which far exceeds the sensitivity of other commercial systems. It does not require an oxygen atmosphere for detection although the presence of oxygen may alter the response. A schematic of the detector is given below. Hydrogen dissociates on the surface of the metal and atomic hydrogen is absorbed into the metal and migrates to the interface between the metal and metal oxide. The resulting dipole layer alters the electronic properties of the diode which can be correlated to the amount of hydrogen in the environment. The complete detector package incorporates a temperature detector and heater in addition to the Schottky diode. The detector is maintained at a temperature of 80°C.

Schottky diode hydrogen detectors have been utilised to form an automated hydrogen gas leak detection system primarily to detect leaks in the main engine of the space shuttle whilst on the launch pad. The system was developed for the NASA Marshall Space Flight Centre by the Gencorp Aerojet Corporation and versions of the system have also been sold for automotive applications. A primary application of the instrument has been for the checking of pressurised systems for leaks. Given the sensitivity of the detector this can be accomplished using, for example, inert 1%H_2 in N_2 mixtures. The detectors are mounted inside a boot which can be placed over say a pipe fitting. When the system is pressurised the rate of increase in hydrogen concentration inside the boot can be converted to a leakage rate. A display gives an image of the boot with the plume of the leak, allowing the leak to be pinpointed.

Current NASA sensors reportedly combine a Schottky diode with a hydrogen sensitive resistor for detection of hydrogen from 0 – 100%. The sensors generally incorporate a silicon semiconductor. However silicon-carbide is also used to enable use in temperatures higher than

600 °C [12]. These sensors do not appear to be widely commercially available as yet and papers report sensor development at or well above room temperature.

Indicative Specification [1], [12]

Range 0-4.4%.

Temperature range Room temperature up to 600 °C

Response time T_{90}: <2 s for jump to 5%

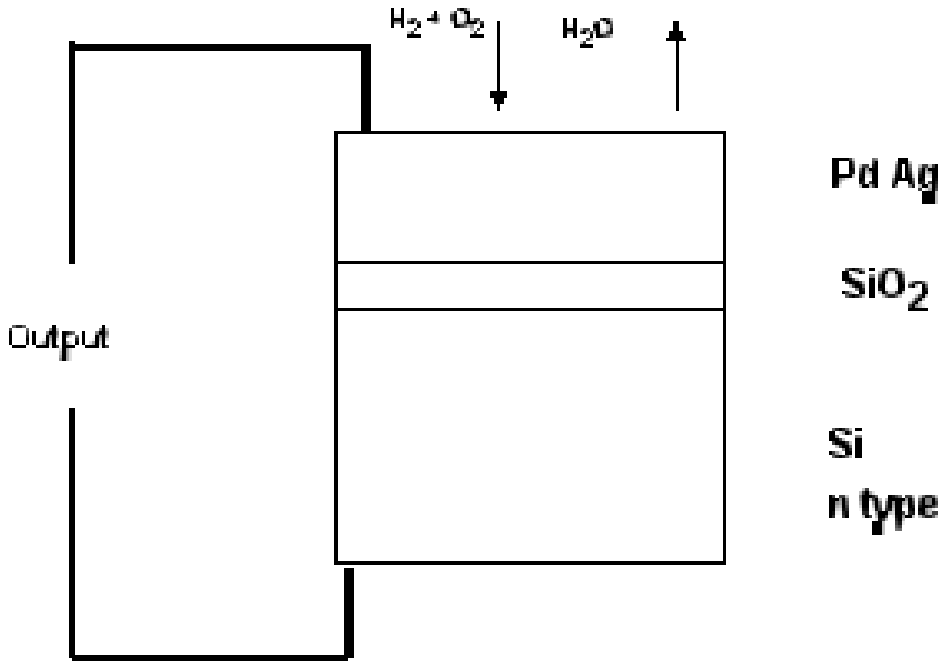

Figure 38 Pd-Ag Schottky diode hydrogen detectors

4.3.7. Sophisticated analytical instrumentation

Traditionally such techniques were laboratory based and required skilled technicians for operation. In recent years systems suitable for online process monitoring have been developed (e.g. vista II GC or Questor mass spectrometer from ABB) have been developed. Such instruments would however normally be considered too complex/expensive for hydrogen monitoring alone. For such instruments to be justifiable there would probably need to be a requirement to perform measurements of a number of gases that could not be accomplished satisfactorily with conventional gas analyser/detector technology or contained other gases that made the use of other techniques impractical. For example in principle mass spectrometry could facilitate the simultaneous monitoring of say H_2, HF and UF_6.

Mass spectrometers operate by first ionising the sample in a high vacuum chamber. The ionised atoms/molecules are then accelerated by an electric field and focused into an ion beam. The ion beam is then projected into a magnetic field causing the beam to scatter into different collectors according to their mass numbers. GC's essentially separate the components of the sample prior to being sent to a detector. If for example an atmosphere contained hydrogen, methane and CO_2 in air a GC with a TC detector could determine the amounts of each gas whereas it would be impossible to calibrate a TC detector alone for hydrogen in situations where there are gases (other than the reference gas) present in any quantity.

Obviously, such instruments will require extensive gas sampling systems and the number of gas streams each unit can handle is limited. Operating and maintenance cost will be relatively high and due to greater complexity are unlikely to be as reliable as say a simple TC detector. Cost can be shared however, by making the instrument sample many locations in sequence via a manifold of solenoid valves operated by a timer.

Very much depends on the specific application. GC based instruments will be capable of detection from ppm levels upwards. Mass spectrometry based instruments are often more sensitive with detection down to low ppb levels. On-line instruments are not usually able to differentiate between species of near identical atomic mass e.g. N_2 and CO (although the relative amounts of fragments of the molecules produced would give an indication).

4.3.8. Acoustic

Rather than detect hydrogen, these detectors identify if there are pressurized gas leaks from storage facilities. When high pressure containers are breached noise occurs at the point of leaking. The noise is not audible to the human ear, but may be detected using ultrasonic detection systems.

Advantages

These methods can be used for both pressurised and vacuum systems and there seems to be a good sensitivity, with identification of leaks occurring quickly and at relatively high distances up to 20m [13]

Disadvantages

These methods are incapable of identifying the size of the leak, and do not give readout in terms of a concentration. It is most appropriate in open areas and they can be affected by site noise. A baseline can be taken and removed. However changes in site noise may result in false positives.

4.3.9. Colorimetric (Draeger) Tubes

These are essentially tubes (ca. 5mm diameter 15cm) packed with a solid material containing reagents that change colour when exposed to a specific gas. A fixed volume of sample gas is drawn through the tube and the length of reagent that has changed colour can be related to the

amount of that gas in the sample. First produced, for carbon monoxide measurement, in the early nineteen hundreds, tubes are now available to detect a wide range of chemicals, including hydrogen.

Advantages

There is little to recommend them specifically for hydrogen in comparison to other flammable gas detectors. They can be useful devices since they can provide real time test results for a wide range of gases and can sometimes be useful in determining unknown contaminants. They are cheap and simple devices used mostly as one-time area clearance/entry tests.

Disadvantages

Cross sensitivity to other compounds and that they only provide a snapshot of the concentration at a single point in time. Some of the tubes available for hydrogen could potentially become hot enough to constitute a source of ignition.

4.3.10 Solid state hydrogen detectors

A significant amount of work in the past has been directed towards various forms of solid-state detectors which promise low cost, reliable hydrogen detection. For hydrogen detection these typically have a three-layer palladium (or alloy of), insulator, semi-conductor structure. Solid state detectors for hydrogen have been available for a number of years but do not appear to have been used extensively. Many solid-state hydrogen detectors take the form of Pd/Ni thin film detectors (described in the previous section), but also Schottky barriers, Metal Insulator Semiconductor Field Effect Transistors (MISFETs), and Metal Insulator Semiconductor capacitors (MIS CAPs). Solid State Fibre optic hydrogen detectors have also been developed. It appears thin film/ layer technology is being favoured for development.

[1] EIGA, SAFETY IN STORAGE, HANDLING AND DISTRIBUTION OF LIQUID HYDROGEN, DOC 06/02/E

4.3.11. Hydrogen visualisation techniques

Hydrogen is a transparent colourless gas, which doesn't fluoresce in the UV region. This makes it more difficult to visualise than most gases. Some methods have been developed in order to track the gas movement. However they often involve quite a significant system size and cost, or the use of seeded tracer gases. Table 2 below lists the methods currently available

Table 5 Summary of flow visualisation/imaging techniques

Methods of Visualisation	**Quality of flow field visualisation**	**Quantification of hydrogen concentration**	**Difficulty of technique**	**Availability of technology**	**Scale of use**	**Suitability for field used**
Acoustic leak detection	No visualisation, but can locate site of a release from pressure	None	Easy	readily available commercial instruments	any	Good
Distributed gas detection networks	Poor. Spatial resolution limited by number of sensors. Detection response is typically seconds so poor temporal resolution	Yes. Good, in so far as the hydrogen concentration can be accurately determined at the measurement points. Response time of detection system can be an issue for fast or transient releases.	Easy, with commercialised sensors	NREL developed HyWAM system is currently being tested (part of the EC PRESLHY project) [3]	any apart from very small scale	Good

Methods of Visualisation	Quality of flow field visualisation	Quantification of hydrogen concentration	Difficulty of technique	Availability of technology	Scale of use	Suitability for field used
Raman Scattering LIDAR	Poor/Fair. Instrument can potentially give an indication of the extent of a flammable plume by scanning over an area. Temporal resolution of transient/fast event is poor and concentrations in effect averaged over time. Turbulent flow/mixing detail not resolved.	Yes. Raman scattering is specific to hydrogen (i.e. no cross sensitivity issues). It is limited in that it is a line of sight integrating optical system.	Fairly complicated requiring laser, optics and beam scanner, but are co-located with the detector to form a single device. Final commercialised instrument might be relatively easy to use	Technique is being developed as a commercial instrument	Suitable for detecting hydrogen releases over tens of metres	Current research looks promising. Some concerns over power/use of lasers (safety)
Rayleigh scattering detection	Poor, essentially remote point measurement	Yes, but scattering signal is not hydrogen specific. Mie scattering by particulate could affect response. It is limited in that it is a	Fairly complicated	Custom built Laboratory technique	small	Probably poor due to Mie

Methods of Visualisation	Quality of flow field visualisation	Quantification of hydrogen concentration	Difficulty of technique	Availability of technology	Scale of use	Suitability for field used
		line of sight integrating optical system.				scattering etc.
Infra Red (IR) leak imaging	Poor/Fair. Instrument can potentially give an indication of the extent of a flammable plume by scanning over an area. Temporal resolution of transient/fast events is poor and concentrations in effect averaged over time. Turbulent flow/mixing detail not resolved.	Not directly, flow would need to be seeded with e.g. methane. With possible exception of DIAL (in some implementations) are a line of sight integrating optical system.	Varies. Can have sophisticated truck mounted DIAL systems or handheld portable BAGI or passive IR systems. Mostly fairly complex technology	A number of different systems available commercially	typically medium/large releases	Instruments mostly designed for field use.
Planar Laser Induced	Planar imaging techniques are	Not directly, flows need to be seeded.	High, Laboratory technique. Low	custom build, expensive	small. 100mm	very poor

Methods of Visualisation	**Quality of flow field visualisation**	**Quantification of hydrogen concentration**	**Difficulty of technique**	**Availability of technology**	**Scale of use**	**Suitability for field used**
fluorescence (PLIF)	quantitative and can offer excellent spatial temporal resolution of flow field concentrations. Often considered the best option for fluid mechanics research		signal to noise ratios can be a significant issue for many gaseous phase applications.	lasers/cameras/optics	high light sheets are typical	
Planar Rayleigh Scattering		Yes, no seeding required but studies reported in literature suggests Resolution down to LFL likely to be difficult				
Planar Raman scattering		In principle can give hydrogen specific response, but weak Raman scattering is likely to make impractical				
Planar Mie Scattering		Difficult to relate scattering by seeding particulate to hydrogen concentration.				
Shadowgraph	Reasonable temporal and spatial detail of flow field structure/mixing	Poor, techniques response depends on second spatial derivative of refractive index. In addition, it is a line of sight integrating optical system. Therefore can't directly determine hydrogen concentration from shadowgram.	Generally easy, depending on particular implementation	Normally custom built. Many types of system are possible, but doesn't necessarily require sophisticated equipment	Potentially any	Yes
Schlieren	Good temporal and spatial	Poor, techniques response depends on first spatial derivative	Fairly easy at small scale.	Generally Custom built	Small/medium	limited

Methods of Visualisation	Quality of flow field visualisation	Quantification of hydrogen concentration	Difficulty of technique	Availability of technology	Scale of use	Suitability for field used
	detail of flow field structure/mixing. Usually more sensitive than shadowgraphy	of refractive index. In addition it is a line of sight integrating optical system. Therefore can't directly determine hydrogen concentration from schlieren image	Much more difficult at large scale. Alignment of optics is important	systems. Require more optical equipment than shadowgraph.	scale. Larger scale possible but very difficult	
Interferometry	Good temporal and spatial detail of flow field structure/mixing.	Yes. Response is related directly to refractive index or gas density (and hence hydrogen concentration), although being a line-of-sight technique is not considered as useful as planar laser techniques for 3D flows. Interpretation of interferograms can be difficult	High. Laboratory based technique. Requires precision alignment of optics. Significantly more difficult than schlieren.	Generally Custom-built systems. Needs monochromatic light source (laser).	small	likely to be poor
synthetic schlieren (BOS)	Reasonable to good temporal and spatial detail of flow field structure/mixing	Poor, techniques response depends on first spatial derivative of refractive index. In addition it is a line of sight integrating optical system. Therefore can't directly determine hydrogen concentration from schlieren image. Based on literature reports, visualising flows	In practical terms very easy. Only requires CCD camera and patterned background. Alignment not critical	Specialist software required but is available commercially	Potentially any	Good

Methods of Visualisation	Quality of flow field visualisation	Quantification of hydrogen concentration	Difficulty of technique	Availability of technology	Scale of use	Suitability for field used
		of 4%(v/v) H_2 in Air mixing with air not possible				

4.4 Conclusions for chapter 4

Overall, there is no one solution to hydrogen release dispersion imaging. All of the techniques discussed have different advantages, limitations and vary in terms of technical difficulty. Some instruments are available off the shelf, some are still primarily laboratory-based research techniques. Some can be used as large-scale others only small scale.

A positive for the aviation industry, however, is there is a large range of hydrogen sensors for a variety of scenarios and environmental conditions. Clearly the best technique will depend to a large extent on how the results are to be used. For hazardous zoning it is the extent of the flammable volume that is of interest. However, the least developed area, that will most likely be extremely useful to any large-scale use of hydrogen is the distributed network of hydrogen sensors. Either an organisation must develop their own network using hydrogen sensing technology, or must wait for those currently being developed and tested. An off the shelf hydrogen sensing network is not yet available.

4.6 References for chapter 4

[1] T. Hubert, L. Boon-Brett, V. Palmisano, G. Frigo, A. Hellstrand, O. Kieswetter and M. May, “Trends in gas sensor development for hydrogen safety.,” in *International Conference of Hydrogen Safety*, Brussels, Belgium, 2013.

[2] H2Sense, “The "H2Sense Hydrogen Sensor Database",” 2014. [Online]. Available: https://netzwerke.bam.de/Netzwerke/Content/EN/Downloads/h2sense-database.pdf?__blob=publicationFile. [Accessed 26th August 2021].

[3] W. Buttner, J. Hall, S. Coldrick, P. Hooker and T. Wischmeyer, “Hydrogen wide area monitoring of LH2 releases.,” *International Journal of Hydrogen Energy,* vol. 46, no. 23, pp. 12497-12510., 2021.

[4] M. Gandhi, J. Rowley, D. Nelson\ and C. Campbell, “Gas Detection in Process Industry – The Practical Approach,” in *ICHEME Hazards 25*, 2015.

[5] DET-TRONICS, “Catalytic Bead Combustible Gas Detector (CGS),” 24 01 2020. [Online]. Available: https://www.det-tronics.com/products/catalytic-combustible-gas-detector. [Accessed 26 08 2021].

[6] T. Hübert, J. Majewski, U. Banach, , M. Detjens, and C. Tiebe, “Response time measurement of hydrogen sensors.,” in *International Conference on Hydrogen Safety*, Hamburg, Germany, 2017.

[7] J. Firth, A. Jones A. and T. Jones , “The principles of the detection of flammable atmospheres by catalytic devices,” *Combustion and Flame,* vol. 21, pp. 303-311, 1973.

[8] P. S. Chauhan and S. Bhattacharya, “Hydrogen gas sensing methods, materials, and approach to achieve parts per billion level detection: A review.,” *international journal of hydrogen energy,* vol. 44, no. 47, pp. 26076-26099., 2019.

[9] AMS, “HLS-440P Factsheet,” 2015. [Online]. Available: https://dtsheet.com/doc/2022844/hls-440p-factsheet. [Accessed 21 08 27].

[10] US Dept. of Energy, “Hydrogen Sensor Success Story: SolidState Sensors for Monitoring Hydrogen,” 2005. [Online]. Available: https://h2scan.com/pdfs/h2_monitoring.pdf. [Accessed 26 08 2021].

[11] R. Jayaraman, “THIN FILM HYDROGEN SENSORS:,” Pennsylvania State University, 2002.

[12] NASA, “Hydrogen sensing technology,” NASA, 10 02 20. [Online]. Available: https://www1.grc.nasa.gov/research-and-engineering/chemical-sensors/gas-sensors/. [Accessed 26 08 21].

[13] D. Nolan, “Ultrasonic leak detection,” in *NDE Handbook: Non-Destructive Examination Methods for Condition Monitoring*, Elsevier, 2014, p. 237.

5. Implications for hydrogen hazard assessment and control on Aircraft

5.1. Summary of hydrogen hazards and mitigation

The hydrogen economy is developing at a rapid rate, and with the increased interest and investment, there has been an increase in technologies and research being developed to maintain the safety of these systems. However, it has been a considerable amount of time since a study was published examining the safety of hydrogen for use in civil-aviation. With increasing interest in this area there is significant need for this assessment on the current state of the industry and technology.

In this work, as part of the ENABLEH2 project, a high-level Preliminary Hazard Analysis, and Bow Tie Diagram analysis demonstrate the interconnected hazards associated with liquid hydrogen use on-board civil-aviation aircraft. A gap analysis has then also been performed identifying current industry needs, including missing fundamental knowledge, and technology deficits, that will be required for hydrogen technology adoption.

This is the first stage of a process that could enable the safe introduction of hydrogen propulsion technology resulting in zero carbon and reduced greenhouse gas emissions, reducing the impact of worldwide aviation on the planet.

5.2. Introduction

The increase in economic growth and prosperity worldwide has resulted in a steady increase in air travel use, with a rise of 5.9% per year for 27 years prior to 2010 [1]. Passengers numbers reached 3.7 billion in 2016, a 6.0 per cent increase over the previous year [2]. Current estimates are that air travel worldwide will double (or increase by more more) by 2035 [3] [4], requiring tens of thousands of new passenger aircraft.

Aviation is a significant contributor to the emission of greenhouse gases (GHGs) such as Carbon Dioxide (CO_2) and Nitrogen Oxides (NO_x), that contribute to rising global temperatures. To address this, a number of government and industry groups have issued mandates, e.g. IATA issued a global commercial aviation mandate to reduce net CO_2 to 50% of 2005 levels by 2050 with carbon neutral growth from 2020 [5]. It is generally accepted that meeting this target, and others, will not be possible while continuing to use hydrocarbon fuels [6], even with additional economy from advances such as boundary layer ingestion. Hence the industry needs to examine alternative energy sources. Among the suggestions in industry are the use of cryogenic fuels, such as liquid hydrogen (LH_2).

The hydrogen economy is a growing, particularly in Europe, with increases in funding [7] and an increasing emphasis on larger infrastructure [8], supporting industries such as public transport freight, and most recently, shipping [9]. The costs of creation and liquefaction of hydrogen (currently often a by-product of other industries) have until recently been prohibitively high [10] but there are an increasing number of projects exploring carbon neutral and renewable hydrogen and economic savings may follow

the investment. Additionally, should green taxes be introduced on Carbon and NOx producing industries, the economic appeal of hydrogen will change quickly [6].

But the use of cryogenic fuels is complex and would require significant and wide-reaching changes to aircraft design, and supporting infrastructure. Many on-board and round support systems, such as storage, refuelling, and combustion systems, require a complete. This work will explore these changes from a safety perspective, examining the interconnected hazards using preliminary hazard analysis, and bow-tie approaches. It will also identify existing safety knowledge gaps that are the current barriers to technology development and industry integration.

5.3. Literature survey

Hydrogen is used in a range of industries. It is also produced as a by-product in industries such as chemical and nuclear, where hydrogen hazards must be managed. There is a large body of work and advice describing hydrogen hazards and control in wider industries such as transport and energy [11] [12]. The major hazards posed from liquid hydrogen (LH_2) in ground-based services can be summarised as flammable, cryogenic, materials compatibility (embrittlement, permeation and temperature), and increased leak propensity as well as the common system issues of pressure and contamination hazards. However, hydrogen use in aviation and aerospace applications poses further difficulty due to the complexity, environmental changes, and safety critical nature of the engineering systems.

Hydrogen gas for aerospace propulsion has been explored and used across the 20th century. It is commonly used for propulsion in spacecraft (in combination with liquid oxygen) and is the proposed fuel for a number of projects in development such as SpaceX, Skylon and SABRE of the EC funded ENABLEH2 project which will be developing aircraft and propulsion & heat management system designs in order to introduce direct propulsion engines into civil aviation aircraft [13]. A major component of this project are the safety analyses (the start of which are covered in this paper) in relation to systems and ground support at airports, which aim to enable safe development and introduction of this environmentally friendly fuel.

While there have been recent papers looking at the conversion of existing engines, development of new engines and modelling of hydrogen combustion in those engines, relatively few of those aircraft-focused studies have paid specific attention to the safety of those systems, and their integration into the wider aircraft industry, with studies often concentrating most on specific areas such as storage [14] and flammability issues [15].

Brewer (1991) [15] determined that hydrogen offer safety advantages in crash survivability due to the increased structure and resilience of the tanks, the dispersive/ buoyant nature of the hydrogen on release, and the lower thermal radiation. Schmidtchen et al (1997) [16], as part of the Cryoplane project, examined hydrogen safety across aircraft and airports, supporting rounder tanks (reducing fatigue and heat loss), and highlighting risks in various components. They also identified key safety areas for which solutions need to be engineered, including disk burst, contamination,

emergency landing, Lightning strike, Fire protection, and Bird strike. Some of the major knowledge gaps identified are large releases of LH_2 and the lack of information on the deflagration and detonation of hydrogen.

Both Verstraete et al (2010) [17] and Khandelwal et al (2013) [18] discuss the importance of tank shape (with cylindrical/spherical identified as best in terms of minimising surface area), tank position (integrated providing support, and reducing weight) and insulation (with heat inflow being key to fuel management and safe storage). Khandelwal et al also compare hydrogen safety to kerosene, however the lack of like-for-like comparison in experimental examples makes this difficult to apply to real scenarios, other than the demonstration that hydrogen fire can be directed upwards and have thermal heat impact.

All of these studies have concluded that safe handling occurs in other areas of industry, and that there is no reason safety in aviation will be less safe than at present if hydrogen is introduced, if the relevant technology and standards are introduced. This study will examine the hazards associated with on-board LH_2 through to hydrogen gas combustion. The interconnected hazards are shown through a preliminary hazard analysis (PHA) and bow tie analysis. These are used to highlight existing knowledge gaps.

5.4. Methodology

The following section details the methodology used for preliminary hazard, bow tie and knowledge gaps analyses for the purpose of examining the hazards associated with liquid hydrogen (LH_2) fuel use on board civil aircraft.

5.4.1. Preliminary Hazard Analysis

A Preliminary Hazard Analysis (PHA) is often the first stage of a risk assessment process. As it is performed in the early stages of a project it can often form the basis for later risk assessment methods. Given the early stage of the ENABLEH2 project a component by component analysis is not possible, and may result in overarching hazards being discounted early, which may affect components added in later. Therefore, following the US DOD [19] approach, a basic system architecture and division has been proposed to analyses areas with similar hazard categories. The system has therefore been split into 4 sections;

1) LH_2 storage,
2) LH_2 transport & heat exchange system
3) Gaseous Hydrogen (GH_2) transport and heat exchange system
4) GH_2 combustion system.

The first stage of a PHA is the creation of a Preliminary Hazard List (PHL); a list of everything that can go wrong with a system or process. This includes things that can cause harm or damage, sources of energy, and interfaces between different systems and components. The PHL process covers both normal conditions (handling of

hazardous system entities and ignition sources under expected flight conditions), and off-normal or fault-conditions (i.e. fault of component/system failure, operator error, and other out–of-tolerance issues).

Two existing lists related to aerospace were used as a starting point [20] [21] but were not regarded as comprehensive. The issues covered in hydrogen standards and guides [12] [20] [21] were also included, as well as the specific scenarios identified in several past projects addressing hydrogen use in aviation [21] [22] [24]

Next an assessment was made for each system, applying each of the hazards on the PHL, with an emphasis put on any area where the inclusion of hydrogen as a fuel significantly changed design or operational considerations. MIL STD 882E [19] and Benson et al (2019) [13] describe the standard rationale employed, in use of the categories from the PHL. The PHA process identifies hazards types, modes by which they can occur and the severity and likelihood of the hazards to eventuate into adverse incidents that affect the safe operation of the systems. The hazards are then also be analyzed to assess their ease of remediation. Where doubts exist around the technology solutions or there is lack of data underpinning the decision this is identified and used to inform the gap analysis later on. Severity and likelihood categories are defined in MIL-STD-882E [19].

5.4.2. Knowledge Gap analysis

The final scoring process of the PHA following mitigation was incomplete due to a lack of meaningful data and research required to properly assess the hazards and risk, and also due to the lack of engineering solutions required for use in aviation conditions. This has been used to perform a gap analysis; is a process by which the difference between the state of the art, and the required technological position for a desired outcome, is defined. This process enables engineers to prioritise scientific and engineering activities, in order to fill these gaps, and bring about the desired outcome more quickly. In this case the gap analysis is performed to see what technology, engineering and fundamental scientific gaps exist in order to enable the safe introduction of hydrogen technology on aircraft.

The uncertainty in scoring for the final stage of the PHA scoring process has been used to identify where gaps in fundamental knowledge and engineering capability exist, using an approach similar to that used by the Hanson et al [27] & the US DOE for the nuclear industry. Where assessment is difficult due to lack of information/ data, and the safety case cannot be justified to a satisfactory degree, further work is required and the major safety barriers to technology development and uptake, and cross cutting needs for all systems are identified. The gap analysis is performed based on doubts in the risk assessment process and can be seen in Table 8.

5.4.3. Bow tie diagrammatical analysis

This PHA has been used as the basis to create a Bow-tie diagram for hydrogen fuel use on board aircraft. A Bow tie diagram is a graphical tool which combines the root

cause analysis methods of fault trees and event trees. The Bow tie diagram starts with causes/ failures at the start and ends with the possible consequences. These events, and control measures that may be used to prevent, change or mitigate issues intersect through a 'top event' which represents the point at which control is lost. A simple example is shown in Figure 39.

Figure 39 A simple example of a bow-tie diagram

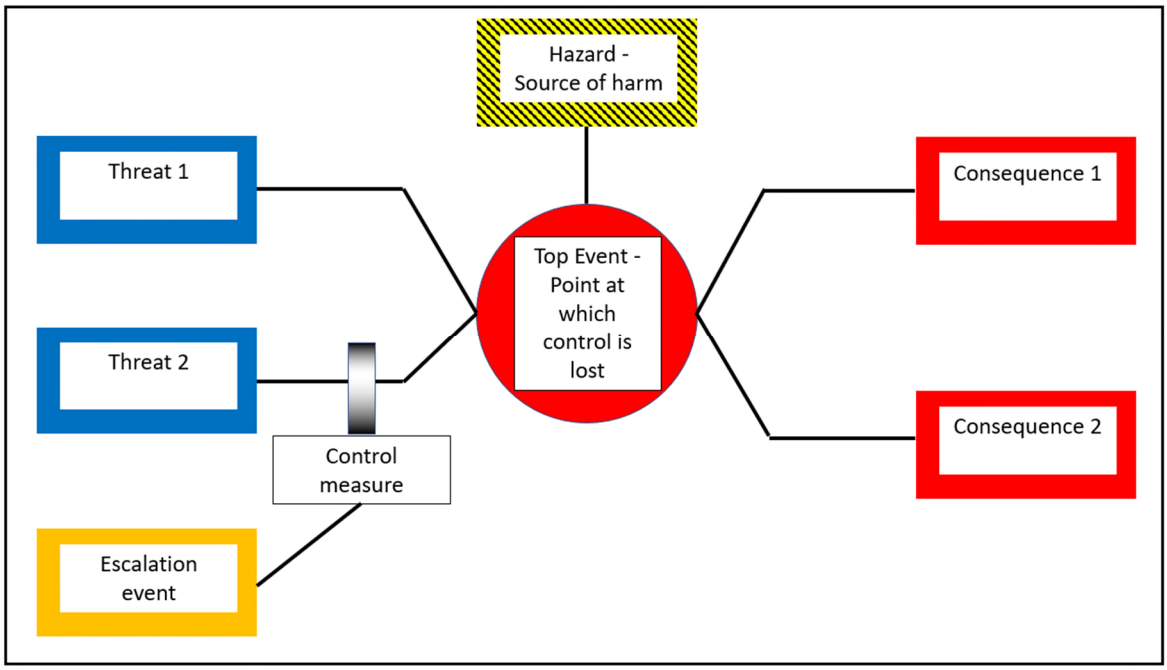

5.5. Results

The following section shows the results of a series of analyses examining hydrogen hazards for LH_2 and GH_2 hydrogen systems on-board civil aviation aircraft.

5.5.1. Preliminary hazard analysis

The Preliminary Hazard Analysis highlights a significant number of hazards currently dealt with in industry that would need to be considered in the incorporation of hydrogen fuel systems into aircraft.

All hazard categories listed in the PHL were applicable for all systems assessed in one form or another. The expression of these problems, severity, likelihood and remediation varied. The hazard type sub-groups for the two LH_2 systems were similar, with some differing modes given the different nature of storage versus a multi component pump, heat exchange and expansion system. The two GH_2 systems were not affected by the cryogenic hazards directly, but otherwise shared similar issues, with additional issues of, for example, danger of deflagration to detonation transition in the combustion chamber and outlet. The systems had common issues concerning preventing system breach from external or internal mechanical factors, the possible

uses of ventilation and inerting, eliminating ignition sources as far as possible/practicable, and a lack of information in the adaptation of these technologies for aviation conditions (including environmental, vibration, and continual use) affecting the attempts to apply control measures. The major hazards identified in relation to the LH_2 and GH_2 hydrogen hazards can be seen in Table 6 and Table 7.

Table 6 Major hazards associated with LH_2 use in civil aviation

Hazard categories	**Storage**	**Heat management/ transport**
Temperature	Cryogenic hazards, heat input	Cryogenic hazards, heat input, 'slush'
Pressure	Expansion, backflow	Expansion, ingress
Chemical	Contamination, leak, compatibility, Ortho-para	Contamination, leak, compatibility
Mechanical	Sloshing, impact, vibration, strain	TAO, hammer, impact, vibration & strain
Leak/ spill	Cryogenic, flammable	Cryogenic, flammable
Physiological	Burn (cold/ heat), asphyxiation	Burn (cold, heat), asphyxiation

Table 7 Major hazards associated with GH_2 use in civil aviation

Hazard categories	**Heat management/ transport**	**Heat management/ transport**
Pressure	Expansion, ingress	Expansion, ingress
Temperature	Properties effect	Properties effect
Mechanical	Impact, vibration, strain	Impact, vibration, strain
Chemical	Compatibility, leak	Compatibility, leak
Leak/ spill	Flammable	Flammable
Physiological	Burn (hot)	Burn (hot)
Fire/ Explosion	Confined explosion, DDT	Confined explosion, DDT

These hazards can be brought about by a number of modes (causes and failures) which were explored as part of the PHA. These are shown in the following Bow-tie analysis section. Some possible control measures to prevent or mitigate these possible hazards are also covered, however this is not an exhaustive list, and, as will be covered in the gap analysis section in section 5.5.2, there many questions around the most suitable mitigation strategies and further work needed to characterise fully the hazards and hence identify suitable control measures.

5.5.2. Gap analysis

The following section details areas of knowledge that have been identified as needing further work to enable LH_2 combustion technology and systems for use on board aircraft. The work in identifies where significant gaps exist in terms of our understanding of hydrogen and the technology it is used in, where no adequate control

measures could be identified, and where the adaptation to aviation industry will require large scale adaptation and safeguards. Table 8 summarises the areas identified as requiring further work, classifying and simplifying issues work discussed in Benson et al (2019).

Table 8 Issues identified in the gap analysis process for integration of LH_2 technology on civil aviation aircraft

Hazard categories and type	**Identified knowledge gaps**
Fundamental knowledge gaps	
Fire (formation of a flammable atmosphere, ignition sources)	There are a number of serious knowledge gaps that need filling in order to be able to fully assess the danger from flammable hazards. Firstly the flammability of hydrogen under flight environmental conditions (low temperature and low pressure) has not been explored in detail. There is a clear need to flame speed, flammability limits, and the behaviour of fire (such as jet fires) under these conditions. Ignition under these circumstances also needs to be addressed in greater detail through definition of, for example, minimum ignition energy, and the probability of ignition by mechanical impact, friction, electrical apparatus, coronal discharge, and lightning. At ground level greater research is still needed in areas identified by __ on large scale ignition, for example at airports, and control measures required.
System containment failure (high pressure release, Increase in internal system pressure, inadvertent release, high temperature, low temperature, fluid compatibility, General leakage to external of system)	Firstly our understanding of LH_2 leaks is limited. There is a need to define dispersion and collection of LH2 and GH2leaks at altitude, as well as the long-identified gap in our understanding of large-scale longer-term releases of LH2 on ground, and the mitigation or control measures that might be used in case of these releases. New detection methods may also have to be developed. Further concern on system breach relates to materials use. Work will be required to examine the novel engineering materials being developed for aircraft use, fuel tanks and insulation, as well as exploring material behaviour for hydrogen systems under cryogenic and cold environment conditions, hot system conditions, and the possibility of embrittlement, and diffusion at altitude.
Mechanical damage (Thermo-acoustic oscillation)	Further work is required to understand the existence and impact of possible thermos-acoustic oscillations and vibrational damage in the combustion system given the change in combustion and flame with hydrogen fuel.
Aviation engineering knowledge gaps	
Fire (Ignition source, Contingencies	Currently fire suppression is a key area of aircraft assessment. The recent ban on halons has resulted in new

	fire suppression system design, primarily around the idea of inerting. Work must be conducted to identify fire suppression capability for hydrogen flames under aviation conditions. Fire fighting techniques are already in place for ground systems that can be used at airports. Further work is needed to assess current engineering ability to protect LH2 storage materials and other systems from lighting strike. Different fire protection measures may be needed for different stages of aircraft operation.
System containment failure (High pressure containment failure, Increase in internal system pressure, Decrease in internal pressure due to inadvertent release, High temperature/Heating elements, Low temperature)	Pressure and temperature effects could have an adverse impact on hydrogen systems. Care will need to be taken in the design and testing of systems to prevent cold (cryogenic and environmental) from blocking or causing the failure of components such as required pressure relief or valves). Emergency off-gassing procedures may be needed in case of high temperature exposure. Engineering and process design must prevent harm occurring due to leaks in refuelling.
Mechanical damage (Impacts/ collision with protected item)	Tank design will be key (as highlighted by prior work in the literature survey). Careful consideration must be given to Tank siting (disk burst and kick up prevention, access for inspection, etc) and damage from sloshing liquids. All systems must be protected, by position or through reinforcement, from loose object impact, acceleration, deceleration and gravity effects, as well as fragments or missiles (engine rotors, fans disks burst and other uncontained engine failure, or bird strike).
Explosion (Deflagration to Detonation risk, Blast overpressure/ seismic wave)	A great deal of thought is required to understand the implications of an explosion, very small or large, on board an aircraft. The preference from a safety perspective is complete prevention through explosion avoidance & control methods. However, future work should also examine the survivability from fireball ignition, rather than a developing blast wave to assess the overall risks involved and required control measures. Further work is needed to characterise hydrogen Boiling-Liquid-Evaporating Gas explosion hazard. Engineering design must pay careful attention to prevent the risk of deflagration to detonation transition, and the increased damage from resulting shockwave, and ensuring relight in combustion systems.
All system effects	The following issues will have to be explored to understand their effect and implications for all systems: take-off and landing, off normal aircraft manoeuvre, changing environmental conditions (wide pressure and temperature

	envelopes), vibration, and longevity/ continual use factors associated with civil aviation aircraft.

5.5.3. Bow tie diagram analysis

The following section will show the widespread and interconnected hazards that have been identified in relation to LH_2 and GH_2 hydrogen systems use on board aircraft. Figure 40 shows the key for the symbols and colours used in this analysis, while Figure 41 key shows the layout of six diagram sections, each describing the threats or consequences, and the identified associated mitigation measures that might be applied in these scenarios. Figure 42 to

Figure *47* show these full sections in greater detail.

Figure 40 Bow tie diagram key

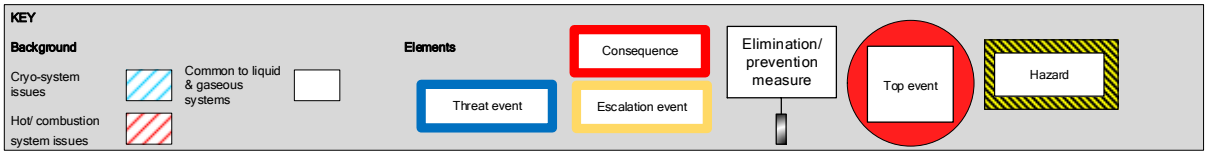

Figure 41 Diagram section key for the bow-tie analysis of threats and consequences associated with hydrogen fuel use on board civil aviation aircraft

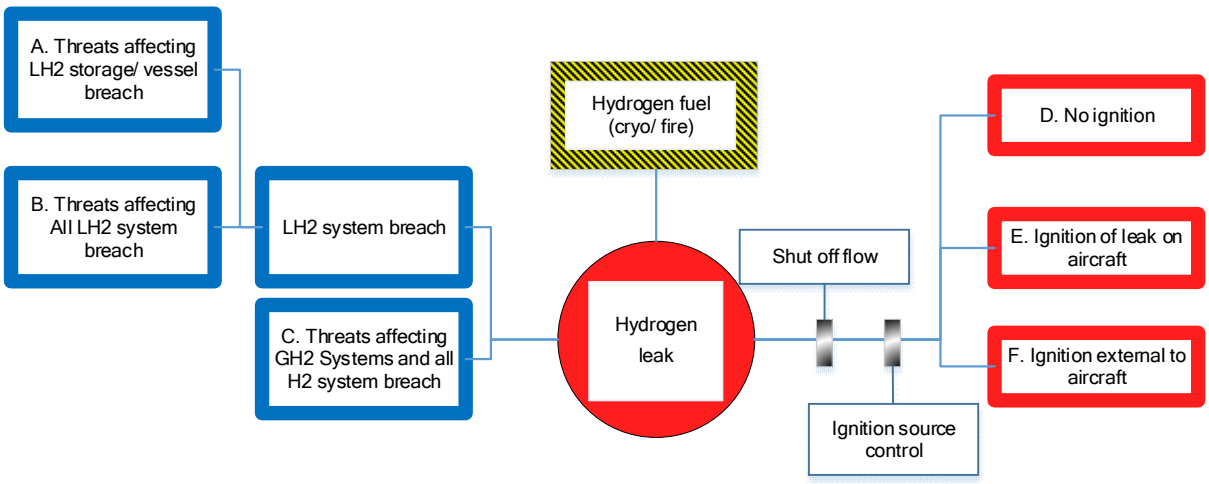

Figure 42: A. Threats associated with only LH_2 storage systems for civil aviation aircraft leading to hydrogen leaks

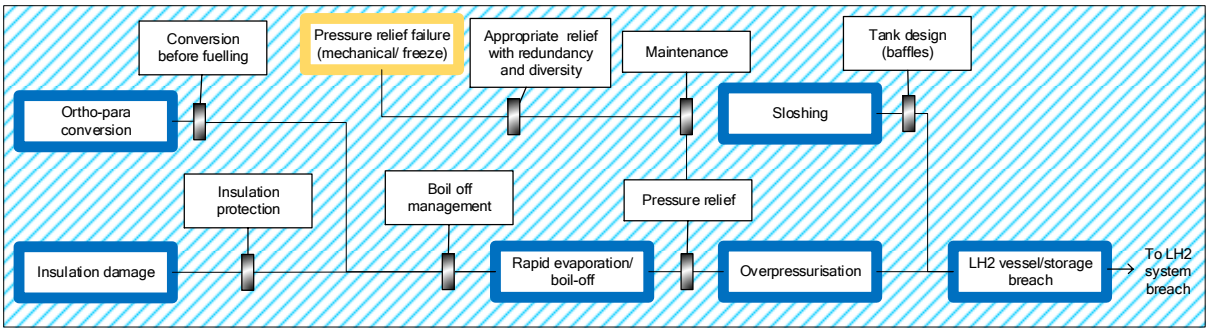

Figure 43: B. Threats associated with LH_2 systems for civil aviation leading to hydrogen leaks.

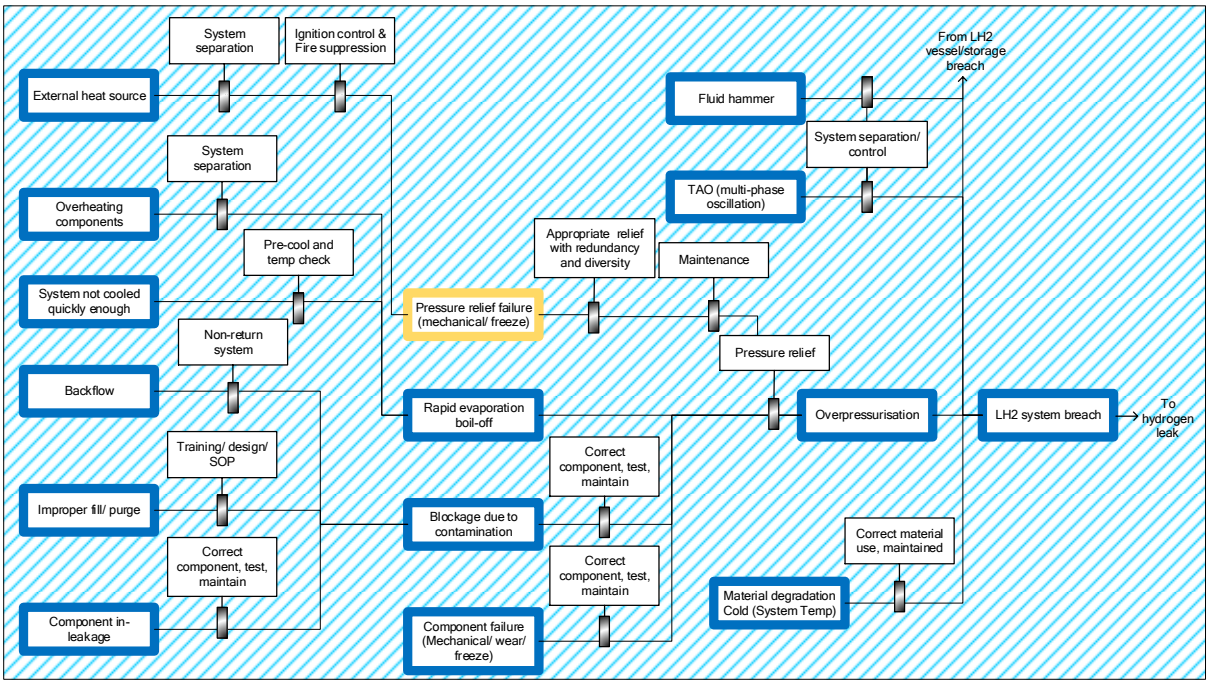

Figure 44: C. Threats associated with hot GH_2 and all hydrogen systems for civil aviation leading to hydrogen leaks

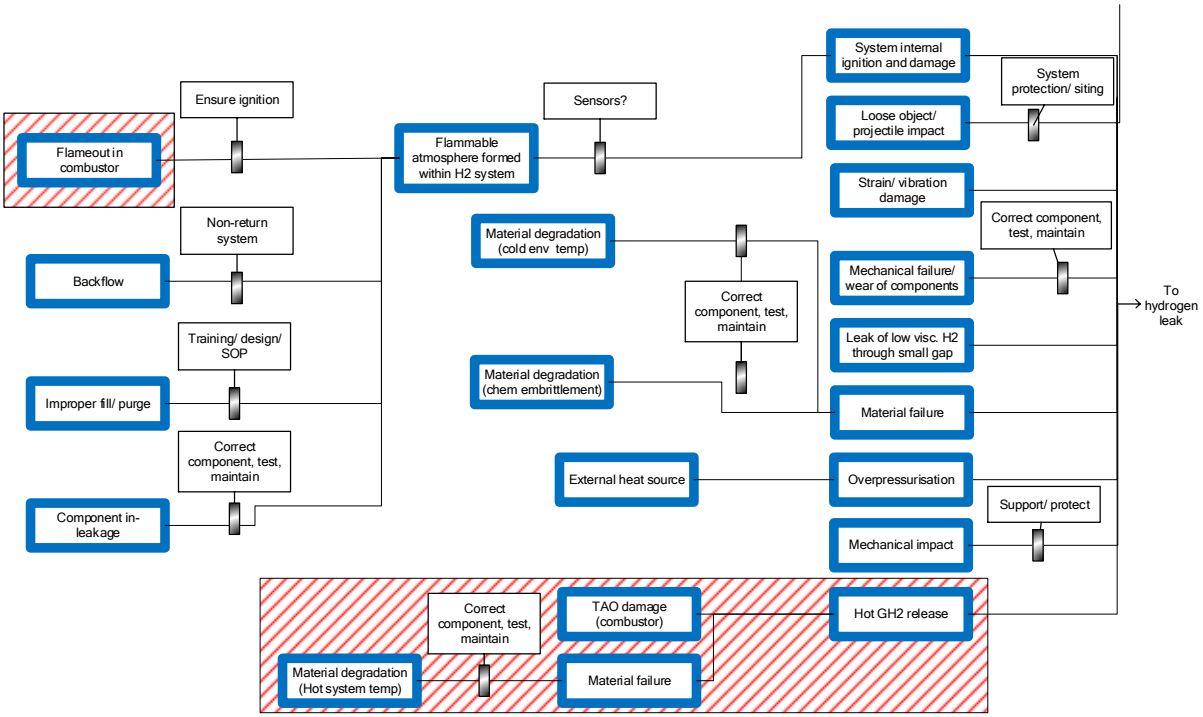

*TAO = Thermo-acoustic oscillation

Figure 45: D. Consequences associated with a hydrogen leak from a civil aviation aircraft in the event of no ignition

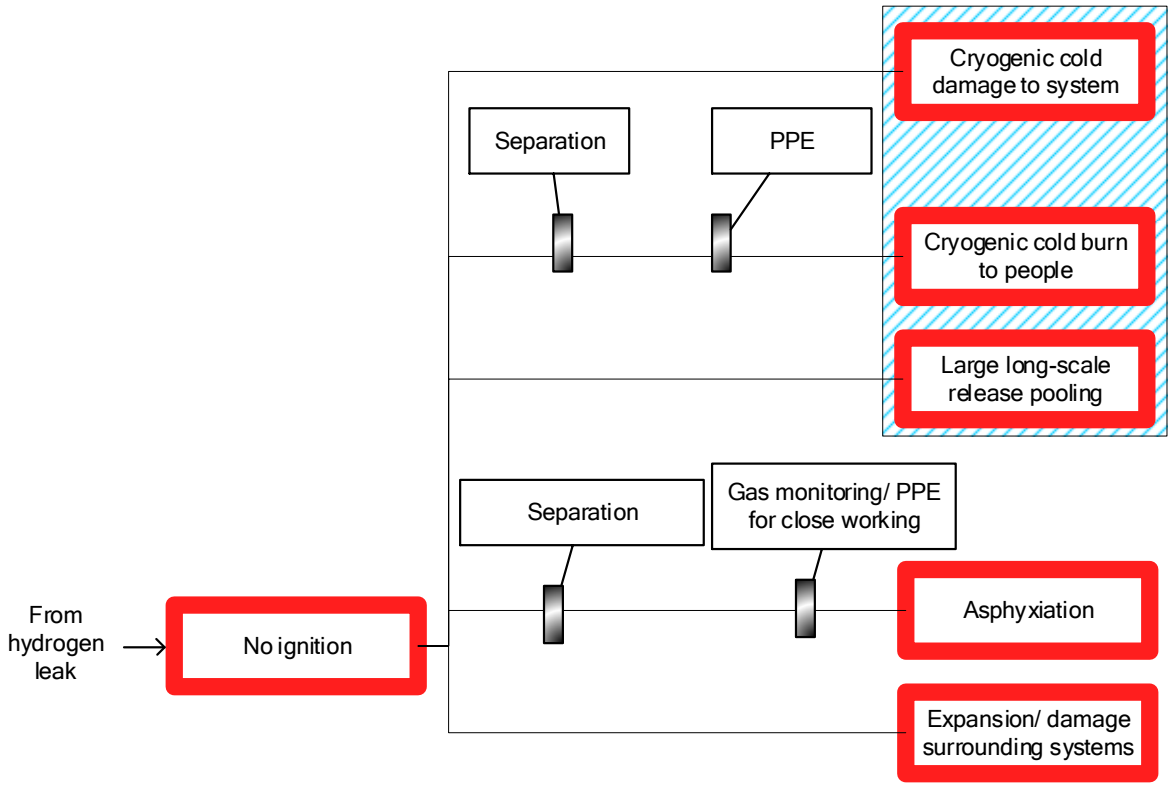

Figure 46: E. Consequences associated with a hydrogen leak from a civil aviation aircraft in the event of an ignition on the aircraft

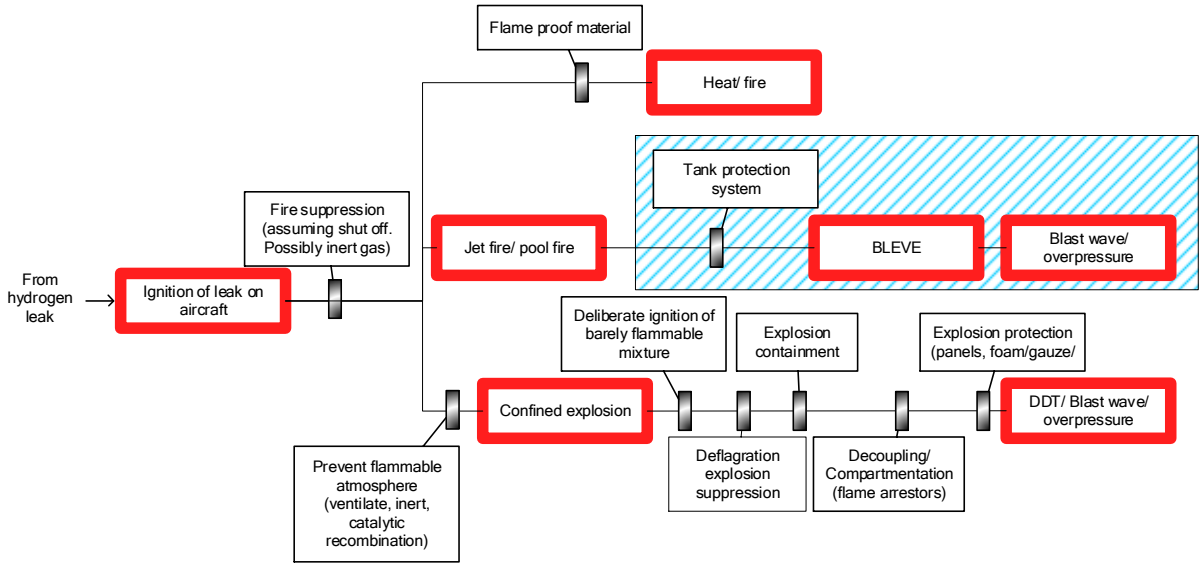

Figure 47: F. Consequences associated with a hydrogen leak from a civil aviation aircraft in the event of an ignition external to the aircraft

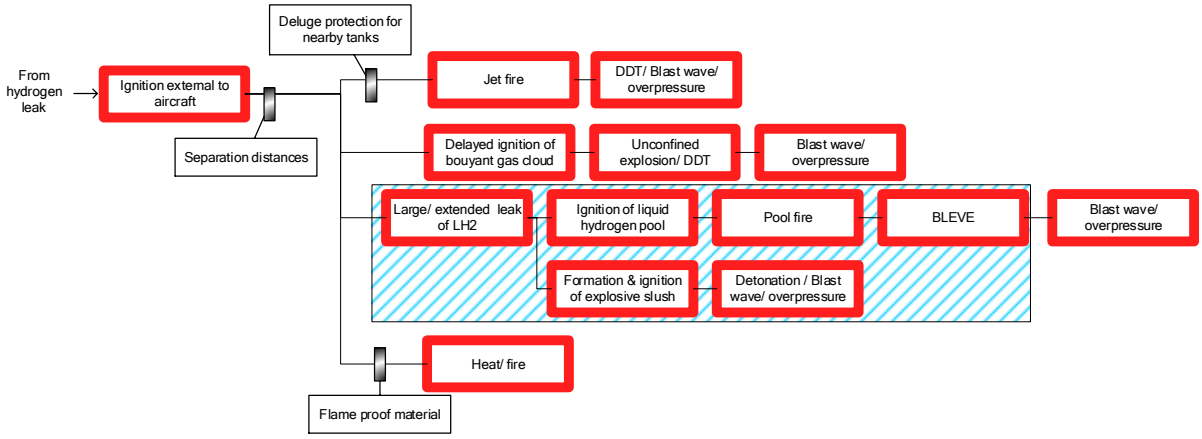

5.6. Discussion

As summarised in the preliminary hazard analysis and highlighted in some areas of the bow-tie analysis, there are a high number of possible hazards associated with LH_2 fuel use on board aircraft.

In terms of threats that are confined to LH_2 storage systems (shown in Figure 42, B) issues include over-pressurisation due to insulation damage (and resulting heat input) or ortho-para conversion (the un-managed quantum state change of hydrogen molecule nuclei spins following liquefaction, releasing heat), combined with pressure relief failure.

Figure 43 (B) shows threats that effect all LH_2 systems. Again, increase in evaporation is a major threat, but with wider and more varied causes of external and

component heat and a failure to cool the system at the start of operation. Overpressure from contamination blockage or component effect is also a problem, which could be caused by improper filling, backflow and most commonly component in-leakage. Mechanical damage through fluid hammer, or thermoacoustic oscillation (due to evaporation and re-cooling inside long pipes) could cause serious system damage. Material degradation and component failure or wear are also threat. Suitable materials are needed for use in aviation that contain a cryogenic fuel, while also withstanding the environmental and chemical conditions (pressure build up, thermal contraction, hydrogen embrittlement, weather). As composites are increasingly being explored due to their light weight (e.g. in hydrogen tanks) understanding the behaviour and how to reinforce these will be necessary.

Figure 44 (C) depict the threats affecting GH_2 that may affect all systems given the possibility of rapid evaporation from LH_2 systems. A threat that can affect systems in multiple ways is the formation of a flammable inside the system. Causes include improper filling, backflow and in-leakage of air, but also include the possibility of a flame-out scenario in combustor, where late relight could cause damage. Mechanical breach can occur from, strain, vibration, component failure, external and internal object impact and projectiles, material failure, the implication being this must be engineered out through design, component and material control and maintenance processes. As well as the danger of flame-out and failure to relight quickly, the combustor is also threatened by the possibility of material failure from heat, but also the possibility of thermoacoustic oscillation causing vibrational damage.

All these threats, unmanaged or unmitigated, have the capability of resulting in a hydrogen leak, shown in Figure 41. These might be stopped or the danger might be reduced by shutting off flow immediately, though this will also have to be considered from an aircraft operation perspective.

The consequences have been split into three distinct areas; no ignition, ignition on the aircraft, and ignition external to the aircraft.

The consequences that can occur even where ignition is prevented are shown in

Figure 45 (D). These are cryogenic damage and injury, and asphyxiation/ damage from the expanding gas.

Figure 46 (E) covers the various explosion and fire consequences that can result from ignition on board an aircraft. Here a range of mitigations are offered, including tank protection, explosion containment and compartmentalisation, fire suppression, and even explosion protection or deliberate ignition of barely flammable mixtures however, as the gap analysis exposes, it is unclear which, if any of these, are suitable for the civil aviation use. It is unlikely the last two listed would be suitable but have been included at this stage. Prevention of a flammable atmosphere has been proposed through use of ventilation, inerting or catalytic recombination, which might be more realistic as leaks cannot be ruled out. Early detection of minor leaks and cracks would

also be necessary before they become serious or fail catastrophically. Hydrogen is more prone to deflagration to detonation transition (DDT) than most other fuels so the flameout, flood and late re-ignition hazards must be assessed.

Figure 47 (F) shows the possible consequences of a release of hydrogen external to the aircraft. It is likely that these will be more serious for larger releases and will have greater implications for nearby populations. The diagram is largely unmitigated due to the limited information on releases in this context. Some practical work by the HSL [28] [29], as well as some more recent modelling work [30] [31] examines some of these issues, but further modelling, and in some cases better validation, is needed to enable the use of this material safely at, for example, airports in large volumes, and know all the risks, including possibility and avoidance of DDT.

The bow-tie analysis which was developed using the PHA demonstrates the threats for LH_2 storage, LH_2 transport/ heat management systems, and the GH_2 systems including transport, heat management and combustion. Bowtie process has used a number of standard industry mitigations however, as the gap analysis highlights, it is not clear how these will work on aircraft under aviation conditions, with wide pressure and temperature envelopes, and with long-range and multiple trip use factored in while also requiring the ability to refuel and maintain systems. The systems operation is far more easily controlled due to existing industry mitigations that can be adapted, such as system separation, boil-off management and pressure relief

5.7. Conclusion and Future work

The ENABLEH2 project is exploring novel hydrogen technology use for civil aviation aircraft. This includes designing and continuing to develop LH_2 storage & heat management systems, and GH_2 transport, heat management & combustion systems.

This work has examined the current state of the art in relation to the safety of LH_2 and GH_2 systems and has explored the use of these systems for propulsion in civil aviation from a safety perspective. Three analyses have been used to explore and demonstrate the interconnected hazards and consequences that surround hydrogen system breach in this scenario. A PHA has shown the large number of hazards that must be considered in aviation fuel integration. There are significant differences between hydrocarbon and hydrogen fuels, and a number of hazards associated with hydrogen (both liquid and gaseous) as well as possible advantages (e.g. lower environmental damage from spills, buoyancy and fast dispersion outside).

A Gap analysis has been used to identify areas required for research in order to enable the development and safe integration of hydrogen into civil aircraft. A bow-tie analysis has been used to demonstrate the systems, hazards and possible control measures (prevention, change, mitigation) that could be used. For some areas lack of mitigation for events also demonstrates areas of need for fundamental and engineering research work in the future if this green fuel is to be adopted. Together these demonstrate that a significant level of research and engineering will be needed to enable the development of a LH_2 propulsion system.

5.8. References for chapter 5

[1] M. Mazraati, “World aviation fuel demand outlook,” *OPEC Energy Rev.,* vol. 34, no. 1, 2010.

[2] ICAO, “Traffic growth and airline profitability were highlights of air transport in 2016,” International Civil Aviation Organization, 2 Janury 2017. [Online]. Available: https://www.icao.int/Newsroom/Pages/traffic-growth-and-airline-profitability-were-highlights-of-air-transport-in-2016.aspx. [Accessed 4 October 2018].

[3] Airbus, “Over 33,000 new planes valued over US$5 trillion for the next 20 years,” Airbus Group Ltd, 11 July 2016. [Online]. Available: https://www.airbus.com/newsroom/press-releases/en/2016/07/over-33-000-new-planes-valued-over-us-5-trillion-for-the-next-20-years.html. [Accessed 4 October 2018].

[4] IATA, “IATA Forecasts Passenger Demand to Double Over 20 Years,” IATA, 18 October 2016. [Online]. Available: https://www.iata.org/pressroom/pr/Pages/2016-10-18-02.aspx. [Accessed 4 October 2018].

[5] C. Bil and T. Conroy, “Life-cycle analysis for alternative aviation fuels,” *Journal of Aerospace Operations,* vol. 4, no. 1-2, pp. 5-29, 2016.

[6] G. Babazzi, P. Gauthier, P. Agarwal, J. McClure and V. Sethi, “NOx emissions Predictions for a Hydrogen Micromix combustion system,” in *ASME TurboExpo 2019*, Arizona, 2019.

[7] EU Fuel Cells & Hydrogen Joint Undertaking, “Who we are,” 6 May 2014. [Online]. Available: https://www.fch.europa.eu/page/who-we-are. [Accessed 25 July 2019].

[8] J. S. S. &. B. T. H. Kurtz, “Review of transportation hydrogen infrastructure performance and reliability.,” *International Journal of Hydrogen Energy.,* 2019.

[9] S. Sen, “Japan: Taking a Lead in Hydrogen,” *The Chemical Engineer,* 1 April 2019.

[10] M. &. W. M. Ball, “The hydrogen economy–vision or reality?.,” *International Journal of Hydrogen Energy,* vol. 40, no. 25, pp. 7903-7919, 2015.

[11] F. Rigas and P. Amyotte, Hydrogen Safety, CRC Press, 2018.

[12] NFPA, “NFPA 2. Hydrogen Technologies Code,” NFPA, Massachusetts, 2016.

[13] C. Benson, J. Ingram, P. Battersby, D. Mba, V. Sethi and A. Rolt, “An analysis of civil aviation industry safety needs for the introduction of liquid hydrogen,” in

ASME Turbo Expo 2019: Turbomachinery Technical Conference and Exposition, Arizona, 2019.

[14] S. Rondinelli, A. Gardi , R. Kapoor and R. Sabatini , “Benefits and challenges of liquid hydrogen fuels in commercial aviation,” *International Journal of Sustainable Aviation,* vol. 3, no. 3, 2017.

[15] G. D. Brewer, Hydrogen Aircraft Technology, CRC press, 1991.

[16] F. Schmidtchen, E. Behrend, H. Pohl and N. Rostek, “Hydrogen aircraft and airport safety,” *Renewable and sustainable energy reviews,* vol. 1, no. 4, p. 1997.

[17] D. Verstraete, P. Hendrick, P. Pilidis and K. Ramsden, “Hydrogen fuel tanks for subsonic transport aircraft.,” *International journal of hydrogen energy,* vol. 35, no. 20.

[18] B. Khandelwal, A. Karakurt, P. R. Sekaran, V. Sethi and R. Singh, “Hydrogen powered aircraft: the future of air transport.,” *Progress in Aerospace Sciences,* vol. 60, 2013.

[19] DoD, US, “Mil-std-882e, department of defense standard practice system safety.,” US Department of Defense., 2012.

[20] B. Goldberg, K. Everhart, R. B. I. N. Stevens, P. Clemens and L. Stout, “NASA Reference Publication 1358 System Engineering “Toolbox” for Design-Oriented Engineers,” NASA, 1994 .

[21] S. Hard, B. Knabenshue, C. Schaeffer and J. Schmidt, “OC-Flight-1 Preliminary Hazard Analysis(PHA),” NASA, 2012.

[22] AIAA, “ G-095A Guide to Safety of Hydrogen and Hydrogen Systems,” AIAA, 2017.

[23] H. Beeson and S. Woods, “Guide for hydrogen hazards analysis on components and systems.,” NASA, 2003.

[24] B. Lowesmith, G. Hankinson and S. Chynoweth, “Safety issues of the liquefaction, storage, transportation of LH2 - IDEALHY,” in *Int. Conf. on H2 Safety*, 2013.

[25] A. Kotchourko, D. Baraldi, P. Bénard, P. Eisenreich, T. Jordan and J. Keller, “State of the art and research priorities in hydrogen safety,” European Commission Joint Research Centre of the European Commission (JRC)., 2014.

[26] Arthur D Little Inc, “An assessment of the crash fire hazard of liquid hydrogen fueled aircraft,” NASA, 1982.

[27] B. Hanson, H. Alsaed, C. Stockman, D. Enos, R. Meyer and K. Sorenson, “USED FUEL DISPOSITION CAMPAIGN. Gap Analysis to Support Extended Storage of Used Nuclear Fuel,” U.S. Department of Energy , 2012.

[28] P. Hooker, B. Willoughby and M. Royle, “Experimental releases of liquid hydrogen,” in *4th Int. Conf. on Hydrogen Safety*, 2011.

[29] J. E. Hall, P. Hooker and D. Willoughby, “Ignited releases of liquid hydrogen : Safety considerations of thermal and overpressure effects,” *International journal of hydrogen energy,* vol. 39, no. 5, 2014.

[30] S. Jallais, E. Vyazmina, D. Miller and J. Thomas, “ Hydrogen jet vapor cloud explosion: A model for predicting blast size and application to risk assessment,” *Process Safety Progress,* vol. 37, no. 3, 2018.

[31] E. Edelia, R. Winkler, D. Sengupta, M. El-Halwagi and M. Mannan, “ A computational fluid dynamics evaluation of unconfined hydrogen explosions in high pressure applications.,” *International Journal of Hydrogen Energy,* vol. 43, no. 33, 2018.

[32] D. Verstraete , “The Potential of Liquid Hydrogen for long range aircraft propulsion. Ph. D. Thesis,” Cranfield University, 2009.

[33] UK Department for Transport, “UK Aviation Forecasts,” Department for Transport, United Kingdom, 2013.

6. Conclusions and future work

An apparatus to find various combustion parameters of hydrogen under flight profile conditions has been built at LSBU. The apparatus has been demonstrated to generate results consistent with previous work.

Lower flammability limit data has been found using the FAA criteria that a pressure rise of less than 3% of the initial pressure constitutes non-flammability. The flammability limits so determined indicate that the lower flammability limit rises slightly as the temperature falls from $20℃$ to $-50℃$ but rises slightly as the pressure falls from $1013\ mbar$ to $240\ mbar$ (absolute). Thus, at $1013\ mbar$ and $20℃$ the LFL was found to be 5.1%, at $572\ mbar$ and $-15℃$ it was 4.95%, and at $240\ mbar$ and $-50℃$ it was found to be 4.7%. This represents a very modest but unfavourable fall in LFL of 8% (0.4 percentage points) at high altitude pressure and temperature compared to ground temperature and pressure.

Upper flammability limit data has been found using the FAA criteria that a pressure rise of less than 3% of the initial pressure constitutes non-flammability. The flammability limits so determined indicate that the upper flammability limit falls slightly as the temperature falls from $20℃$ to $-50℃$ and also falls slightly as the pressure falls from $1013\ mbar$ to $240\ mbar$ (absolute). Thus, at $1013\ mbar$ and $20℃$ the UFL was found to be 76.2%, at $572\ mbar$ and $-15℃$ it was 73.6%, and at $240\ mbar$ and $-50℃$ it was found to be 63.4%. This represents a significant, favourable fall in UFL of 17% (12.8 percentage points) at high altitude pressure and temperature compared to ground temperature and pressure.

Therefore, at high-altitude temperature and pressure $(-50℃, 240\ mbar)$ the flammability limits of hydrogen are narrower than at ground conditions $(20℃, 1013\ mbar)$, dropping to a range of 58.7% from 68.5%.

Limiting oxygen concentration (LOC) for combustion was determined at hydrogen concentrations of 6% and 25% at pressures of $240, 572$ and $1013\ mbar$ and temperatures of $20, -15$ and $-50℃$. The combined effect of higher altitude pressure-temperature pairs was to favourably increase the LOC at both hydrogen concentrations. At 6% hydrogen the LOC increased from 4.95% at ground conditions $(20℃, 1013\ mbar)$ to 5.7% at high altitude $(-50℃, 240\ mbar)$. This represents a 15% increase (0.75 percentage points) in LOC at altitude for a 6% hydrogen mixture.

For a 25% hydrogen mixture the effect was more pronounced, 4.8% LOC at ground and 5.8% at altitude, representing a 20% increase in LOC at altitude (1 percentage point).

A range of hydrogen detection and visualisation technologies have been reviewed but there is no clear winner. The technology most likely to be useful on the large-scale use of hydrogen is the distributed network of hydrogen sensors. This is the least-developed option and a proprietary hydrogen-sensing network is not yet available. As commercial options are not available, there is the possibility of forming a consortium with relevant partners to develop a system for use in the aviation industry.

There are still gaps in knowledge of combustion parameters under flight profile conditions. Minimum Ignition Energy (MIE) and laminar burning velocity (LBV) data under flight profile conditions have yet to be determined, although the equipment to determine them has been developed at LSBU. The possibility of using the existing apparatus to continue these investigations is open.

A large hydrogen leak might generate temperatures lower than $-50℃$ and so it might be worthwhile to investigate combustion properties at even lower temperatures. However, this would not be possible with the current LSBU apparatus.

Grant Agreement: 769241

Call identifier: H2020-MG-2016-2017/H2020-MG-2017-Two-Stages

Project full title: ENABLEH2 – ENABLing cryogEnic Hydrogen-based CO2-free air transport

Grant Agreement: 769241

Call identifier: H2020-MG-2016-2017/H2020-MG-2017-Two-Stages

Project full title: ENABLEH2 – ENABLing cryogEnic Hydrogen-based CO2-free air transport

ENABLEH2

D4.2b - Analytical studies into large scale behaviours and hazards posed by liquid hydrogen use in civil aviation

Deliverable lead beneficiary: London South Bank University
Authors: Paul Holborn, James Ingram, Claire Benson

Abstract:

The aim of this work package has been to study the large-scale hazards posed by the use of liquid hydrogen in civil aviation. Analytical studies have been carried out to examine liquid hydrogen release and dispersion behaviour for different LH_2 tank storage and aircraft tank failure/rupture accident scenarios. The FLACS CFD model has been used to simulate the potential hazard effects following an accidental LH_2 leak, including the extent of the flammable LH_2 clouds formed, magnitude of explosion overpressures and pool fire radiation hazards. A comparison has also been made between the relative hazard consequences of using LH_2 with conventional Jet A/A1 fuel. Specific modelling studies have been carried out for:

- LH_2 leaks and flammable cloud dispersion behaviour.
- Leaks from a LH_2 storage tank at an engine test facility.
- A serious aircraft crash scenario comparing LH_2, LNG and Jet A/A-1 pool fire hazards.
- LH_2 and Jet A/A-1 fuel spills during aircraft refuelling operations resulting in pool fires.
- LH_2 spills during aircraft refuelling operations resulting in flammable clouds, flash fires and explosions.
- Continuous releases of LH_2 and Jet A/A-1 from aircraft and airport storage tanks resulting in pool fires.

The results of the study indicate that, in the event of accidental fuel spill, LH_2 has some safety advantages over Jet A/A-1. Modelling of LH_2 pool fires suggests they exhibit a smaller thermal radiation hazardous distance and deliver a lower thermal dose than those found for comparable Jet A/A-1 pool fires. The rapid vaporisation of instantaneous, unconstrained, LH_2 spills produces short duration fires such that the fuel spills will completely evaporate and burn-out rapidly. Hydrogen fires will also emit a lower fraction of their heat as radiation and are clean burning such that no toxic smoke is produced (unless other materials become involved).

However, the use of LH_2 fuel and associated dense gas cloud dispersion behaviour will also introduce additional hazards not found with Jet A/A-1 that will need to be carefully managed and mitigated against. The largest hazardous distances are predicted to occur for LH_2 tank BLEVE (boiling liquid expanding vapour explosion) accident scenarios – particularly airport storage tank BLEVEs. The results suggest that there will also be additional hazards associated with LH_2 leaks and spills due to dense gas cloud

This project has received funding from the European Union's Horizon 2020 research and innovation programme under grant agreement no 769241

dispersion behaviour that is predicted and the extent of flammable gas cloud that can be formed at ground level downwind of the spill and potential for accompanying flash fire/jet fire and explosion hazards. The hazard consequences produced may be accentuated if the prevailing wind could transport the cloud under the body of the aircraft where it could be partially confined, towards the airport terminal building, or to the side of the aircraft where passengers' egress.

There is significant uncertainty with current models and the limitations should be borne in mind when interpreting or making judgements based on the results. There is also an urgent requirement for more large-scale experimental test data for LH_2 releases and associated hazard behaviour in order to reduce uncertainty and allow models to be further developed and validated to improve confidence in their predictions.

This work forms part of a programme of work being carried out for the EU ENABLEH2 project, examining the feasibility of using LH_2 in commercial aviation. The usage of LH_2 in aviation will require the development of new types of aircraft and cryogenic fuel tank design, as well as the need for the provision of large-scale LH_2 storage facilities at airports. The results are intended to assist with assessing the safety of future LH_2 aircraft and large-scale airport LH_2 storage facilities, being considered as part of ENABLEH2.

Table of Contents

1 Introduction

The contribution of the aviation sector to global CO_2 emissions and its associated impact upon the climate is already significant - emitting 900 million tons of CO_2 per year or around 2% of the total. Even allowing for more efficient conventional aircraft being developed this could more than double by 2050 [Fleming and Ziegler, 2016].

In order to meet internationally agreed commitments to reduce global CO_2 emissions by 2050, the aviation sector urgently needs to develop environmentally friendly alternatives to the traditional hydrocarbon-based fuels (Jet A[1]) that are currently used for aircraft. The use of hydrogen as an aviation fuel would eliminate in-flight CO_2 emissions. Hydrogen propulsion has the potential to play a major part in reducing the climate impact and meeting the decarbonization targets of the aviation sector [McKinsey, 2020].

The high density of liquid hydrogen (LH_2), when compared with gaseous hydrogen, allows for significantly more efficient storage, transport and distribution as much larger quantities can be stored at low pressure in lighter tanks. Consequently, liquid hydrogen, generated from renewable energy sources, can play a key role in the development of the hydrogen economy, helping to reduce greenhouse gas emissions, and address concerns over climate change.

The usage of liquid hydrogen as an aviation fuel will require the development of new types of aircraft and cryogenic fuel tank design, as well as the need for large-scale LH_2 aircraft refuelling operation and storage facilities at airports. A key challenge that will need to be met in order to allow such a transition is that of safety.

Hydrogen has unique properties and behaves very differently to conventional aircraft fuel (kerosene - Jet A). Key differences include [Rigas and Amyotte, 2012]:

- *Cryogenic liquid*. As a cryogenic liquid, liquid hydrogen must be maintained at extremely low temperatures (20.4 K at atmospheric temperature) to be kept as a liquid. Above this temperature it will vaporise and boil vigorously releasing hydrogen gas.

- *Flammable range* – hydrogen has very wide flammability limits 4 - 74% at NTP in comparison to Jet A – and thus will form flammable gas mixtures over a much greater range, particularly if released in a confined or enclosed space. Jet A/A1 has a narrow flammable range and does not vaporise or generate flammable gas clouds to a significant degree at ambient temperatures.

- *Very low MIE* – hydrogen has an extremely low minimum ignition energy MIE – an order of magnitude less than kerosene for a stoichiometric fuel-air vapour mixture. Hence it can be ignited much more readily. In contrast Jet A contains additives that inhibit ignition and flame spread behaviour making it much easier to handle safety as an aircraft fuel (difference with Jet A and JP-1).

- *Buoyancy* - At ambient temperatures hydrogen gas is extremely buoyant and will rise and disperse rapidly if released in an open environment. However, at very low temperatures of 22 K or less hydrogen has a density which is greater than that of air and hence under certain circumstances it also has the potential to behave as a dense gas.

- *Burning behaviour* – hydrogen has different combustion properties (higher heat of combustion and flame temperature) and radiative characteristics (low emissivity and radiative heat fraction) than Jet A.

- *DDT behaviour* – hydrogen has a much greater propensity to detonate and can undergo a DDT (deflagration to detonation transition) under a wide range of circumstances (e.g. congestion or confinement) and fuel-air mixture ratios producing a highly damaging detonation.

[1] Note that the expression “Jet A” is used in this report as a generic term referring to both Jet A and Jet A-1 (apart from in section 2.5.3).

Given these differences, it is natural to ask how the safety of LH_2 compares with that of Jet A in terms of the hazards and challenges it will present if it is to be used as a fuel for commercial aircraft. However based upon previous studies, only a limited amount of information is available examining the behaviour and the extent of flammable gas clouds, pool fires and explosions resulting from LH_2 spills, particularly in the context of the aircraft and airport safety. As part of the ENABLEH2 (ENABLing cryogEnic Hydrogen based CO_2 free air transport) project [ENABLEH2, 2021], an analysis has therefore been carried out herein, using modelling studies (with the FLACS-CFD code), to examine and predict the behaviour of accidental LH_2 releases in terms of the hazards and safety challenges they could present and how these compare with the existing hazards posed by using conventional aviation fuel (Jet A).

The main aim of the work has been to study the large-scale hazards posed by LH_2 use in civil aviation carry out LH_2 release and dispersion modelling of large-scale releases and their potential hazard effects for airport storage and aircraft tank failure/rupture/leak scenarios. A variety of different hazard types and accident scenario case studies have been considered.

Chapter 2 examines the previous work that has been carried out on LH_2 hazards, particularly in relation to its use as a fuel for aviation. A review of research on LH_2 pool spills and flammable cloud dispersion behaviour, fire and explosion hazards is presented. A summary of previous studies looking at the safety of LH_2 aircraft and airports is also given.

Chapter 3 provides an overview of the FLACS CFD code that has been used in this study to model the hazardous behaviour of fuel leaks/spills, including flammable cloud dispersion, pool fires and gas explosions.

Chapter 4 looks at the application of FLACS to model LH_2 leaks and cloud dispersion behaviour. Comparisons are made with the results of large-scale LH_2 dispersion tests experimental tests carried out by NASA during the 1980s. The effect of both wind speed and pool ground properties on the extent of the flammable cloud produced by a LH_2 spill are examined. Both transient and continuous spills are considered. The results can be used to predict the hazardous distance for flammable clouds produced by accidental spills from both LH_2 aircraft and fixed tank storage at airports.

In Chapter 5 the results of a case study examining the potential consequences of a large LH_2 leak occurring from an LH_2 storage tank at an engine test facility are examined (based upon the Reaction Engines TF1 facility design). With a capacity of 4.5 tonnes the LH_2 storage tank examined is of a similar size to that which will be required for an LH_2 aircraft. It also represents a natural stepping-stone for analysis on the way to the larger LH_2 storage tanks that will be required for airports operating LH_2 aircraft.

Chapter 6 considers a serious aircraft crash scenario resulting in an instantaneous spill of the entire fuel tank contents and a large pool fire. A comparison is made between the hazard consequences produced for LH_2, LNG and Jet A fuels.

Chapter 7 examines the consequences of the immediate ignition of an instantaneous fuel spill occurring during aircraft refuelling operations resulting in a pool fire. A comparison is made between the fire behaviour and thermal hazard produced for instantaneous spills of LH_2 and Jet A, ranging in size from 100 L to 5000 L. The effect of the pool fire on the aircraft was also investigated.

Chapter 8 considers the consequences of the delayed ignition of an instantaneous LH_2 fuel spill occurring during aircraft refuelling operations resulting in flammable cloud dispersion and a flash fire or explosion. The influence of a representative LH_2 aircraft geometry was included in the simulations. The effect of different leak locations, wind directions and leak duration upon flammable cloud dispersion behaviour was examined.

Chapter 9 examines the consequences of the immediate ignition of a continuous fuel spill either from an aircraft (due to a hole in a tank or leak from an engine fuel line) or an airport fuel storage tank resulting in a pool fire.

Finally, Chapter 10 discusses some of the implications of the research and identifies knowledge gaps, challenges and areas for future work, whilst Chapter 11 presents the main conclusions of the study.

2 Literature Review - Previous Studies of LH_2 Hazards

2.1 Overview of LH_2 Hazards

Figure 2.1 illustrates the potential hazards and harmful effects that could result from an accidental leak or spill of liquid hydrogen.

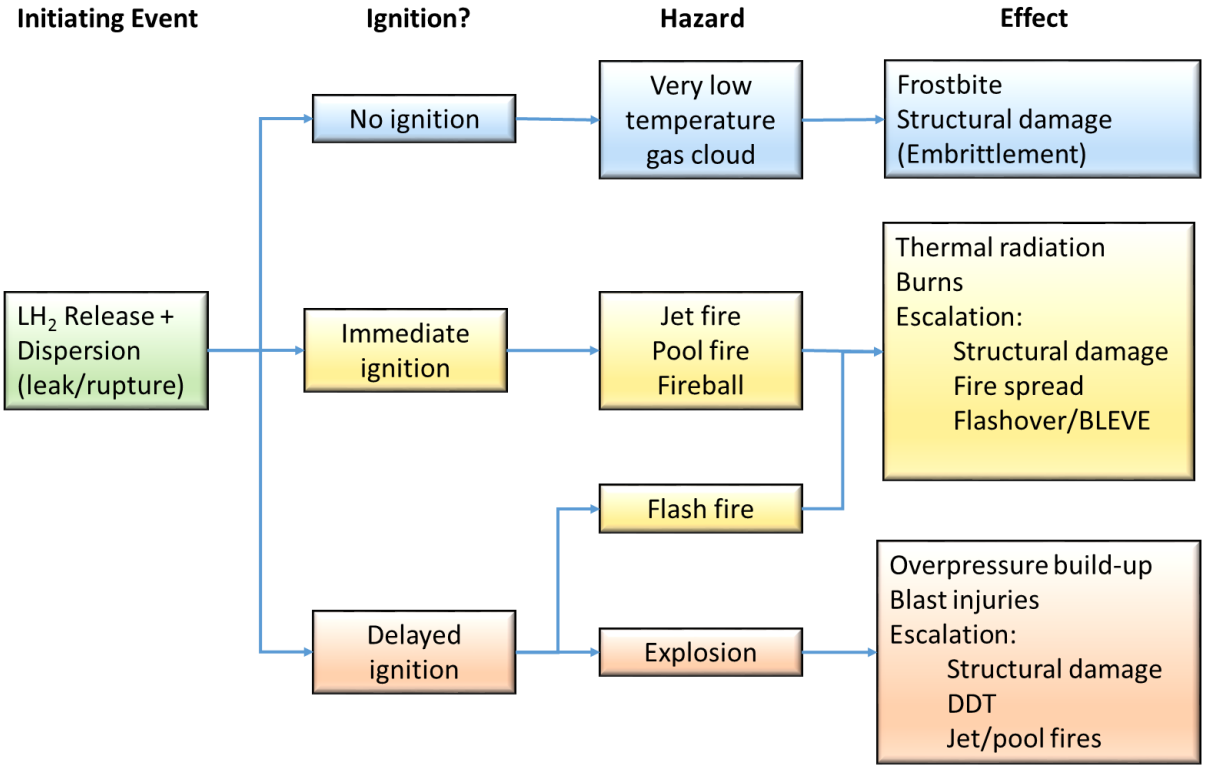

Fig. 2.1 – Hazards and effects that could results from an accidental LH_2 leak or spill.

Following a LH_2 release due to an accidental leak or rupture (initiating event) a range of different hazards and consequent effects can occur depending upon the nature of the release and as to whether or when an ignition source is introduced (Rigas and Amyotte [2012]):

- *No ignition - Low temperature gas cloud*: Even if no ignition source is present, the cold gas cloud released could still represent a low temperature hazard that is capable of causing harm via frostbite and lung injuries/fatalities to any people and/or structural damage to unprotected equipment that it comes into contact with.

- *Immediate ignition – Fire*: In the event of an immediate ignition of the LH_2 release the hydrogen will burn as a fire, emitting thermal radiation and causing harm via burn injuries/fatalities, structural damage and incident escalation. The type of fire behaviour exhibited will be dependent upon the nature of the release. If the LH_2 leak forms a liquid spill pool on the ground, it can vaporise to produce a flammable hydrogen-air gas mixture above the pool, which if immediately ignited will then burn as a pool fire (burning gas flame fed by a vaporising liquid pool). If the release of vaporised hydrogen gas is very rapid and of short duration (driven by buoyancy or momentum) it can burn as a fireball - a rapidly rising expanding ball of flame. If the LH_2 leak is released as an atomized liquid or gaseous jet, which is then ignited it will burn as a jet fire.

- *Delayed ignition - Flash Fire\Explosion*: In this case the hydrogen gas release will disperse and travel away from the spill point forming a flammable gas cloud. If it should then encounter a

remote ignition source then the cloud could ignite resulting in a flash fire causing burn injuries/fatalities or (if in a congested or confined area) a vapour cloud explosion causing harm via blast injuries/fatalities, structural damage and incident escalation. The flame can also propagate back to the LH_2 pool producing a pool fire.

For LH_2 stored in a tank the initiating LH_2 release event can also take the form of a catastrophic rupture, resulting in a boiling liquid expanding vapour explosion (BLEVE). Such an explosion can occur for liquids, such as LH_2 when, they are stored at temperatures above their boiling point at atmospheric pressure, resulting in a rapid expansion of the contents if the vessel should fail. Tank BLEVEs can be triggered via heating of the tank by an external fire, a violent impact, failure of pressure relief valve, or a fault in the vessel insulation. The hazardous consequences of a tank BLEVE are manifested through the generation of a pressure wave, the production of missiles and fragments as the vessel is torn apart and if ignited, a fireball (Rigas and Amyotte [2012], Ustolin et al. [2020]).

Previous research studies that have been carried out on LH_2 hazards will be considered in the following sections.

2.2 LH_2 Pool Spills and Flammable Cloud Dispersion Behaviour

Unfortunately, the existing experimental test data on the behaviour of large scale LH_2 spills and the flammable clouds formed is relatively limited. In the 1960s, Arthur D. Little [1960] carried out an experimental programme, for the United States Airforce, to determine the potential hazards associated with the handling and storage of LH_2. Instrumentation of the tests was limited, with no measurements made of hydrogen concentration or temperature in the gas cloud formed. Instantaneous LH_2 ground spills of 1.25, 32, 600 and 5000 gallons (4.7, 121, 2271 and 18,927 L) formed by emptying an insulated storage vessel were examined. In terms of the larger scale releases, the 600 gallon (2271 L) LH_2 spill demonstrated the effects of cloud dispersal, at a wind velocity of 20 mph (8.9 m/s), with the visible cloud dispersing downwind along the ground for 8 seconds, before it was deliberately ignited. The largest 5000 gallon (18,927 L) LH_2 spill was ignited immediately, resulting in a pool fire, so no cloud dispersion behaviour was observed for this case. Some experiments, representing a LH_2 pipeline rupture, using a more continuous release of LH_2 (e.g. 16 l/min [1.1 kg/s] for 1 min, wind speed 7.6 m/s) were also performed. In this case the visible cloud, formed by the LH_2 spill, was observed to remain close to the ground over a distance of 600 feet (183 m) from the point of release.

A series of large-scale experimental liquid hydrogen dispersion tests were carried out by NASA at the White Sands Test Facility, New Mexico, during the 1980s (Witcofski and Chirivella [1984], Chirivella and Witcofski, [1986]). The tests were intended to provide information on large, rapid LH_2 spills and the associated flammable hydrogen-air cloud dispersion behaviour that might result as a consequence of the rupture of a large scale LH_2 storage facility. The experiments consisted of large ground spills of LH_2 of up to 5.7 m3 (~400 kg) with spill durations varying between 35 and 120s. The results of these experiments suggested that rapid liquid hydrogen spills, of the type corresponding to the rupture of a storage tank, produced large flammable gas clouds which would travel along the ground for a distance of 50-100 m, before rising off the ground at an angle and dispersing below the flammable limit. In contrast, slower spills, of the type corresponding to a ruptured liquid hydrogen pipeline, were characterised by lower levels of dispersion and flammable clouds that exhibited prolonged ground level travel.

Some large scale near ground release LH_2 releases between two buildings were conducted by Battelle/BAM for the Euro-Quebec-Hydro-Hydrogen-Pilot-Project in the 1990s (Statharas et al. [2000]). The buildings each of length 49.5 m and width 13.4 m had a separation of 23.9 m. LH_2 was released into a pan of diameter 0.4 m and 0.1 m high, located next to end of one of the buildings, from which it could spill onto a 2 m by 2 m aluminium plate, situated 0.2 m above the ground. A total of six experiments were carried out. The resulting hydrogen gas concentrations were monitored by sensors positioned at several locations. Unfortunately, the release rate used in each test was uncertain due to lack of metering and could only be estimated to average approximately 0.4 kg/s over a period of around 2 minutes. There were also significant uncertainties over the prevailing wind conditions for each test and their effect upon the flammable clouds formed.

A series of large scale LH_2 release tests were also carried out by the Health and Safety Laboratory (HSE), at Buxton, UK, to investigate the hazards associated with liquid spills of LH_2 (Royle and Willoughby [2014]). The tests were intended to replicate the failure of a LH_2 hose line during a tanker refuelling operation. The tests were carried out on a 32 m diameter concreted pad. The LH_2 (stored at 2 bara) was released at 60 L/min (0.071 kg/s) via an outlet orifice diameter 26.3 mm. The hydrogen gas cloud formed passed through an array of 30 temperature thermocouples (used to infer hydrogen concentration) which could be moved to align with the prevailing wind direction. Ground thermocouples were also used to characterise the spreading behaviour of the LH_2 pool formed. The hydrogen dispersion behaviour and formation of liquid pool on the ground was investigated for different orientations of spill. The results for four LH_2 unignited tests were reported - two horizontal releases, one located at ground level, the other at a height of 0.86 m, and for two releases directed vertically downwards from a spill point positioned 0.1 m above the ground. The test results suggested the flammable gas cloud formed extended at least 9 m downwind of the release point. The cloud dispersion was also extremely sensitive to wind speed, with clouds becoming buoyant at wind speeds of 3 m/s or less and staying close to the ground at wind speeds greater than 5 m/s. A LH_2 pool was formed for the downward release once the substrate was sufficiently cooled. However, the horizontal release of LH_2 at 60 l/min, 0.86 m above ground resulted in total evaporation, with no evidence of rainout or an LH_2 pool being formed.

To address some of the main gaps in knowledge the EU funded PRESHLY (Prenormative Research for Safe Use of Liquid Hydrogen) project (2018 - 2021) has recently carried out an experimental programme looking at the LH_2 and cryogenic GH_2 release and mixing, ignition and combustion phenomena that were judged to have the highest research priorities (PRESLHY [2021], Jordan et al. [2019]). The hydrogen release and mixing experiments performed included:

- *DisCha facility* - cryogenic GH_2 blowdown release behaviour through different size nozzles from a small-scale cylindrical vessel (diameter 0.16 m, height 0.14 m) at a temperature of 80 K and elevated pressures up to 200 bar. Pressure, temperature, and concentration time histories were obtained.

- *Cryostat facility* - steady releases of LH_2 (30 K at pressures up to 5 bar) from a 225 L vessel via a 4 mm diameter nozzle. . Pressure, temperature, and concentration time histories were obtained.

- LH_2 *pool facility* - LH_2 release into a 0.5 m x 0.5 x 0.2 m basin filled (to a height of 0.1 m) with different ground substrate materials of concrete, gravel, sand and water, instrumented with thermocouples, hydrogen concentration sensors and monitoring the mass of LH_2 in the basin which was positioned on top of some scales. In each test the pool was usually filled with LH_2 three times. The evaporation rate for the gravel substrate was observed to be significantly higher than for concrete or sand. Ventilation rates across the pool up to 5 m/s did not significantly enhance the evaporation rate.

- *Steady* LH_2 *release (20 K, 1 barg) trials* - carried out by HSL investigating cloud dispersion behaviour LH_2 vaporisation and pool formation for elevated release locations (0.5 m and 1.5 m high, horizontal). The test setup was similar to that used in previous trails carried out by HSL described above. The tests showed that no rainout occurred for any of the above ground LH_2 releases.

CFD modelling of large-scale LH_2 spills has primarily focused on model validation and comparisons with the available experimental data. Middha et al. [2011] used the FLACS CFD (pool) model to simulate LH_2 pool spread and gas cloud dispersion behaviour for the NASA White Sands Experiments - Test 6 (as reported in [8]). The predicted hydrogen concentration results (assuming stable atmospheric conditions) were found to be in good agreement with the peak concentrations observed at several instrument tower sensor locations in the test. However, they also found that the predicted hydrogen concentration was strongly underestimated at one of the sensor locations (tower 7 – height 9.4 m). To improve agreement with experiment, a “meandering” wind model (Hanna et. al. [2004], Hansen et al. [2010]) was used in Midda et al. [2011] to simulate wind gust effects. The FLACS pool model was also used to predict the variation of the LH_2 pool radius and evaporation rate. On the basis of their study, the authors concluded that the FLACS pool model provides an efficient and accurate tool for investigating accidental release scenarios involving cryogenic liquids such as LH_2.

Ichard et al. [2012] also used FLACS to simulate liquid hydrogen releases for two of the test performed at HSL Buxton, UK, in 2010: Test 6 - a vertical downward release 100 mm above the ground and Test 7 - a horizontal release 860 mm above the ground. In order to better represent two-phase (gas/liquid) flow behaviour they used a Homogeneous Equilibrium Model (HEM) which they implemented in FLACS, assuming both phases were in local thermal and kinematic equilibrium (this effectively treats inter-phase transport as if it occurs at an infinitely fast rate). In the HSL tests modelled, the LH_2 (stored at 2 bara) was released at 60 L/min (0.071 kg/s) via an outlet orifice diameter 26.3 mm. In order to account for uncertainty in LH_2 release source term (i.e. the fraction of liquid flashing to vapour) five different gas mass fractions were modelled at the leak outlet. The source term best matching the experimental release behaviour in Test 7 was identified (corresponding to a gas mass fraction at the outlet of 0.65). For Test 6 the FLACS Pool model was used to simulate the spread and vaporisation of LH_2 on the ground. The effect of including or neglecting O2 and N2 condensation was also examined. The results suggested that the process of air condensation could be neglected for Test 7 but could have a significant effect on the temperature field for Test 6 (i.e. for a release close to the ground) releasing energy and causing the hydrogen gas cloud to become more buoyant and reach higher altitudes.

The ADREA-HF CFD code has been applied to model the BAM, NASA WSTF and HSL experimental LH_2 spill tests. Statharas et al. [2000] modelled BAM experimental test 5. They found that ground heating had a strong effect upon the dispersion of the LH_2 pool and that dispersion of the gas cloud exhibited dense gas behaviour close to the spill and significant buoyant behaviour further away. They also noted wind direction had a significant effect upon the cloud dispersion behaviour due to the shielding effect of the surrounding buildings. Venetsanos and Bartzis [2007] applied ADREA-HF to model NASA test 6. They found that modelling LH_2 source as a downward two-phase jet, with a pond fence, and contact heat transfer to the ground produced the best agreement with experiment. However, they found that gas concentrations were overestimated at lower levels and underestimated at higher levels and that the model was unable to reproduce the sudden changes in cloud structure observed experimentally or the high concentration levels measured at tower 7.

Giannissi et al. [2014] used ADREA-HF to simulate HSL LH_2 spill tests 5, 6 and 7, examining the effect of atmospheric humidity, and two phase models - HEM (no slip) and NHEM (with slip so two phases can have different velocities) - upon gas dispersion behaviour. They concluded that simulations including both humidity and slip effect produced the results that were in better agreement with experiment. In a later paper, Giannissi and Venetsanos [2018] compared the results obtained for Test 7 with and without sub-models for water vapour, nitrogen and oxygen phases and no slip, algebraic slip and momentum slip models. Their results indicated that the buoyancy of the gas cloud was increased and the downwind flammable distance to the LFL was reduced significantly (by as much as 35%) when the phase change effects of water vapour (and to a lesser extent the components of air) were taken into account.

Verfondern and Dienhart [1997, 2007] describe the LAuV code, developed by FZJ, which can be used to simulate the spreading and vaporisation behaviour of a LH_2 pool by solving the 2-D shallow-layer equations for pool height and velocity. LAuV was used to simulate the LH_2 pool formed for NASA Test 6 predicting a maximum pool radius of 6.5m – around double that inferred from the experimental test results (although the predicted vaporisation time of 43.5 s was very close to that estimated from the test). The discrepancy was attributed to the effect of percolation of liquid into the sand, furrowing of the test site increasing surface contact area and the LH_2 spill splashing from a deflection plate before hitting the ground.

Jin, Liu and co-workers have employed a model for predicting LH_2 spill dispersion behaviour, using ANSYS FLUENT CFD. Both the liquid and gas phases of hydrogen are represented and assumed to be in thermal equilibrium. The mass transfer between the two phases is described using Lee's model, with the mass transfer coefficient "tuned"(to a value of 0.25) using the WSFT NASA-6 experimental test results. The model was validated using the large-scale NASA WSTF Test 6 experiment and found to produce acceptable agreement. They have subsequently published a series of papers modelling the flammable gas clouds formed by liquid hydrogen spills and examining the effect of a range of different factors including: ground temperature, wind speed, and ambient temperature (Jin et al. [2017a]); the evolution of the flammable cloud with time and role of turbulent diffusion (Jin et al. [2017b]); different LH_2 source conditions - spill amount, duration, and liquid mass fraction (Liu et al. [2018]); air humidity (Liu et al. [2019a]); the effect of dikes positioned around the LH_2 spill (Liu et al. [2019b]); the effect of continuous LH_2 spills (Liu et al. [2019c]); and dilution of the flammable vapor cloud by wind and turbulence (Liu et al. [2020]).

Shao et al. [2018] have also used ANSYS FLUENT CFD to investigate the dispersion history of flammable clouds formed by LH_2 spills under different weather conditions. Their model employed a Non-Homogeneous Equilibrium Model (NHEM) approach to represent the two-phase hydrogen release. Mass transfer between the two phases was again described using Lee's model and they adopted mass transfer coefficient value of 0.25 used by Jin et al. [2017a]. However, in this case the LH_2 liquid phase was represented using a particle slip model, with an estimated diameter of 10 µm. The model was validated using the WSFT NASA-6 experimental test results. It was then used to examine the effect of ambient temperature, wind speed and atmospheric pressure upon dispersion behaviour. They found that increasing wind speed enhanced the dispersion of the cloud, but was impeded by increasing atmospheric pressure.

Jäkel et al. [2019] have also developed a CFD model (implemented in the ANSYS-CFD), for liquid hydrogen releases and the resulting gas cloud dispersion behaviour, which they validated against the NASA WSTF (Test 6) and HSL (Tests 5, 6, 7 and 10) experimental tests. A HEM approach was adopted to model the liquid and gas hydrogen phases. Surface heat transfer due to vaporization of liquid hydrogen was modelled using correlations for the nucleate, transition and film boiling regimes. The effect of water vapour condensation was also considered and found to slightly increase the buoyancy of the resulting hydrogen gas cloud. On the basis of their results they concluded that the predictions from their model (LH_2 pool size and hydrogen and temperature distributions) were qualitatively consistent with the available experimental test data and modelling results obtained by other researchers. However, there were also significant quantitative deviations which they attributed to uncertainties in relation to the specification of ground and atmospheric boundary conditions in the available experimental tests.

Hansen [2020] has recently shown that LH_2 releases can exhibit dense gas behaviour under certain conditions. The FLACS CFD code was used to make a comparison between the LH_2 and LNG hazard distances predicted for horizontal and downward releases from a pressurised tank (5 barg) through a 10 mm diameter instrument connection, in a 2 m/s wind. As a result of dense gas behaviour, the LFL-distances found for the LH_2 releases were significantly longer than for comparable LNG releases. In the case of the horizontal release the hazardous distance to the 4% LFL was 122 m - five times that found for LNG, whilst for the downward release it was 67 m – double that found for LNG.

2.3 LH_2 Fire Hazards

Relatively few research studies have directly looked at LH_2 fire hazards. In the 1960s, Arthur D. Little [1960] carried out an experimental programme, for the United States Airforce, to determine the potential hazards associated with the handling and storage of LH_2, including a number of tests igniting LH_2 spills that resulted in pool fires. Note that the film taken of the spill tests suggests that fuel spills were made into a pit which constrained their area. The ignition of an LH_2 spill test of 32 US Gallons (121 L) triggered a pool fire that emitted a low level of thermal radiation and evaporated in approximately 30 seconds. The results were also compared with 32-gallon spill tests for JP4 and gasoline to examine differences in the thermal radiation hazard. The thermal flux density was found to be 12 times that observed for the LH_2 pool flame. The JP4 and gasoline pool fires respectively took 7 minutes and 5 minutes to evaporate. A larger scale 5000-gallon (18,927 L) spill test resulted in a LH_2 pool fire with a flame height of around 150 feet (46 m). The study concluded that thermal radiation was the primary hazard resulting from large-scale LH_2 spills. The level of thermal radiation produced by LH_2 pool fires was less than that found for both JP4 and gasoline. However, hydrogen's low ignition energy and wide flammability limits would also make the ignition of a LH_2 spill more likely.

Zabetakis and Burgess [1961] carried out some small-scale experimental tests igniting the hydrogen-air mixtures produced by transient LH_2 spills of varying amounts up to 90 L onto the ground. They observed the development of the resulting flames above the LH_2 spill which initially formed mushroom shaped fireballs that then evolved into detached hemi-spheres, floating upwards at rates of approximately 20 feet per second (6 m/s). The effect of different ignition delays on the development of flame and radiation heat flux produced was also examined and found to have a significant impact on both the total radiant energy released and the release rate.

A series of large scale LH_2 release tests were also carried out by Health and Safety Laboratory, at Buxton, UK, to investigate the hazards associated with ignited releases of LH_2 (Royle and Willoughby

[2014]). The tests were intended to replicate the full-bore failure of a LH_2 hose line during a tanker refuelling operation. The tests were carried out on a 32 m diameter concreted pad. The LH_2 (stored at 2 bara) was released at 60 L/min (0.071 kg/s) via an outlet orifice diameter 26.3 mm. In the ignition tests, LH_2 was released horizontally from the hose outlet along the ground. Four chemical igniters were used, located at different positions and distances from the outlet. The radiation heat flux was monitored by six fast response radiometers, mounted on poles located at different distances downwind of and parallel to the release point, at a height of 1.8 m. Once ignited the flame initially typically burnt back from the ignition source, through the horizontal flammable gas cloud to the release point, to then produce a jet fire, with an estimated flame length of approximately 5 m, and with a maximum heat flux of around 10 kW/m^2 at a distance of 6.5 m parallel to the flame.

Two concurrent LH_2 aircraft crash safety studies carried out for NASA in the early 1980s by Arthur D. Little [1982] and Lockheed [Brewer et al., 1981] concluded that, following a crash, a LH_2 pool fire would be the main hazardous outcome that would need to be considered. In the Arthur D. Little study [1982], the LH_2 pool fire hazard was characterised by using a simplified analytical model of cryogenic liquid spill behaviour developed by Raj [1981], along with flame height correlation, derived by Thomas [1963] (based upon data obtained for wood crib fires) was used to estimate the resulting (time-averaged) spill pool diameter, fire duration and flame height as a function of the instantaneously released liquid spill volume. They also calculated the flame emissivity, thermal radiative fraction and maximum heat flux that would be delivered to an aircraft fuselage immersed in the resulting pool fire. Their results suggested that although the pool fires resulting from LH_2 spills would have a taller flame, they would have a smaller diameter with a lower flame emissivity (except for very large spills), smaller radiation hazard distance and burn out more rapidly. Similarly, in the parallel study carried out by Lockheed [Brewer et al., 1981] it was concluded that even if an LH_2 spill were to be ignited the resulting pool fire would only be of very short duration, and so would have insufficient time to heat the aircraft fuselage to the point where it might be compromised. Hence, they suggested that passengers could stay safely aboard the aircraft until the LH_2 pool fire burned out.

In terms of radiation there is a significant difference in the behaviour shown between LH_2 and hydrocarbon fuels. The main combustion product of burning hydrogen is water vapour. Hence the thermal radiation from hydrogen flames is mainly produced by excited water molecules. However, when hydrocarbon fuels burn most of the thermal radiation is produced by carbon-based species, particularly soot which are more efficient thermal radiators (approximately blackbody). Consequently, although hydrogen has a higher flame temperature than hydrocarbon fuels, a hydrogen fire releases a smaller fraction of its heat as thermal radiation. A range of different values for the thermal radiation fraction (fraction of total combustion heat released as radiation) from hydrogen flames have been proposed in different studies. After reviewing the available data Arthur D Little [1982] suggested that the thermal radiation fraction for a hydrogen flame was in the range 8.5-25%, whereas for methane it was 10.3-33% and for kerosene (Jet A) it was 30-40%. Similarly a comparison given in Beyler [2016] indicated the value of the radiative fraction for a hydrogen-air flame was around 20%, whereas for a hydrocarbon fuel like kerosene (Jet A) it was around 40%. Based upon the studies carried out by Zabetakis and Burgess [1961], Hord [1978] suggested that the thermal energy radiated from a hydrogen flame was between 17 to 25%, versus 23 to 33% for methane and 30 to 42% for gasoline. However, Klebanoff et al. [2017] estimated that radiant fraction would be only 4.5% for a hydrogen pool fire resulting from a spill of 1200 kg of LH_2, but 10% (i.e. 2.2 times the radiant energy) for a methane pool fire burning an energy equivalent amount of methane (3199 kg). By assuming a 5 kW/m^2 threshold for thermal radiation injury to skin, they also calculated that the closest safe approach to a hydrogen fire burning 1200 kg LH_2 would be around 19 m, whilst for a methane fire burning the energy equivalent amount of LCH4 (3199 kg) it would be around 58 m – three times as far.

Rather than emitting radiation over a broad spectrum, a hydrogen-air flame behaves as a band emitter. Unlike hydrocarbon flames, hydrogen flames emit significant amounts of ultraviolet radiation from excited OH* molecules. However, to produce an equivalent level of damage the dose of ultraviolet radiation needs to be around double that of infrared radiation [LaChance et. al, 2011]. Hence it is the radiation emitted by the excited water molecules in the infrared region that dominate, with strong emission bands located at around 1800, 2700 and 6300 nm [Schefer et al., 2009].

Since the radiation produced by a hydrogen flame is emitted by excited water molecules it can also be readily absorbed by the water vapour present in the surrounding atmosphere. This can significantly reduce the amount of radiant heat transmitted. Thus, for example, Klebanoff et al. [2017] estimated that

approximately 30% of the thermal radiation produced by a hydrogen fire would be blocked by atmospheric water vapour over a distance of 4.7 m.

While hydrogen-air flames are often thought of as being invisible, Schefer et al. [2009] have suggested that although the visible emissions from hydrogen flames are significantly weaker than for hydrocarbon flames, they would nonetheless, in most cases, still be visible at lower light levels.

2.4 LH_2 Explosion Hazards

The experimental test programme carried out for the United States Airforce by Arthur D. Little [1960] also looked at the potential explosion hazards that might result from the delayed ignition of an LH_2 spill. In the initial small-scale tests, 1.25 US gallons (5.7 L) of LH_2 was spilled into a pit and the vapour ignited with a spark source, varying the spark time delay and height of the source above the spill, to see if a detonation would occur. Fifty tests of this type were performed. No detonations were observed, and the resulting explosion overpressures (if any) were very small. Tests carried out for 32 gallon (121 L) spills of LH_2 and using a strong (explosive charge) ignition source also produced similar results with no detonations observed. On the basis of the test work, it was concluded that the ignition of even sizeable LH_2 spills would not result in a detonation occurring. Note however that these tests did not consider the effect of confinement or congestion upon the ignited vapour cloud. Under confined and congested conditions, the propagation of the flame front for hydrogen-air mixtures can, under some circumstances, become accelerated by the generation of turbulence by confinement and/or obstructions producing a feedback loop between the flame and the unburnt fuel/air mixture ahead such that it undergoes a deflagration to detonation (DDT) event. Solid air and liquid hydrogen mixtures were also tested. It was found that these would detonate if the oxygen level was enriched to at least 40%.

Zabetakis and Burgess [1961] carried out some small-scale experimental tests igniting the hydrogen-air mixtures produced by transient LH_2 spills between 16 and 90 L onto the ground and measuring the associated explosion overpressure produced. They found that the maximum explosion overpressure generated was relatively small and inversely related to the square of the distance, for distances from the spill between 80 and 160 feet (24 -49 m).

A series of large scale LH_2 release tests were also carried out by Health and Safety Laboratory, at Buxton, UK, to investigate the hazards associated with ignited releases of LH_2 [Hall, 2014]. The tests were intended to replicate the full-bore failure of a LH_2 hose line during a tanker refuelling operation. The tests were carried out on a 32 m diameter concreted pad. The LH_2 (stored at 2 bara) was released at 60 L/min (0.071 kg/s) via an outlet orifice diameter 26.3 mm. In the ignition tests, LH_2 was released horizontally from the hose outlet along the ground. Four chemical igniters were used, located at different positions and distances from the outlet. The radiation heat flux was monitored by six fast response radiometers, mounted on poles located at different distances downwind of and parallel to the release point, at a height of 1.8 m. Once ignited the flame initially typically burnt back from the ignition source, through the horizontal flammable gas cloud to the release point, to then produce a jet fire. However, in one test a secondary explosion also occurred emanating from the LH_2 pool formed at the release point, creating an 8 m diameter hemispherical fireball and producing a maximum heat flux of 120 kW/m^2 at a distance of 7.1 m from the release point (possibly due to generation of solid deposits and oxygen enrichment effects).

The PRESHLY [2021] project has recently carried out an experimental programme for the LH_2 and cryogenic GH_2 combustion phenomena that were judged to have the highest research priorities to allow their safe daily use in urban areas. The experiments performed included tests for a LH_2 pool facility with LH_2 released into a 0.5 m x 0.5 m x 0.2 m basin and then introducing an ignition source above the LH_2 pool and varying the substrate type (concrete, sand, water and gravel) and height of the ignition source. Varying degrees of damage were caused to the facility. Whilst the pool in the test using water was virtually undamaged (minor burning), some of the sand and concrete tests resulted in more significant damage with ripping of the pool insulation. However, the ignition of the LH_2 pool with the gravel substrate produced a “highly energetic event” resulting in the complete destruction of the test facility. The results suggest that repeated spills of LH_2 on gravel beds (but not concrete or sand) might condense and freeze oxygen from the surrounding air and then be made to detonate. Combustion tube experiments were also carried out to determine the FA and DDT criteria for cryogenic hydrogen at temperatures down to 80 K and for varying blockage ratios. The results suggest that greater pressure loads can be generated

for cryogenic GH_2 mixtures than are found at 300 K for tests using the same volume, hydrogen concentration and blockage ratio, due to density effects. They also showed that the run-up required for a DDT was reduced for cryogenic hydrogen mixtures.

2.5 LH_2 Aircraft and Airport Safety – Previous Studies

2.5.1 Aircraft Safety

Two major studies of LH_2 aircraft safety and crash hazards were carried out in the early 1980s for NASA by Arthur D Little [1982] and the Lockheed Corporation [Brewer, 1981]. The motivation for the development of these LH_2 aircraft designs and safety studies was the 1970s oil crisis, with the intention being to reduce the USA's reliance on oil as fuel for aviation, by using LH_2 as alternative fuel source with a more secure supply (ironically derived from coal!)

In their study, Arthur D. Little [1982] examined the relative crash fire hazards associated with LH_2 fuelled aircraft in comparison with liquid methane (LCH_4) and conventional jet fuel (for a 400 passenger reference design aircraft). Four different aircraft crash scenarios (specified by NASA) were considered:

- Scenario 1: A non-normal landing or ground accident resulting in damage to the fuel system and/or the fuel system insulation allowing fuel to leak out of a punctured tank or fuel line.
- Scenario 2: Crash take-off or landing resulting in damage causing a massive release of fuel after the aircraft comes to rest.
- Scenario 3: Crash take-off or landing resulting in damage causing a massive release of fuel before the aircraft comes to rest.
- Scenario 4: Catastrophic crash resulting in an explosion (maximum rate of energy release).

Pool fires were judged to be the most likely aircraft crash scenario hazard outcome, with a small leak (scenario 1) producing a steady pool fire, a massive leak (scenarios 2 and 3) producing an expanding circular pool fire, and a catastrophic leak (scenario 4) producing a fireball. They also identified the different fuel system failure modes that would result in a fuel release occurring and estimated fuel release rates for both fuel line and tank leaks.

In the case of LH_2 pool fires, a simplified analytical model of cryogenic liquid spill behaviour developed by Raj [1981], along with flame height correlation, derived by Thomas [1963] (based upon data obtained for wood crib fires) was used to estimate the resulting (time-averaged) spill pool diameter, fire duration and flame height as a function of the instantaneously released liquid spill volume. They also calculated the flame emissivity, thermal radiative fraction and maximum heat flux that would be delivered to an aircraft fuselage immersed in the resulting pool fire.

Based upon a review of the available thermal radiation data, they employed a simple analytical model to compare the fireball radiation hazard distance (assuming a 5 kW/m^2 burn injury threshold) as a function of the instantaneous liquid spill volume released for a catastrophic aircraft crash scenario. Their results suggested that the estimated fireball radiation hazard distance for a given spill volume of LH_2 would be less than that found for both LCH4 and conventional aviation jet fuel – due to the higher burning rate and lower flame emissivity of hydrogen. Their results also suggested that the pool fires resulting from LH_2 spills would produce a smaller radiation hazard distance, burn out more quickly and have a smaller diameter (although taller flame) with a lower flame emissivity (except for very large spills).

Based upon the results of their study they concluded that the aircraft crash fire hazards for the three different fuel types were not significantly different when compared in general, although LH_2 did offer some survival benefits in most cases where a rapid fire occurred. However, although it was

acknowledged that it could be a potential problem, they did not consider flammable gas cloud dispersion or accumulation of hydrogen in confined spaces and associated delayed ignition hazards (flash fire and explosion) in their study since it was assumed that, for the severe crash scenarios being examined, ignition was so likely that gas cloud dispersion with delayed ignition at large distances from the crash would not be a credible outcome.

In the parallel study carried out for NASA by Lockheed, Brewer et al. [1981], also made an assessment of the relative crash fire hazards associated with LH_2 fuelled aircraft in comparison with liquid methane (LCH4) and conventional jet fuel for the same four aircraft crash scenarios (which had been specified by NASA). On the basis of their analysis, they concluded that LH_2 was the safer fuel than the other alternatives, with both passengers and people and property in the surrounding area being exposed to less hazard, because:

- LH_2 fuel tanks being mounted in the fuselage and designed to withstand a higher pressure (in the reference design considered) were less likely to be damaged.

- In the event of a tank rupture a LH_2 spill would quickly evaporate, immediately becoming buoyant and dispersing rapidly into the atmosphere.

- Even if an LH_2 spill were to be ignited the resulting pool fire would be of very short duration, and so would have insufficient time to heat the aircraft fuselage to point where it might be compromised. Hence passengers could stay safely aboard the aircraft until the LH_2 pool fire burned out.

However, the authors also acknowledged that their study only represented a preliminary investigation and that many other cases and circumstances remained to be analysed. When modelling the dispersion of fuel spills, pool fires and thermal hazards to fuselage many of their computer program runs exhibited instabilities. Hence, they also concluded that the modelling tools used to carry out the analysis needed to be improved and the results validated against suitable experimental test data.

Interest in using LH_2 as a potential fuel for commercial aviation was renewed in the 1990s by a joint German-Russian consortium (and later as an EU project led by Airbus in the early 2000s) with the advent of the CRYOPLANE [2003] project. The project considered the conceptual basis that would be required to transition from using kerosene to hydrogen in aviation, including safety.

Due to the lower density and cryogenic nature of LH_2 they concluded that it was not suitable for storage in wing fuel tanks, as is done for conventional aircraft using kerosene. Alternative fuel tank arrangements were therefore considered instead. The CRYOPLANE aircraft design was based on a modification of a twin-engine Airbus A310, with a total fuel load of 17 t or 240 m^3 LH_2 stored in four LH_2 tanks (two large and two small) located on top of the fuselage. This design, locating the fuel tanks above the fuselage, was intended to offer improved safety in the event of an LH_2 leak since it was argued that the release would rapidly vaporise and rise upwards and hence not pose a threat to the passengers situated below. It was also recognised that the liquid storage system used onboard the aircraft would need to be able to cope with the pressure fluctuations that would occur during flight.

The main aircraft safety aspects examined in the study were: disk burst; lightning strike; bird strike; emergency landing; fire protection and fuel system. It was concluded that, although LH_2 posed some specific safety challenges, the hydrogen fuelled aircraft designs examined in the study would be at least as safe as conventional kerosene aircraft.

The study also reviewed safety requirements for adaptation of airport infrastructure to use LH_2. It was recommended that the amount of hydrogen that could be released in the airport area be restricted to low levels at all times (e.g. through the use of shut-off valves) and that appropriate measures be used to confine potential accident consequences and prevent their escalation via domino effects (e.g. by employing appropriate safety distances).

A number of knowledge gaps were identified in the study which required further work including:

- the release of large amounts of liquid and gaseous hydrogen
- the formation and vaporization of large liquid pools

- the dispersion of large hydrogen clouds
- the likelihood of sufficiently large free clouds to detonate
- the results of damage to storage tanks (drop, fire, force, crush, shots etc.)
- the material embrittlement due to the low temperature in case of release
- the suitability of valves, connections, seals, materials etc. for cryogen temperature
- the accumulation of oxygen inside the fuel system

2.5.2 Airport Requirements

Brewer [1991] - Chapter 7 Airport Requirements, outlined the airport requirements and infrastructure that would need to be put in place to support LH_2 fuelled commercial aircraft. The work used San Francisco International Airport (SFO) as a case study. In order to meet the estimated aircraft refuelling demand, it was suggested that a LH_2 liquefaction plant be located at SFO airport, consisting of four modules, each capable of producing 250 tons LH_2/day. The accompanying LH_2 storage facility consisted of five spherical LH_2 tanks 71 ft (21.6 m) in diameter each containing 1 million gallons (3,835 m^3) of LH_2. The LH_2 liquefaction plant and storage facility would need to be located so as to minimise the effects of accidents in other airport operations e.g. away from kerosene storage and runway centrelines [Schmidtchen et al., 1997]. The low storage temperature of LH_2 meant that the tank walls must be well insulated to prevent the surrounding air freezing and liquefying and potentially forming an oxygen rich mixture around the tank. For the SFO airport case study design the LH_2 was to be distributed around the airport via a vacuum insulated circular pipeline hydrant system, located in an open trench, covered by grills.

A similar conceptual design study for the conversion of airport infrastructure to service the operation of long-haul (400-passenger, 10,186 km range) LH_2 aircraft was carried out by Boeing [1976] for Chicago O'Hare airport. In this case the LH_2 liquefaction plant design was specified to produce a total of 726 tonnes of LH_2/day to meet the projected aircraft demand of 544 t/day. The LH_2 produced was stored in four, 23.2 m diameter, spherical LH_2 tanks at a nominal storage pressure of 110 kPa, and having a total capacity of 1452 tonnes,

The main airport safety requirements identified in the study were:

- sufficient separation of LH_2 facilities from roads, buildings, runways etc.
- adequate ventilation for enclosed areas to prevent flammable mixtures
- prevention of air ingress into LH_2 systems
- automatic sensing of malfunctions and system shutdown
- confinement and control of large LH_2 spills
- ignition source control

On the basis of the available data on where aircraft come to rest after crashes occurring during take-off and landing, a safety distance of 305 m (1000 ft) was specified between the runway centreline and the LH_2 liquefaction and storage facilities. This minimum clearance was judged to be sufficiently far from the runway so as to make aircraft direct impact or fire damage to the LH_2 facility highly unlikely. This safety distance of at least 305 m from the runway to LH_2 plant was also suggested by Sefain and Jones in the CRYOPLANE project (referenced in Haglind et al. [2006]). Based upon the results of the CRYOPLANE study, Schmidtchen et al. [1997] suggested that the safety distances specified in existing building regulations should also be sufficient for an LH_2 storage plant. They argued that since they are derived based on experience for LPG and hydrocarbon gases, they should be conservative when applied to hydrogen, since it does not travel along the ground to the same extent. However, this would seem to neglect the potential for the flammable hydrogen clouds formed by LH_2 spills to behave like a heavy gas under some circumstances, as well as the greater propensity for hydrogen to undergo a DDT event and detonate.

2.5.3 Aircraft Refuelling

After considering the different options, Brewer [1991] advocated that LH_2 aircraft be refuelled at gate positions located near to the terminals and be carried out in parallel to boarding/disembarkation of passengers, cleaning and maintenance operations in the same way as today's kerosene fuelled aircraft. During refuelling operations, the LH_2 aircraft fuel tank would be refuelled via the tail cone which would be connected to two hoses (one supplying LH_2 to the tank the other collecting GH_2 expelled from the tank), using a special refuelling vehicle, to the airport LH_2 supply located in a hydrant pit below the tail. To allow for the possibility of mechanical failure of a fuelling hose or adapter occurring during a LH_2 fuelling operation Brewer [1991] recommended that a zone of radius of 90 ft (27.4 m) around the tail cone should be kept spark free. It was also suggested that the aircraft cabin and cargo hold be maintained at a slight positive pressure to prevent hydrogen from any leak accumulating inside the aircraft.

Although there would appear to be little if any information currently available about the likelihood or consequences of LH_2 spills occurring during aircraft refuelling operations, studies have been made of Jet A-1 spills from aircraft. Jet A and Jet A-1 (a kerosene type fuel) is the main type of fuel that is currently used for civil aviation. Jet A is used in the United Sates, whilst Jet A-1 is used in the rest of the World. The main difference between the two is that Jet A-1 has a lower freezing point. It also contains a mandatory anti-static additive. Jet A-1 is five times heavier than air so any spills will be relatively slow to disperse.

The flashpoint of a combustible liquid is the lowest temperature at which a flammable vapour/air mixture exists at the surface of the liquid [Drysdale, 1998]. To be ignited the Jet A/A-1 liquid spilled has to be heated above its flashpoint with an ignition source present (or heated above the temperature where spontaneous combustion occurs). Jet A/A-1 has a much higher flashpoint than aviation gasoline (AVGAS). This has been a major factor in reducing fuelling risk because it significantly reduces the likelihood of ignition and speed of flame spread across a Jet A/A-1 spill.

Following a number of major fuel spills that occurred on the ramp at UK airports a study of the risk associated with aircraft refuelling operations involving Jet A-1 was carried out by WS Atkins for the UK Health and Safety Executive [Jones, 2000]. The study reviewed historical incidents which had resulted in fuel spills occurring during fuelling of an aircraft. It found that a number of major fuel spills of aviation Jet A/A-1 had occurred at airports around the world. The types of failure incident identified were:

- underwing couplings becoming detached from the aircraft;
- nozzle quick disconnects separating;
- vehicle impact damage to hydrant couplers;
- failure of hydrant couplers due to incorrect re-assembly after being modified;
- hose ruptures;
- failure of valve or poppet to close; and
- accidental disconnection of a coupling after the failure of an interlock

A fuel spill size frequency distribution was derived based upon historical information on Jet A-1 fuel spills that had occurred at UK airports. Several thousand spill events occurred over a couple of years, but only two ignitions were observed. Based upon this data they estimated the probability of ignition of an "average" Jet A/A-1 fuel spill event to be of the order of 10^{-4}. An assessment of fire and/or explosion risk from aircraft fuelling operations involving Jet A/A-1 was also made. The study identified failure events that could result in a fuel spill on the ramp occurring during aircraft fuelling, maintenance and defueling operations. It was also found that hydrant fuelling presented a higher risk that using a refueller vehicle.

In an emergency an isolation valve should close in 2 to 5 second (hydrant system supply) to limit the size of any spill. To reduce the risk of ignition fuelling zones are defined around the refuelling connection point with aircraft - 6 m (fuel zone), 15 m (limit to proximity of buildings) and 30 m (no testing of radar and HF equipment).

The main consequence of a Jet A/A-1 fuel spill was determined to be a pool fire if the spill were to be ignited. The resulting pool fire will release thick black toxic smoke.

The potential harmful effects were identified as:

- thermal radiation/engulfment from fire
- explosion overpressure (blast wave) and impact (flying missiles/fragments)
- smoke inhalation of toxic combustion products

2.6 Summary

On the basis of previous studies a number of knowledge gaps have been identified in relation to the behaviour and the extent of flammable gas clouds, pool fires and explosions resulting from LH_2 spills, particularly in the context of the aircraft and airport safety. An analysis has therefore been carried out in this report, using modelling studies performed with the FLACS-CFD code, to examine and predict the behaviour of accidental LH_2 releases in terms of the hazard effects (flammable gas clouds, pool fires, explosions) and safety challenges they could present for some representative accident scenarios (aircraft refuelling leak, crash landing, fuel tank storage leak) and see how these compare with the existing hazards posed by using conventional aviation fuel Jet A/A-1.

3 Methodology

3.1 The FLACS CFD Model

The numerical simulations were performed using the FLACS CFD model. FLACS was originally developed in the 1980 and 90s for use in the Oil and Gas industry. It provides capabilities for carrying out safety studies by simulating accident scenarios involving fluid flow behaviour in complex 3D geometries by modelling flammable gas hazard effects such as:

- Dispersion of flammable gases
- Gas explosions and blast waves
- Pool and jet fires

FLACS is a structured Cartesian grid, finite volume CFD code. The code solves the compressible conservation equations for mass, momentum, enthalpy, mass fraction of chemical species, turbulent kinetic energy and dissipation rate of turbulent kinetic energy [Gexcon, 2019]. The numerical treatment used in FLACS solver employs a second order scheme in space, and a first/second order in time. The pressure and velocity fields are coupled via the SIMPLE solution algorithm [Patankar, 1980]. A standard k-ε turbulence model is also utilised incorporating modifications for generation of turbulence behind sub-grid obstacles and turbulent wall functions.

FLACS employs the Porosity/Distributed Resistance method to model the turbulence generated by subgrid scale objects [Gexcon, 2019]. This allows for the efficient simulation of gas dispersion behaviour in complex geometries using relatively coarse numerical grids.

The convergence of solutions in FLACS is managed through the Courant-Friedrich-Levy (CFL) number [Gexcon, 2019]. An adaptive time step routine is used, with the time step adjusted to meet CFL number stability criteria based upon both the speed of sound (CFLC) and the fluid flow velocity (CFLV). Each time step length is selected so that both sound waves and the fluid may propagate only a limited distance, equal to the average control volume length multiplied by the CFLC/CFLV number.

3.2 FLACS Atmospheric Dispersion Modelling

The stability of the atmospheric boundary layer plays an important role in determining the level of turbulence and hence the resulting gas dispersion behaviour. In FLACS, the atmospheric stability is characterised by using the concept of the Pasquill-Gifford stability class (A to F) [Gexcon, 2019]. Here, Pasquill classes A-C correspond to unstable, D neutral, and E-F stable atmospheric conditions [Pasquill, 1961]. Under stable atmospheric conditions turbulent fluctuations and mixing behaviour are damped. Hence the level of dispersion is reduced, and high gas concentrations can persist over greater distances than is the case for unstable conditions.

Atmospheric boundary layer flows are modelled in FLACS by introducing profiles for wind velocity, temperature and turbulence on the flow inlet boundaries [Gexcon, 2019]. Buoyancy effects are accounted for by introducing additional source terms in the momentum and turbulence model equations.

The wind inlet velocity profiles are assumed to be logarithmic in form and are specified as a function of the Monin-Obukhov length, L (m), and the surface roughness length, z_0 (m):

$$U(z) = \frac{u_*}{\kappa}\left(\ln\left(\frac{z}{z_0}\right) - \psi_u(z)\right) \tag{3.1}$$

where κ is the von-Karman constant (-), z is the height above the ground (m), and u_* is the friction velocity (m/s):

$$u_* = \frac{U_0\,\kappa}{\ln\left(\frac{z_{ref}}{z_0}\right) - \psi_u(z_{ref})} \tag{3.2}$$

where U_0 is the wind velocity (m/s) at the reference height, z_{ref} (m). The stability function ψ_u (-) is a function of z and L:

$$\psi_u(z) = \begin{cases} 2\,\ln\left(\frac{1+\xi}{2}\right) + \ln\left(\frac{1+\xi^2}{2}\right) - 2\arctan(\xi) + \frac{\pi}{2} & \text{for } L < 0 \\ -17\left(1 - \exp\left(-0.29\,\frac{z}{L}\right)\right) & \text{for } L > 0 \end{cases} \tag{3.3}$$

and

$$\psi_u(z) = 0 \quad \text{for Pasquill Class D} \tag{3.4}$$

Where

$$\xi = \left(1 - \frac{16\,z}{L}\right)^{1/4} \tag{3.5}$$

In FLACS, the Monin-Obukhov length scale is estimated by relating it to the specified Pasquill-Gifford stability class using an approach based on work by Golder [1972]. By using a table relating the Pasquill Class to specific values for two parameters L_s (m) and z_s (m) the Monin-Obukhov length, L (m), can then be estimated using the relation:

$$\frac{1}{L} = \frac{1}{L_s}\log\frac{z_0}{z_s} \tag{3.6}$$

The temperature boundary profile is assumed to be uniform. The boundary profiles used for turbulent kinetic energy (k) and dissipation (ε) are taken from Han et al. [2000].

Further details of the wind boundary model implemented in FLACS can be found in [Gexcon, 2019]. The model has been tested for a wide variety of scenarios including buoyant and dense gas releases [Hanna, 2004; Hansen et al., 2010].

3.3 The FLACS Pool Model

The FLACS pool model [Gexcon, 2019] allows the deposition and spread of a pool of liquid from a spill onto the ground simulated and the release source term to the gas dispersion model to be calculated. The model was originally developed for use with LNG spills but has also been applied to liquid hydrogen releases [Middha, 2011; Ichard et al., 2012]. In the FLACS pool model the liquid (incompressible) and gaseous (compressible) states are modelled separately. Hence, the model does not consider or employ relations expressing the thermodynamic state or slip velocity between two phases co-existing in the same control volume. Treatment of the liquid phase is restricted to the pool. This acts as a source term to the gaseous phase via heat and mass transfer due evaporation from the pool.

The behaviour of the spreading liquid pool is approximated by solving the shallow-water equations on a two-dimensional Cartesian grid along the ground (identical to the x-y grid defined in FLACS) and assuming that the pool, properties (velocity, temperature etc.) are uniform across the height of the pool. The pool model solves conservation equations for mass (expressed in terms of spill height), momentum (spill velocity) and enthalpy for the pool. The spill height, h (m) is given by the equation:

$$\frac{\partial h}{\partial t} + \frac{\partial h u_i}{\partial x_i} = \frac{\dot{m}_L - \dot{m}_V}{\rho_l} \tag{3.7}$$

while the momentum equation is:

$$\frac{\partial h u_i}{\partial t} + u_j \frac{\partial h u_i}{\partial x_j} = F_{g,i} + F_{\tau,i} \tag{3.8}$$

where $\dot{m}_L$ is the liquid mass spill rate per unit area (kg/m^2/s), $\dot{m}_V$ is the mass vaporisation rate per unit area (kg/m^2/s), ρ_l is the density of the liquid (kg/m^3) and u_i is the velocity component of the spill (m/s) in direction x_i. The terms on the right-hand side of the momentum equation (m^2/s^2) represent the effects of gravity, and the shear stress between the pool and the substrate, respectively:

$$F_{g,i} = hg\Delta \frac{\partial (h+z)}{\partial x_i} \tag{3.9}$$

$$F_{\tau,i} = \frac{1}{8} f_f \, u_i \, |u_i| \tag{3.10}$$

where g is gravitational acceleration (m/s^2), Δ is a factor (-) that equals unity for pools on solid ground and $(1 - \rho_l/\rho_w)$ for pools on water, z is the elevation of the ground (m), which allows the effects of sloping terrains, obstacles and embankments to be accounted for, and f_f is a friction factor between the pool and substrate (-) which is calculated for either laminar or turbulent flow regimes (whichever is greater). Note that here, and in what follows "(-)" denotes an expression with dimensionless units. In the laminar regime the laminar friction factor is given by:

$$f_{f,lam} = \frac{64}{4\,\mathrm{Re}_h} \tag{3.11}$$

Where Re_h is the Reynolds number for the pool fluid flow (-). For turbulent flows the turbulent friction factor is given by:

$$f_{f,turb} = \begin{cases} \left\{-1.8 \log\left(\frac{1.72}{Re_h} + \left(\frac{\varepsilon_g}{12h}\right)^{1.11}\right\}^{-2} & \text{if } \frac{\varepsilon_g}{h} < 0.2 \\ 0.125 \left(\frac{\varepsilon_g}{h}\right)^{1/3} & \text{if } \frac{\varepsilon_g}{h} \geq 0.2 \end{cases} \tag{3.12}$$

Where ε_g is the ground roughness (m). The friction factor is then taken to be:

$$f_f = \max\left(f_{f,lam}, f_{f,turb}\right) \tag{3.13}$$

The transport equation for the specific enthalpy of the pool, θ (J/kg), is given by:

$$\frac{\partial h\theta}{\partial t} + u_i \frac{\partial h\theta}{\partial x_i} = \frac{\dot{m}_L}{\rho_l}\left(\theta_L - \theta\right) + \frac{1}{\rho_l}\left(\dot{q}_c + \dot{q}_{rad} + \dot{q}_g + \dot{q}_{evap}\right) \tag{3.14}$$

where θ_L is the liquid enthalpy (J/kg), the first term on the right hand side is the enthalpy due to spill, $\dot{q}_c$ is the convective heat transfer between the pool and the surrounding air (J/m²/s), $\dot{q}_{rad}$ is the radiative heat transfer from the surroundings and the sun (J/m²/s), $\dot{q}_g$ is the heat transfer to the pool from the substrate (J/m²/s), and $\dot{q}_{evap}$ is the heat loss due to evaporation (J/m²/s).

For pools formed of liquid hydrogen, heat transfer to the pool is typically dominated by heating from the substrate, given by:

$$\dot{q}_g = \left(\dot{q}_{g,cond}^3 + \dot{q}_{g,conv}^3\right)^{1/3} \tag{3.15}$$

where, for solid and rough ground and for all ground types under non-boiling conditions, the conductive heat transfer between the pool and substrate (W/m²) is given by:

$$\dot{q}_{g,cond} = \begin{cases} \dfrac{\lambda_g\left(T_g^{\infty} - T_p\right)\left(1.5 - 0.25\left(t - t_{gw}\right)\right)}{\sqrt{\pi\,\alpha_g}} & \text{if } t < 4s \\ \dfrac{\lambda_g\left(T_g^{\infty} - T_p\right)}{\sqrt{\pi\,\alpha_g\left(t - t_{gw}\right)}} & \text{if } t \geq 4s \end{cases} \tag{3.16}$$

where λ_g is the thermal conductivity of the ground substrate (W/m/K), T_g^{∞} is the ground temperature at an infinite depth below the pool - equal to the ground temperature before it is wetted by the pool (K), T_p is the pool temperature (K), t_{gw} is the point in time when the ground is wetted (s) and α_g is the thermal diffusivity of the ground (m²/s).

The convective heat transfer between the pool and substrate (W/m²) is given by:

$$\dot{q}_{g,conv} = 0.0133\, Re_h^{0.69}\, Pr_l^{0.4}\, \frac{\lambda_l}{h}\left(T_g^s - T_p\right) \tag{3.17}$$

where λ_l and Pr_l are the conductivity (W/m/K) and the Prandtl number of the pool liquid, Re_h is the local Reynolds number of the spreading pool, and T_g^s is the ground temperature at the surface (K) given by:

$$T_g^s = T_g^{\infty} + 2\frac{\dot{q}_s}{\lambda_g}\sqrt{\frac{\alpha_g\left(t - t_{gw}\right)}{\pi}} \tag{3.18}$$

The convective heat transfer between the pool and the surrounding air, is based on boundary layer theory and is given by:

$$\dot{q}_c = \frac{\rho\, C_\mu^{1/4} k^{1/2} c_p\,(T - T_p)}{T^+} \tag{3.19}$$

Where ρ is the gas density (kg/m3), C_μ is the constant in the k-ε turbulence model equation (-), k is the turbulent kinetic energy (m^2/s^2), c_p is the specific heat capacity at constant pressure of the gas (J/kg/K), T is the gas temperature (K), and T^+ is the dimensionless temperature (-) used in the model's wall functions, given by:

$$T^+ = \begin{cases} \Pr y^+ & \text{if } y^+ < E^+ \\ E^+ \Pr + \frac{Pr_T}{\kappa} \ln\left(\frac{y^+}{E^+}\right) & \text{if } y^+ \geq E^+ \end{cases} \tag{3.20}$$

Where Pr and Pr_T are respectively the laminar and turbulent Prandtl numbers for the gas (-), E^+ is the wall function constant (-) and y^+ is the dimensionless wall distance (-) given by:

$$y^+ = \frac{\rho\, C_\mu^{1/4} k^{1/2}\, y}{\mu} \tag{3.21}$$

Where y is the wall distance (m) and μ is the dynamic viscosity (Pa s).

The radiative heat transfer from both the surroundings and the sun to the pool is given by:

$$\dot{q}_{rad} = (1 - \omega)\dot{q}_{sun} + \varepsilon\sigma T^4 - \varepsilon_p \sigma T_p^4 \tag{3.22}$$

Where ω is the albedo of the pool (-), ε and ε_p are the emissivity of the gas and the pool (-), σ is the Stefan-Boltzmann constant (J/m^2/s/K^4) and $\dot{q}_{sun}$ is the radiative heat flux from the sun to the pool (J/m^2/s).

The mass vaporisation rate of liquid from the pool, $\dot{m}_v$ (kg/m^2/s) is determined by the convective and boiling mass transfer rates:

$$\dot{m}_v = \dot{m}_c + \dot{m}_{boil} \tag{3.23}$$

Where the convective mass transfer from the pool to the gas (kg/m^2/s) is given by:

$$\dot{m}_c = \frac{\rho\, C_\mu^{1/4} k^{1/2} \frac{p_0}{RT_p}(X - X_{sat})}{X^+} \tag{3.24}$$

X and X_{sat} are the mole fraction of the evaporated liquid in the air (mol/mol) and the saturated mole fraction of evaporated liquid in the air at the same temperature as the pool surface (mol/mol) and X^+ is given by:

$$X^+ = \begin{cases} \mathrm{Sc}\, y^+ & \text{if } y^+ < E^+ \\ E^+ \mathrm{Sc} + \frac{Sc_T}{\kappa} \ln\left(\frac{y^+}{E^+}\right) & \text{if } y^+ \geq E^+ \end{cases} \quad (3.25)$$

and *Sc* and Sc_T are respectively the laminar and turbulent Schmidt numbers for the gas (-).

The boiling mass transfer rate from the pool (kg/m^2/s) is given by:

$$\dot{m}_{boil} = \max\left\{\frac{\dot{q}_g + \dot{q}_c + \dot{q}_{rad}}{\Delta h_{fg}} - \dot{m}_c,\ 0\right\} \quad (3.26)$$

Where Δh_{fg} is the heat of evaporation of the pool liquid (J/kg)

The heat transfer due to evaporation from the pool (J/m^2/s) is then given by:

$$\dot{q}_{evap} = -(\dot{m}_c + \dot{m}_{boil})\Delta h_{fg} \quad (3.27)$$

For further details about the FLACS Pool Model see [Gexcon, 2019].

Hansen at al. [2010] carried out a validation of FLACS pool model against experimental data sets from the model evaluation database for LNG vapour dispersion. They concluded that FLACS successfully meets the quantitative criteria for LNG vapour dispersion model validation specified in the model valuation protocol [Ivings, 2016].

3.4 The FLACS Explosion Model

In order to model explosion behaviour FLACS employs a combustion model [Gexcon, 2019]. This is comprised of a flame model and a burning velocity model. A one-step reaction kinetic model is assumed with the rate of reaction determined by the burning velocity of the fuel mixture. A chemical equilibrium model is used to estimate the composition of the combustion products. In most practical engineering simulations the flame reaction zone is typically thin compared to the grid resolution. To overcome this problem, in the β flame model employed in FLACS, the flame is artificially thickened so that its structure may be fully resolved by a relatively coarse grid. The flame zone is thickened by increasing the diffusion coefficient by a factor β and reducing the reaction rate by a factor 1/β. The factor β used to achieve this is proportional to the grid size and inversely proportional to the integral length scale, giving the flame a constant thickness equal to 3-5 grid cells and guarantying that the flame propagates with the specified burning velocity.

The burning velocity model is comprised of three sub-models with burning velocities corresponding to the laminar, quasi-laminar and turbulent combustion regimes. The FLACS code switches the value of the effective burning velocity used in the model depending upon the relative magnitude of these three burning velocities. In the *laminar combustion regime* (typically close to the ignition source) the flame front is assumed to be smooth and the burning velocity is calculated using a look-up table where it is expressed as a polynomial function of the equivalence ratio and flammability limits (fitted to empirical data obtained for laminar premixed hydrogen-air flames). The flammability limits of hydrogen-air mixtures are used in FLACS to prevent flame propagation when the concentration is above the upper limit (74%) or below the lower limit (4%). Thus, if there are regions above 74% hydrogen in air at the point of ignition, the flame will not propagate and ignition will fail. As the flame propagates further away from the ignition source it begins to deform and wrinkle due to the effect of flame instabilities (e.g.

Rayleigh-Taylor and thermal diffusive) resulting in an increase in the burning velocity. Finally, in the *turbulent combustion regime* the turbulent burning velocity is expressed as a function of the turbulent flow intensity and length scale – based upon experimental data obtained by Abdel-Gayed et al. [1987].

The FLACS explosion model has been validated against a wide range of experiments (at small, medium and large scale) and has received specific validation for simulating hydrogen-air dispersion and explosion behaviour [Popat et al., 1996; Hansen et al., 2005; Middha et al., 2010; Gallego et al., 2007; Venetsanos et al., 2009; Papanikolaou et al., 2011; Jordan et al., 2007; Venetsanos et al., 2010; Middha et al., 2009b; Makarov et al., 2009, Middha, 2010; Vyazmina and Jallais, 2016; Tolias et al., 2018].

In order to simplify and reduce the number of explosion scenarios that need to be considered when evaluating a flammable gas cloud hazard, Gexcon have developed a concept called the Equivalent Stoichiometric Cloud method [Gexcon, 2019; Hansen et al., 2013], via the FLACS output parameter Q9, which is used to represent real flammable clouds with an equivalent stoichiometric cloud volume, taking both the maximum flame speed and maximum expansion into account:

$$\mathrm{Q9}(m^3) = \sum \mathrm{Volume}_{\mathrm{Fuel}} \times \frac{S\,E}{(S \times E)_{max}} \tag{3.28}$$

where the sum is performed over all the control volumes containing a flammable gas mixture, *S* denotes the laminar burning velocity and *E* the expansion ratio for the actual gas mixture.

3.5 The FLACS-Fire Model

FLACS-Fire allows the modelling of the non-premixed gas combustion (diffusion-flame) behaviour exhibited by accidental pool and jet fires [Gexcon, 2019]. It can predict fire growth and behaviour, heat transport from the fire (convective and radiative) and the heat fluxes incident on surfaces. It also provides fire hazard results such as wall temperature, wall heat flux and thermal radiation dose that can then act as input for further analysis to determine the consequence effects on people and structures.

3.5.1 Combustion Model

In order to model the diffusion flame, a transport equation for the (density weighted/Favre-averaged) fuel mass fraction, $\tilde{Y}_{fuel}$, is solved:

$$\frac{\partial \bar{\rho}\tilde{Y}_{fuel}}{\partial t} + \frac{\partial \bar{\rho}\tilde{Y}_{fuel}\tilde{u}_j}{\partial x_j} = \frac{\partial}{\partial x_j}\left(\bar{\rho}D\frac{\tilde{Y}_{fuel}}{\partial x_j}\right) - \frac{\partial}{\partial x_j}\left(\bar{\rho}\widetilde{Y''_{fuel}u''_j}\right) + \bar{\rho}\widetilde{\omega}_{fuel} \tag{3.29}$$

Where $\bar{\rho}\widetilde{Y''_{fuel}u''_j}$ is a turbulent diffusion term, modelled using a gradient diffusion assumption, *D* is a diffusion coefficient and $\widetilde{\omega}_{fuel}$ is the fuel species source term obtained from the combustion model. The combustion process is modelled using the Eddy Dissipation Concept (EDC) [Magnussen and Hjertager, 1976], which represents the interaction between turbulent flow and chemical reaction. In the EDC the fuel species source term is given by:

$$\widetilde{\omega}_{fuel} = -\frac{\dot{m}\chi}{1-\gamma^*\chi}\tilde{Y}_{min} \tag{3.30}$$

$$\tilde{Y}_{min} = \min\left(\tilde{Y}_{fuel}, \frac{1}{r}\tilde{Y}_{ox}\right) \tag{3.31}$$

Where r is the stoichiometric ratio of fuel to oxygen for the combustion reaction, $\tilde{Y}_{ox}$, the oxidant mass fraction, and γ^* and χ are model parameters.

The parameters used in the model are given by:

$$\gamma_\lambda = \min\left(0.8, 2.13\left(\frac{\nu\tilde{\varepsilon}}{\tilde{k}^2}\right)^{1/4}\right) \tag{3.32}$$

$$\gamma^* = \gamma_\lambda^3 \tag{3.33}$$

$$\dot{m}^* = 2.433\left(\frac{\tilde{\varepsilon}}{\nu}\right)^{1/2} \tag{3.34}$$

$$\dot{m} = \gamma^*\dot{m}^* \tag{3.35}$$

$$\chi_1 = \frac{\left(\tilde{Y}_{min}+\tilde{Y}_{prod}/(1+r)\right)^2}{\left(\tilde{Y}_{fuel}+\tilde{Y}_{prod}/(1+r)\right)\left(\tilde{Y}_{ox}/r+\tilde{Y}_{prod}/(1+r)\right)} \tag{3.36}$$

$$\chi_2 = min\left(\frac{1}{\gamma_\lambda}\frac{\tilde{Y}_{prod}/(1+r)}{\tilde{Y}_{prod}/(1+r)+\tilde{Y}_{min}}, 1\right) \tag{3.37}$$

$$\chi_3 = \frac{1}{\gamma_\lambda} min\left(\frac{\gamma_\lambda\left(\tilde{Y}_{prod}/(1+r)+\tilde{Y}_{min}\right)}{\tilde{Y}_{min}}, 1\right) \tag{3.38}$$

$$\chi = \chi_1\chi_2\chi_3 \tag{3.39}$$

The EDC model assumes a single, one-step reaction and infinitely fast reaction kinetics, where the rate of fuel consumption is controlled by the rate of mixing. For further details see Gexcon [2019].

3.5.2 Radiative heat transfer

FLACS-Fire uses the Discrete Transfer Model (DTM) to model radiative heat transfer in the near field [Lockwood and Shah, 1981]. The DTM model solves the Radiative Transfer Equation (RTE) for the radiation intensity a number of representative rays traced through the volume from the domain boundaries and solid surfaces defined in the geometry. The rays are traced from hemispheres formed about each radiating element which are divided into a number of discrete solid angles. Radiative heat transfer boundary conditions are used to determine the intensity of the rays traced from the domain boundaries. The tracing of a ray provides information about the distance travelled and the control volumes that are passed through. Each ray is traced until it hits another surface. It is then traced back along this path to the point of origin whilst solving for the radiation intensity as it enters and exits each control volume on that path. An iterative procedure is used until a converged solution for the radiation intensity is obtained. The advantages of the DTM method are that it is geometrically flexible, can be used to solve conjugate heat transfer problems and is very accurate for a wide range of optical

thicknesses. The main disadvantage is that solving a problem requiring a large number of rays can be very numerically intensive, especially for large domains.

In the far-field, FLACS-Fire employs a multipoint source model to model radiative heat transfer [Mumby, 2010]. In this case radiation is assumed to be emitted from a number of source points, *n*, located along the length of the flame. The radiative heat flux received at a given target location is then given by:

$$q = \sum_{i=0}^{n} \frac{\tau_i Q_i}{4\pi S_i^2} \quad (3.40)$$

Where *i* is the *i*th point source located along the flame, S_i is the distance of the path from source to the target location (m), τ_i is the atmospheric transmissivity along the path and Q_i is the strength (power) of each point source *i* (W), with each point radiating 1/*n* of the total emissive power. The values of Q_i are found by identifying the longest axis of the flame, considering *n* grid planes perpendicular to this axis and then adding the radiative source term for source *i* corresponding to the hottest cell in grid plane *i*. The atmospheric transmissivity is found using a relationship obtained by Moorhouse and Pritchard [1982]:

$$\tau = 0.998^S \quad (3.41)$$

which was derived for infrared radiation produced by hydrocarbon flames and is valid for distances up to 300 m.

In FLACS-FIRE CO_2 and H_2O are treated as the participating gases that can emit and absorb radiation, depending upon the temperature of the gas mixture. A weighted sum grey gas model (WSGGM) is used (by default) to determine the radiative properties of the gaseous mixture [Yin, 2013]. The formation of soot can have a significant effect on the thermal transport properties of the flame particularly with regard to the emission and absorption of thermal radiation. To model soot production a simple fixed conversion soot mode has been used, which converts a fixed fraction of carbon into soot (soot yield).

Further technical details of the FLACS-Fire model can be found in the FLACS User's Guide [Gexcon, 2019].

3.6 HyRAM - Hydrogen Risk Assessment Models

The HyRAM (Hydrogen Risk Assessment Models) research software, developed by Sandia National Laboratories, provides a toolkit of methods and engineering models for performing quantitative risk assessment and consequence modelling for hydrogen infrastructure and transportation systems [Ehrhart et al., 2020].

The latest version of the software, HyRAM 3.0, provides the capability of modelling cryogenic hydrogen releases from liquid hydrogen systems (saturated vapor and saturated liquid releases), by using the NIST equation of state and property equation model, based on a Helmholtz energy function using the approach developed by Leachman et al. [2009], which is valid for pressures up to 2000 MPa and temperatures between 14 K and 1000 K.

HyRAM includes experimentally validated hydrogen release and flame physics models allowing the calculation of:

- The hydrogen concentration for an unignited jet plume
- The temperature and trajectory of a jet flame

- The radiative heat flux contours produced at different distances from a jet flame

A hydrogen release is modelled as flow through an orifice, assuming isentropic gas flow, and expansion to atmospheric pressure using one of five different notional nozzle models. Gaussian profiles are assumed for the properties of both jet plumes and diffusion flames. A one-dimensional model approach is used to calculate the trajectory of the hydrogen jet plume (Houf and Winters [2013]) or flame (Ekoto et al. [2014]) which can also account for the upward curvature of the plume/flame produced by buoyancy. The radiative heat flux from the jet flame to the surrounding is calculated using a weighted multi-source model (Hankinson and Lowesmith [2012]).

Fig. 3.1 shows an example of a hydrogen jet plume calculated using HyRAM for a leak from a LH_2 aircraft fuel tank. Fig 3.2 shows the corresponding jet flame and radiative heat flux contours produced at different distances from the flame.

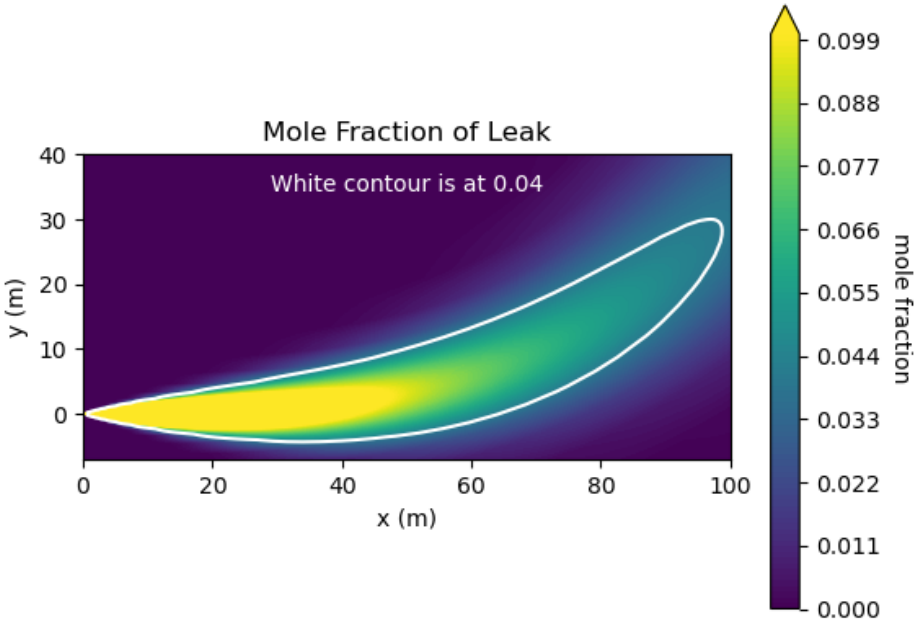

Fig. 3.1 – Example of the hydrogen jet plume predicted using HyRAM for an aircraft fuel tank hydrogen leak scenario.

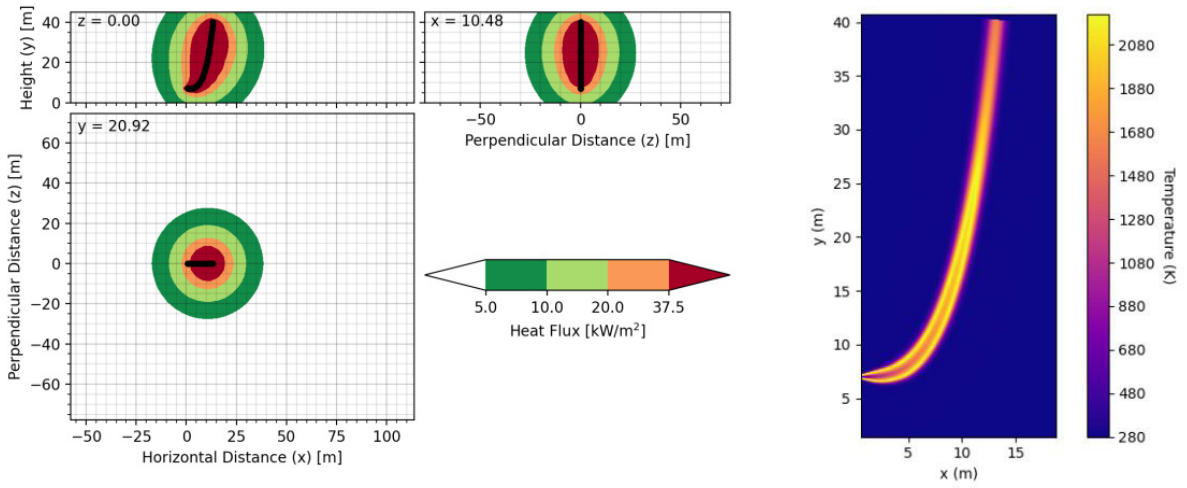

Fig. 3.2 – Example of the radiative heat flux contours and jet flame predicted using HyRAM for an aircraft fuel tank hydrogen leak scenario.

For further details about the hydrogen hazard assessment models implemented in HyRAM see Ehrhart and Hecht [2020].

3.7 Harm criteria

In order to gauge and compare the level of harm presented by the hazard effects modelled in this study the following harm criteria have been adopted.

3.7.1 Fire - Thermal radiation heat flux thresholds

The most direct measure of the amount of harm caused by the thermal radiation produced by a fire is the level of the thermal radiation heat flux at the target.

Harm criteria: In terms of thermal radiation heat flux the following range was adopted for the analysis (LaChance et al. [2011]):

5.0 kW/m^2 - pain after 20 s exposure; first degree burn

37.5 kW/m^2 – 1% fatality after 10 s; structural damage after 30 mins

3.7.2 Fire - Thermal Radiation Dose

The level of harm inflicted by the thermal radiation released from a fire depends both upon the intensity of the thermal radiation flux received by the target and the duration of exposure. This harm level is usually expressed in terms of the thermal radiation dose given by: $(q)^{4/3}\ t_{eff}$ in units of $(kW/m^2)^{4/3}$ s (also referred to as the thermal dose unit or tdu), where q is the radiation heat flux (kW/m^2) and t_{eff} is the effective exposure time (s). When considering harm to people the exposure time depends upon how long the persons takes to react to the fire and find shelter. An upper bound of t_{eff} = 30 s is often assumed, and is adopted here for cases where the duration of the fire is greater than 30 s.

The effect of a particular radiation dose level can be related to the harm it causes through either burn injuries/fatalities or structural damage by defining harm criteria in terms of a given dose threshold (Hankinson and Lowesmith [2013]; Assael and Kakosimos [2010] pg. 127).

Harm criteria: the following thermal dose thresholds causing harm to people were adopted for the analysis (based on LaChance et al. [2011]):

Burn (First degree) – 100 TDU

Burn (Second degree) - 240 TDU (Pew)

Dangerous dose (1% fatality) – 420 TDU (Tsao and Perry)

Fatality (LD50: 50% fatality) – 1050 TDU (Tsao and Perry)

In the above, a dangerous dose is where 1% of exposed population would die. The LD50 is the lethal dose (LD) where 50% of the exposed population would be expected to die.

3.7.3 Flammable Gas Cloud - Flash Fire

Harmful consequences can occur due to the delayed ignition of a flammable hydrogen cloud resulting in a flash fire or explosion. In the case of a flash fire, a relatively slow propagation of flame through the

flammable gas cloud will occur (as might be the case for very lean or rich fuel-air mixtures). In this case there is likely to be sufficient time that significant heat transfer from the burning flame and hot gas region to a target could take place. A person located within the flammable region of the cloud when ignition occurs could therefore suffer a fatal injury.

Harm criteria: The hazard associated with flash fire has been characterised in terms of the area/region of the cloud formed that is above LFL of hydrogen (assumed to be 4% v/v for hydrogen-air although this may be different at cryogenic temperatures) or the maximum downwind distance from the spill origin to the LFL boundary of the cloud.

3.7.4 Flammable Gas Cloud - Explosion

In the case of an explosion, a rapid flame propagation through the flammable gas cloud can occur. In this case the main source of harm is likely to be the overpressure generated by the explosion, which can be enhanced by any confinement and/or turbulence generated by congestion encountered by the travelling flame front. The following explosion overpressure harm criteria was adopted for the analysis (Hankinson and Lowesmith [2013]):

Harm criteria: The hazard associated with an explosion was characterised in terms of level of overpressure reached in the range 0.07 to 0.48 barg. Overpressure predicted in a localised region greater than 0.07 barg threshold criteria, could result in casualties and damage and were regarded as being relatively high. The upper threshold of 0.48 barg was regarded as representing the overpressure level where the probability of the explosion resulting in a fatality or structural damage was around 50%.

4 LH_2 leaks and Cloud Dispersion Behaviour

4.1 NASA White Sands Experimental Tests

A series of large-scale experimental liquid hydrogen dispersion tests were carried out by NASA at the White Sands Test Facility (WSTF), New Mexico, during the 1980s (Witcofski. and Chirivella [1984]; Chirivella and Witcofski [1986]). The experiments consisted of large ground spills of LH_2 of up to 5.7 m^3 (~400 kg) with durations of approximately 35 - 120 s. The tests were intended to provide information on large, rapid LH_2 spills and the associated flammable hydrogen-air cloud dispersion behaviour that might result as a consequence of the rupture of a large scale LH_2 storage facility. Some tests for longer duration spills were also carried out to try to replicate the behaviour of smaller/slower releases, corresponding to the rupture of a LH_2 pipeline.

Liquid hydrogen, stored in a 5.7 m^3 Dewar, was transported to the spill site, through a 15.5 cm diameter, 30 m long spill line, where it was released, via a downward facing diffuser (approximately 0.5 m × 0.5 m in area), into a 9.1m diameter spill pond, formed from a compacted sand base and earthen sides 0.6 m high. A 1.2 m × 1.2 m steel plate (1.27 cm thick) was located directly below the diffuser to prevent erosion of the spill point.

Nine, 19.5 m high, instrumented towers were located “downwind” of the centre of the spill pond (1, 2 and 3 at a radius of 9.1 m, 45° apart, 4, 5, and 6 at a radius of 18.3 m, 45° apart, and 7, 8 and 9 positioned a distance 33.8 m in a straight line from the spill origin and spaced 22.5° apart). The instruments on each tower were used to collect data on temperature, hydrogen concentration and turbulence levels. Hydrogen sampling bottles were mounted (in clusters of eight) at heights of 1, 9.4 and 18.6 m on towers 1, 3 and 5, and at heights of 9.4 m and 18.6 m on the remaining towers, apart from tower 2 where they were located at heights of 1 m, 6.7 m and 13.1 m. The bottles were opened individually, at pre-determined times, during the course of each test. The three towers located on the centre line (2, 5 and 8) were fitted with UVW turbulence indicators (anenometers).

Details of the seven LH_2 spill tests carried out and results obtained for some of the tests (primarily Test 6) were initially presented in Witcofski. and Chirivella [1984] but were later reported in revised form in Chirivella and Witcofski [1986]. Thus, for example, the mean wind speed for Test 6 was initially reported as 2.2 m/s, but was later revised to 1.75 m/s. Variation in the prevailing wind direction during the tests meant that the direction of travel of the gas cloud was typically orientated at an angle relative to the central line of the instrumented towers (2, 5 and 8). Hence, the gas cloud did not necessarily pass through the instrument towers.

The most extensive set of test results reported (hydrogen concentration versus time at different sensor locations) was obtained for Test 6. Hence, data from Test 6 has served as the main basis for model comparison. Results were also reported in Chirivella and Witcofski [1986] for the farthest downwind distance and height of the flammable cloud, the time to vaporization of the LH_2 pool, and the duration of the visible cloud for many of the spill tests.

4.2 Simulation Details

The initial validation simulations were performed on a domain 200 m × 60 m × 80 m in the X, Y and Z directions (-30 m to 170 m, -30 m to 30 m, 0 to 80 m). The “standard” grid employed had a total of 177,284 cells (82 × 47 x 46 cells). In the pool region a grid cell size of 0.5 m was used in the X and Y directions and 0.12 m in the Z direction. Outside this region the grid cell size was increased, by using an expansion factor of 1.2, and setting a maximum grid cell size of 4 m. A finer “hi-res” grid of 924,000 cells (150 × 80 x 77 cells) was also used to test the grid sensitivity of the results, with a smallest grid cell size (in the pool region) of 0.25 m in the X and Y directions and 0.06 m in the Z direction, and a maximum cell size of 2 m. For subsequent simulations the size of the domain and number of grid cells was increased, firstly only in the X-direction, to 400 m × 60 m × 80 m (82 × 47 × 46 - 285,384 cells) and then to 400 m × 80 m × 80 m (169 × 74 × 48 - 600,288 cells) in the X, Y and Z directions to allow the simulation of the larger flammable clouds and LH_2 pool areas that are produced (without a pool fence) for higher spill rates and longer spill durations.

For the initial base-line simulations of NASA WSTF Test-6, the wind speed was set to 1.75 m/s at a height of 10 m. The wind direction used in the simulation was aligned to run along the positive x-axis (wind direction 270°). A set of monitor points was defined to represent the sensors in the NASA Tests located on instrument tower 2 (1 m high), tower 5 (1 m and 9.4 m high) and tower 7 (9.4 m high). The direction of the prevailing wind during Test 6 was orientated at an angle relative to the central line of the instrumented towers (2, 5 and 8). An additional set of monitor points were also therefore introduced into the simulation with the instrument tower sensor x and y positions translated to replicate the direction of the prevailing wind being at an angle of 24° (midpoint of wind variation range indicated in [9]) to the centre line of the instrumented tower. Although FLACS has the capability to model different wind orientations, this would have required the use of a larger simulation domain (with increased run times) and multiple runs. Representing the change in wind direction by shifting the relative position of the monitor points, was more efficient and enabled the effect of multiple wind directions to be simulated using a single run. The results obtained are expected to be the same.

Values for CFLC = 20 and CFLV = 1 were used in the simulations. The ambient temperature was set to 15°C. The ground roughness length for the wind profile was set to 3 mm. The Pasquill stability class was set to class F – stable (produced best match in Middha et al. [2011]). The wind profile parameter values used in the simulation (corresponding to class F) were L_s = -31.323 m and z_s = 19.36 m [Gexcon, 2019]. The pool model spill point was set at the origin (0, 0, 0). The inlet boundary (type WIND) was defined at 30 m upwind of this point. A pool fence, 0.6 m high, was defined at radius of 4.25 m from the spill point. This was aligned with the grid and thickened in the horizontal direction, making it two grid cells wide, to ensure it would act as a solid obstruction and would not allow dispersion of the cloud through the fence. The thermal conductivity and thermal diffusivity of the ground used in the pool model were set to 3.72 W/m/K and 1.45 × 10^{-6} m^2/s, to replicate the thermal properties of wet coarse sand [Hamdhan and Clarke, 2010]. The ground was also assumed to be adiabatic outside of the pool region. Fig. 4.1 illustrates the boundary conditions, the domain and the grid used in the initial base-line simulations.

The pool release was started after 10 seconds of simulation time to allow the wind field to become established. Liquid hydrogen in the pool model was released at 9.5 kg/s for a duration of 38 s. In order to comply with FLACS Best Practice User Guidelines (so as to adequately resolve the pool region and produce a circular pool shape) the radius of the leakage area used in the pool model was set equal to the length of 3 grid cells (1.5 m for the “standard” grid, 0.75 m for the “hi-res” grid), rather than the physical dimension of the experimental diffuser used in the tests. As a limiting case to examine the effect of the largest possible LH_2 pool (i.e. a conservative assumption with regard to the formation of the liquid pool and the subsequent dispersion behaviour), it was assumed that all of the LH_2 release was deposited into the LH_2 pool and the effects of flash vaporisation were neglected. Such releases may approximate conditions where LH_2 is stored at low gauge pressures above atmospheric (such as is the case with LH_2 tanks to be used in aircraft) and there is consequently expected to be a relatively low level of flashing.

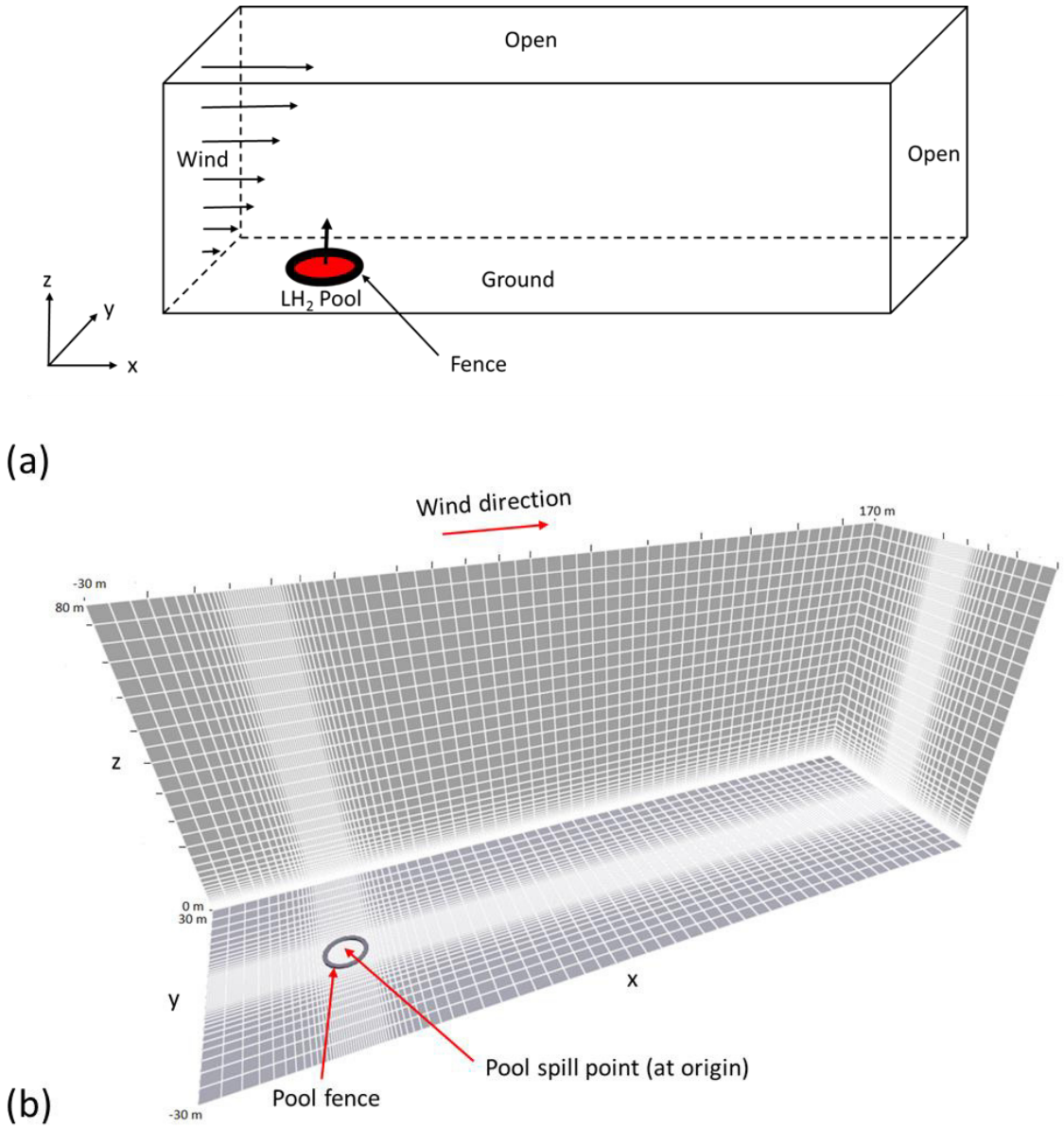

Fig. 4.1 - (a) Illustration of the boundary conditions used in the base-line simulations; (b) the grid and domain used in the base-line simulations.

4.3 Results

4.3.1 Model Comparison for NASA Test 6

Fig. 4.2 shows a comparison of the hydrogen concentrations observed experimentally with those predicted by the model at the four instrument tower sensor locations in NASA Test 6, using both standard and hi-res grids and for wind directions (relative to the central axis of the instrumented towers) of 0° and 24°.

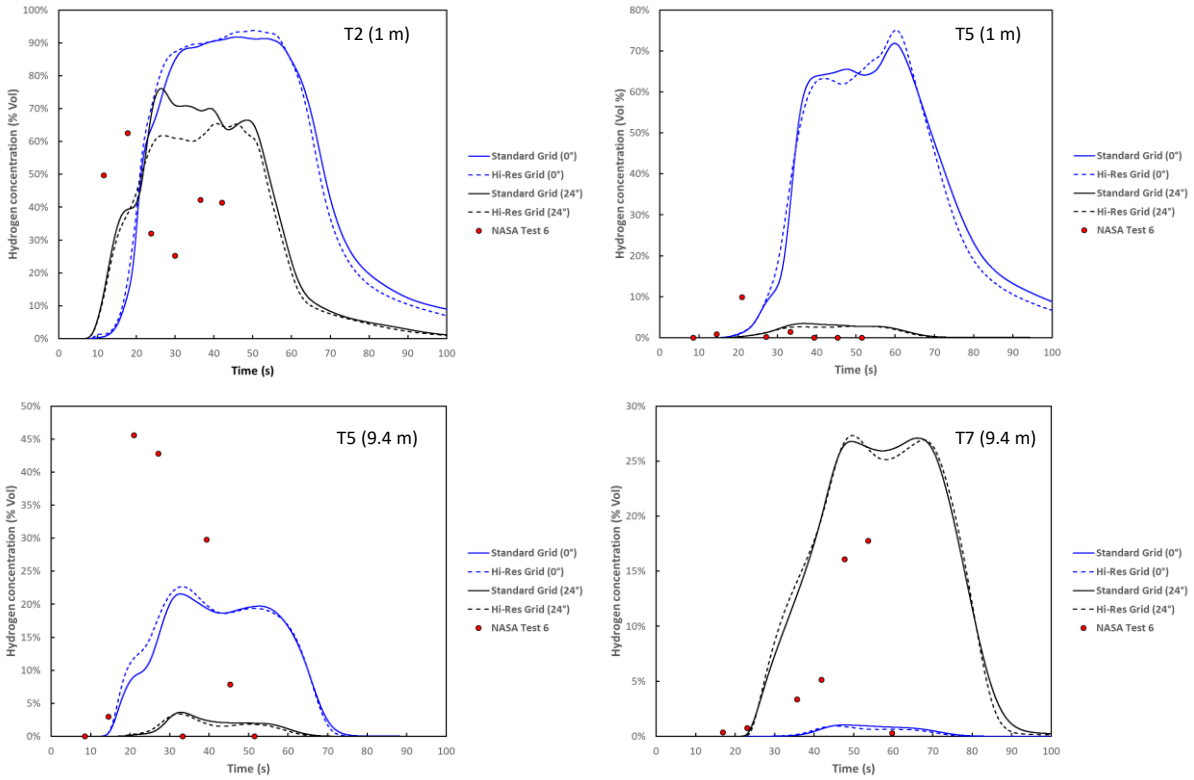

Fig. 4.2 - Comparison of hydrogen concentration results for NASA Test 6 with FLACS predictions standard and hi-res grids and for original sensor locations (0°) and rotated by an angle of 24° to replicate a shift in mean wind direction: Tower 2 (height 1 m); Tower 5 (height 1 m); Tower 5 (height 9.4 m) and Tower 7 (height 9.4 m).

The results obtained for both the standard and hi-res grids are broadly consistent suggesting that a reasonable level of grid independence has been achieved using the standard grid, which was therefore adopted for use in this study. Using a wind direction of 0°, the model over-predicts the peak hydrogen concentrations observed at T2 (1 m) and T5 (1 m) and under-predicts those observed at T5 (9.4 m) and especially for T7 (9.4 m). By comparison, using a wind direction of 24°, a better level of agreement between the predicted and observed peak hydrogen concentrations is achieved at T2 (1 m) and T5 (1 m) and particularly for T7 (9.4 m), as the gas cloud now passes through this sensor location. However, the predicted peak hydrogen concentrations are very low at T5 (9.4), compared with those observed in the test, suggesting that the model is under-predicting the level of buoyancy of the gas cloud produced by the spill.

Fig. 4.3 shows a comparison of the hydrogen gas concentrations for the cloud along the centre-line, downwind of the spill point, observed experimentally in NASA test 6, around 20 seconds after the start of the spill [8], with those predicted by the FLACS pool model. It can be seen that the predicted cloud is reasonably similar in form to the experimental one, but that the experimental results suggest a greater level of upward dispersion and travel downwind.

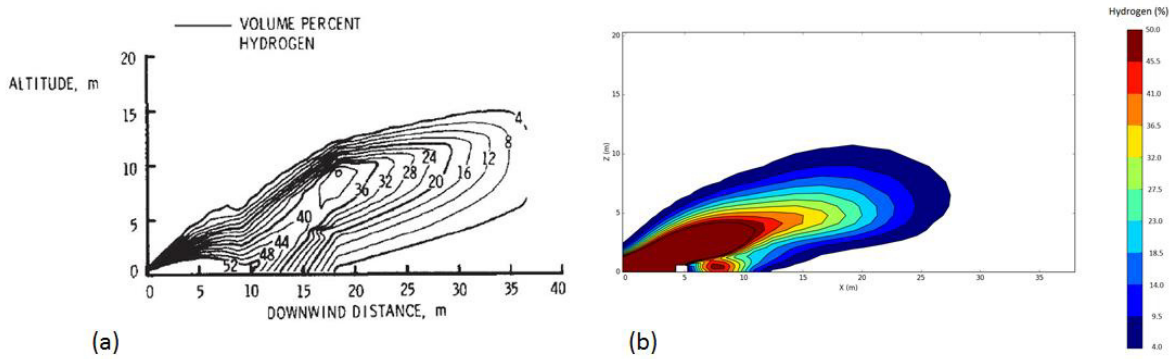

Fig. 4.3 – The hydrogen gas cloud concentration contours: (a) observed experimentally after 21.33 s [8]; (b) predicted by the FLACS pool model after 20 s.

Fig. 4.4, shows the development of the flammable gas cloud predicted by the model for test 6. The head of the flammable cloud rises upward whilst the body travels along the ground. Both downwind extent and the maximum height of the head of the flammable cloud increase with time as does the distance over which the cloud travels along the ground before starting to rise. The tail end of the cloud remains anchored to origin of the spill throughout the lifetime of the cloud. After the end of the release at 38 s the cloud continues to extend further downwind whilst gradually dispersing, to lower concentrations, and then below the flammable limit.

Fig. 4.5(a), show the radius of the LH_2 pool versus time predicted by FLACS (for both standard and refined grids) compared with the experimental pool size range estimated for NASA test 6 and the predictions of another model – LauV [Verfondern and Dienhart, 1997, 2007]. The FLACS pool results can be seen to be broadly consistent with those inferred from test 6 – predicting a slightly larger maximum pool radius and a very similar time to complete vaporization of the LH_2 pool (around 45 seconds). The corresponding LH_2 pool vaporisation rate predicted by FLACS is shown in Fig. 4.5(b). It initially peaks at a value of 0.11 m^3/s before falling sharply and then gradually rising again in a fluctuating pattern approaching 0.1 m^3/s before dropping to zero after 45 seconds. By contrast LAuV predicts a lower and a steadier maximum vaporisation rate of around 0.07 m^3/s. LAuV assumes that heat conduction from the ground is the dominant source of heat transfer for vaporization of a cryogenic pool and uses an expression similar in form to equation (16). The discrepancy of the LAuV results compared with the FLACS results (and also with NASA test results) may be at least partly attributable to differences in the heat transfer properties for the ground substrate (thermal conductivity and thermal diffusivity) that were assumed when modelling the NASA test. The FLACS results obtained for a concrete ground type (see below), suggest that the pool radius can be significantly larger if a lower value for thermal conductivity of the substrate is assumed.

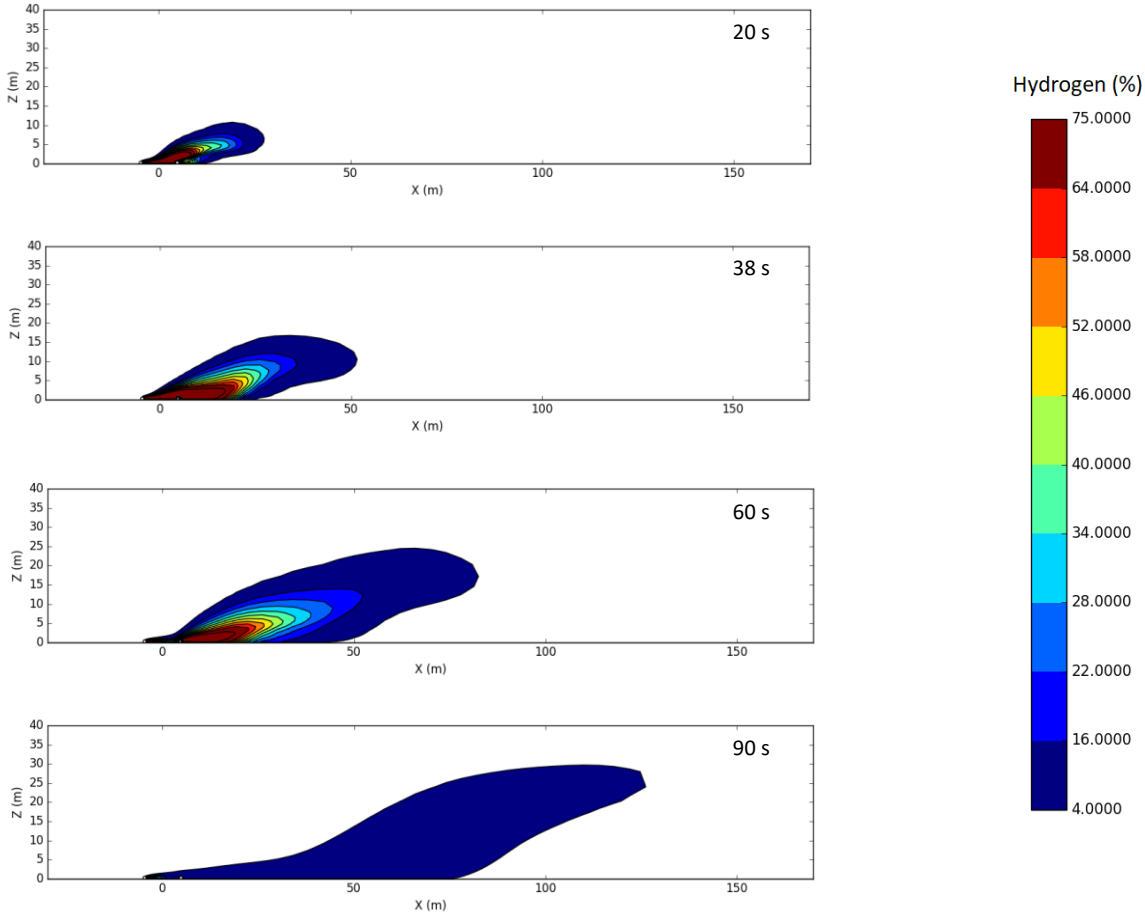

Fig. 4.4 – Development of the predicted flammable hydrogen gas cloud with time after start of spill.

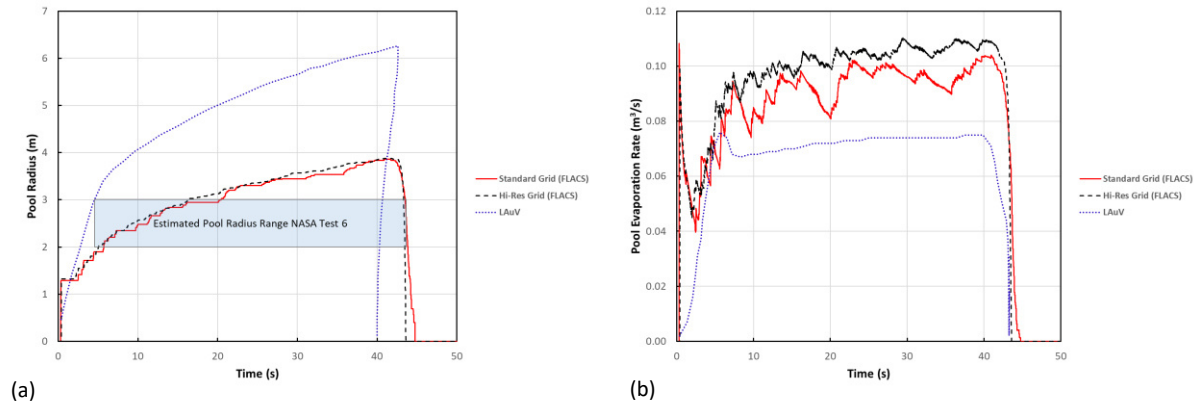

Fig. 4.5 - (a) Comparison of LH_2 pool radius development with time (form start of spill) predicted by FLACS (using standard and hi-res grids) and LAuV with range estimated from NASA Test 6. (b) Comparison of pool evaporation rate variation with time predicted by FLACS and LAuV.

4.4 Flammable distance for NASA Tests

The results of the NASA WSTF experiments reported in [9] provides details of the hydrogen gas clouds produced during the LH_2 spill tests, including the maximum downwind distance of the cloud to the reach the LFL (4% v/v hydrogen in air), the maximum flammable height, time to total vaporisation of the LH_2 pool and duration of the visible cloud (taken to indicate the approximate duration of the flammable cloud).

Table 4.1 presents a comparison between the observed and predicted results for three of the NASA tests. For the base-line Test 6 (release rate 9.5 kg/s, release duration 38 s, wind speed 1.75 m/s) the predicted and observed maximum downwind flammable distances are the same, but the predicted flammable height is only half that found in the experiment. For Test 7, where a slower release spill rate (1.67 kg/s) was used over a long duration (120 s), at a higher mean wind speed (4.16 m/s), both the downwind flammable distances are lower than those found for Test 6, but the observed distance is less than half the predicted one. On the other hand the flammable heights in this case are both relatively low suggesting that the gas cloud remains close to the ground. Finally, for Test 4, where a similar spill rate (10.3 kg/s) and duration (35 s) to Test 6 was used, but the mean wind speed was almost double (3.38 m/s), the downwind flammable distances are both higher than those found for Test 6, although the predicted distance is about 30% greater than that observed. In this case the predicted flammable height is also less than half that found in the experiment. For tests where the data is available FLACS predicts very similar pool vaporisation times to those observed experimentally, but over predicts the duration of the visible cloud. The latter may be at least partially attributable to the difference between the visible cloud limit (at dew point - typically around 8% v/v [Witcofski and Chirivella, 1984] and LFL limits (4% v/v).

Table 4.1 - Comparison between observed and predicted results for three NASA test conditions.

Trial	Release Rate (kg/s)	Duration (s)	Wind Speed (m/s)	Max Flammable Distance to LFL (m)		Max Flammable Height (m)		Time to Total Vaporization (s)		Visible Cloud Duration (s)	
				Expt.	FLACS	Expt.	FLACS	Expt.	FLACS	Expt.	FLACS
6	9.5	38	1.75	160	160	65	32	43	45	90	140
7	1.67	120	4.16	61	144	9	7	-	-	-	-
4	10.3	35	3.38	212	285	53	21	42	42	90	140

The model reproduces similar qualitative trends with regard to the effect of spill rate, spill duration and wind speed on the flammable cloud behaviour to those observed in the experimental tests, although significant quantitative differences in the results are apparent.

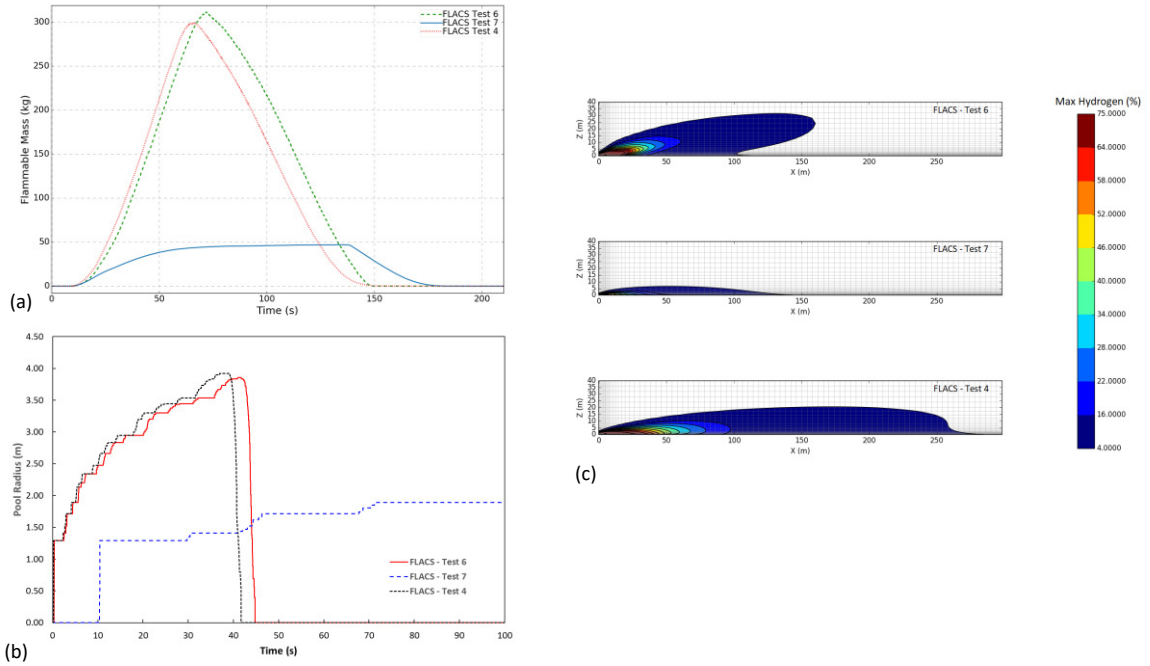

Fig. 4.6 – Comparison between FLACS results predicted for NASA test conditions 6, 7 and 4: (a) flammable mass of gas cloud versus time; (b) LH_2 pool radius versus time; (c) Contour plot of maximum hydrogen concentration registered in each cell over the course of the simulation along the central x-z plane.

Fig. 4.6 shows a comparison between the results predicted by FLACS for the three test conditions. Fig. 4.6(a) compares the predicted total mass of the flammable cloud versus time for the three tests. The curves predicted for Test 6 and Test 4 display a similar peak flammable mass and flammable time. In contrast, Test 7 exhibits a much lower maximum flammable mass and a longer flammable time. The results suggests that in this case the spill rate and duration (rather than wind speed) are the main factors determining the shape of the flammable mass curve.

Fig. 4.6(b) compares the predicted LH_2 pool radius versus time for three tests. As with the flammable mass curves, the pool radius variation predicted for both Test 6 and Test 4 are very similar, where-as the curve for Test 7 displays a much slower rate of growth and reaches a maximum radius which is around half that found for the other two tests.

Fig. 4.6(c) compares the maximum concentrations for the flammable cloud along the central X-Z plane predicted for three tests. Note that these contour plots show the maximum hydrogen concentration produced in a given control volume over the duration of the simulation. Hence, they do not show the hydrogen gas concentration at a particular instant of time, but instead provide a composite of the maximum values over time – indicating any location where the concentration has been greater than 4% v/v. Hence, they demarcate the maximum flammable extent of the gas cloud over the course of the simulation. Compared to Test 6, the cloud predicted for Test 7 is shorter and remains close to the ground. Conversely the predicted cloud for Test 4, has a much greater flammable extent than Test 6. The results suggest that spill rate, duration and wind speed all play a role in determining the downwind flammable distance and height.

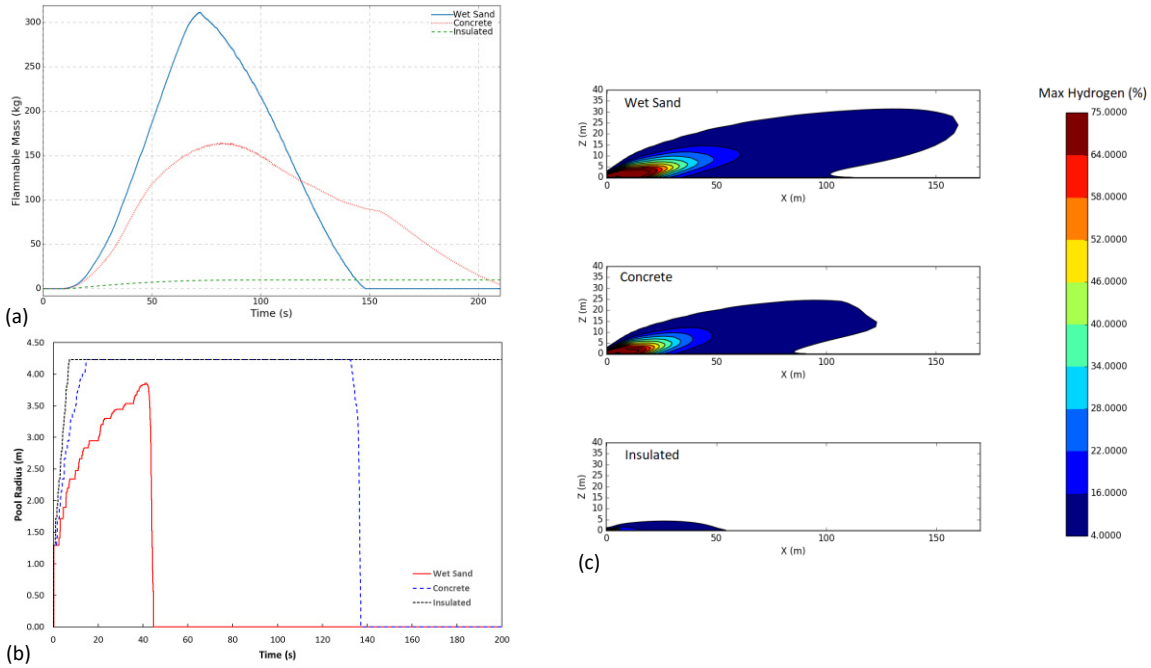

Fig. 4.7 – Effect of pool ground type on the predicted results for: (a) flammable mass versus time; (b) pool radius versus time; (c) maximum hydrogen concentration of flammable cloud.

4.5 Effect of Pool Ground Type

Fig. 4.7 shows a comparison between the flammable mass, flammable hydrogen cloud and LH_2 pool size results predicted by FLACS for three different pool model ground types – wet coarse sand, concrete and insulated (characterised in terms of thermal conductivity and thermal diffusivity values given in Table 4.2). In each case the analysis has been performed for the Test 6 release scenario – but with an adjustment made to the ground substrate type.

Table 4.2. Pool model ground properties.

Ground Type	Thermal Conductivity (W/m/K)	Thermal Diffusivity (m^2/s)
Wet coarse sand	3.72	1.45×10^{-6}
Concrete	1.1	1.0×10^{-6}
Insulated	0.0	10^{30}

Both concrete and particularly the wet coarse sand used for the Nasa Tests have a relatively high thermal inertia, meaning that the ground take longer to cool and so maintains greater temperature difference and rate of heat transfer to the LH_2 pool. Hence the higher level of heat transfer from the concrete and particularly for the wet sand produces a much greater level of vaporisation of the LH_2 pool (smaller maximum pool radius and shorter time to total vaporisation), cloud dispersion and greater peak flammable mass and flammable extent but for a shorter duration. In contrast for the insulated pool, there is no heat transfer from the ground to the pool - which rapidly grows to the maximum size of the pool, thereafter resulting in a slow steady vaporisation of the LH_2 pool, and producing a sustained long duration flammable cloud with a relatively low flammable mass and a smaller flammable extent.

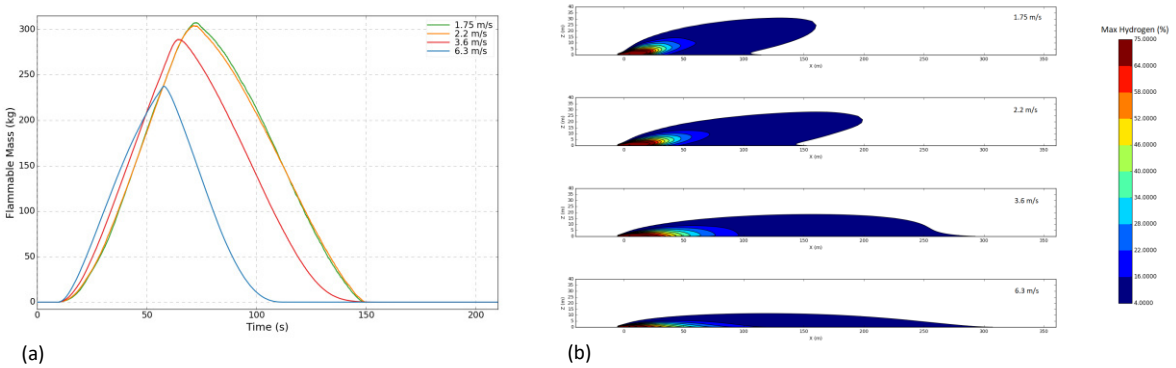

Fig. 4.8 – Effect of wind speed on the predicted results for: (a) flammable mass versus time; (b) maximum hydrogen concentration contour plots of the flammable cloud.

4.6 Effect of wind speed

Fig. 4.8 shows a comparison between the flammable mass and flammable hydrogen clouds predicted by FLACS for different wind speeds. At lower wind speeds the head of the cloud becomes buoyant rising away from the ground. At higher wind speeds the cloud becomes restricted to travelling along the ground, increasing the maximum downwind flammable distance and reducing the maximum flammable height reached. However, the level of dilution of the cloud also increases at higher wind speeds, with both the peak flammable mass and duration of the flammable cloud being reduced. This serves to limit the maximum flammable extent of the cloud. Thus, increasing the wind speed from 3.6 m/s to 6.3 m/s has only a small effect (5% difference) on the maximum downwind flammable distance reached by the cloud.

4.7 Transient LH_2 Spills

A series of transient LH_2 spills were simulated, using different release rates and spill durations, for a fixed total LH_2 release mass of 1444 kg (without the spill pond fence). The conditions used for these simulations were the same as for the NASA Test 6 scenario: wet sand ground type, wind speed 1.75 m/s, and stability class F. Table 4.3 summarises the spill conditions simulated.

Table 4.3 – The transient LH_2 spill conditions simulated for a fixed total LH_2 mass of 1444 kg

Run	Leak Rate (kg/s)	Duration (s)
T1	9.5	152
T2	4.75	304
T3	19	76
T4	38	38
T5	76	19

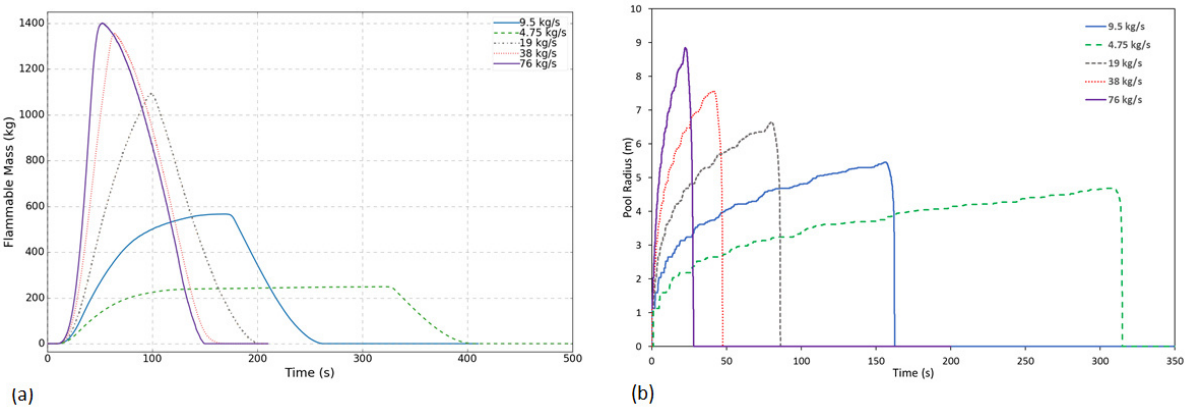

Fig. 4.9 – Comparison of predicted results varying the spill rate for a 1444 kg transient LH_2 spill: (a) flammable mass versus time; (b) LH_2 pool radius versus time.

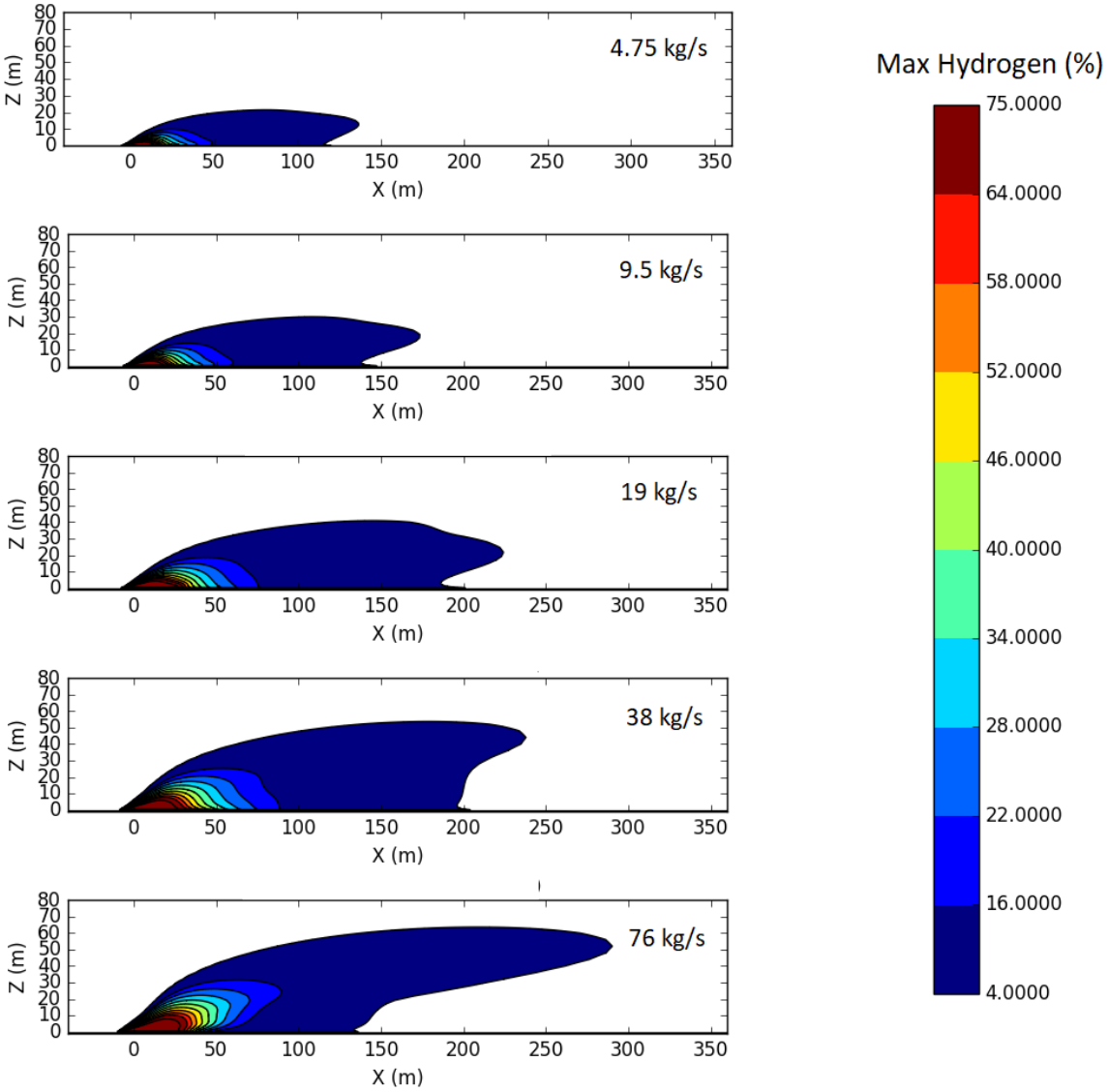

Fig. 4.10 - Predicted maximum concentration contours for the flammable cloud along the central X-Z plane, at the different spills rates, for a 1444 kg transient release.

Fig. 4.9 shows a comparison between the results predicted by FLACS for the different transient spills examined. Fig. 9(a) compares the flammable mass of the gas cloud versus time. At the lowest spill rate, 4.75 kg/s, the flammable mass of the gas cloud formed is sustained at a relatively low level (around 250 kg) over a long period of time. As the spill rate is increased the maximum flammable mass rises significantly, with the curve at higher spill rates tending towards a limiting form with a sharp peak (around 1400 kg) for a shorter period of time.

The corresponding LH_2 pool radius versus time curves, shown in Fig. 9(b) follow a similar pattern. At the lower spill rates the resulting pool exhibits a slow steady growth over a long time period. Conversely, at higher spill rates the pool grows rapidly, becoming significantly larger, but with a much shorter total vaporisation time.

Fig. 4.10 shows the variation in the predicted maximum concentration contours for the flammable cloud along the central X-Z plane, for the different spills. As the spill rate is raised the downwind extent of the flammable cloud increases as does the maximum height reached by the flammable cloud. At the highest spill rate, 76 kg/s, the distance travelled by the cloud before leaving the ground is also reduced relative to those predicted at some of the lower spill rates. The flammable extent of the cloud along the ground is governed by the interaction between the wind transporting the cloud along the ground and the vaporisation rate of the pool producing dispersion/mixing/buoyancy and upward transport of the cloud. It could be that, by producing a larger pool and greater vaporisation rate, the higher spill rate is enhancing the dispersion/mixing/buoyancy and consequently the upward movement of the gas cloud relative to downwind transport along the ground by the wind, thus causing the cloud to rise more readily and reducing the flammable extent of the cloud along the ground.

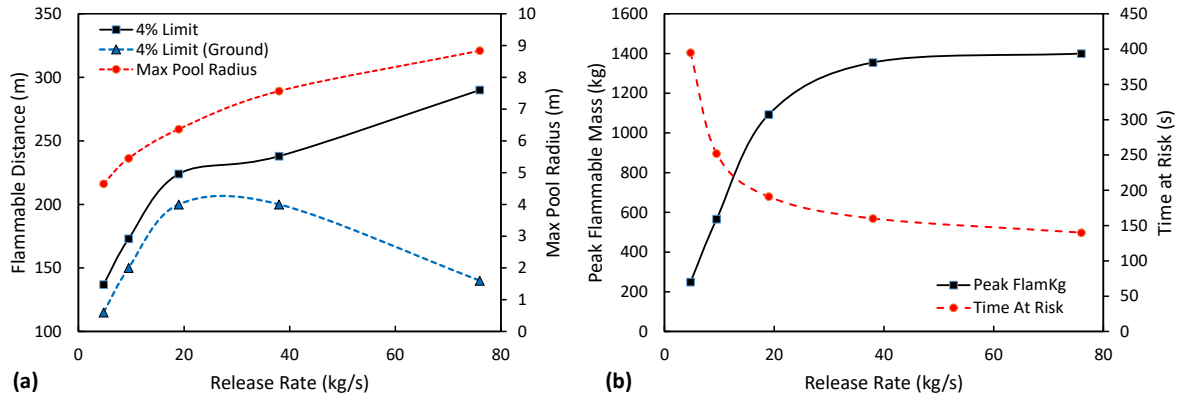

Fig. 4.11 – Predicted variation with release rate for transient 1444 kg spill of: (a) flammable distance of 4% Limit and maximum radius of LH_2 pool; (b) Peak flammable mass of gas cloud and time period over which gas cloud is flammable (time-at-risk).

Fig. 4.11(a) shows the effect of the spill rate on both the maximum downwind flammable distance reached by the cloud (for any height and also just at ground level) and the maximum radius of the LH_2 pool formed. Both the predicted maximum flammable distance at any height and the pool radius respectively increased from 137 m and 4.65 m at 4.76 kg/s to 290 m and 8.84 m at 76 kg/s. However, it can also be seen that, in contrast to the maximum flammable distance at any height, the maximum flammable distance reached at ground level does not continue to rise as the release rate is increased, but instead falls back for release rates above 38 kg/s. Hence the results suggest that, in terms of the flammable extent of the cloud produced at ground level, the level of hazard for higher spill rates may be reduced (for the specific wind conditions and ground type examined). Fig. 11(b) shows the variation of both the peak flammable mass and the time-at-risk over which the gas cloud is flammable, with the release rate of the transient spill. As the spill release rate is increased the flammable cloud mass rises

steeply before approaching a limiting value of around 1400 kg. Conversely the time-at-risk of the flammable cloud is reduced significantly to around 140 s.

4.8 Continuous Spills (600 seconds)

To examine the relationship between maximum downwind hazardous distance (and LH_2 pool radius) and spill release rate for continuous spills, a series of simulations were performed at different steady LH_2 spill release rates (between 0.1 and 20 kg/s) using a fixed spill duration of 600 seconds (to approximate the results found under continuous release – steady state conditions).

The model parameters adopted in these FLACS simulations were based upon those recommended for use in the dispersion modelling of LNG designs spills [NFPA-59A, 2016; Taylor, 2007; Woodward and Pitblado, 2010] where the maximum duration of the release is set to 10 minutes (600 seconds) intended to represent worst case dispersion conditions (at least for LNG clouds):

- Atmospheric stability Pasquill-Gifford Class F
- Wind speed 2.0 m/s measured at 10 m
- Surface roughness of 0.03 m
- Concrete pool substrate

4.9 Relationship between flammable distance and release rate

As well as the 4% v/v lower flammability limit for hydrogen, the 8% v/v hydrogen (limit for downward flame propagation) and 18% v/v hydrogen (limit for H_2-air detonation) and a gas cloud temperature of 200 K (temperature threshold taken for cryogenic injury to occur) were also used as criteria to set the location of the maximum downwind hazardous distance.

Fig. 4.12 shows the maximum downwind hazardous distances (at ground level) predicted by FLACS for the gas cloud as a function of the LH_2 spill release rate, using the 4%, 8% and 18% v/v hydrogen-air concentration limits, and the 200 K cryogenic temperature limit (taken as the temperature threshold for cryogenic injury [Woodward and Pitblado, 2010]. In all cases the hazardous distance exhibits an approximately power law relationship with the LH_2 spill release rate. The 4% LFL criteria sets the longest (most conservative) hazardous distance, whilst the hazardous distance of the cloud from the spill to the 200 K temperature threshold for cryogenic injury is significantly shorter.

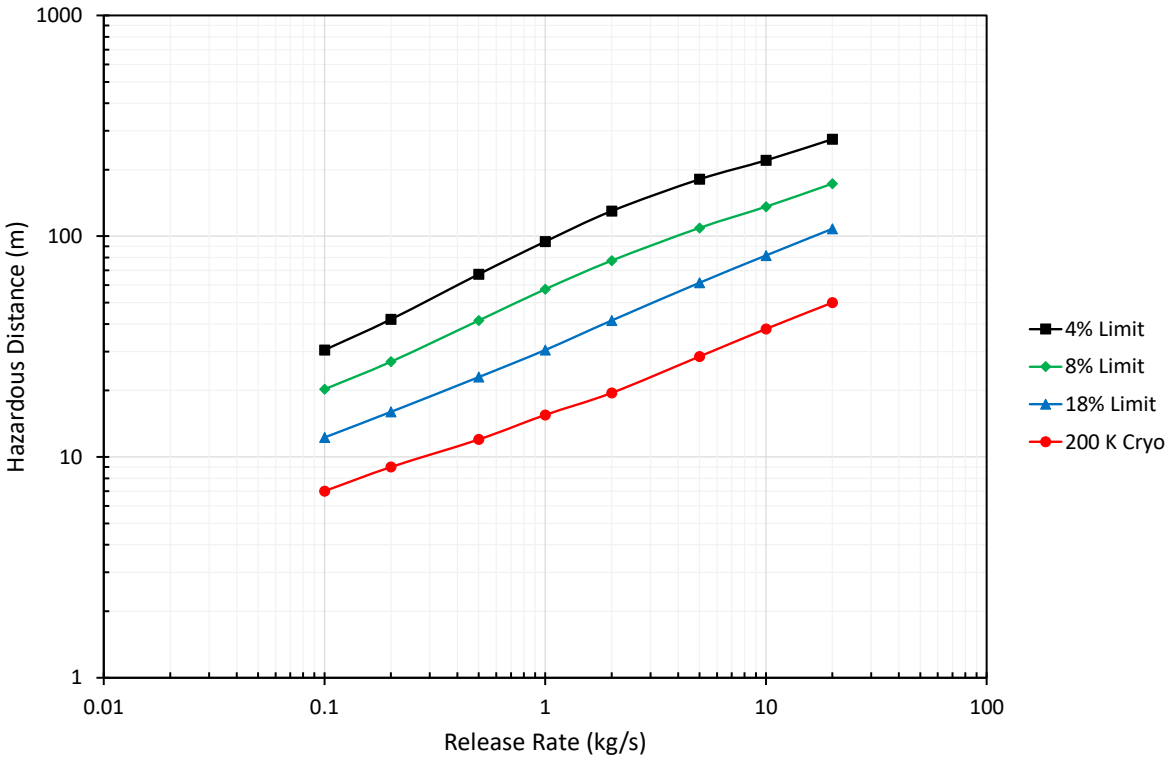

Fig. 4.12 – The maximum downwind hazardous distances predicted by FLACS for 4%, 8% and 18% hydrogen concentration limits and 200 K temperature limit as a function of the release rate for a continuous 600 s spill.

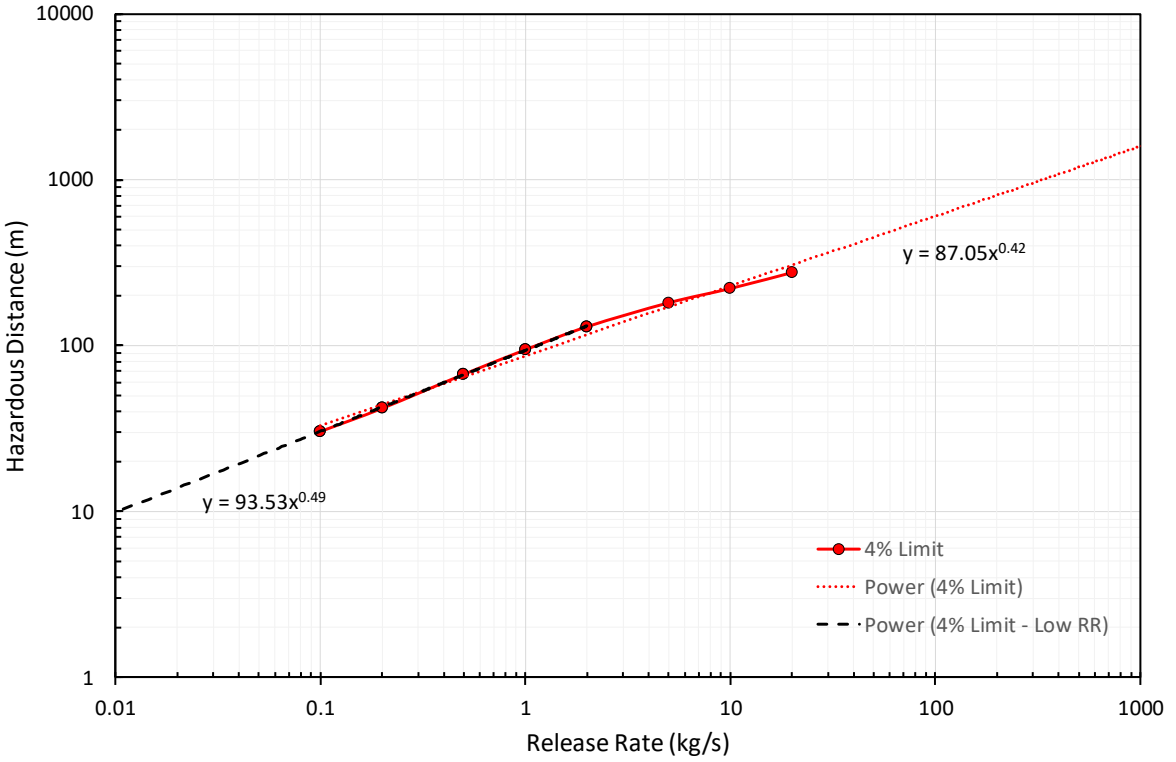

Fig. 4.13 Power law correlations fitted to the 4% hazardous distance limit data.

In order to obtain a correlation that could be used to estimate the hazardous distance (at ground level) for a given LH_2 release spill rate a power law relationship was fitted to the FLACS 4% limit data (see Fig. 4.13). Two correlations were obtained. The first fit was performed across the entire FLACS 4% limit data set:

$$x_H = 87.05\ (F_{dis})^{0.42} \tag{4.1}$$

Where x_H is the hazardous distance to the 4% limit (m) and F_{dis} is the discharge rate of the spill (kg/s).

However, it is also apparent from the FLACS 4% limit data, that at higher release rates the points are tending to curve downwards, below the fitted linear relationship (on a log-log plot) than may be projected from the points at lower release rates. This may reflect the effect of the flammable cloud lifting away from ground level, after a certain distance, at higher release rates (as was observed for the transient spills – see Fig 4.10.), thus reducing the hazardous extent of the cloud at ground level. In contrast to the transient spills, where the hazardous distance at ground level was found to decrease at the highest spill rate, the hazardous distance found for the continuous spills, shown in Figs. 4.12 and 4.13, continues to increase across the range of spill rates considered. However, the downward curvature of the line indicates that it might exhibit a similar trend at high enough spill rates. This suggests that the extrapolated correlation for hazardous distance (at ground level) may be conservative at higher spill rates (but possibly excessively so).

A second fit was also performed to the FLACS results obtained at lower release rates, to try to give an estimate of the hazardous distance behaviour for low release rates:

$$x_H = 93.53\ (F_{dis})^{0.49} \tag{4.2}$$

Note that Eqn. 4.2 is based on an extrapolated fit to five data points – so can only be regarded as being indicative.

The correlations could also be used to estimate the hazardous distance for LH_2 release rates, outside the range of those simulated. However, such extrapolated results should obviously be treated with caution as the physical behaviour of the system may change at different scales. It should also be kept in mind that this correlation has been derived from modelling results obtained for a specific ground type (concrete) and reference wind speed (2 m/s). A different wind speed or pool ground type might produce a different correlation. Hence, they should be used with caution.

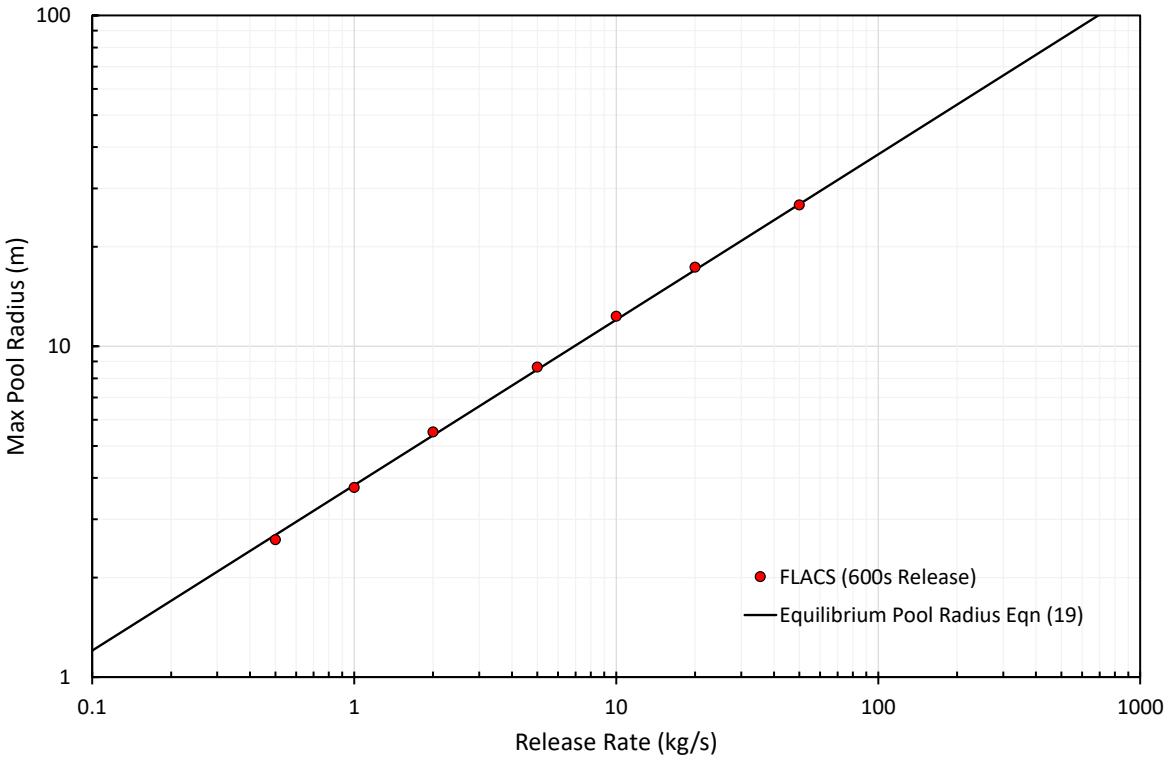

Fig. 4.14 – Equation for equilibrium pool radius equation fitted to FLACS results.

4.10 Maximum Pool Radius versus Release Rate

For a continuous LH_2 spill release rate, maintained over a sufficiently long time, the size of the pool formed should eventually reach a steady-state equilibrium (when the evaporation rate from the pool equals the discharge rate into the pool). Woodward and Pitblado ([2010] pg. 137) give an expression for the equilibrium pool radius, R_{eq} (m), of an LNG pool (which should also be valid for LH_2 spills) as:

$$R_{eq} = \left(\frac{F_{dis}}{\pi\, G_{evap}}\right)^{1/2} \tag{4.3}$$

where G_{evap} is the steady-state evaporation rate of the pool per unit area (kg/m^2/s).

Fitting the equation for R_{eq} to the FLACS 600 s simulation results, for the maximum pool radius predicted at different LH_2 spill release rates, the FLACS results can be seen to be in excellent agreement with Eqn. 4.3, as shown in Fig. 4.14. Based upon this fit, the value of G_{evap} is estimated to be 0.022 kg/m^2/s for the concrete ground type used. However, this value is between 15-25% higher than the corresponding pool evaporation rates per unit area estimated directly from the FLACS pool model simulations. The reason for this is that, even after 600 s, the pool still hasn't reached a steady-state condition, and the spill rate into the pool remains in excess of the evaporation rate from the pool.

4.11 Possible explanations for under-predicting gas cloud dispersion

In section 5 a comparison of the experimental results for NASA Test 6 with those predicted by the model suggested that the FLACS pool model is under-predicting the level of gas cloud dispersion. Possible explanations for the enhanced levels of dispersion observed in the experimental test are:

i. Variable wind speed and direction – The model is only using a mean wind velocity and direction – but significant variations in both wind speed and direction were observed to occur during the course of the experimental test. Such wind fluctuations would enhance dispersion of the gas cloud.

ii. Turbulence generated by LH_2 spill – it was observed in the experimental tests that significant turbulence was generated at higher spill rates, via the momentum of spill and the violent boiling and vaporisation of the liquid hydrogen pool formed, promoting higher levels of dispersion of the hydrogen gas cloud.

iii. Neglecting flash vaporisation – A significant fraction of the LH_2 (which was released under pressure) may have undergone flash vaporisation during transport and release in NASA Test 6. This flash vaporised vapour release could have produced enhanced dispersion levels.

iv. Neglecting effect of condensed water vapour, oxygen and nitrogen from the atmosphere. The gas cloud formed by the vaporising LH_2 is extremely cold (20K) upon release, causing water vapour in the atmosphere to condense into water vapour (at its dew point) when in come into contact with hydrogen cloud. The latent heat released during phase change from gas vapour to liquid, will heat the hydrogen gas cloud, increasing its temperature and reducing it density – hence enhancing its buoyancy and level of dispersion. See for example [Ichard et al. 2012; Giannissi and Venetsanos, 2019].

v. The FLACS pool model does not include direct heating of the gas cloud by the ground – outside of the LH_2 pool region - which might be expected to increase the buoyancy of the cloud in contact with ground and hence reduce the hazardous distance of the cloud along the ground.

4.12 Comparisons with EN 60079-10-1

As part of the standard BS EN 60079-10-1 [2015] (IEC 60079-10-1), concerned with classifying areas where flammable gas or vapour hazards may arise, a method for estimating the extent of a hazardous zone formed by the release of a flammable substance, including from an evaporative pool formed from a gas liquefied by refrigeration, such as LH_2, is given. In this method the hazardous distance is expressed in the form of a chart and expressed as a function of the release characteristic (m^3/s), given by:

$$\frac{W_g}{(\rho_g \times k \times LFL)} \tag{31}$$

Where W_g is the gaseous mass release rate (evaporation rate) of flammable substance (kg/s), ρ_g is the density of the gas formed (kg/m^3), k is a safety factor associated with the LFL, typically between 0.5 and 1, and LFL is the lower flammability limit for the gas release (0.04 v/v for hydrogen).

Fig. 4.15 compares the maximum downwind hazardous distance predicted by FLACS for the 4% limit with the curve given in (BS) EN 60079-10-1 ([42] Annex D – Figure D.1) for a heavy gas release (note that this curve been extrapolated – broken line - to match the release characteristic range covered the FLACS results). Two limit lines are shown for the FLACS results. The first of these ("FLACS – Spill Rate") calculates the release characteristic by assuming that the rate of evaporation from the pool is equal to the spill rate as would occur under steady-state conditions. The second line ("FLACS – Evap Rate") calculates the release characteristic using the pool mass evaporation rate calculated by FLACS after 600 s. It can be seen that the "FLACS – Evap Rate" line lies slightly above the "FLACS – Spill Rate" line indicating a larger hazardous distance (by around 10 m) for a given release characteristic value.

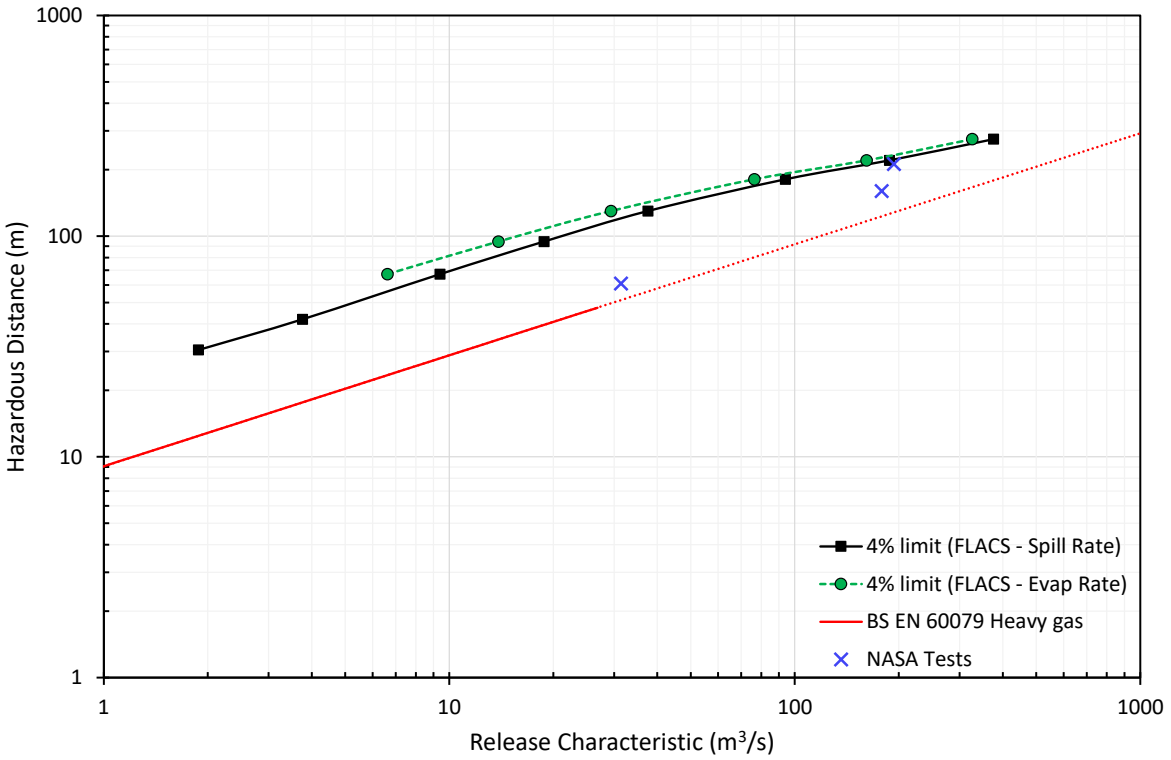

Fig. 4.15 – Comparison of 4% flammable limit hazardous distance versus release characteristic predicted by FLACS with the (extrapolated curve) given in EN 60079 for a heavy gas.

At lower release rates the FLACS predictions for the 4% LFL hazardous distance of the cloud appear to follow a similar power law scaling relationship (i.e. similar gradient) with release characteristic to the EN 60079 heavy gas curve. However, the FLACS hazardous distances are somewhat more conservative than those suggested by EN 60079, by a factor of approximately two. The downwind flammable distances estimated from the size of the visible cloud for some of the NASA WSTF tests are also shown - to provide a comparison with experiment. The hazardous distance for the lower release rate test lies closer to the EN 60079 line, but for the higher release rate tests the hazardous distance is significantly higher than the limit predicted by EN 60079, and closer to the limit predicted by FLACS.

Note that the release characteristic calculated for these tests assumes that the evaporation rate from the LH_2 pool is equal to the release spill rate, which may not be appropriate for these transient releases. If the pool evaporation rate is less than spill rate, as would be the case for a growing pool, then the release characteristic for the tests would shift to lower values, increasing the distances above the EN 60079 line and improving the match with the limit predicted by FLACS. Since the flammable distances for the tests are estimated from the size of the visible (water vapour) cloud they may also underestimate the location of the 4% hydrogen-air flammability limit. Hence, comparison with the limited experimental

test data available suggests that the more conservative hazardous distances predicted by FLACS for LH_2 pool spills may be plausible.

It is possible that the greater hazardous distances predicted by FLACS in comparison to the heavy gas curve given in EN 60079-10-1 may reflect limitations in the modelling approach employed in the FLACS pool model (e.g. neglecting the effect of heat transfer to the cloud from the ground outside the pool region). However, in a recent research paper Hansen [2020] has shown that liquid hydrogen releases do indeed exhibit dense gas behaviour and found that the hazardous distance for an LH_2 release can be significantly longer than for other gases exhibiting dense gas behaviour, such as LNG. Hence, it may be that the heavy gas curve given in EN 60079, whilst applicable to other heavy gases, is under-predicting the true hazardous distance when applied to the case of a LH_2 release.

Few details of the methodology used to obtain the heavy gas curve chart presented in Figure D.1 in BS EN 60079-10-1 [2015], beyond that it is based upon the continuity equation and selected CFD simulations, assuming a dispersion distance proportional to the square root of the X axis and also noting that the results have been moderated for the purpose of the standard. Hence, it is difficult to determine the limitations of the methodology applied in EN 600079 to predicting the hazardous behaviour of dense gases in comparison to that used by FLACS, or whether those predictions could be expected to apply in the case of LH_2.

Finally, although the hazardous distance predicted for large scale LH_2 pool spills are significant it should also be kept in mind that such releases are expected to be rare events. If the regulations and standards for LH_2 safety are not to be overly onerous, it has been recommended in NFPA-2 [2016] that a risk informed approach to safety assessments should be adopted. Hence, both the consequences and the frequency of occurrence of a LH_2 spill scenario should be taken into account when assessing the overall level of risk.

4.13 Summary

The FLACS CFD model has been used to simulate large scale LH_2 pool releases to examine their behaviour and predict the LH_2 pool size, downwind hazardous distance, and flammable mass of the hydrogen-air clouds formed for different environmental conditions and release scenarios.

Comparisons with large-scale NASA LH_2 spill data for test 6 suggests that the FLACS pool model is under-predicting the level of dispersion of the gas cloud produced by the LH_2 spill. This may be attributed to: (i) variations in both the wind speed and direction occurring during the course of the experimental test; (ii) enhanced levels of turbulence generated by the LH_2 spill observed in the tests; and (iii) the model neglecting the effect of condensed water vapour, oxygen and nitrogen from the air. The FLACS model predictions of LH_2 pool size are consistent with those observed in the test.

A comparison between the observed and predicted behaviour of the flammable gas cloud, including the maximum downwind distance of the cloud to the reach the LFL, the maximum flammable height, time to total vaporisation of the LH_2 pool and duration of the visible cloud was made for three of the NASA tests. The FLACS model reproduces similar qualitative trends with regard to the effect of spill rate, spill duration and wind speed on the flammable cloud behaviour to those observed in the experimental tests, although significant quantitative differences in the results are also apparent. The results also suggest that spill rate, duration and wind speed all play a role in determining the downwind flammable distance and height of the cloud, but that spill rate and duration (rather than wind speed) are the main factors determining the shape of the flammable mass curve.

Using the model to examine the effect of different pool ground types, materials with a higher thermal conductivity (e.g. wet sand) were found to produce a cloud with a greater peak flammable mass and flammable extent, but for a shorter duration.

At lower wind speeds the head of the cloud becomes buoyant rising away from the ground, while at higher wind speeds the cloud becomes restricted to travelling along the ground, increasing the downwind flammable distance. However, the level of dilution of the cloud also increases with wind speed, serving to limit the maximum flammable extent reached by the cloud.

A series of transient LH_2 spills were simulated, using different release rates and spill durations, for a fixed total LH_2 release mass of 1444 kg (without the spill pond fence).

At higher spill rates the downwind extent of the flammable cloud increases as does the maximum height reached by the flammable cloud. The distance travelled by the cloud before leaving the ground is also reduced.

FLACS simulations were also performed at a number of different continuous LH_2 spill release rates (between 0.1 and 20 kg/s) using a fixed spill duration of 600 seconds to try to approximate the results found under steady state conditions.

The FLACS pool model was used to predict the maximum downwind hazardous distances as a function of the LH_2 spill release rate for the 4%, 8% and 18% v/v hydrogen-air concentration limits, and the 200 K cryogenic temperature limit and were found to exhibit a power law relationship.

Correlations were obtained using the FLACS 4% limit data allowing the hazardous distance for a given LH_2 release spill rate to be estimated.

The dependence of the maximum pool radius upon LH_2 release rate predicted by FLACS for the 600 s simulations was also examined and found to be in excellent agreement with an analytical expression for the equilibrium pool radius, with the steady-state evaporation rate of the LH_2 pool per unit area estimated to be 0.022 $kg/m^2/s$ for a concrete type ground.

Finally, the maximum downwind flammable distances predicted by FLACS for the 4% limit were compared with the method for estimating hazardous distance of a release given in BS EN 60079-10-1 (Annex D – Figure D.1) for a heavy gas release. The hazardous distances found using FLACS are somewhat more conservative than those suggested by BS EN 60079, by a factor of approximately two. Comparison with the limited experimental test data available suggests that the more conservative hazardous distances predicted by FLACS for LH_2 pool spills may be plausible.

5 Leak from a LH_2 Storage Tank at an Engine Test Facility

5.1 Background

A case study has been carried out herein to examine the potential consequences of a large LH_2 leak occurring from an LH_2 storage tank at a rocket engine test facility (based upon the Reaction Engines TF1 facility design) forming a LH_2 pool which then vaporises to produce a flammable gas cloud. With a capacity of 4.5 tonnes the LH_2 storage tank examined is of a similar size to that which will be required for an LH_2 aircraft. The case study thus represents a natural stepping-stone for analysis on the way to the larger LH_2 storage tanks that will be required for airports operating LH_2 aircraft. Hence, it was regarded as providing a good case study for modelling LH_2 accident scenarios that will be relevant to the aims of the ENABLEH2 project.

Two different LH_2 release scenario categories were considered:

- Rupture of a LH_2 supply pipe during engine testing forming a LH_2 pool for a number of different leak rates, durations and locations (particularly the containment shelter)
- Catastrophic failure of the LH_2 storage tank – a conceivable, if highly unlikely, event

The experimental nature of the engine development and testing process mean that failures such as LH_2 leaks and ignition sources would be expected to be more likely to occur in the vicinity of the rocket engine under test, than elsewhere on the test facility. Hence the test facility also has a containment shelter around the rocket engine being tested to mitigate the consequences of any engine failure event and in particular protect the LH_2 storage tank, H_2 gas cylinders and compressor from exposure to high overpressures and prevent the occurrence of a domino effect. However, should a LH_2 leak occur in the confinement shelter, the shelter will also serve to confine the hydrogen gas cloud formed, which, if ignited, could exacerbate the resulting explosion overpressure.

The FLACS CFD model has been used to represent the engine test facility geometry and simulate the consequences of large LH_2 leaks due to supply pipe rupture and catastrophic tank failure scenarios. The flammable gas cloud dispersion behaviour produced by different LH_2 releases in the engine test facility has been studied. The effect of different mitigation measures upon consequences of the LH_2 leak scenarios has also been examined to gauge the resilience of the test facility with respect to:

- The effect of using a bund around the LH_2 tank
- The engine containment shelter – intended to mitigate the consequences of engine failure e.g. shrapnel

In the latter case, the containment shelter will offer protection to the rest of the facility should a catastrophic engine failure occur but will also serve to increase the level of confinement of a flammable hydrogen cloud formed in the shelter following a LH_2 leak. If ignited this could exacerbate the consequences of the resulting gas explosion overpressure on the surrounding facility (e.g. LH_2 storage tank). To test this FLACS has therefore been used to simulate the explosion overpressure following ignition of a flammable gas cloud in the shelter.

5.2 LH_2 Leak Release Scenarios

Two different LH_2 release scenarios were considered in the study:

(a) ***Rupture of a LH_2 supply pipe during engine testing forming a LH_2 pool.*** A 9.5 kg/s leak rate was assumed corresponding to the rupture of a liquid hydrogen supply pipe. This leak rate corresponds to the maximum liquid hydrogen supply flow rate of 7 kg/s to the engine required during engine tests multiplied by a factor of 1.35 to account for possible back pressure effects following the rupture [Taylor, 2007]. For the LH_2 pipe rupture scenario leak durations of 30 s were examined. Three different pipe rupture locations at the test facility were considered: (i) at the LH_2 storage tank; (ii) at the hydrogen mixer; and (iii) in the engine containment enclosure. For the

case of a pipe rupture leak in the engine containment shelter a 9.5 kg/s leak rate with a shorter duration of 10 s and a lower 0.5 kg/s leak rate were also both considered. Longer 180 s duration leaks were also examined for the pipe leak located at the LH_2 storage tank to determine the impact of the bund upon longer duration LH_2 spills.

Table 5.1 - The different LH_2 release scenarios examined.

Case	Leak Rate (kg/s)	Duration (s)	Leak Location	LH_2 Tank Bund?
1	9.5	30	LH_2 Tank	yes
2	9.5	30	LH_2 Tank	no
3	9.5	30	H_2 Mixer	n/a
4	9.5	30	Containment Shelter	n/a
5	0.5	30	Containment Shelter	n/a
6	9.5	10	Containment Shelter	n/a
7	9.5	180	LH_2 Tank	yes
8	9.5	180	LH_2 Tank	no
9	225	20	LH_2 Tank	yes
10	225	20	LH_2 Tank	no

(b) ***Catastrophic failure of the LH_2 storage tank.*** The catastrophic LH_2 storage tank failure was characterised by a LH_2 leak rate of 225 kg/s discharging the entire contents of the tanks (4.5 tonnes) in 20 s.

For both of the scenarios considering a leak at the LH_2 storage tank the impact of using a bund around the LH_2 storage tank on the resulting LH_2 spill and the flammable gas cloud formed was also studied.

Table 5.1 summarises the different LH_2 release scenarios examined in the study.

5.3 Simulation Details

5.3.1 Geometry of Engine Test Facility

Fig. 5.1(a) shows the geometry of the engine test facility modelled, surrounded by 5 m high (banked) protective outer walls. Fig. 5.1(b) shows a closer view of the facility located inside the walls. Notable features represented include the LH_2 storage tank, the engine containment shelter, compressor

enclosure, H_2 mixer, GH_2 gas cylinder storage, LN2 tank and vaporisers, compressed air tank and flare stack.

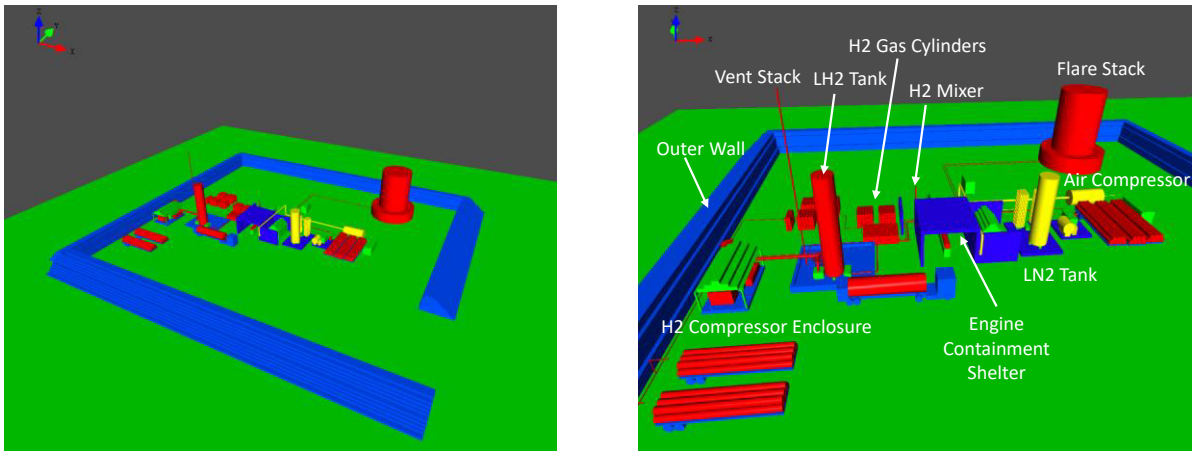

(a) (b)

Fig. 5.1 - Geometry of LH_2 Test Facility model used in FLACS.

Fig. 5.2 shows a close-up of the location of 9.5 kg/s LH_2 pool leak modelled in the vicinity of the LH_2 tank. Fig 5.2(a) shows the case where the raised platform on which the LH_2 tank is standing has a 0.5 m high bund running around its perimeter, whilst Fig 5.2(b) shows the case without the LH_2 tank bund. Similarly, Fig. 5.3 shows a close-up of the location of 9.5 kg/s LH_2 pool leak: (a) modelled at the location of the H_2 mixer situated at the rear of the engine containment shelter; and (b) modelled in the engine containment shelter.

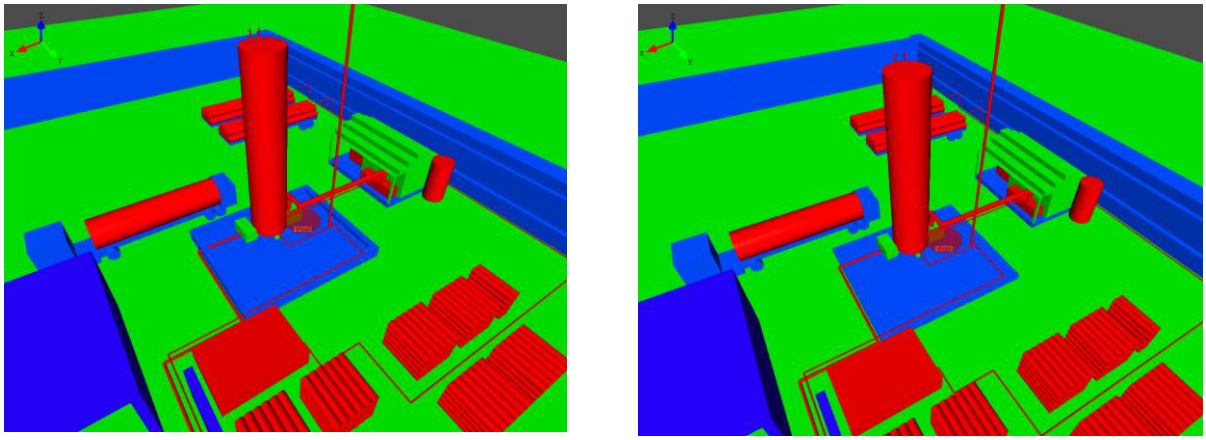

(a) (b)

Fig. 5.2 LH_2 pool leaks located at LH_2 storage tank: (a) with 0.5 m high bund running around platform perimeter; (b) without bund running around platform perimeter.

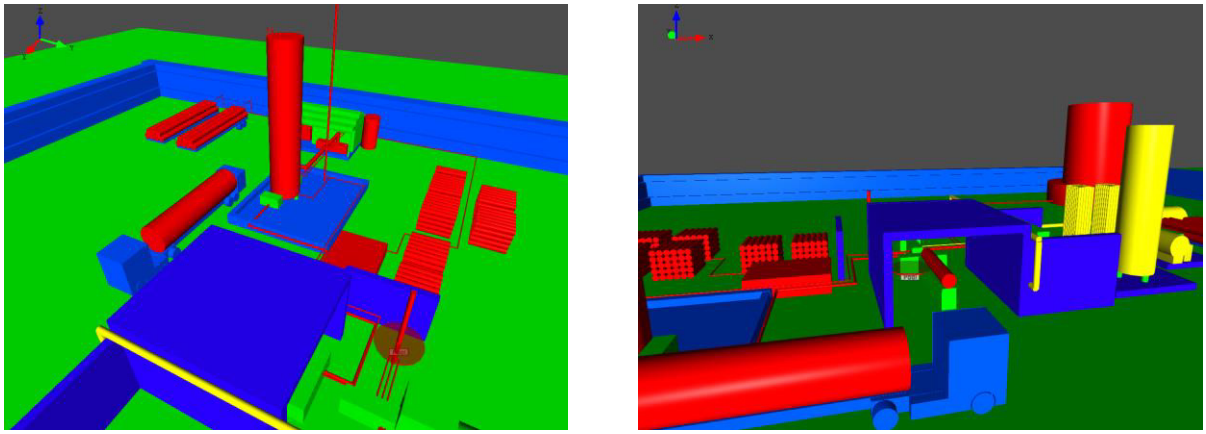

(a) (b)

Fig. 5.3 Additional LH_2 pool leak scenarios: (a) leak located at H_2 Mixer; (b) leak located in engine containment shelter.

5.3.2 Domain and Grid

The LH_2 pipe rupture dispersion simulations were performed on a domain 230 m × 180 m × 40 m in the X, Y and Z directions (-30 m to 200 m, -30 m to 150 m, 0 to 40 m). A 1 m cell size was used in the core region encompassing the test facility (-5 m to 125 m, 10 m to 115 m, 0 to 10 m). Outside this region the grid cell size was increased, by using an expansion factor of 1.2, and setting a maximum grid cell size of 4 m.

An initial grid sensitivity study was made comparing the standard grid (1 m x 1 m x 0.5 used in the core region) with a finer grid (0.5 m x 0.5 m x 0.25 m used in the core region). This suggested that the results were reasonably insensitive to the finer grid cell size (e.g. a 2% change in the peak Q9 value and a 5% difference in maximum hydrogen concentrations at the monitor locations). For the remaining simulations a hybrid grid was employed, based on using the standard grid in the core region, but now refining only the grid around the area of the LH_2 pool release (as recommended by FLACS user guidelines for pool simulations [Gexcon, 2019]), so that a refined grid cell size of 0.5 m was used in the X and Y directions and 0.25 m in the Z direction. This hybrid grid was found to produce very similar results to the original fine grid case. A total number of 885,060 control volumes (180 x 149 x 33) were used (850,608 for the LH_2 leak located at the H_2 mixer).

For the catastrophic LH_2 tank failure dispersion simulations the size of the domain was extended to 330 m × 180 m × 80 m in the X, Y and Z directions (-30 m to 300 m, -30 m to 150 m, 0 to 80 m) with a 1 m x 1 m x 0.5 used in the core region, refined to 0.5 m x 0.5 m x 0.25 around the LH_2 leak, giving a total of 1,313,435 control volumes (205 x 149 x 43).

The FLACS explosion simulations were performed on a domain 330 m × 280 m × 80 m in the X, Y and Z directions (-130 m to 200 m, -80 m to 200 m, 0 to 80 m). A uniform cubical 1 m cell size was used in the core region encompassing the test facility (-50 m to 120 m, -15 m to 140 m, 0 to 20 m). Outside this region the grid cell size was increased, by using an expansion factor of 1.2, and setting a maximum grid cell size of 4 m, giving a total of 218 x 195 x 40 cells (1,700,400 cells). Grid sensitivity was tested by using a uniform cubical 0.5 m cell size in the core region encompassing the test facility (-50 m to 120 m, -15 m to 140 m, 0 to 20 m) with an expansion factor of 1.2, to a maximum grid cell size of 2 m, giving a total of 346 x 306 x 59 cells (6,246,684 cells). The results suggested a moderate degree of grid

sensitivity between the standard and fine grid (e.g. approximately 20% difference in peak overpressures for monitor points located at the LH_2 storage tank).

5.3.3 Model Parameters

The ambient temperature was set to 20°C. The Pasquill atmospheric stability class was set to class F – stable. The characteristic wind speed was set to 2.0 m/s, at a reference height of 10 m, with a wind direction of 270° (i.e. running along the x-axis from –ve to +ve). The ground roughness length for the wind profile was set to 0.03 m. The FLACS pool model ground was set to type “Concrete” (thermal conductivity 1.1 W/m/K, thermal diffusivity 10^{-6} m^2/s).

The pool release was started after 10 seconds of simulation time to allow the wind field to become established. As a conservative assumption with regard to formation of liquid pool and subsequent dispersion behaviour, it was further assumed that all of the LH_2 release was deposited into the LH_2 pool and that the effects of flash vaporisation were neglected.

For the FLACS explosion simulations a stoichiometric hydrogen cloud of the appropriate volume (based upon the maximum Q9 value obtained for a given dispersion scenario) and location was defined in the facility and the explosion simulated for a number of different ignition point locations in the cloud.

5.4 Results

5.4.1 LH_2 Pipe Rupture Leak for 30 s

Fig. 5.4 compares the development of the LH_2 pool, at three different times, formed by the 30 second (9.5 kg/s) leak located at the LH_2 tank, both with (left) and without a bund (right). With the bund present the LH_2 spill remains contained to the area of the tank platform. Without the bund, LH_2 spills over the side of the platform onto the surrounding ground, covering a larger area, but with a shallower depth.

Consequently the pool vaporises more rapidly, and has almost completely evaporated after 54 seconds, while the pool contained by the bund still persists.

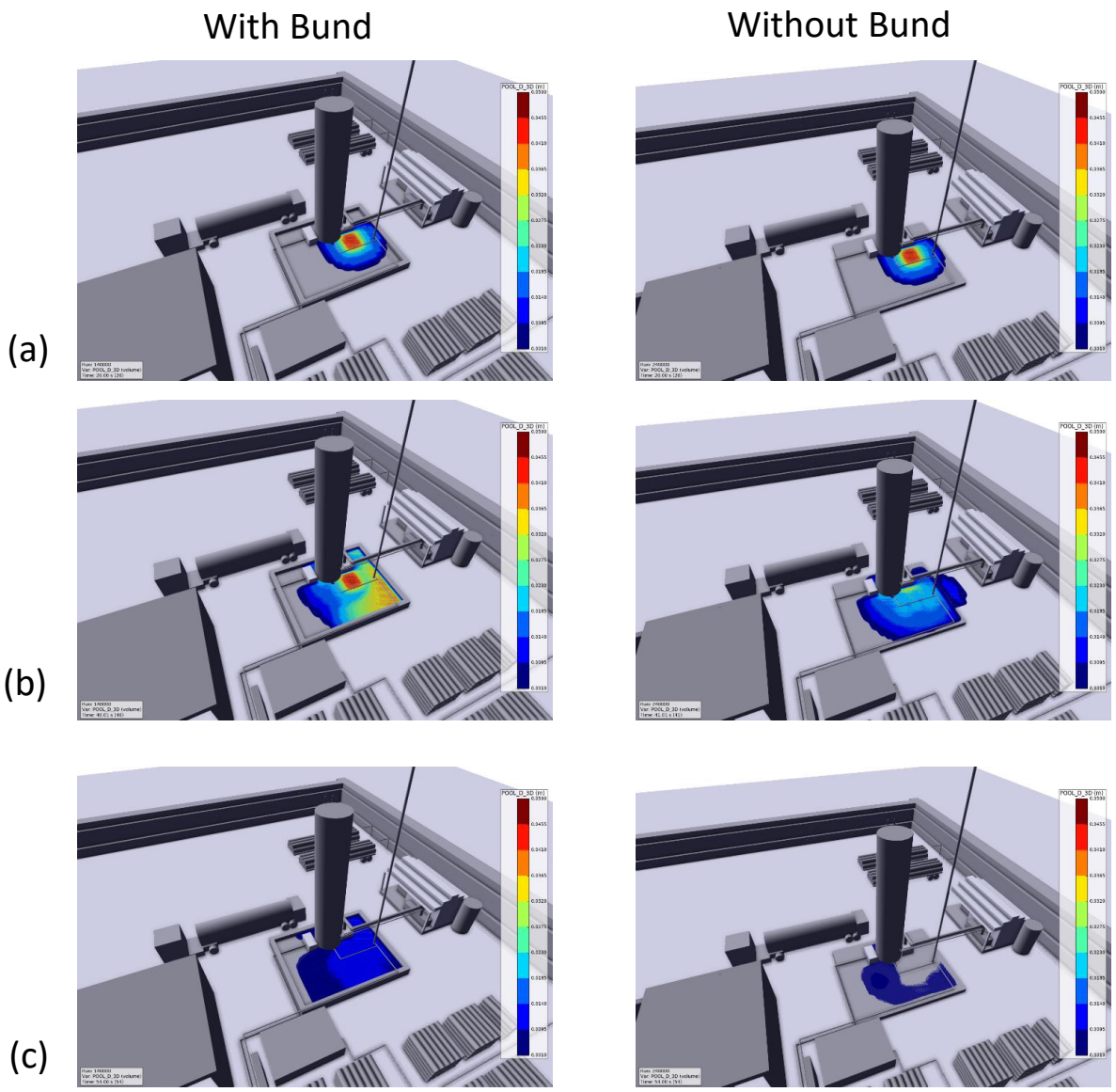

Fig. 5.4 Comparison of LH_2 pool development for 9.5 kg/s release for 30 s at the LH_2 storage tank with bund (left) and without bund (right) at: (a) 20 s; (b) 40 s; (c) 54 s.

Fig. 5.5 shows the development of the flammable hydrogen gas cloud formed by the LH_2 spill for case 1 (with a bund). It can be seen that the as the gas cloud develops, it rises up the leeward side of LH_2 Tank, where it is shielded from the wind. Consequently a significant flammable cloud develops

downwind, in the wake of LH_2 Tank (a-b), becoming buoyant (c) and extending above and beyond the outer wall (d).

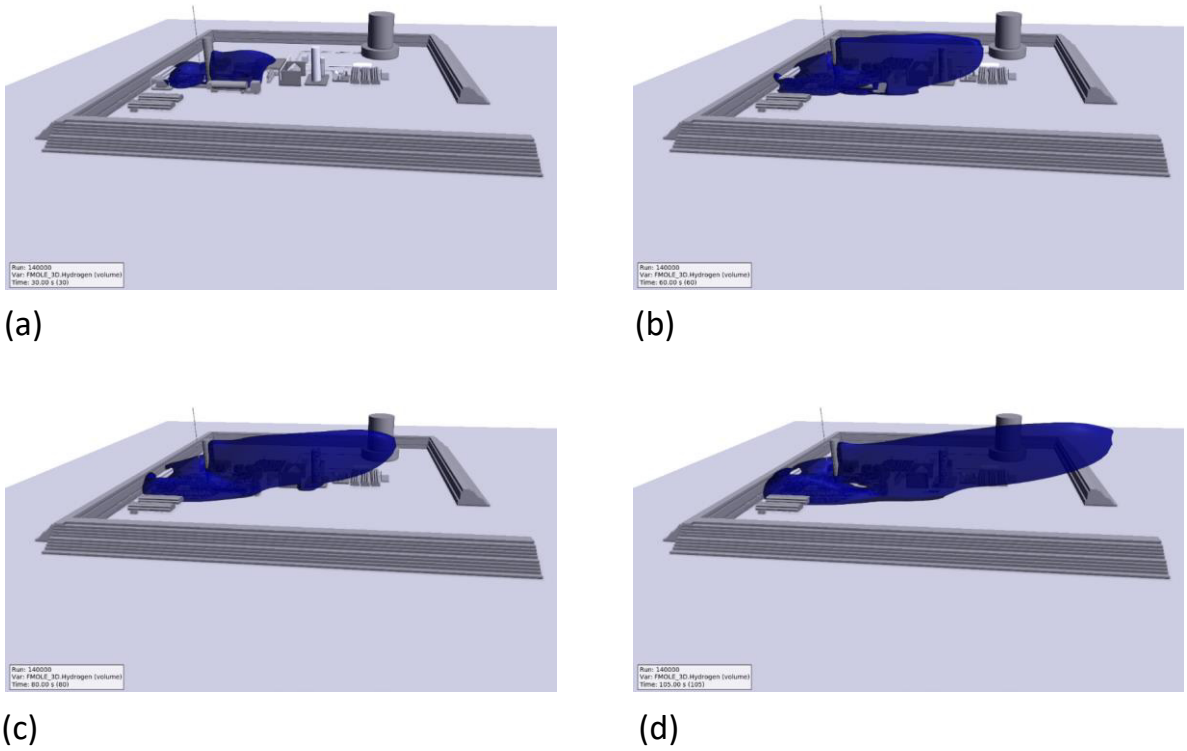

(a) (b)

(c) (d)

Fig. 5.5 Flammable cloud development (4% v/v hydrogen iso-surface) for Case 1 – 9.5 kg/s 30 s with LH_2 leak located at LH_2 storage tank with bund at: (a) 30 s; (b) 60 s; (c) 80 s; (d) 105 s. The results illustrate how the cloud develops up the leeward side of the LH_2 tank where it is shielded from the wind (running west to east).

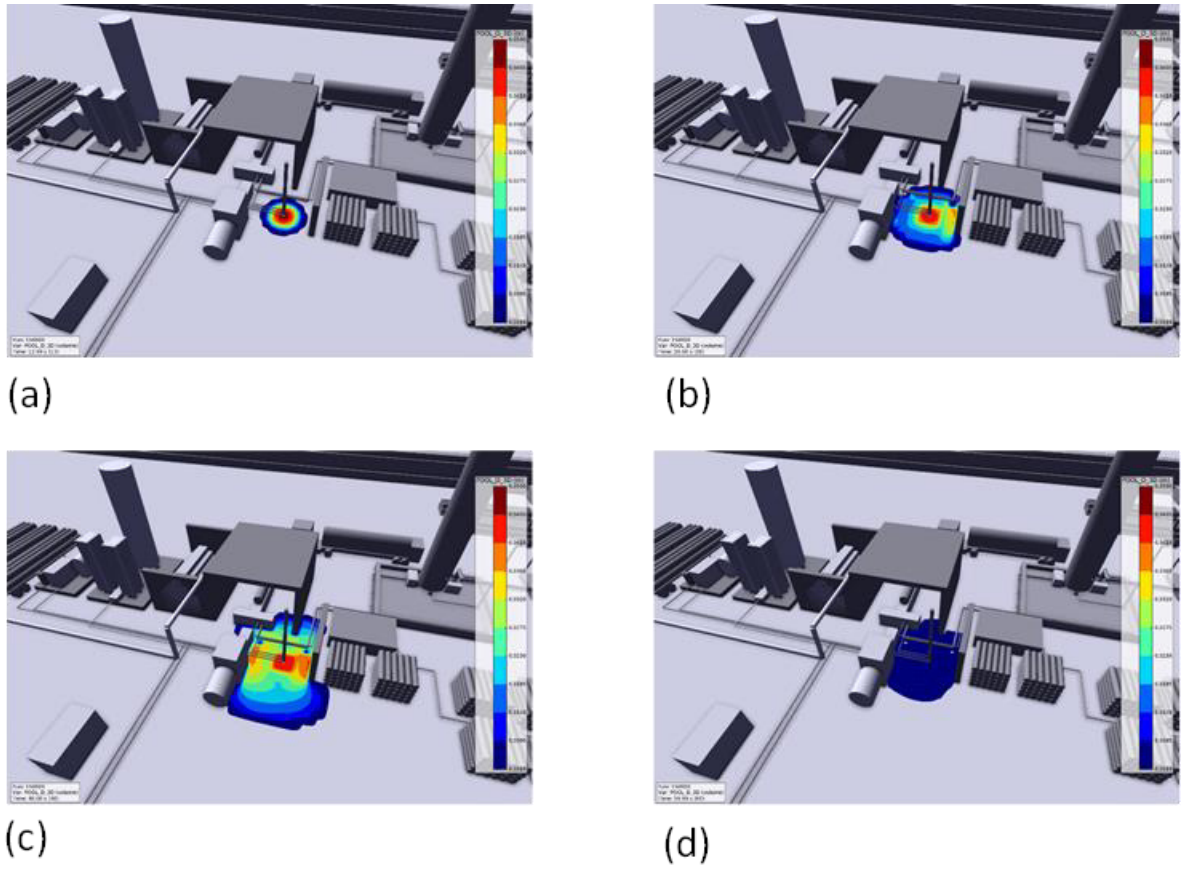

Fig. 5.6 Development of LH_2 pool for a 9.5 kg/s, 30 s leak from H_2 Mixer at: (a) 13 s; (b) 20 s; (c) 40 s; (d) 60 s.

Fig. 5.6 shows the development of the LH_2 pool formed by the 30 second (9.5 kg/s) leak located at the H_2 mixer. In this case the pool spreads between the GH_2 gas cylinder wall and engine silencer towards the engine containment shelter. Similarly Fig. 5.7 shows the development of the LH_2 pool formed by the

30 second (9.5 kg/s) leak in the engine confinement shelter. The LH_2 pool spreads between the shelter wall and engine support and out of the openings at either end of the shelter.

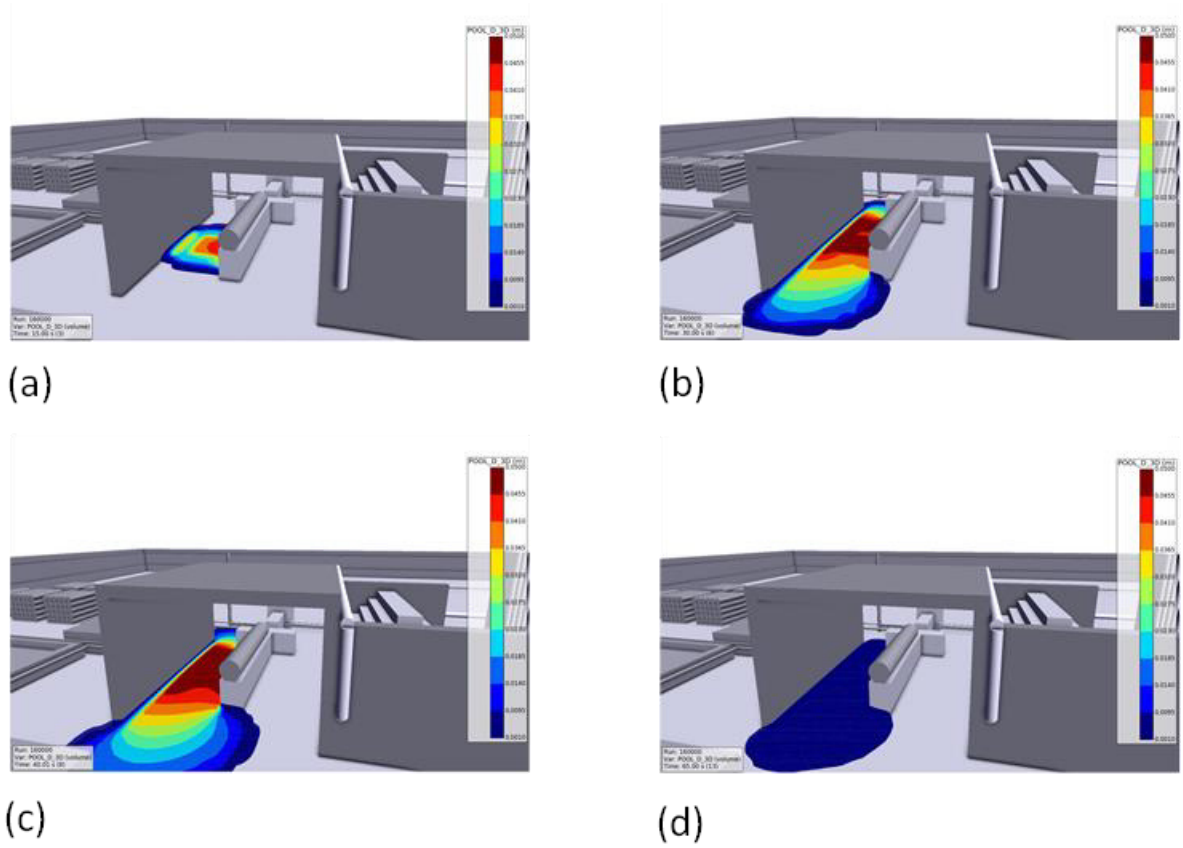

Fig. 5.7 Development of LH_2 pool for a 9.5 kg/s, 30 s leak in Engine Containment Shelter at: (a) 15 s; (b) 30 s; (c) 40 s; (d) 65 s.

Fig 5.8. shows the variation of LH_2 pool area versus time predicted for the four different 30 s pipe rupture (9.5 kg/s) release cases 1-4 (LH_2 release for tank with bund, without bund, at H_2 mixer and in the containment shelter). Comparing the curves obtained for the LH_2 tank release, it is evident that the LH_2 tank bund slightly reduces the maximum area of the LH_2 pool, and extends the vaporisation time for the pool from 54 to 70 s. The release for the H_2 mixer, achieves a similar peak pool area to the un-bunded LH_2 tank case, but takes longer to vaporise, probably as a consequence of its spread being impeded by the presence of the GH_2 cylinder wall and engine silencer. The LH_2 leak in the containment shelter reaches a similar peak pool area, but also takes longer time to grow and vaporise, due to its spread being restricted by the shelter walls and engine support.

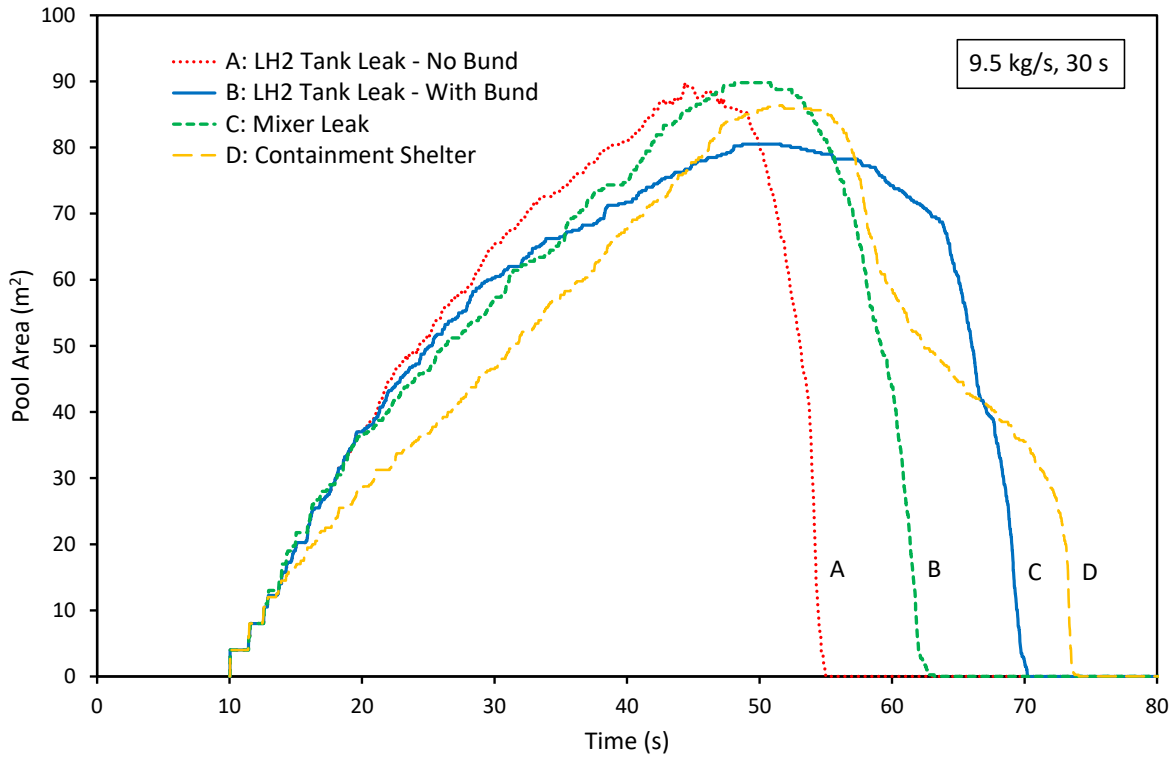

Fig. 5.8 Comparison of the predicted LH_2 Pool Area versus time for the four 9.5 kg/s, 30 s leak scenario cases (1-4).

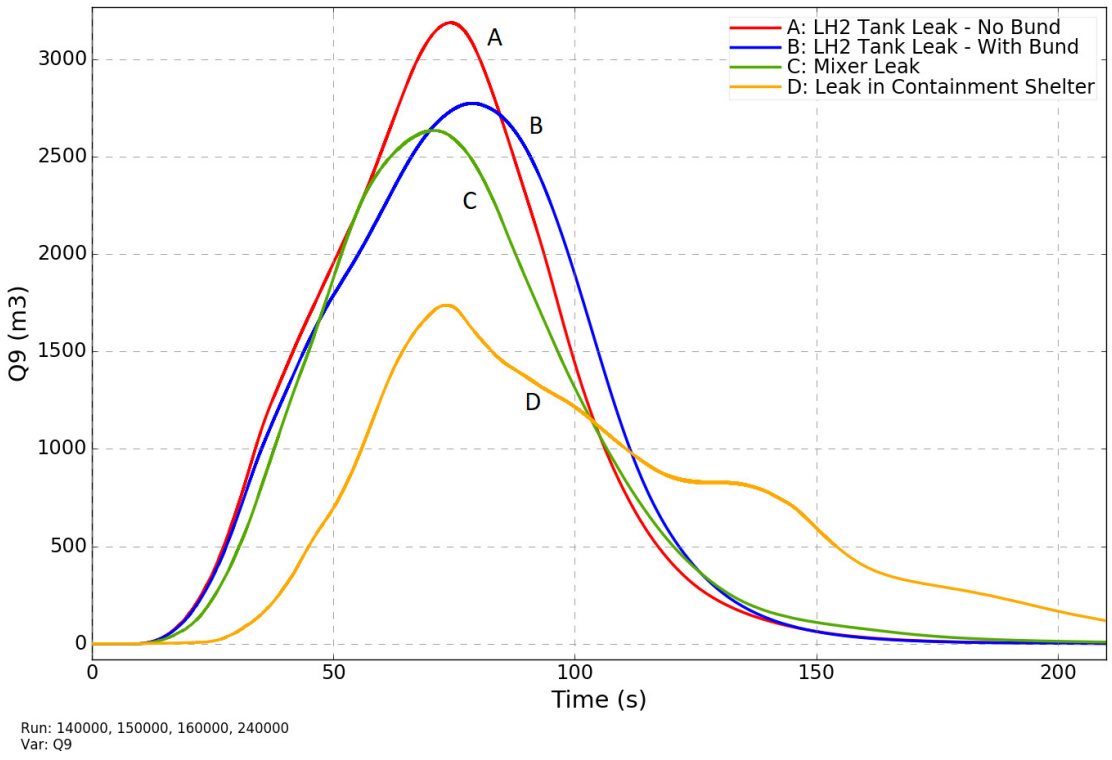

Fig. 5.9 Comparison of the predicted Q9 equivalent stoichiometric gas cloud volumes versus time for the four 9.5 kg/s, 30 s leak scenario cases (1-4).

Fig 5.9. shows the Q9 equivalent stoichiometric gas cloud volumes versus time predicted for the four cases. The LH_2 tank release, without the bund, produces the highest maximum Q9. Conversely the LH_2 leak in the containment shelter is predicted to produce a significantly lower peak Q9 than the other three cases (due to dispersion of the flammable cloud being restricted by the shelter). All four cases reach a maximum at a broadly similar time - around 70 s.

5.4.2 Containment Shelter – LH_2 leak scenarios

Fig. 5.10 compares the variation of the LH_2 pool area with time for the three different leak scenarios simulated in the confinement shelter. It can be seen that reducing the leak rate from 9.5 kg/s to 0.5 kg/s (Case B) results in an LH_2 pool with a very small maximum area. Likewise decreasing the duration of the 9.5 kg/s leak from 30 s to 10 s (Case C), reduces the peak area of the LH_2 pool to around half that of the 30 s case. It also reduces the total vaporisation time for the spill. Fig. 5.11 shows the corresponding Q9 equivalent stoichiometric gas cloud volumes versus time predicted for the three cases. The spill rate of 0.5 kg/s (Case B) produces a much lower peak Q9 (around 200 m^3) whilst the lower release time of 10 s (Case C) results in an intermediate peak Q9 of 500 m^3, around a third of the 1500 m^3 peak Q9 predicted for the 30 s leak (Case A).

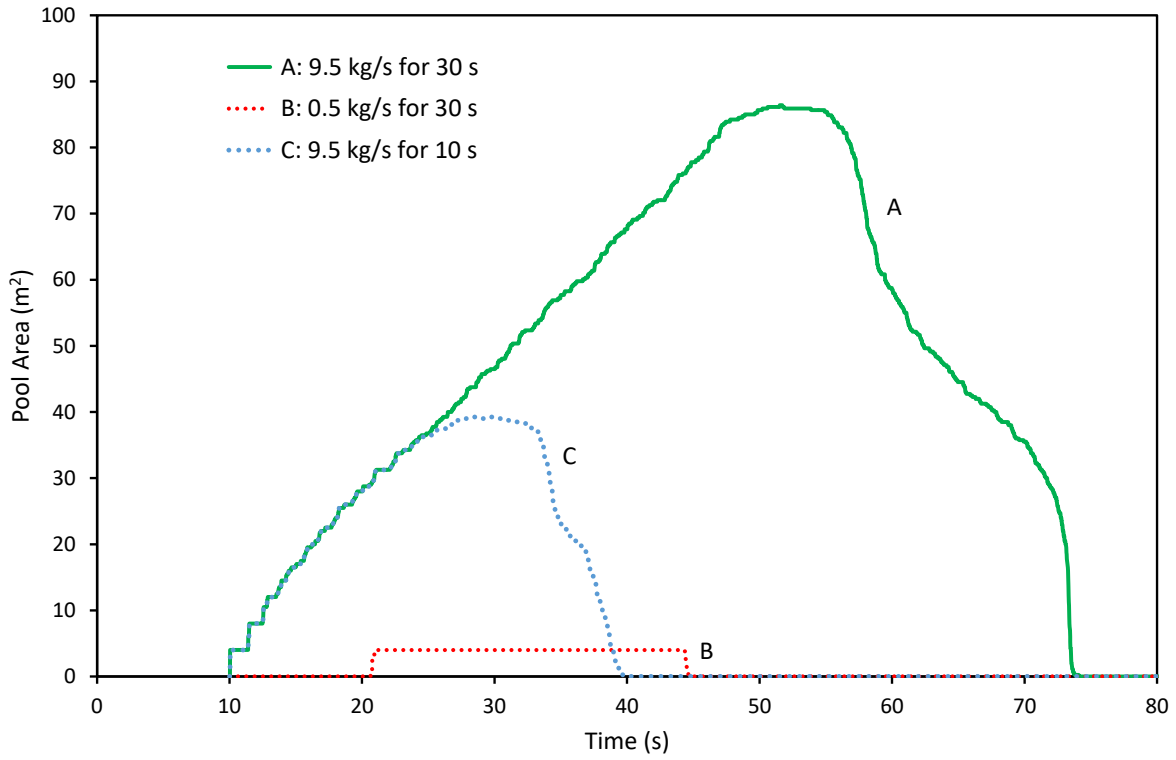

Fig. 5.10 Comparison of the predicted LH_2 Pool Area versus time for the three leak scenario cases modelled in the Engine Containment Shelter (4-6).

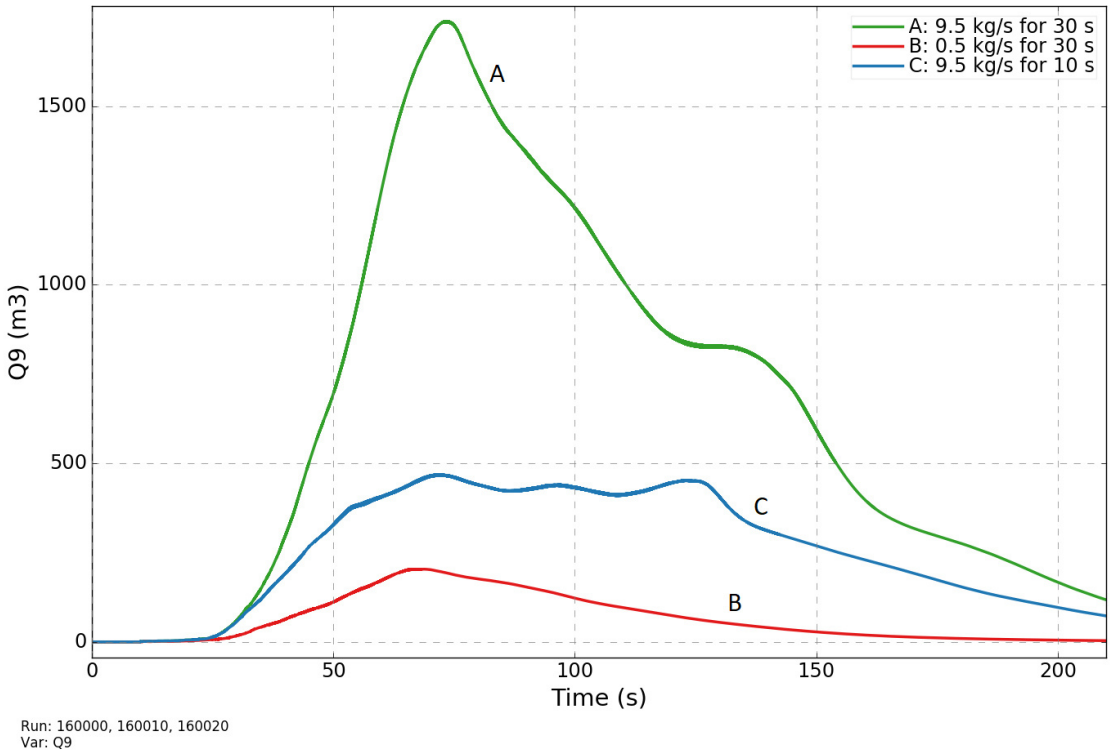

Fig. 5.11 Comparison of the predicted Q9 equivalent stoichiometric gas cloud volumes versus time for the three leak scenario cases modelled in the Engine Containment Shelter (4-6).

5.4.3 LH_2 Tank Pipe Rupture Leak for 180 s

Fig. 5.12 compares the development of the LH_2 pool, at three different times, formed by the extended 180 second (9.5 kg/s) leak located at the LH_2 tank, both with (left) and without a bund (right). For the longer release time, the differences between the two cases become far more pronounced, with the un-bunded spill spreading over a much larger area, but also vaporising far more rapidly (only a small shallow patch remains after 220 s). In contrast the bunded release remains contained, forming a deep pool which is still present after 410 s.

Fig. 5.13 shows the variation of LH_2 pool area versus time predicted for the two 180 s pipe rupture release cases 4 and 5 (LH_2 release for tank with and without bund). As would be expected the pool area of the bunded case is capped at a maximum (95 m^2) reached after 70 s, which is then maintained for the duration of the simulation (410 s). In contrast the pool without the bund continues to grow

achieving a maximum area that is approximately 2.5 times larger (238 m^2), than the bunded case, but which vaporises much more rapidly, disappearing after 225 s.

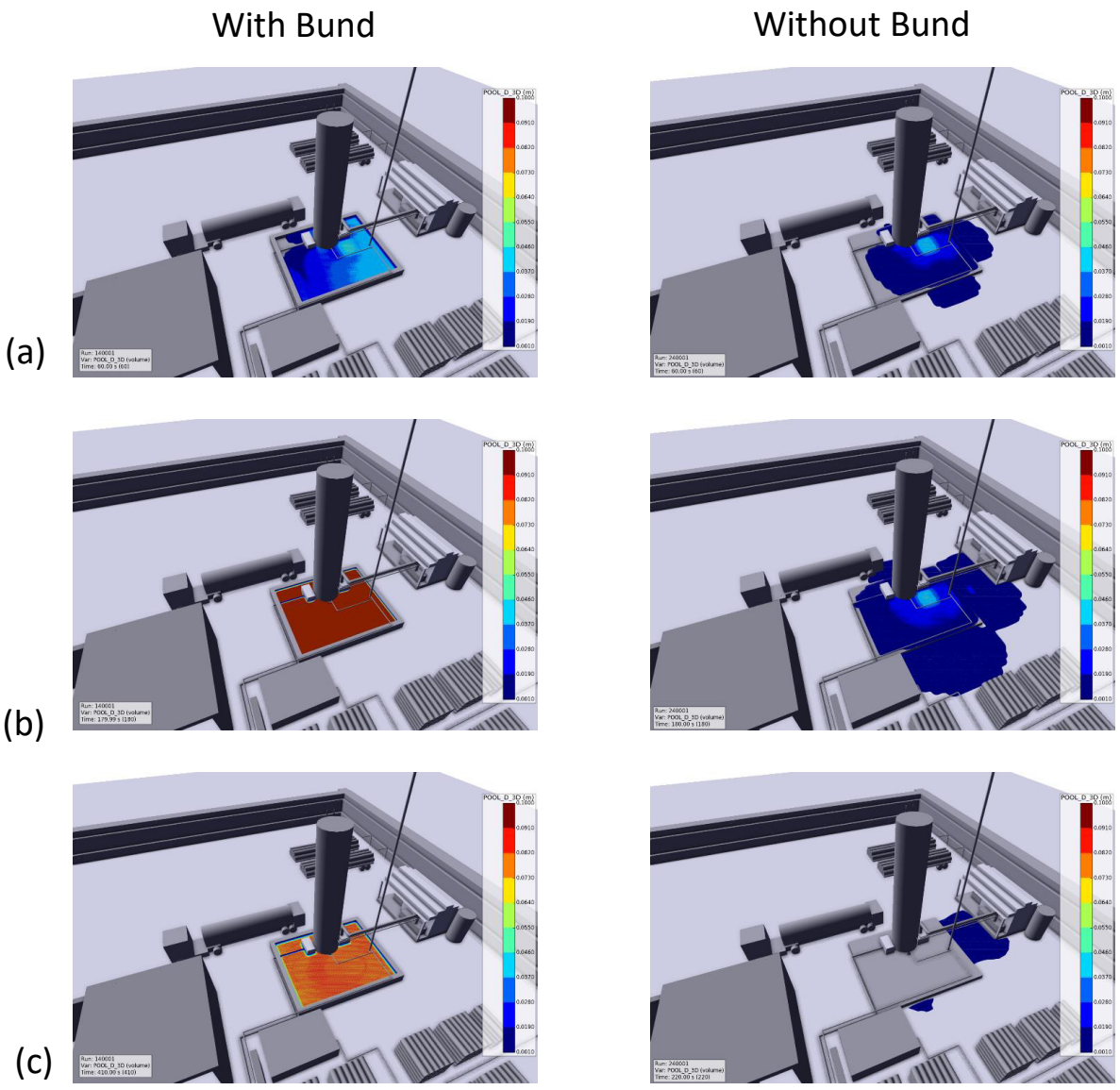

Fig. 5.12 Comparison of LH_2 pool development for 9.5 kg/s release for 180 s at the LH_2 storage tank with bund (left) and without bund (right) at: (a) 60 s; (b) 180 s; (c) left – after 410 s (LH_2 pool still present in bund); right – after 220 s (LH_2 pool almost completely vaporised).

Fig 5.14. compares the Q9 equivalent stoichiometric gas cloud volumes versus time predicted for the two 180 s pipe rupture release cases. It is evident that the larger area, shallower more rapidly vaporising LH_2 pool produced for the un-bunded case results in a significantly higher maximum Q9 gas cloud volume (approx. 2.5 times greater) than for the case where a bund is present.

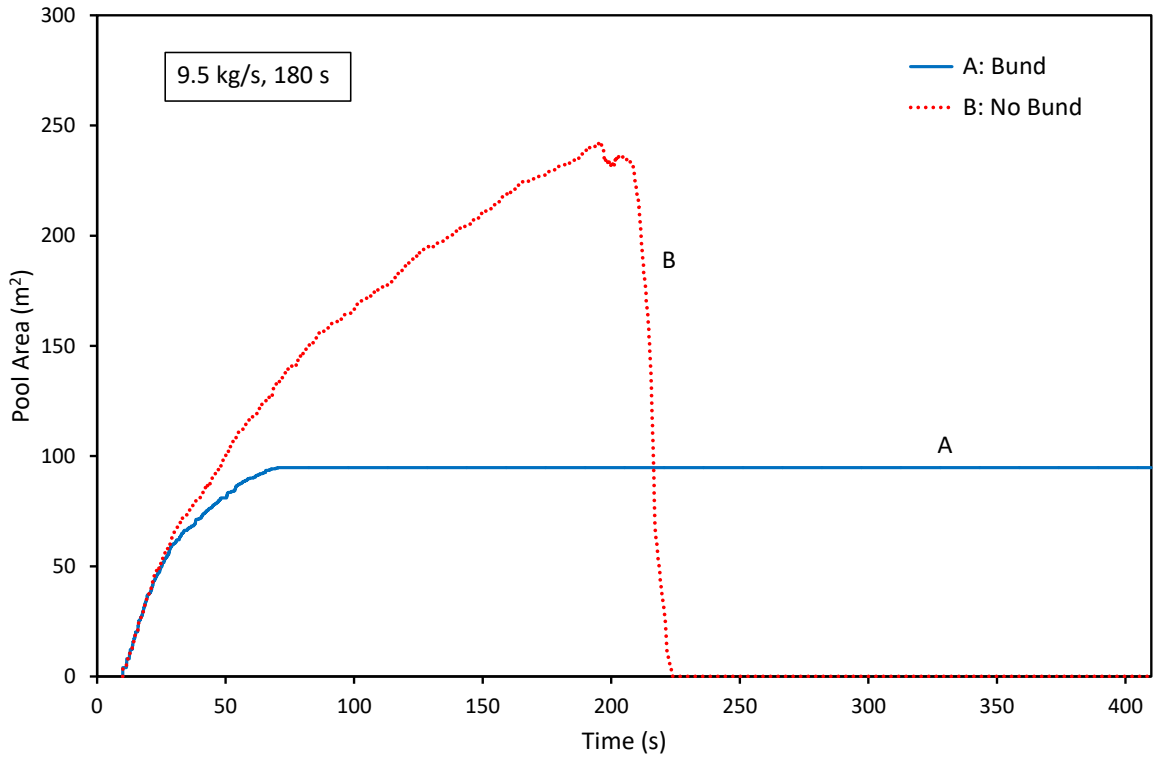

Fig. 5.13 Comparison of the predicted LH_2 Pool Area versus time for the two 9.5 kg/s, 180 s leak scenario cases (7-8) with and without a LH_2 storage tank bund.

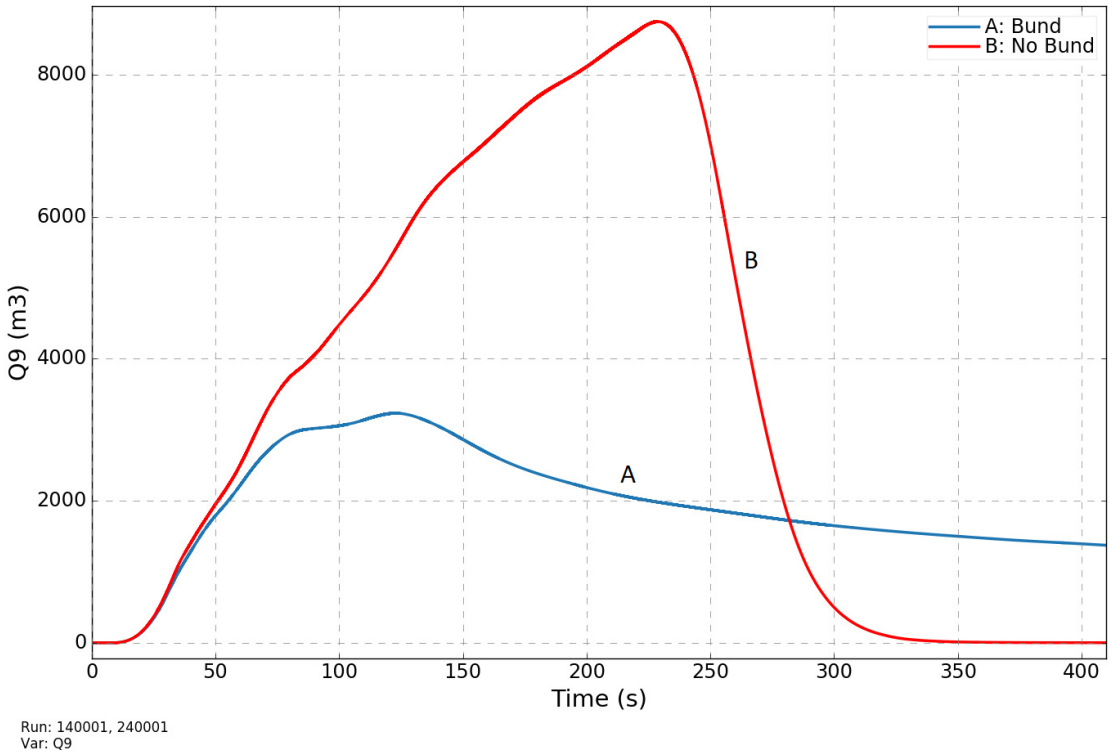

Fig. 5.14 Comparison of the predicted Q9 equivalent stoichiometric gas cloud volumes versus time for the two 9.5 kg/s, 180 s leak scenario cases (7-8) with and without a LH_2 storage tank bund.

5.4.4 Catastrophic failure of LH_2 storage tank

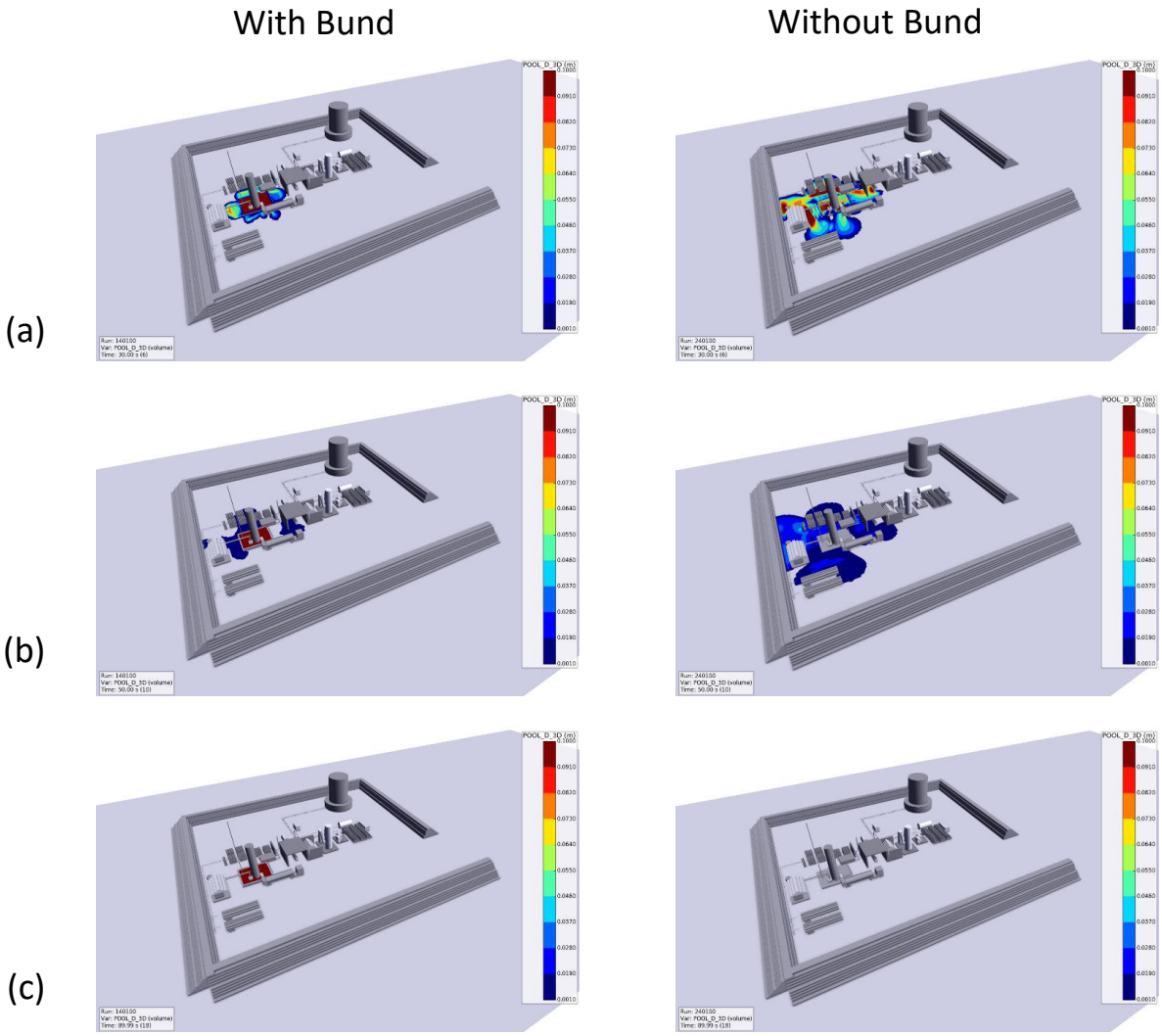

Fig. 5.15 Comparison of LH_2 pool development for a catastrophic 225 kg/s release for 20 s at the LH_2 storage tank with bund (left) and without bund (right) at: (a) 30 s; (b) 50 s; (c) 90 s.

Fig. 5.15 compares the development of the LH_2 pool, at three different times, resulting from the catastrophic failure of the LH_2 storage tank (225 kg/s leak over 20 s) both with (left) and without a tank bund (right). For such a high release rate, even the 0.5 m high bund fitted around the perimeter of the tank platform is unable to prevent LH_2 spilling over into the surrounding area – see Fig. 5.15(a), at the end of the spill (30 s). However, it can also be seen that, without the bund, the area of the spill region is significantly larger and deeper (right). The over-spill outside the tank bund quickly vaporises away (Fig. 5.15(b) left) to leave a deep LH_2 pool contained inside the bund which persists over a long period of time (Fig. 5.15(c) left).

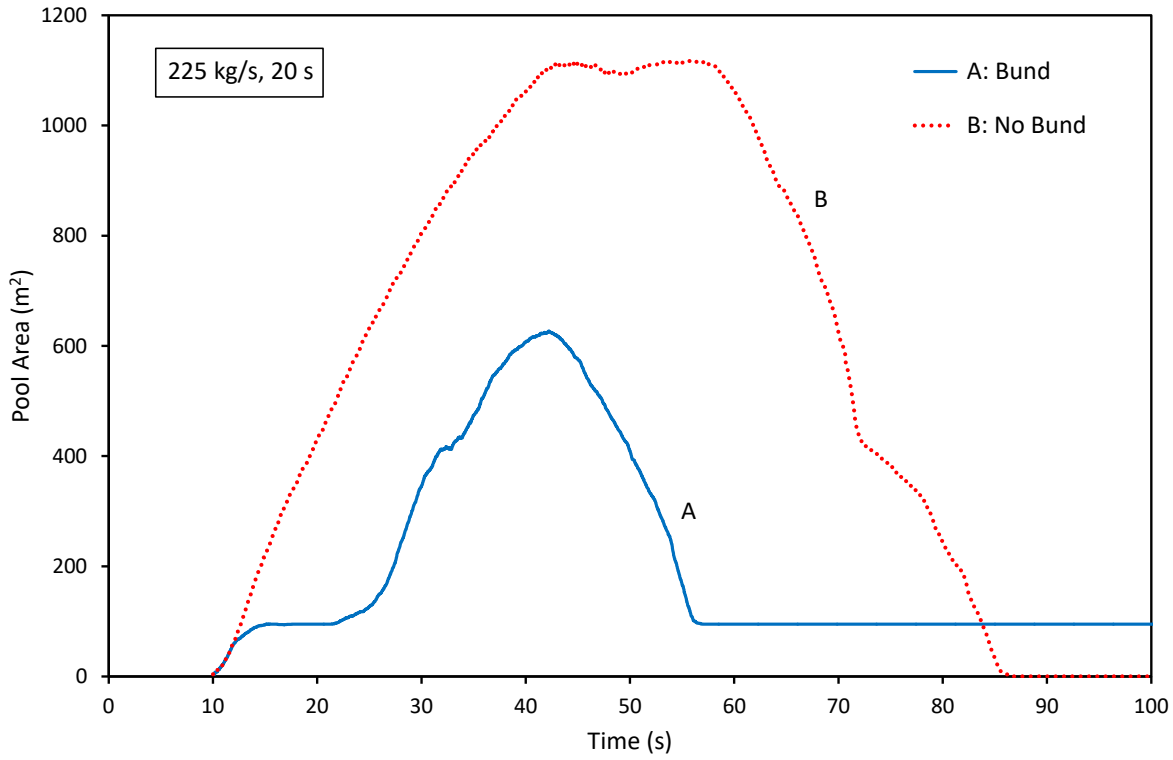

Fig. 5.16 Comparison of the predicted LH_2 Pool Area versus time for the two catastrophic 225 kg/s, 20 s leak scenario cases (9-10) with and without a LH_2 storage tank bund.

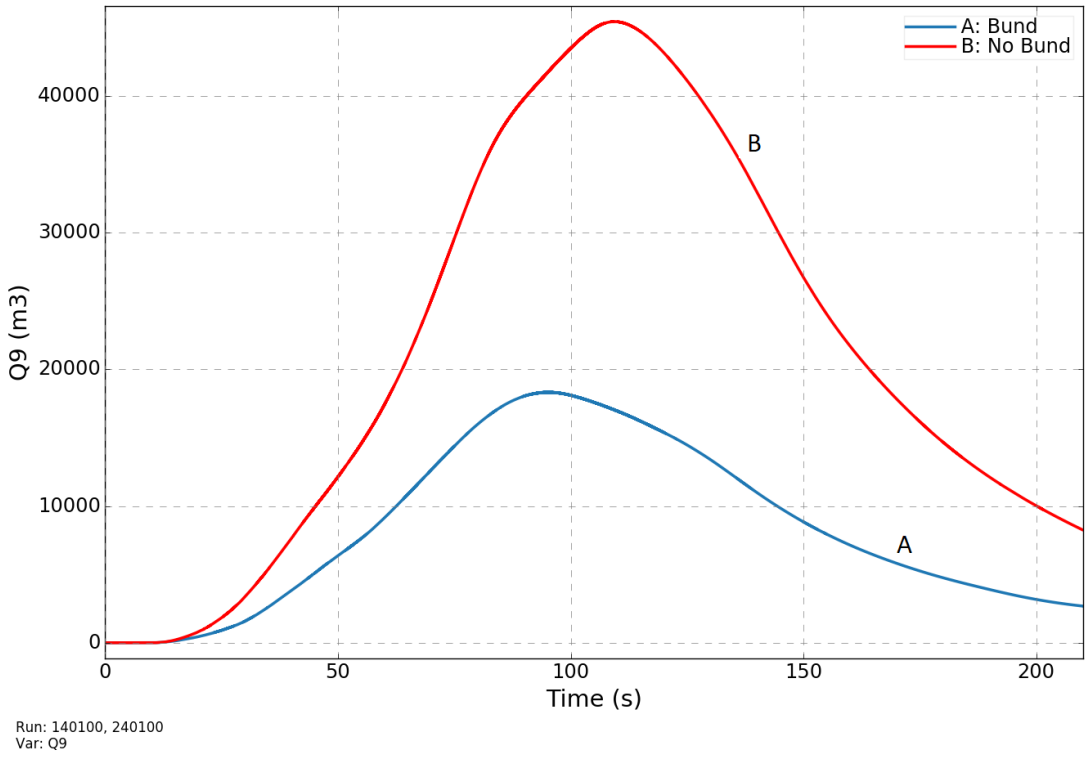

Fig. 5.17 Comparison of the predicted Q9 equivalent stoichiometric gas cloud volumes versus time for the two catastrophic 225 kg/s, 20 s leak scenario cases (9-10) with and without a LH_2 storage tank bund.

In contrast the area of the LH_2 spill for the unbunded tank is larger (Fig. 5.15(b) right) but has completely vaporised after 90 s (Fig. 5.15(c) right).

Fig. 5.16 shows the variation of LH_2 pool area versus time predicted for the two catastrophic LH_2 tank release cases 9 and 10 (for tank with and without bund). The overspill produced for the bunded tank mean that the maximum LH_2 pool area is no longer capped at 95 m^2, but increases to around 600 m^2. However, it is still significantly less than that predicted for the unbunded tank, where the maximum LH_2 pool area is 1100 m^2, almost double that found for the bunded case. After reaching a peak, the LH_2 pool area bunded case rapidly drops back to 95 m^2, after 57 s, whilst the unbunded LH_2 pool has completely vaporised after 85 s.

Finally, Fig. 5.17 compares the corresponding Q9 equivalent stoichiometric gas cloud volumes versus time predicted for the two catastrophic LH_2 tank release cases 9 and 10 (for tank with and without bund). Once again the LH_2 release for the unbunded tank, produces a significantly higher maximum Q9 gas cloud volume (approx. 2.5 times greater) than for the case where a bund is present.

5.4.5 Explosion Consequences for LH_2 Leak in Engine Containment Shelter

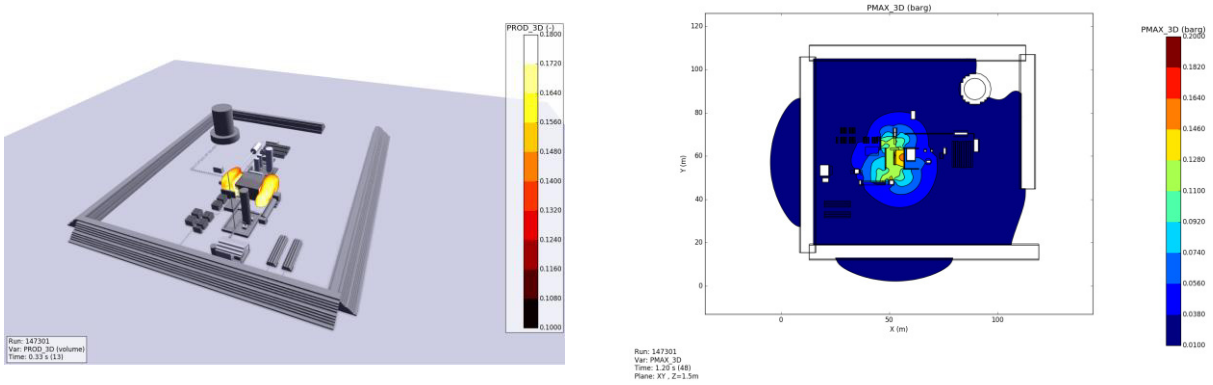

(a) (b)

Fig. 5.18 Explosion simulation results for ignition of a stoichiometric hydrogen gas cloud filling the Engine Containment Shelter: (a) Flame front after 0.3 s after ignition; (b) Maximum overpressure in the test facility on a horizontal plane located 1.5 m above ground level.

To examine the potential effect of an explosion overpressure being enhanced, for a LH_2 leak in the containment shelter, a stoichiometric flammable cloud of volume equivalent to the peak Q9 – corresponding to that found for case 6 was introduced into the region of the containment shelter. FLACS was then used to model the ignition of the flammable gas cloud and predict the resulting explosion overpressures.

Fig. 5.18 show an example of (a) the flame front development and (b) maximum overpressures predicted for the ignition of a stoichiometric cloud filling the containment shelter. It can be seen that the region of higher overpressures is confined to the vicinity of the shelter and the areas around the openings at either end – directed along the axis of the shelter and that the maximum overpressure in the vicinity of the LH_2 storage tank and gas cylinders is predicted to be less than 0.1 barg.

A table of damage to structures and equipment from overpressure events [Rigas and Amyotte, 2012; LaChance at al., 2011] suggest an indicative overpressure of 0.5 barg to cause displacement of a cylindrical storage tank and failure of pipes. Hence, even allowing for an uncertainty of a factor of two,

the predicted results suggest that the overpressure exposure of the LH_2 storage tank and gas cylinders following ignition of a flammable gas cloud in the shelter could remain at a tolerable level.

5.5 Discussion

5.5.1 Shielding from wind by LH_2 storage tank and outer walls

The model dispersion results suggest that the dispersing hydrogen gas cloud formed by the LH_2 spills developing downwind of facility structures and walls, and in particular the LH_2 storage tank, were shielded from the effect of the wind. Consequently the flammable gas cloud was able to rise up the leeward side of LH_2 Tank and form a significant flammable cloud in its wake. Similar behaviour was observed by Statharas et al. [2000] who found that the wind direction had a significant effect upon the cloud dispersion behaviour due to the shielding effect of the surrounding buildings when they modelled the BAM experimental tests.

5.5.2 Effect of LH_2 tank bund

The results suggest that for longer duration LH_2 pipe ruptures and even for a catastrophic LH_2 tank failure the presence of a bund around the LH_2 tank could produce a significant difference in the size of the flammable cloud formed. With a bund, LH_2 from the spill is contained, resulting in the accumulation of a deep LH_2 pool. This vaporises relatively slowly and continues to sustain the flammable gas cloud after the release has stopped. However, both the area of the LH_2 spill and the maximum flammable mass and Q9 equivalent stoichiometric gas cloud volumes are significantly reduced when compared with the un-bunded tank scenario.

Hence in the (unlikely) event of a LH_2 tank supply pipe rupture or catastrophic LH_2 tank failure, the results support the use of a LH_2 tank bund in restricting the spread of the LH_2 pool (both in terms of area and preventing the spill reaching other sensitive areas of the test facility such as GH_2 cylinders, engine containment shelter and compressor enclosure) and the size of the flammable gas cloud and Q9 volume. However, this must also be balanced against the extended life and vaporisation time of the LH_2 pool – which may then present a greater pool fire risk in the vicinity of the LH_2 tank. Hence, the results would appear to indicate that there could be a potential trade-off in terms of the mitigating the consequences of an LH_2 spill - not using a bund could enhance vaporization and dispersion of LH_2 and reduce time at risk of ignition, and ground level travel distance, but may also serve to increase the ultimate size of the resulting flammable gas cloud.

The predicted effectiveness of the bund or dike around the LH_2 storage tank in reducing the size of the flammable cloud would also appear to contradict the guidance given in standard NFPA-2 [2016] recommending that LH_2 spills not be diked. For example it is stated in section 6.14 Spill Control, Drainage, and Secondary Containment that:

"***6.14.2 LH_2.*** *Diking shall not be used to contain an [LH_2] spill. [55:11.3.1.2]*"

and for the notes given in section A.8.2.2.3.9.4(B):

"The intent of these provisions is to make certain that the cryogenic installation is not exposed to the potential of a pool fire from the release of flammable or combustible liquids. Cryogenic fluids are not diked in order that they are allowed to dissipate should leakage occur. Studies conducted by NASA (NSS 1740.16, Safety Standard for Hydrogen and Hydrogen Systems) show that the use of dikes around liquid hydrogen storage facilities serves to prolong ground-level flammable cloud travel and that the dispersion mechanism is enhanced by vaporization-induced turbulence. The travel of spilled or leaked cryogenic fluid to distances greater than a few feet (meters) from the source given the nature of

the typical leak is considered to be implausible due to the character of cryogenic fluids and their ability to quickly absorb heat from the surrounding environment. [55: A.8.13.2.6.4.1]"

This would seem to refer to a "typical" (i.e. smaller) leak rather than the large LH_2 leaks considered herein. The recommendation appears to be based upon NASA NSS 1740.16 which has now been replaced by ANSI/AIAA G-095A-2017 Guide to Safety of Hydrogen and Hydrogen Systems [ANSI, 2017], and which states: (pg. 56) that:

"The use of dikes or barricades around hydrogen storage facilities should be carefully examined because it is preferred to disperse any leaked or spilled LH_2 *or S*LH_2 *as rapidly as possible. Dikes or berms generally should not be used unless their purpose is to limit or contain the spread of a liquid spill because of nearby buildings, ignition sources, and so forth. However, such confinement may delay the dispersion of any spilled liquid by limiting the evaporation rate and could contribute to conditions that result in a combustion event."*

and on pg. 94:

"LH_2 *or S*LH_2 *spills, such as those that might occur from the rupture of a storage vessel, could result in a brief period of ground-level flammable cloud travel. The quick change from a liquid to a vapor and the thermal instability of the cloud cause the hydrogen vapors to mix quickly with air, disperse to nonflammable concentrations, warm up, and become positively buoyant. The presence of S*LH_2 *briefly prolongs this time period. Site specific information should determine whether natural dispersion of the spill or confinement of the spill is preferred."*

Hence the guidance given in ANSI/AIAA G-095A-2017 with regard to diking of LH_2 spills appears to be less clear-cut that NFPA 2/55 might suggest, particularly when a LH_2 spill may have the potential to spread into other sensitive areas of the facility e.g. areas containing hydrogen gas cylinders.

It could also be that the FLACS pool model is over-predicting the area of the LH_2 pool formed and/or under-predicting the spill and vaporisation induced turbulent dispersion. The FLACS pool model predictions obtained by Middha et al. [2011] are consistent with the LH_2 pool size inferred from NASA test 6 – but in this test, made for a release of 9.5 kg/s for 38 seconds onto a sand substrate, the pool only reached a maximum radius of 1–2 m [Witcofski and Chirivella, 1984]. Further validation work against suitable experimental data obtained for large-scale long duration LH_2 spills onto concrete substrates would be required to test this.

5.5.3 Effect of Engine Containment Shelter

The results suggest that for ignition of stoichiometric hydrogen air clouds filling the volume of the engine containment shelter (around 500 m^3) the resulting peak overpressure exposure in the surrounding facility – particularly around the LH_2 tank – remain tolerable. This flammable cloud volume (Q9) is equivalent to a pipe rupture leak (9.5 kg/s) running for 10 seconds. This would suggest that in order to maximise effective mitigation systems it would be desirable to be able to detect LH_2 pipe rupture and cut-off supply to limit leak duration to 10 s.

5.5.4 Risk informed approach

Although the hazardous cloud size predicted for the LH_2 leak scenarios considered are very large it should also be kept in mind that such releases are expected (with the possible exception of LH_2 leaks within the engine containment shelter) to be extremely rare (although still conceivable) events. If regulations and standards for are not to be overly onerous it has been recommended in NFPA-2 [2016] that a risk informed approach should be adopted. Hence both the size/rate of spill and the frequency of occurrence of LH_2 release scenario should be taken into account when assessing the overall levels of risk.

5.6 Summary

The consequences of extreme LH_2 leaks at a rocket engine test facility due to LH_2 supply pipe rupture and catastrophic LH_2 tank failure events have been examined. The FLACS CFD model has been used to simulate these LH_2 leaks and the resulting flammable gas cloud dispersion behaviour was characterised in terms of the variation with time (and maximum) of the LH_2 pool area and the size of the resulting equivalent stoichiometric flammable cloud formed (via the FLACS Q9 parameter). The engine test facility modelled, was surrounded by 5 m high (banked) protective outer walls and featured a LH_2 storage tank, engine containment shelter, compressor enclosure, H_2 mixer, GH_2 gas cylinder storage, LN2 tank and vaporisers, compressed air tank and flare stack.

In the case of LH_2 pipe rupture a number of different leak locations (LH_2 storage tank, gas mixer, and containment shelter), leak durations (10 s, 30 s, 180 s) and leak rates (0.5 kg/s, 9.5 kg/s) were considered. The catastrophic LH_2 storage tank failure was characterised by a LH_2 leak rate of 225 kg/s discharging the entire contents of the tanks (4.5 tonnes) in 20 s. Based upon the simulation results the following conclusions were drawn:

Size of flammable cloud limited by LH_2 storage tank bund - The results suggest that the presence of a LH_2 storage tank bund could significantly reduce both the maximum pool area and size of the Q9 equivalent stoichiometric gas cloud formed for LH_2 tank leak scenarios (long duration pipe ruptures) and catastrophic tank failure. Further experimental validation work would be required to confirm this.

Shielding effect of structures - the flammable hydrogen gas cloud formed by the LH_2 tanks spill rises up the leeward side of LH_2 Tank, where it is shielded from the wind. Consequently a significant flammable cloud develops downwind, in the wake of LH_2 storage tank, becoming buoyant and extending above and beyond the outer wall.

Effect of containment shelter - For ignition of a stoichiometric hydrogen cloud filling the volume of the engine containment shelter (around 500 m^3) the results predicted by FLACS suggest that the maximum overpressures in the surrounding facility – particularly around the LH_2 tank – could remain tolerable.

6 Aircraft Crash Scenario

Simulations of a serious aircraft crash scenario, resulting in an instantaneous spill of the entire fuel tank contents, which is immediately ignited to produce a large pool fire, have been carried out using FLACS-Fire. The hazardous effects of the resulting LH_2 pool fires have been compared with those found for equivalent LNG and Jet A fuelled aircraft.

6.1 Simulation details

The crash scenario examined assumed an instantaneous spill of the entire fuel tank contents of the aircraft. The total fuel load for the LH_2 aircraft was assumed to be 5,000 kg (based upon the "tube and wing" short-medium range cryogenic LH_2 aircraft design developed for ENABLEH2). Energy equivalent fuel loads of 12,000 kg for LNG and 13,889 kg for Jet A were assumed for the other aircraft fuel types, based upon an equivalent stored energy of 600 GJ.

Curves relating the pool mass vaporisation rate per unit area as a function of time were derived from FLACS pool model simulation results, for both LH_2 and LNG fuels, as shown in Fig 6.1 For both cryogenic fuels, the mass vaporisation rate is initially very high, but falls extremely rapidly (proportional to $t^{-1/2}$) as the ground in contact with the pool cools and the rate of conductive heat transfer from the substrate to the pool is reduced (see Section 3.3). A constant fuel mass vaporisation rate per unit area was assumed for Jet A, based upon test data for kerosene [Ahmadi et al., 2019].

A constant spill pool area was assumed, based upon an expression for the maximum radius of an instantaneous spill pool given by Fay [2007]:

$$R_{max} = \left\{ \frac{8}{3} \frac{\sqrt{2\,g}}{v_E} \left(\frac{V_{spill}}{\pi} \right)^{\frac{3}{2}} \right\}^{\frac{1}{4}} \tag{6.1}$$

The maximum pool radius for a spill with an instantaneous volume, V_{spill}, was calculated using the values of the maximum liquid regression rates with fire, v_E, given for each fuel type by Arthur D Little [1982]. Table 6.1 summarises the parameter values and estimated pool size used to characterise the fire for each fuel type.

Table 6.1 – The parameter values used to characterise the pool fire for each fuel type.

Fuel Type	LH_2	LNG	JET A
Spill Scenario	4 × Tanks	4 × Tanks	All Wing Tanks
Spill Fuel Mass (kg)	5,000	12,000	13,889
Total Volume Spilled, V_{spill} (m^3)	70.62	28.44	18.52
Estimated Max Regression Rate, v_E (m/s)	3.3×10^{-3}	2.3×10^{-4}	1.06×10^{-4}
Fay Model Pool, R_{max} (m)	24.8	34.4	35.5
Assumed Pool Diameter (m)	50	70	70
Estimated lifetime of pool (s)	10	12	57

The lifetime of a fuel spill pool, used to characterise a leak, was estimated by calculating the time when the cumulative mass of fuel vaporised was equal to the total mass of fuel spilled. In the case of LH_2 and LNG this was done using the curves given in Fig 6.1, along with the constant pool area value via numerical integration.

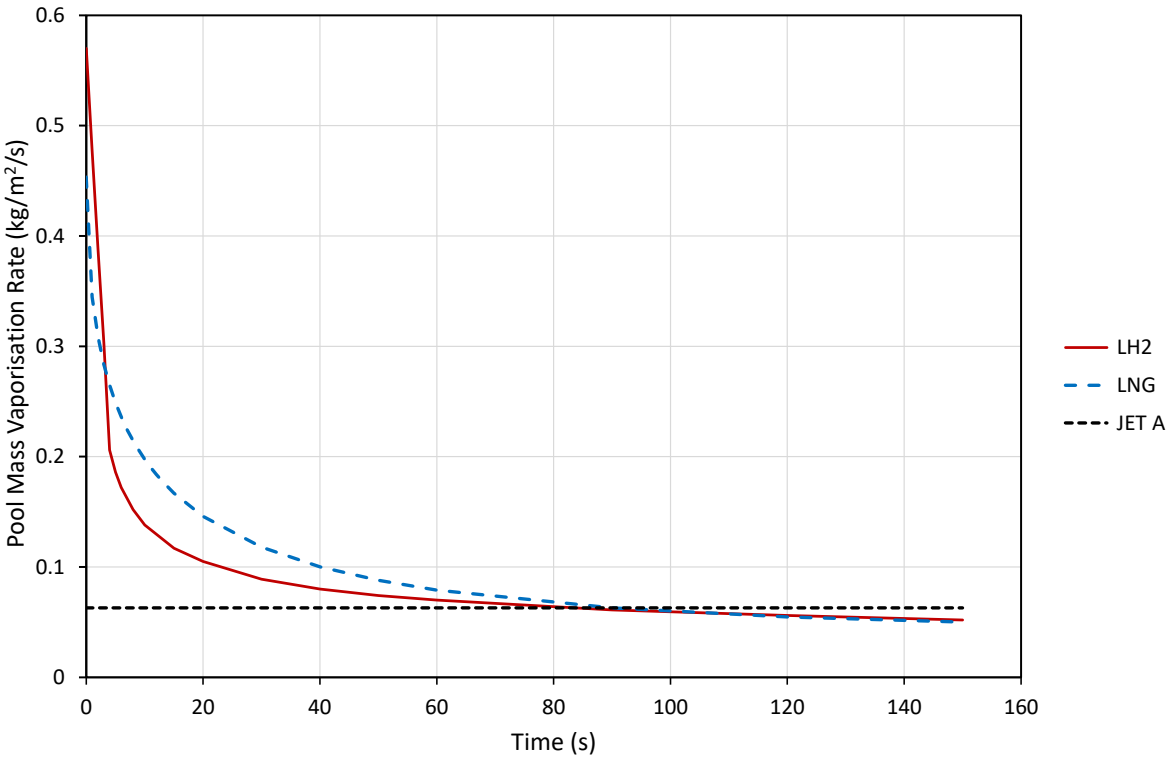

Fig. 6.1 – The pool mass vaporisation rate as a function of time for each fuel type.

For Jet A the mass vaporisation rate used was also constant and the lifetime of the pool was given by:

$$t_{life} = \frac{\rho_{fuel} V_{spill}}{\pi R_{max}^2 \dot{m}''_{vap}} \quad (6.2)$$

The fuel vapour source released by the spill pool was represented as a constant area leak in the FLACS-Fire model. The size and mass flow rate of this leak were defined using the pool area and $\dot{m}''_{vap}$ at a given time using the appropriate curve shown in Fig 6.1.

The FLACS-Fire pool fire simulations of the aircraft crash scenario were performed using a domain 520 m × 520 m × 700 m in the X, Y and Z directions (-260 m to 260 m, -260 m to 260 m, 0 to 700 m). A uniform cubical 2.5 m cell size was used in the core region encompassing the pool fire region (-50 m to 50 m, -50 m to 50 m, 0 to 500 m) in accordance with FLACS user guidelines for a fire simulation. Outside this region the grid cell size was increased, by using an expansion factor of 1.2, giving a total of 72 x 72 x 216 cells (1,119,744 cells).

In the FLACS-Fire simulations, the FLACS fuel types “Hydrogen”, “Methane” and “Dodecane” were used to represent LH_2, LNG and Jet A respectively. The default parameter values set for the FLACS-Fire radiation model were used in the simulations. The Eddy Dissipation Concept (EDC) combustion model was used as suggested by FLACS used guidelines [Gexcon, 2019]. For the LH_2 and LNG (methane) fire simulations no soot model was used. For the Jet A fire simulations the “Fixed conversion factor” soot model was enabled with the soot yield set to 0.042 (Ahmadi et al. [2019]).

The gas released by the area leak during the FLACS-Fire simulation was ignited after a time interval of 1.0 s from the start of the simulation, to give it time to mix with the surrounding air and form a flammable mixture.

Five radiation monitor points (RD1 to RD5) were located at 50 m distance intervals from the centre of the pool fire.

6.2 Results

Fig 6.2 compares combustion product temperature and radiation heat flux produced for pool fire produced by LH_2, LNG and JET A for an instantaneous spill of entire fuel tank contents of an aircraft following a crash. For scale the red monitor points (RD1-5) are spaced at 50 m intervals, with the most central one located 50 m from the centre of the pool fire. Both the LH_2 and LNG pool fires behave in a similar way. Shortly after ignition, the ignited fuel vapour forms into a large fireball - a rapidly rising expanding ball of flame. Over the next 10 - 12 seconds, the spherical fireball region continues to rise and expand in size with a central "stalk" of flame formed below. After this fireball region starts to cool before completely burning out and disappearing. The corresponding radiation heat flux region incident on the ground surface expands in both size and intensity as the fireball rises and grows, reaching a maximum 10 - 12 s after ignition, and then contracting again as the fireball burns out and disappears. In contrast to the short duration, rising fireball found for LH_2 and LNG spills, the Jet A spill burns as a continuously fluctuating fire plume, anchored on the ground, for around a minute. The size of the radiation heat flux region incident on the surrounding ground area also fluctuates accordingly.

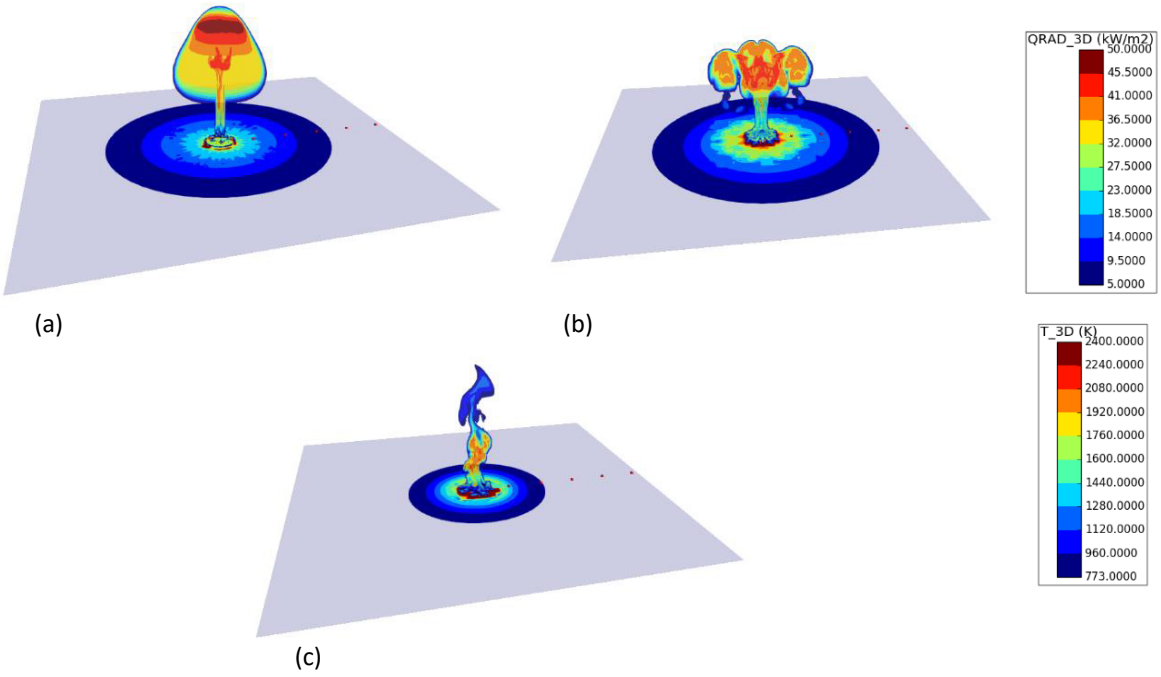

Fig. 6.2 – The predicted 3D temperature and ground surface radiation heat flux contour plots produced by post-crash aircraft pool fires for: (a) LH_2 after 10 s; (b) LNG after 12 s; (c) Jet A after 40 s.

Fig 6.3 shows a comparison of the heat release rate versus time curves predicted for the LH_2, LNG and Jet A pool fires. LH_2 pool fire exhibits the highest peak HRR curve (90 GW) with the shortest duration (around 15 s). LNG behaves in a similar way to LH_2 but with a lower peak HRR (60 GW) and slightly longer duration (around 20 s). By comparison the JET A spill is predicted to produce a pool fire with a much lower peak heat release rate (around 10 - 15 GW), but with sustained burning spread over a significantly longer period of time (around 60s).

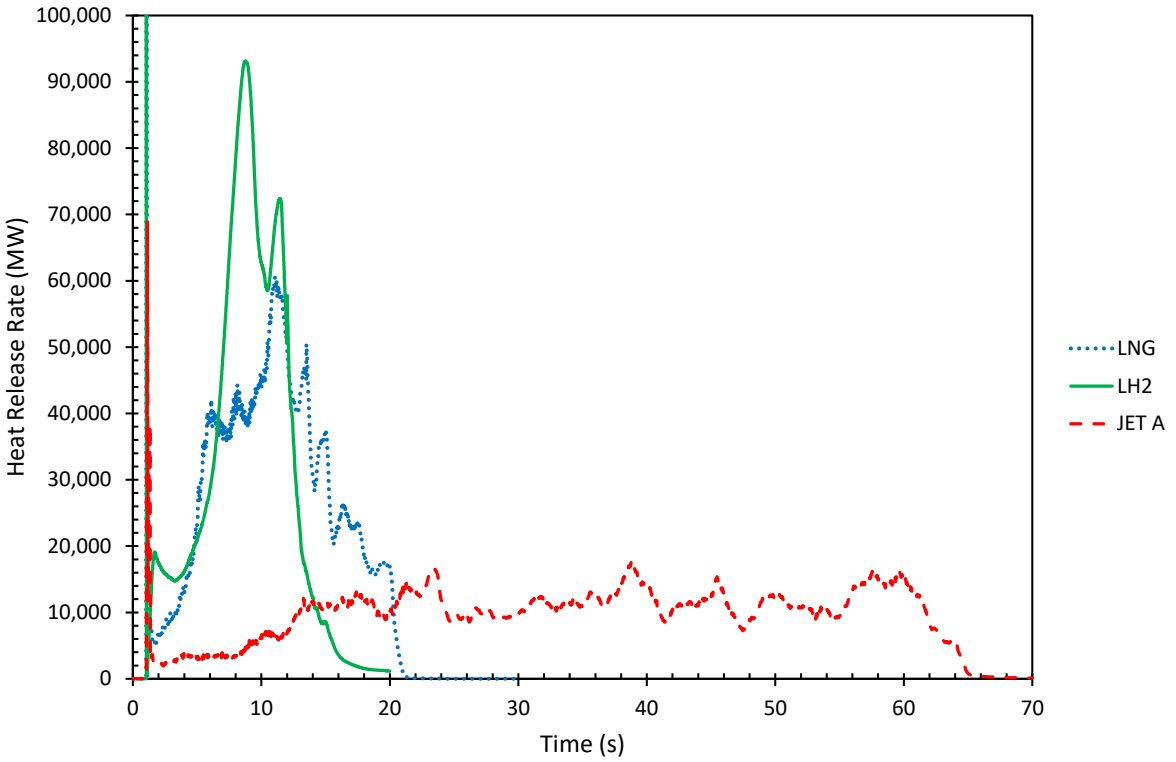

Fig. 6.3 – The post-crash pool fire heat release rate versus time profiles produced for each fuel type.

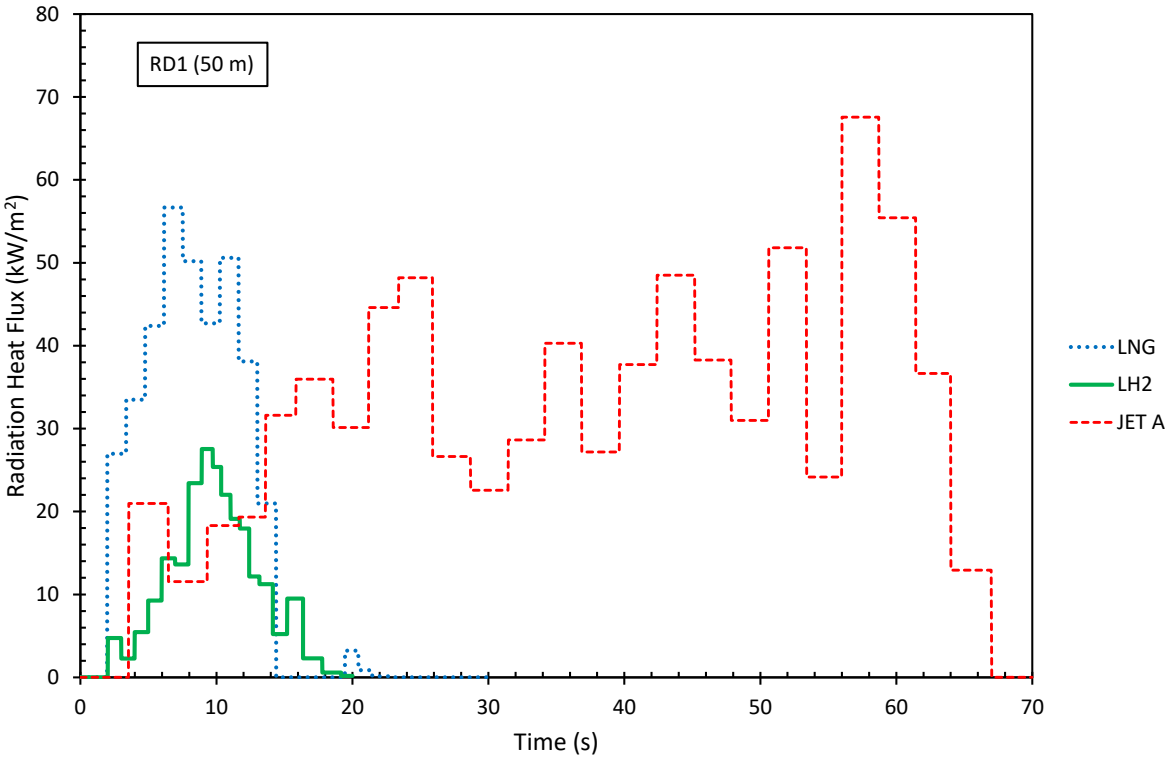

Fig. 6.4 – A comparison of the radiation heat flux received at a distance of 50 m from the pool fire origin for the three different fuel types.

A comparison between the radiation heat flux received at the closest monitor point (RD1), located 50 m from the centre of the pool fire, for the three different fuels is shown in Fig 6.4. It is evident that the radiation heat flux from the LH_2 pool fire is predicted to be significantly lower than for the other two fuels, with a peak value which is around half that expected for LNG and Jet A. The duration of the radiation peak produced for LH_2 and LNG is relatively short (around 20 s), where-as the radiation from the Jet A pool fire is sustained over significantly longer period of time (around 3 times longer).

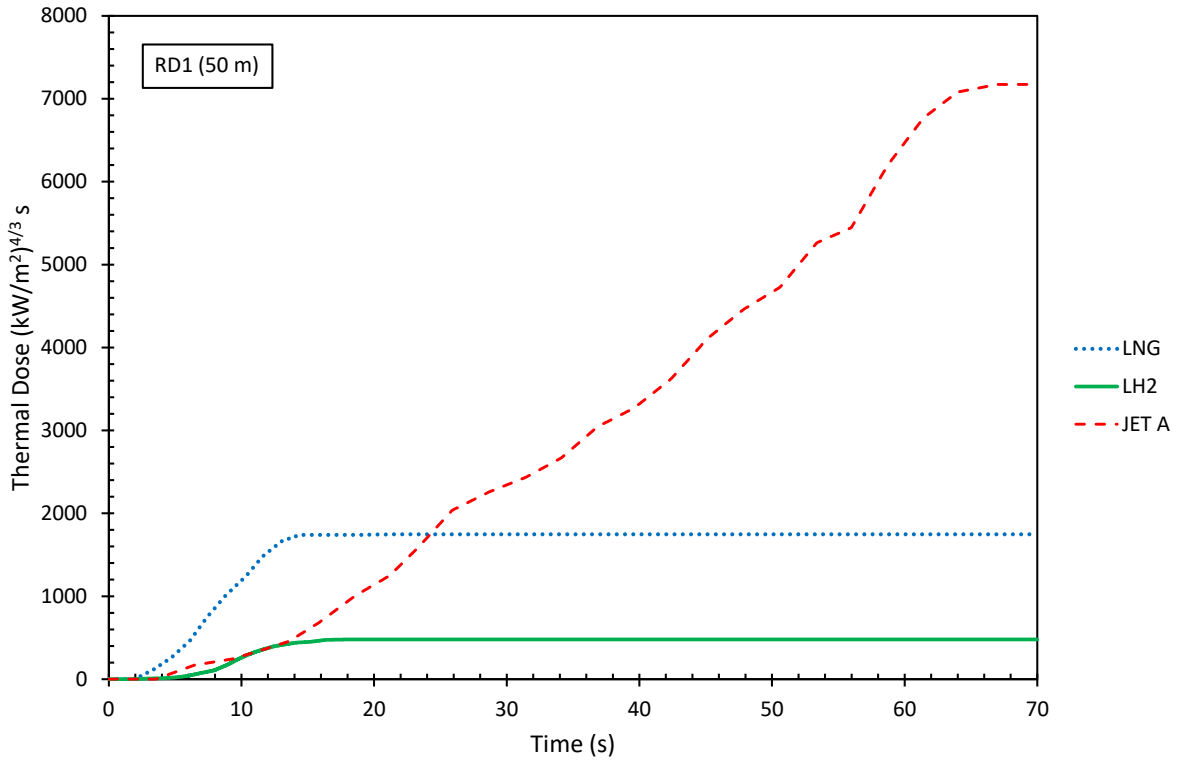

Fig. 6.5 – A comparison of the radiation heat dose received at a distance of 50 m from the origin of the pool fire for the three different fuel types.

Fig 6.5 shows a comparison of the corresponding thermal radiation dose received at RD1 for the three different types of fuel. The combination of a smaller pool size, lower peak radiative heat flux and short burning duration exhibited by the LH_2 pool fire result in a relatively low cumulative thermal dose (479 TDU). By comparison, the LNG pool fire produces a cumulative thermal dose that is around 3.5 times higher (1747 TDU), while the sustained burning of the Jet A fuel results in a cumulative thermal dose that is almost 15 times higher (7172 TDU) than that found for LH_2.

Fig 6.6 shows a comparison between the variation in peak radiation heat flux with distance (received at the five radiation monitor points) predicted for the three different fuel types. At 50 m from the centre of the pool fire the peak radiation heat flux received from the LH_2 pool fire is substantially lower than for the other two fuels. However further away from the pool fire the difference becomes less significant, although the peak radiation heat flux for LNG remains higher than for the other two fuels.

A similar comparison between the variation in cumulative thermal radiation dose with distance for the three different fuel types is shown in Fig 6.7. It is evident that the Jet A pool fire produces a significantly higher thermal dose than the other fuels, particularly at close range to the pool fire.

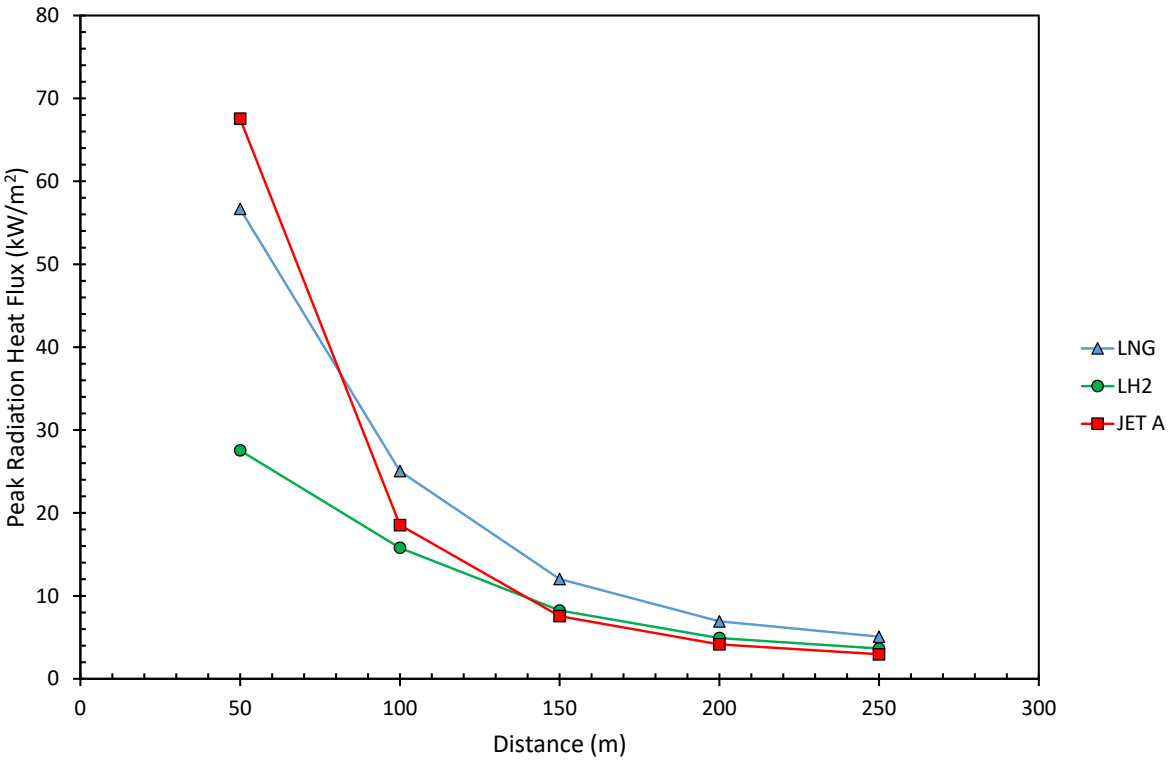

Fig. 6.6 – A comparison of the variation in peak radiation heat flux versus distance from the fire origin predicted for the three different fuel types.

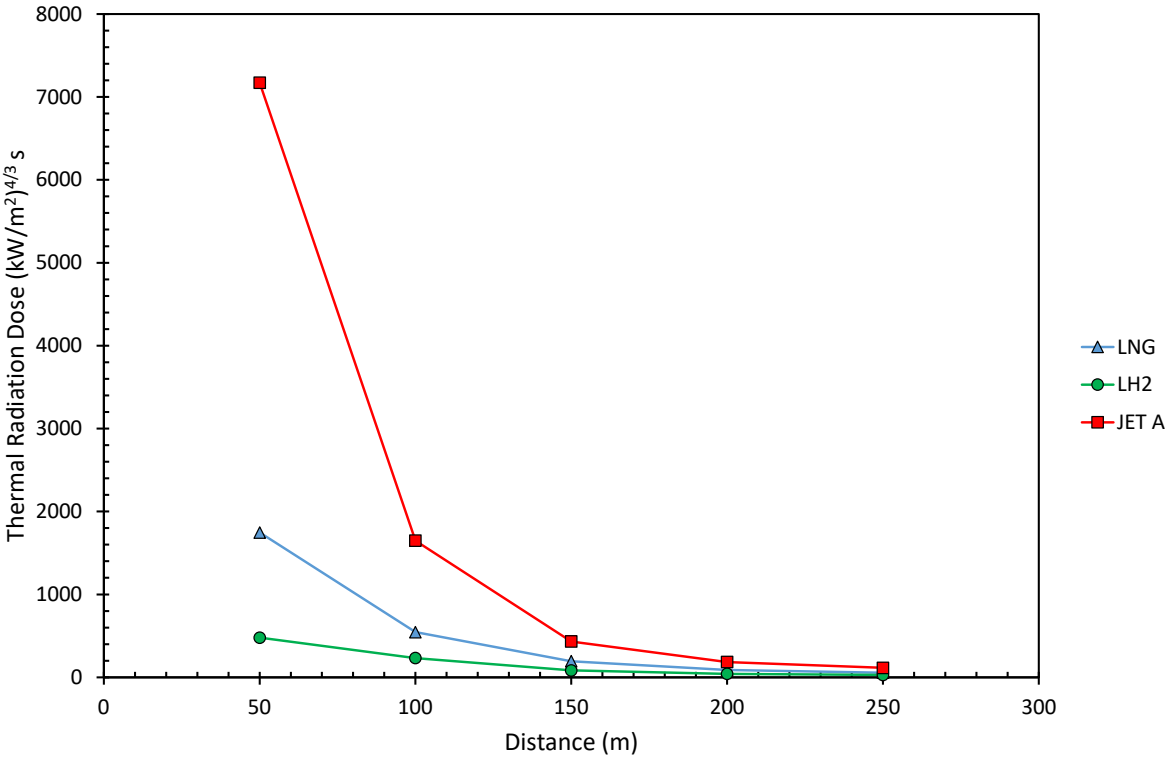

Fig. 6.7 – A comparison of the variation in the cumulative thermal radiation dose versus distance from the pool fire origin for the three different fuel types.

6.3 Summary

A comparison has been made between LH_2, LNG and Jet A fuelled aircraft for a serious aircraft crash scenario, resulting in an instantaneous spill of the entire fuel tank contents, which is immediately ignited to produce a large pool fire. The simulation results obtained with the FLACS-Fire CFD code, suggest that the spills of cryogenic fuels - LH_2 and LNG produce high intensity, short duration pool fires, behaving like a fireball. By comparison the JET A spill is predicted to produce a pool fire with a lower peak heat release rate, but with sustained burning over a longer period of time. A comparison of the pool fires produced for each of the fuel types also suggests that the magnitude of the predicted peak radiation heat flux and thermal radiation dose is significantly lower for the LH_2 pool fire.

7 Aircraft Refuelling Spill (Immediate Ignition) - Pool Fire Simulations

7.1 Instantaneous LH_2 spills – size of spill

In order to examine pool fire scenarios resulting from an accidental fuel spill or leak occurring during aircraft refuelling operations it is first necessary to characterise the size (radius/area) of the spill pool (assumed circular) that is formed when a particular volume of fuel is released. The limiting case, considered in this section, is that the spill occurs instantaneously – with the entire spill volume being released immediately.

7.1.1 Simulation Setup

A series of simulations were carried out using the FLACS pool model to characterise the variation in the size (radius) of a LH_2 spill versus time for an (approximately) instantaneous spill of a fixed volume of LH_2 (with the entire spill volume being released over a period of 1 s).

In accordance with FLACS Best Practice User Guidelines [Gexcon, 2019] a uniform grid cell size was employed across the pool region and the initial pool radius for the spill was set to three times the grid cell size (in order to produce a circular pool). An initial grid sensitivity study was carried out using both a 0.25 m grid cell size with and 0.75 m initial pool radius (rt230500) and a finer 0.125 m grid cell size with a 0.375 m initial pool radius (rt240500). The results (particularly the vaporisation time of the spill) were displayed a degree of sensitivity to the grid cell size (in respect to the initial pool radius set) and hence the finer grid cell size of 0.125 m (with a 0.375 m initial pool radius) was adopted for the pool spill size characterisation study. The thermal conductivity and thermal diffusivity of the ground used in the pool model were set to 1.1 W/m/K and 1.0×10^{-6} m^2/s, to replicate the thermal properties of concrete.

A series of simulations were carried out for LH_2 spill volumes of 100 L (0.1 m^3), 318 L (0.318 m^3), 500 L (0.5 m^3), 1,000 L (1.0 m^3) and 5,000 L (5.0 m^3) - with the entire spill volume being released over a period of 1 second - to determine the variation in the size of the LH_2 pool with time (and hence the maximum pool size reached and the time for the pool to completely vaporise with the pool radius returning to zero). An additional simulation releasing 63.5 L/s (equivalent to 4.5 kg/s) over 5 seconds, corresponding to a total spill volume of 318 L, was carried out to allow comparison between the pool size time histories produced by an instantaneous spill will a more sustained spill (over 5 seconds) of an equivalent volume of LH_2 (as might occur in the case to a ruptured fuel line). Some further simulations were also carried out for larger volume spills of 10,000 L (10.0 m^3), 17,655 L (17.7 m^3) and 70,621 L (70.6 m^3) with the latter two corresponding to a single fuel tank (1250 kg) and the entire fuel tank load (5000 kg) of the LH_2 “tube and wing” short-medium range aircraft design developed for ENABLEH2.

7.1.2 Results

Fig. 7.1 shows the pool radius versus time histories predicted by the FLACS pool model for LH_2 fuel spills ranging in size from 0.1 m^3 to 71 m^3. Similarly, Fig. 7.2 shows the pool radius versus time histories for smaller volume LH_2 spills of 100 L to 5000 L. For the smallest 100 L LH_2 spill, the pool radius increases (from the initial radius of 0.375 m) reaching a maximum of 1.59 m at 2 s, and then contracts back to zero, with the pool completely vaporising after 3.3 s. The curves obtained for larger spill volumes are similar in form. As would be expected, increasing the volume of the spill increases both the maximum radius of the pool and the spill vaporisation time. It is evident that, even for the largest spill volumes considered, the LH_2 pool is predicted to completely vaporise in a relatively short period of time (e.g. in 7.1 s in the case of the 5000 L spill). The predicted pool radius versus time curve is also shown for the 63.5 L/s release rate spill occurring over 5 s. Comparing with the instantaneous 318 L curve

(which has the same total spill volume) it can be seen that 5 second release takes significantly longer to reach a maximum and completely vaporise.

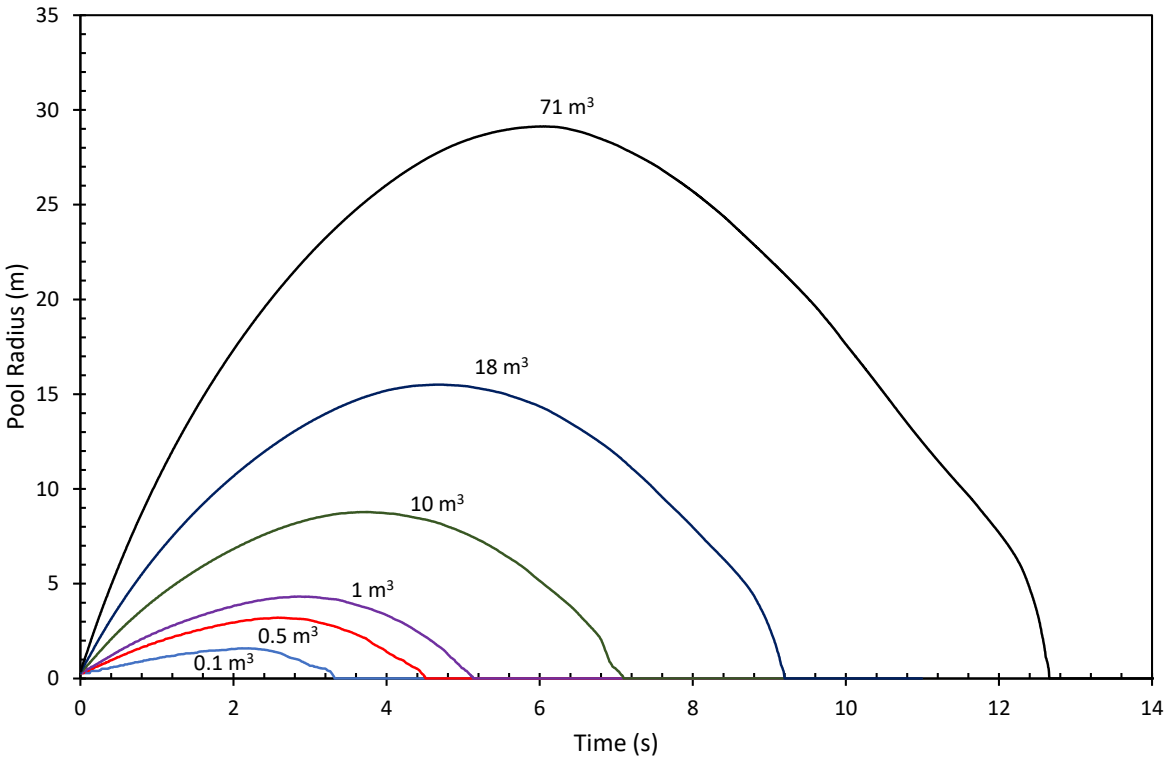

Fig. 7.1 – The pool radius versus time profiles predicted for different instantaneous LH_2 spill volumes.

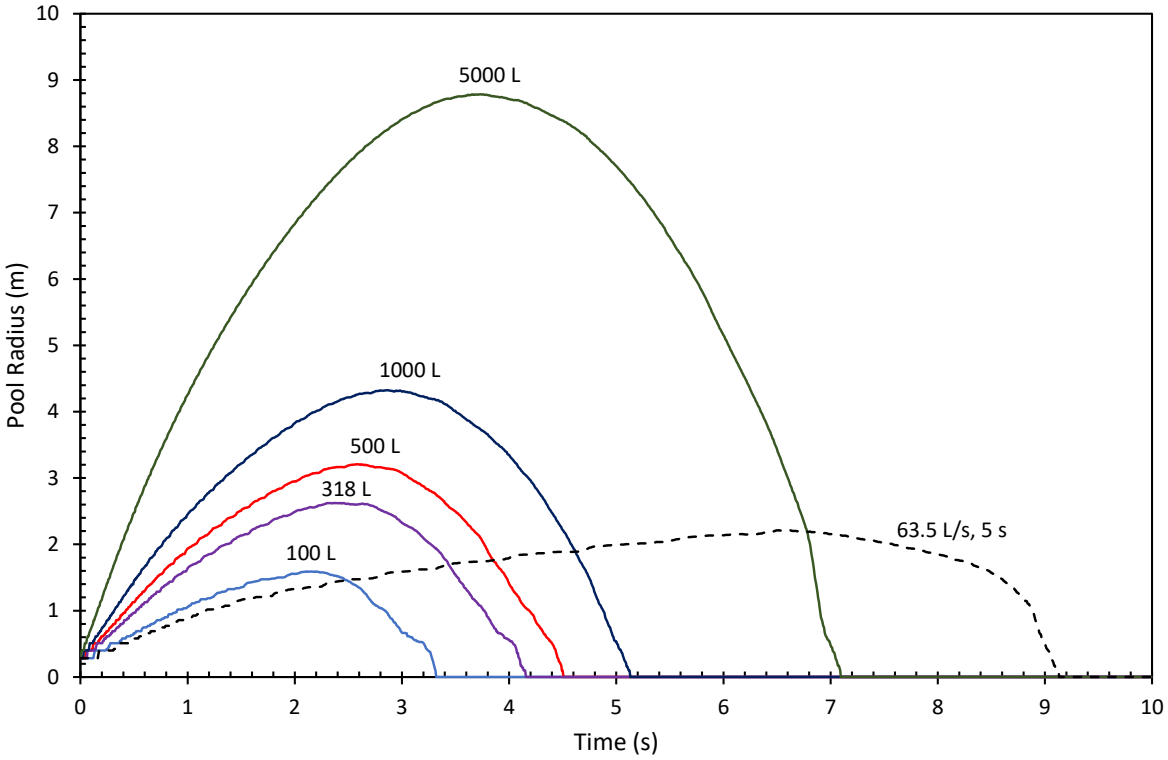

Fig. 7.2 – The pool radius versus time profiles predicted for smaller volume LH_2 spills.

The maximum pool size radius and pool vaporisation time predicted for each LH_2 spill volume simulated are summarised in table 7.1. The table also shows the time averaged pool area and radius, the average pool mass vaporisation rate (kg/s) and mass vaporisation rate per unit area (kg/m^2/s) calculated for each of the LH_2 pool spill volumes considered.

Table 7.1 – Summary of the predicted LH_2 pool spill characteristics.

Spill Size (L)	Mass (kg)	R_{max} (m)	t_{evap} (s)	Time Averaged			
				Pool Area (m)	Pool Radius (m)	M_{vap} (kg/s)	m''_{vap} (kg/m^2/s)
100	7.08	1.59	3.3	4.0	1.0	2.1	0.53
318	22.5	2.62	4.2	11.1	1.7	5.4	0.49
500	35.4	3.20	4.5	16.7	2.1	7.9	0.47
1,000	70.8	4.32	5.1	31.2	2.9	13.8	0.44
5,000	354	8.78	7.1	127.3	5.8	49.9	0.38
10,000	708	11.98	8.1	240.3	8.0	87.1	0.35
17,655	1250	15.51	9.2	402.9	10.4	135.9	0.32
70,621	5000	29.13	12.7	1442.2	19.8	395.0	0.28

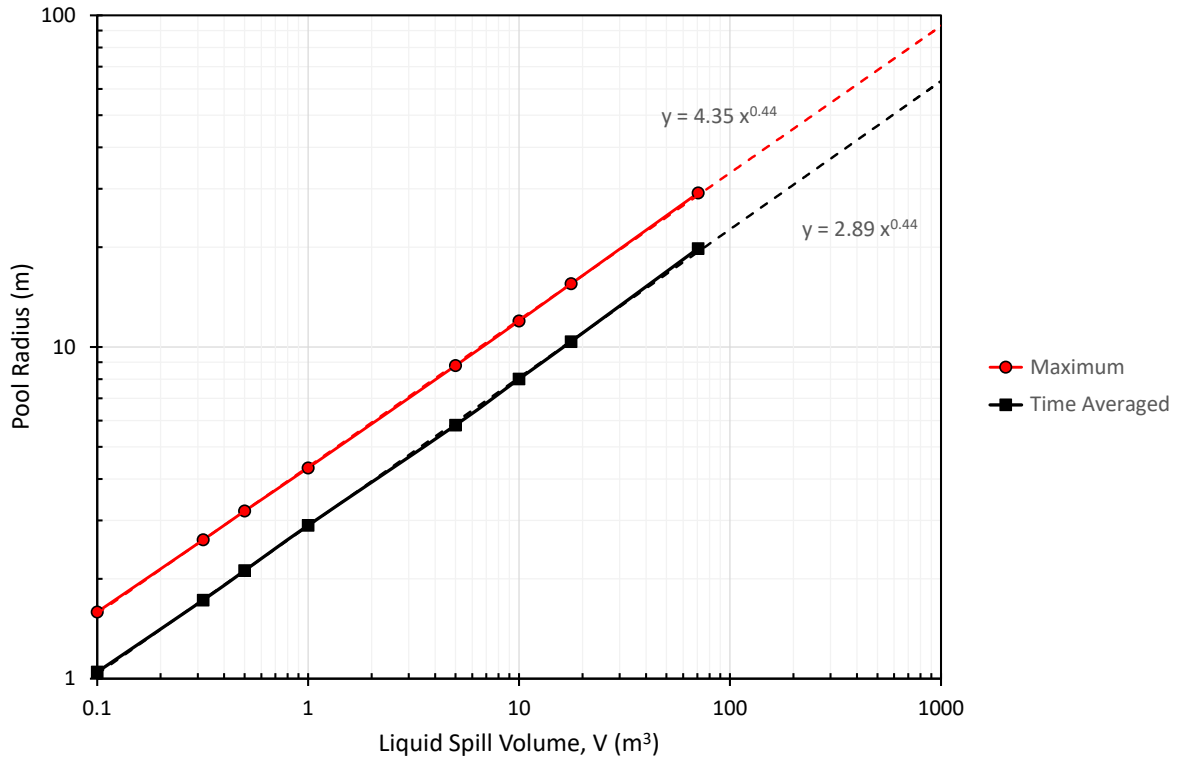

Fig. 7.3 – Variation in pool radius versus spill volume predicted for instantaneous LH_2 spills.

Fig. 7.3 shows the both the maximum, R_{max} (m), and time averaged, R_{ave} (m), pool radius predicted by FLACS as a function of the instantaneous LH_2 spill volume, V (m^3) assuming that an unconstrained pool is formed. In both cases the pool radius exhibits a power law relationship with the LH_2 spill volume. In order to obtain a correlation that could be used to estimate the max or average pool size, for a given LH_2 release volume, power law relationships were also fitted to the FLACS data (see Fig. 7.3) to obtain the following correlations (for a concrete ground type):

$$R_{max} = 4.35\, V^{0.44} \tag{7.1}$$

$$R_{ave} = 2.89\, V^{0.44} \tag{7.2}$$

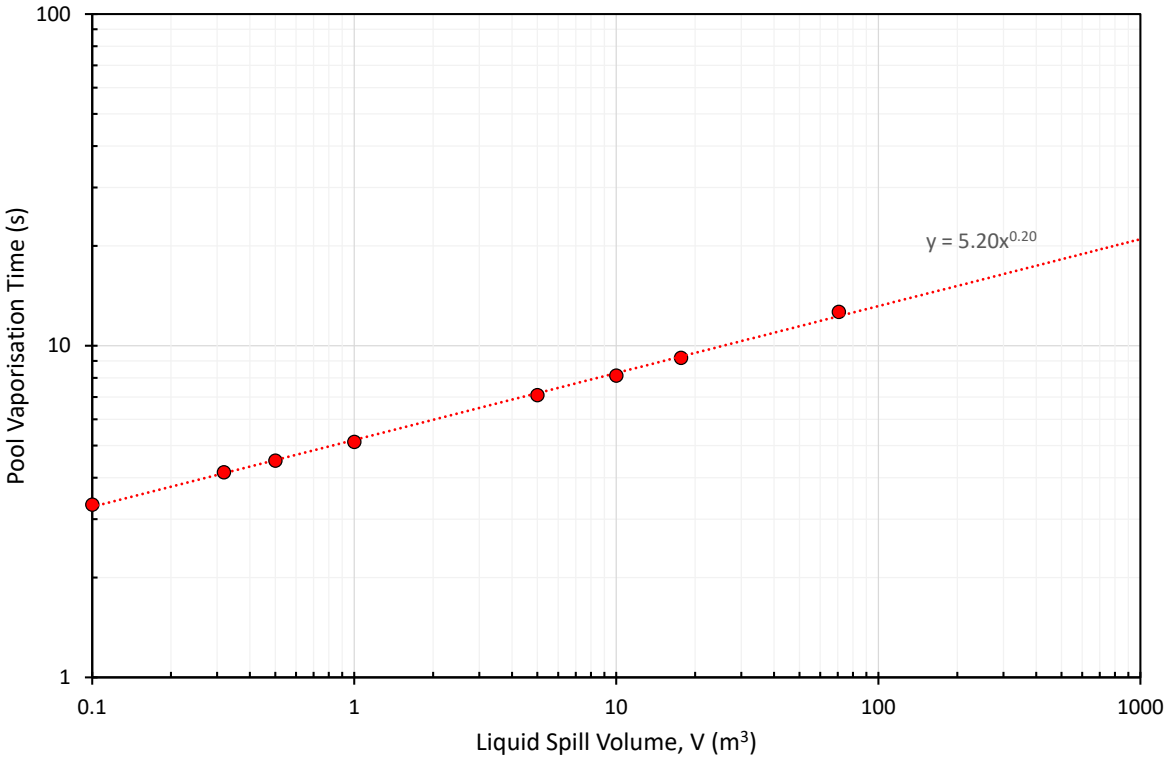

Fig. 7.4 – The variation in pool vaporisation time with spill volume predicted for instantaneous LH_2 spills.

Fig 7.4 shows the time taken for the pool to vaporise, t_{vap} (s) predicted by FLACS as a function of the instantaneous LH_2 spill volume, V (m^3). The results once again exhibit a power law relationship fitted by the correlation:

$$t_{vap} = 5.20\, V^{0.20} \tag{7.3}$$

It is evident from these results that even large volume instantaneous spills of LH_2 forming unconstrained pools are predicted to completely vaporise rapidly in a short period of time.

These correlations can be used to estimate the size and vaporisation time of the pool that would result from an instantaneous spill of LH_2 of a given volume onto a concrete ground. They assume that the spill (fitted in the range 0.1 to 71 m^3) is instantaneous, unconstrained and made onto a concrete substrate.

7.2 Pool fire simulations for an instantaneous 100 L LH_2 spill

7.2.1 Simulation Setup

Some initial simulations were carried out using the FLACS-Fire model to simulate the LH_2 pool fire resulting from the ignition of an instantaneous LH_2 spill of 100 L. The predicted results have been compared with those observed in one of the experimental tests described by Zabetakis and Burgess [1961], where 89 L of LH_2 was spilled onto a surface and ignited. In the test the radiation heat flux produced by the LH_2 flames was monitored at a distance 110 feet (33.5 m) away from the centre of the LH_2 spill/pool fire. Some cross-sections of the flames produced in this experimental test at various time intervals after ignition were also plotted.

For an instantaneous spill of 100 L of LH_2 the results from section 7.1 suggest that the maximum radius of the pool formed will be approximately 1.6 m with a duration of 3.3 s before completely evaporating. The hydrogen gas release generated by this rapidly vaporising LH_2 spill was represented as an area leak in the FLACS-Fire model. The variation in the size (area) and mass vaporisation rate of this leak was defined via a FLACS input leak file based upon the data predicted by the FLACS pool model for the 100 L spill of LH_2 (see 100 L time history curve in Fig. 7.2). The hydrogen gas released by the area leak during the FLACS Fire simulation was ignited after a time interval of 1.0 s from the start of the simulation, to give it time to mix with the surrounding air and form a flammable mixture.

The default parameter values set for the FLACS-Fire radiation model were used in the simulations. The Eddy Dissipation Concept (EDC) combustion model was used as suggested by FLACS user guidelines (Gexcon [2019]). For the LH_2 fire simulations no soot model was used.

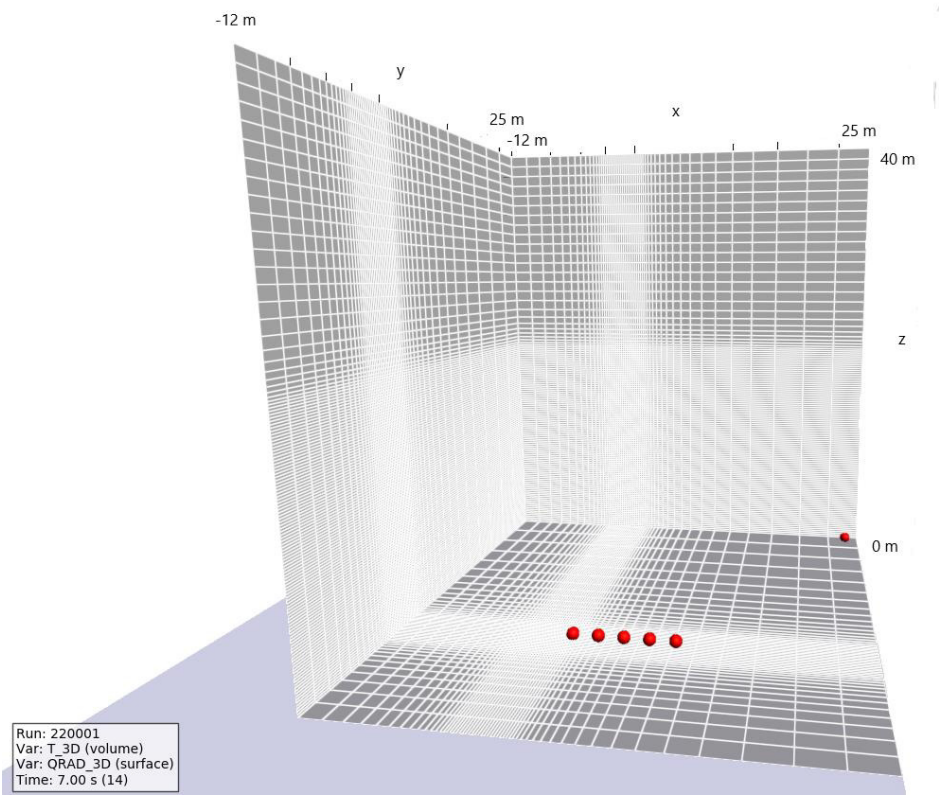

Fig. 7.5 – The domain and grid used in the FLACS-Fire 100 L LH_2 spill pool fire simulations. The red dots indicate the location of radiation monitor points.

The initial pool fire simulations were performed on a domain -12 m to 25 m, -12 m to 25 m and 0 to 40 m in the X, Y and Z directions. The “standard” grid employed had a total of 338,000 cells (52 × 52 x 125 cells). A 0.2 m uniform grid cell size was used in core the region (-2 m to 2 m, -2 m to 2m, 0 to 20 m) around the pool fire area which was centred on the origin. The size of the core region in the XY plane

was chosen so that it would contain the maximum radius of the pool. Outside of the core region the grid cell size was stretched, by using an expansion factor of 1.2, and setting a maximum cell size of 3 m in the X and Y directions and 1 m in the Z direction. The size of domain was extended in the positive x and y directions in order to enable the location of a radiation monitor point to defined (along the diagonal at 23.7m, 23.7m, 0.45 m) at the same distance from the pool fire (33.5 m) as was used experimentally by Zabetakis and Burgess [1961]. Additional monitor points to record the radiation heat flux were also located at distances of 2, 4, 6, 8 and 10 m from the centre of the pool fire (at a height of 0.45 m). Fig 7.5 shows the domain, grid, and monitor points used in the "standard" grid simulations. A finer "hi-res" grid of 1,429,189 cells (79 × 79 x 229 cells) with a smaller grid cell size of 0.1 m defined in the core region, was also used to allow the grid sensitivity of the results to be examined.

7.2.2 Results

Fig 7.6(a-d) shows the evolution in the temperature of the simulated transient pool fire resulting from the ignition of the 100 L LH_2 spill. In order to visualise the fire plume formed, a temperature threshold of 773 K (such that the flame temperature excess is around 500 K above ambient [Fay, 2006]), has been used to demarcate the boundary of the flaming region. The radiation heat flux received on the surface of the ground around the pool fire (in the range 5 kW/m^2 to 37.5 kW/m^2) is also shown. Shortly after ignition (0.5 s), the ignited hydrogen gas has formed into a fireball - a rapidly rising expanding ball of flame (Fig 7.6(a)). Over the next couple of seconds, the spherical fireball region continues to rise and expand in size with a central "stalk" of flame formed below (Fig 7.6(b-c)). By three seconds after ignition the hydrogen in the rising fireball region has been consumed and starts to cool (Fig 7.6(d)) before shortly after completely burning out and disappearing. The corresponding radiation heat flux region incident on the ground surface can be seen to expand in both size and intensity as the fireball rises and grows, reaching a maximum 2 s after ignition, and then contracting again as the fireball burns out and disappears.

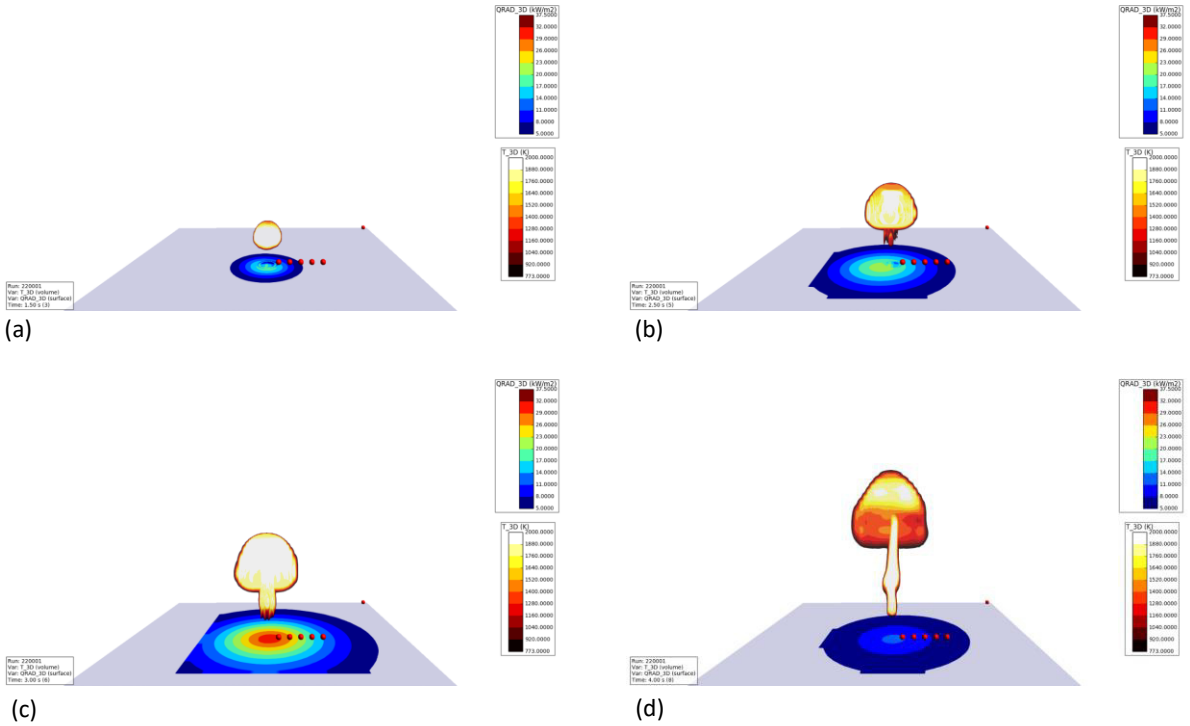

Fig. 7.6 – The evolution of the 100 L LH_2 spill pool fire: (a) 0.5 s after ignition; (b) 1.5 s after ignition; (c) 2.0 s after ignition; (d) 3.0 s after ignition.

Fig 7.7 shows a series of 2-D (X-Z) temperature contour plots taken through the centre of the simulated 100 L LH_2 spill fireball as it develops at several different time intervals (0.5 – 2.5 s) after ignition. These plots can be compared with vertical cross-sections of flame for the experimental 89 L LH_2 spill/fire

observed by Zabetakis and Burgess at the same time intervals after ignition (Fig. 7.8). The simulated LH_2 spill flame shows some broadly similar qualitative behaviour to that observed in the test. In both cases the diameter and height of the fireball's "head" above the ground increases with time and it also develops a central fire plume column (or "stalk") of flame below the fireball. However, the fireball region in the experimental test is initially located close to the ground and its central plume remains anchored.

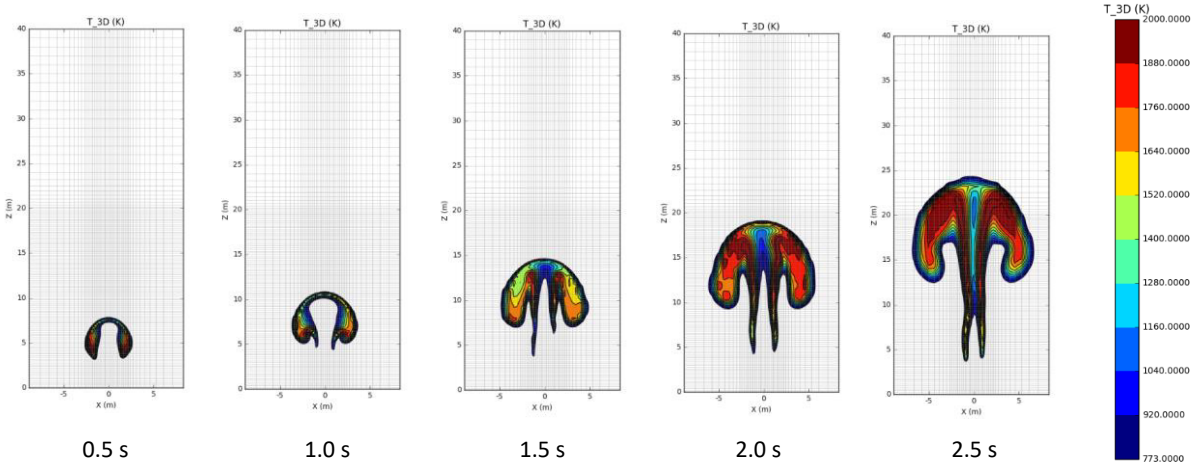

Fig. 7.7 – 2D temperature contours showing the development of the 100 L LH_2 spill fireball at different times after ignition.

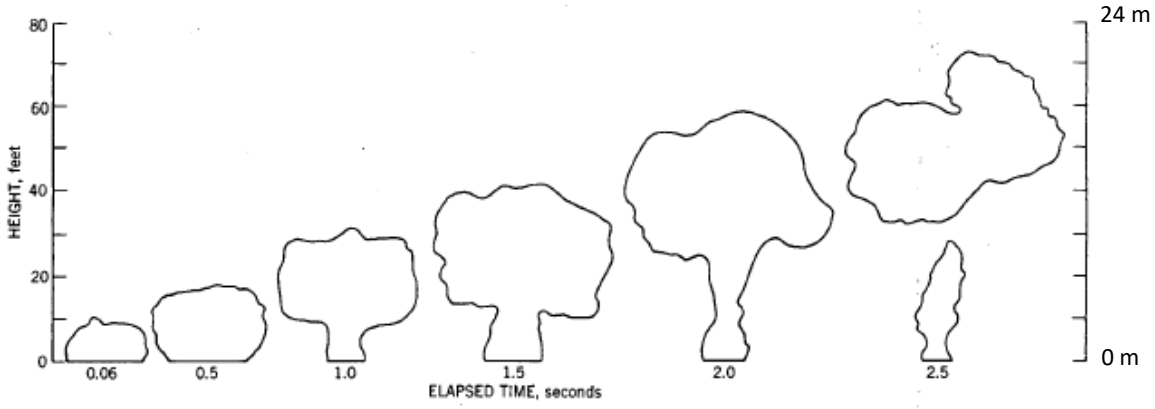

Fig. 7.8 – Experimental flame profiles observed at various time intervals after the ignition of a spill of 89 L of LH_2 [Zabetakis and Burgess, 1961].

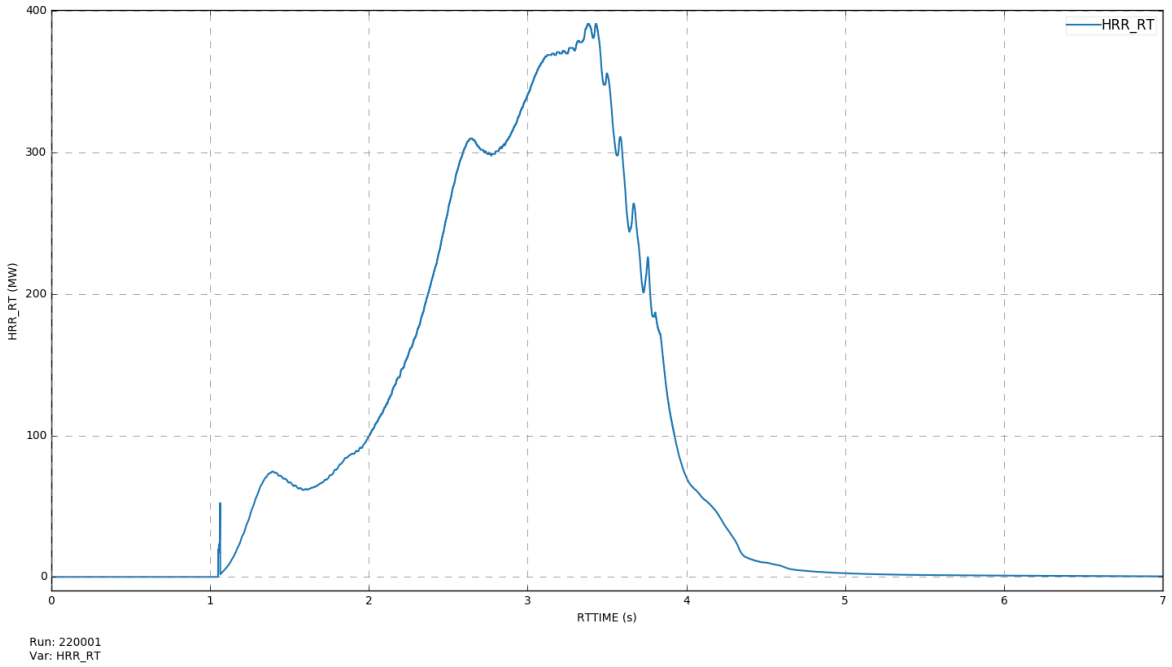

Fig. 7.9 – The heat release rate versus time curve predicted for the 100 L LH_2 spill pool fire.

The heat release rate (HRR) of the simulated 100 L LH_2 spill fire is shown in Fig 7.9. Following ignition at 1 s, the HRR rises rapidly over the next 2 seconds before reaching a peak (~380 MW) around 3.5 s (i.e. 2.5 s after ignition) and then falling sharply back towards zero over the next second.

Fig 7.10 shows a comparison between the predicted thermal radiation heat flux received at the monitor point MP1 located at a distance of 33.5 m from the centre of the 100 L LH_2 spill/fire for both the "standard" (0.2 m cell) and "hi-res" (0.1 m cell) grid. A comparison of the radiation heat flux curves predicted for both grid resolutions suggests that a degree of grid independence has been achieved and that the "standard grid" produces adequate results for this scenario. The figure also shows the radiation heat flux versus time history observed in the experimental test at a distance of 33.5 m from the LH_2 spill fire (for ignition at 1.4 s). The magnitude of the predicted peak radiation heat flux (4 kW/m^2) is significantly higher than was observed experimentally (0.5 kW/m^2).

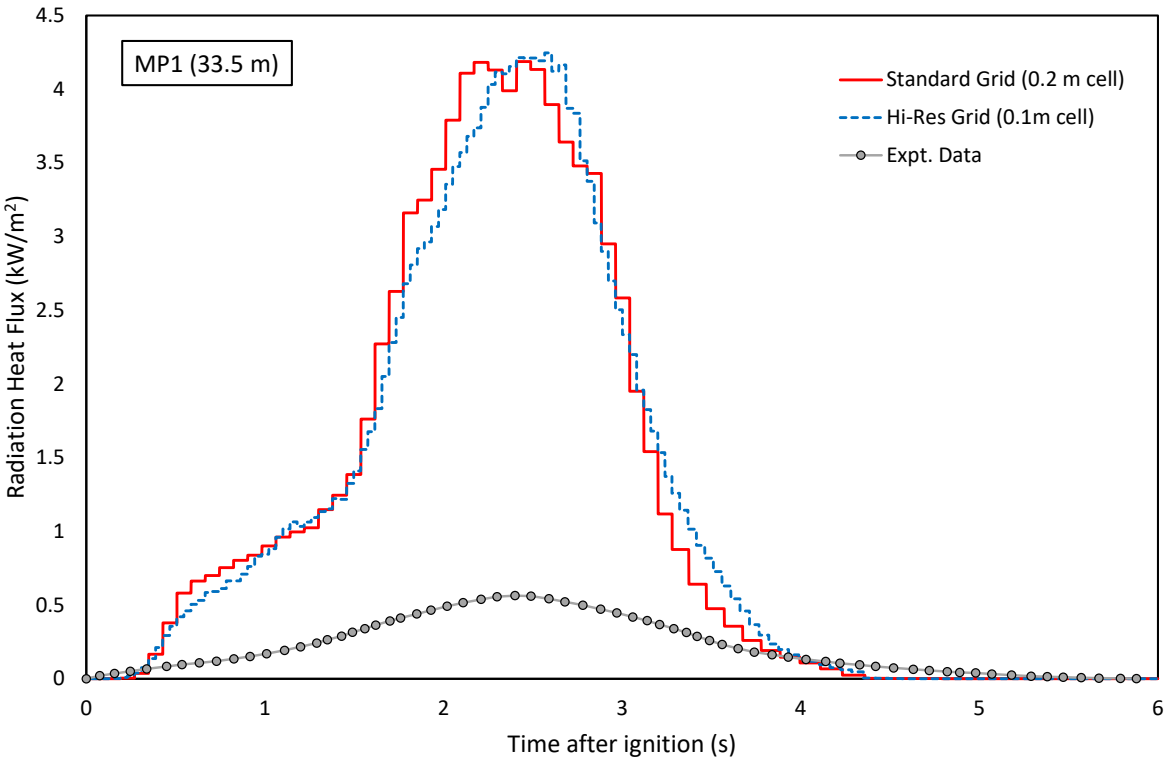

Fig. 7.10 – The radiation heat flux received at a monitor point located at a distance of 33.5 m from the origin of the LH_2 pool spill.

For far-field radiation calculations, FLACS-FIRE uses Eqn. (3.41) to calculate the transmissivity of infrared radiation through the atmosphere. However, this relationship was derived for the radiation from hydrocarbon flames and does not include the effect of water humidity on the transmissivity. Hence, it does not take into account the significant thermal absorption of radiation released form a hydrogen-air flame by the surrounding water vapour present in the atmosphere. In the case of the experimental test carried out by Zabetakis and Burgess [1961], the radiation travels a distance through the atmosphere, S = 33.5 m, so Eqn. (3.41) would suggest the transmissivity at this distance is:

$$\tau = 0.998^{33.5} = 0.935 \tag{7.4}$$

However, Zabetakis and Burgess also obtained a relationship for transmissivity of radiation (based upon some small-scale experiments performed for a hydrogen flame measuring the absorption of the radiation from by steam) given by:

$$\tau_z = \exp\left(-0.015\, w\, r\right) \tag{7.5}$$

Where w is the water vapour content (%) and r is the distance (in feet). In the case of the LH_2 spill/fires observed by Zabetakis and Burgess, the tests were carried out under relatively humid conditions, with w in the range of 1– 2%, suggesting a significantly lower level of radiation transmissivity at a distance of 110 feet (33.5 m) in the range 0.037 to 0.192. This range of reduction in the thermal radiation flux (0.04 to 0.2) compared with Eqn. (7.4) is consistent with the difference in peak radiation heat flux (0.5/4 = 0.125) shown in Fig 7.10.

Thus, the level of radiation heat flux predicted by FLACS-FIRE in the far-field for a hydrogen flame would be expected to be conservative (over-predicted) in scenarios where the effect of atmospheric humidity on transmissivity is significant, as is the case in the experimental LH_2 spill/fire tests carried out by Zabetakis and Burgess.

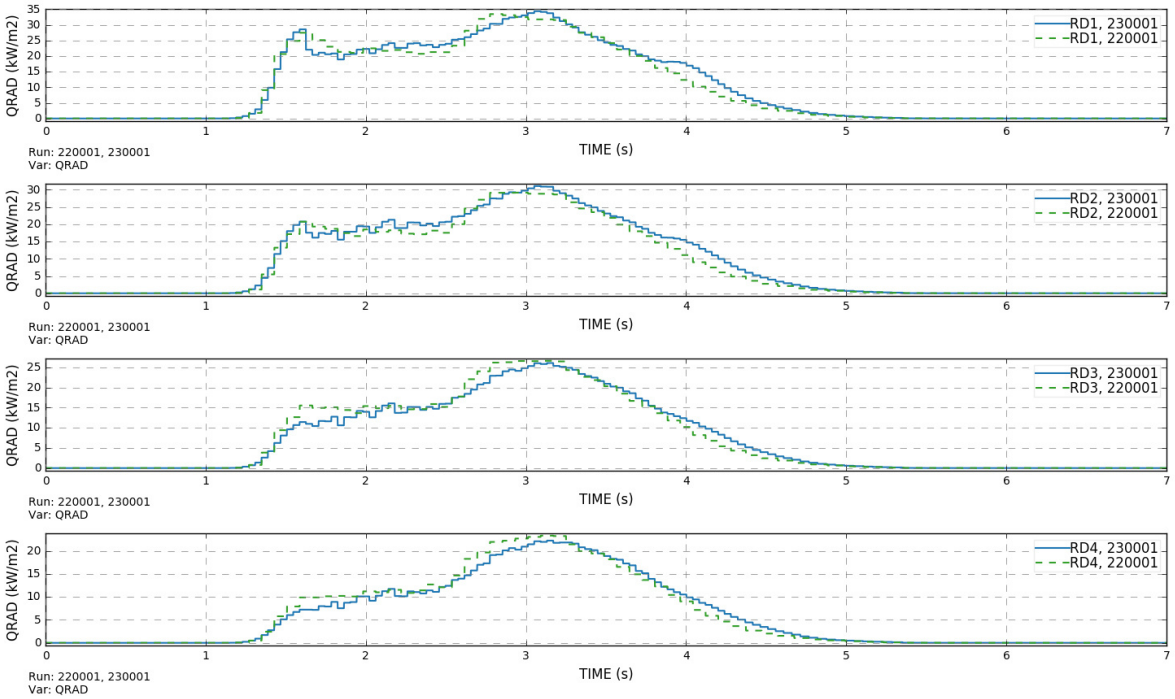

Fig. 7.11 – Comparison of the predicted radiation heat flux received at 2 m (RD1), 4 m (RD2), 6m (RD3) and 8 m (RD4) from the origin of the 100 L LH_2 spill pool fire for "Standard grid" (dashed green line) versus "Hi-res grid" (solid blue line).

Fig 7.11 shows a similar comparison between the predicted thermal radiation heat flux received at the monitor point located at positions closer to the 100 L LH_2 spill/fire at RD1, RD2, RD3 and RD4 (located at 2, 4, 6 and 8 m from the origin) for both the "standard" (0.2 m cell) and "hi-res" (0.1 m cell) grid, again suggesting that a degree of grid independence has been achieved for this scenario.

The thermal dose received at the different monitor location for the 100 L LH_2 spill/fire scenario is shown in Fig 7.12. As would be expected the thermal dose reflects the behaviour of the fireball increasing very rapidly for the first couple of seconds after ignition (particularly at close range) before levelling off after 5 s, as the fireball burns out and disappears.

Comparison of the radiation dose results obtained for the "standard (0.2 m)" and "hi-res grid (0.1 m)" suggests that the predictions are reasonably consistent, with a difference in the final cumulative thermal dose received ranging from 2 to 15% between the results obtained using the two grids at the different monitor locations.

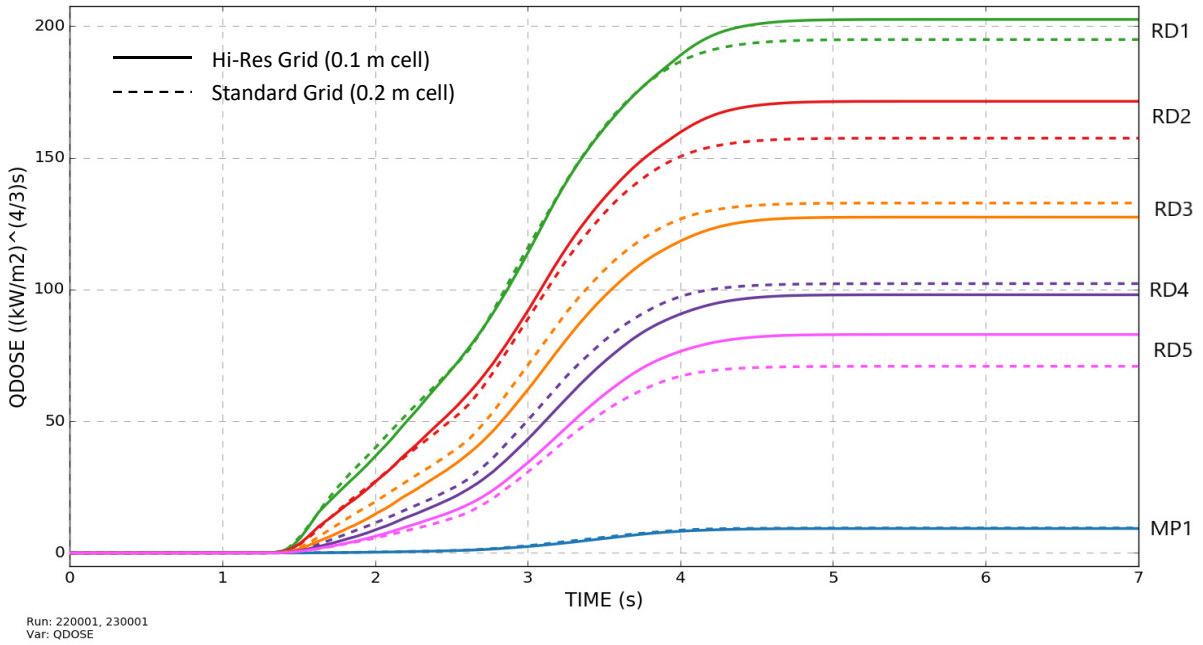

Fig. 7.12 - Comparison of the predicted thermal radiation dose received at 2 m (RD1), 4 m (RD2), 6m (RD3) and 8 m (RD4) and 33.5 m (MP1) from the origin of the 100 L LH_2 spill pool fire for the "Standard grid" (dashed line) versus "Hi-res grid" (solid line).

7.3 Comparison between pool fires for instantaneous spills of LH_2 and Jet A

A series of simulations were carried out using the FLACS-Fire model to simulate the pool fires resulting from instantaneous spills of LH_2 and Jet A, ranging in size from 100 L to 5000 L, broadly corresponding to the range of fuel spill volumes (for Jet A) that have been observed to occur during aircraft refuelling operations in practice at airports [Jones et al., 2000], to allow a comparison to be made between the behaviour and level of thermal hazard presented by the two different fuel types.

7.3.1 Simulation setup

In the case of LH_2 spills, the hydrogen gas release generated by each spill volume considered was represented as an area leak in the FLACS-Fire model. The variation in the size (area) and mass vaporisation rate of this leak versus time was defined via a FLACS input leak file based upon the results predicted by the FLACS pool model for the vaporisation of that LH_2 spill volume, using the results from section 7.1.2. The maximum radius of the pool and vaporisation time used for a given spill volume was taken from table 7.1.

In the case of instantaneous release of Jet A the maximum radius of the pool formed for a given spill volume, V_{spill} (m^3), was calculated using [Ponchaut et al., 2016]:

$$R_{max} = \sqrt{\frac{V_{spill}}{\pi\, h_{min}}} \tag{7.6}$$

where h_{min} (m) is the minimum pool thickness. For typical spills the pool will spread until it reaches a minimum pool thickness equal to the characteristic surface roughness. A value of h_{min} = 0.005 m (5 mm) was used here, which is representative of a relatively smooth surface like concrete [van den Bosch, 2005]. It was also assumed that the released liquid instantaneously spreads to the minimum pool thickness and immediately reaches the maximum pool size.

In the FLACS-Fire simulations, the FLACS fuel type "Dodecane" (ρ_{fuel} = 750 kg/m^3) was used to represent Jet A, and a constant fuel mass vaporisation rate per unit area $\dot{m}''_{vap}$ of 0.063 kg/m^2/s was assumed (based upon test data for kerosene [Ahmadi et al., 2019]).

The burning lifetime of the Jet A pool fire is then found using:

$$t_{life} = \frac{\rho_{fuel} V_{spill}}{\pi R_{max}^2 \dot{m}''_{vap}} \quad (7.7)$$

Note that for a Jet A fire with an instantaneous release with R_{max} given by Eqn. (7.6), t_{life} becomes:

$$t_{life} = \frac{\rho_{fuel} h_{min}}{\dot{m}''_{vap}} \quad (7.8)$$

Hence, the burning lifetime of the Jet A fire is independent of the instantaneous spill volume and (for the constant parameter values assumed here) has a constant value of around 60 s.

In the case of Jet A spills, the gas generated by each spill volume considered was represented as a constant area leak in the FLACS Fire model, with a duration given by Eqn (7.8). The size (area) and mass flow rate of this leak were defined using the value of R_{max} given by Eqn. (7.6) and $\dot{m}''_{vap}$. The initial temperature of Jet A fuel vapour gas was set to 216°C (corresponding to vaporization temperature of Jet A/kerosene fuel).

The default parameter values set for the FLACS-Fire radiation model were used in the simulations. The Eddy Dissipation Concept (EDC) combustion model was used as suggested by FLACS used guidelines. For the LH_2 fire simulations no soot model was used. For the Jet A fire simulations the "Fixed conversion factor" the soot model was enabled with the soot yield (fraction of fuel carbon converted to soot) set to 0.1 (10% yield typical for hydrocarbon fuels [Gexcon, 2019]). The gas released by the area leak during the FLACS-Fire simulation was ignited after a time interval of 1.0 s from the start of the simulation, to give it time to mix with the surrounding air and form a flammable mixture.

The computational domains employed in the Jet A pool fire simulations were set in general accordance with FLACS-Fire pool fire modelling guidelines [Gexcon, 2019], using uniform grid cells in the core region across and above the pool area with the cell size selected so as to maintain around 20 cells across the pool diameter (and so at least 13 cells across the characteristic diameter of the flame which is typically 70-80% of the pool fire diameter). Outside of the core region the grid cell size was stretched, by using an expansion factor of 1.2. The height of domain was selected to be a minimum of 6 times the pool diameter in the vertical direction (with half of this height being in the core region using the unform grid cell size). In cases without wind the domain in the XY-plane was equally spaced around the leak. The horizontal extent of the domain in the XY plane was set to be at least of 2-3 times the pool diameter each side of the pool region. In the case of the LH_2 pool fire simulations the vertical extent of the domain used was extended to a minimum of 10 times the pool diameter (with half of this height being in the core region using the unform grid cell size) to allow for the greater flame height/fireball behaviour exhibited by hydrogen pool fires, when compared to hydrocarbon fuels.

The baseline conditions used in the FLACS-Fire simulations assumed still atmospheric conditions without wind flow. The ambient temperature was set to 20°C.

Some additional simulations were also carried out to examine the effect of a wind flow on the behaviour of the 500 L instantaneous spill pool fires, with the characteristic wind speed, at a reference height of 10 m, set to 2 m/s. Atmospheric stability was set to Pasquill class F (stable), with a ground surface

roughness of 0.03 m. The wind direction used in the simulation was aligned to run along the positive x-axis (wind direction 270°). In accordance with FLACS-Fire user guidelines [Gexcon, 2019] the grid was extended in the downwind direction (to more than 4 times the pool diameter) to allow for the effect of the wind on the flame.

Table 7.2 summarises the number of grid cells and core region cell size used in the FLACS-Fire pool fire simulations of instantaneous fuels spills.

Table 7.2 – Summary of instantaneous fuel spill pool fire simulations.

Case	Scenario	Fuel	Rmax (m)	NX	NY	NZ	Core Cell Size (m)
IP-1	100 L Spill	LH_2	1.59	52	52	125	0.20 m
	100 L Spill	Jet A	2.50	60	60	96	0.25 m
IP-2	500 L Spill	LH_2	3.20	48	48	152	0.50 m
	500 L Spill	Jet A	5.64	74	74	97	0.60 m
IP-3	1000 L Spill	LH_2	4.32	52	52	138	0.70 m
	1000 L Spill	Jet A	7.98	64	64	109	0.80 m
IP-4	5000 L Spill	LH_2	8.77	52	52	152	1.0 m
	5000 L Spill	Jet A	17.84	58	58	75	1.8 m
IP-5	318 L Spill	LH_2	2.62	42	42	143	0.40 m
	4.5 kg/s LH_2 for 5 s	LH_2	2.15	42	42	143	0.40 m
IP-6	500 L Spill - 2 m/s Wind	LH_2	3.20	77	48	152	0.50 m
	500 L Spill - 2 m/s Wind	Jet A	5.64	74	74	97	0.60 m
IP-7	1,250 kg Spill of Single Fuel Tank	LH_2	15.48	60	60	117	1.5 m
	4,630 kg Spill of Tanks on One Side	Jet A	19.82	58	58	75	2.0 m
IP-8	5,000 kg Spill of Entire Fuel Load	LH_2	29.03	60	60	117	3.0 m
	13,889 kg Spill of Entire Fuel Load	Jet A	34.34	70	70	100	2.5 m

7.3.2 Results for 500 L fuel spill pool fires

In order to visualise and compare the fire plume results obtained in the different fire simulations performed a temperature threshold of 773 K has been used to demarcate the boundary of the flaming region. Similarly, the radiation heat flux received on the surface of the ground around the pool fire (in the range 5 kW/m^2 to 37.5 kW/m^2) has also been plotted.

Fig 7.13(a-d) shows the evolution in the temperature of the simulated transient pool fire resulting from the ignition of the 500 L LH_2 spill. At 2 s after ignition the ignited hydrogen gas has formed into a fireball - a rapidly rising expanding ball of flame (Fig 7.13(a)). Over the next couple of seconds, the spherical fireball region continues to rise and expand in size with a central “stalk” of flame formed below (Fig 7.13(b-c)). By 5 seconds after ignition the hydrogen in the rising fireball region has been consumed and starts to cool (Fig 7.13(d)) before shortly after completely burning out and disappearing. The corresponding radiation heat flux region incident on the ground surface can be seen to expand in both

size and intensity as the fireball rises and grows, reaching a maximum around 3 s after ignition, and then contracting again as the fireball burns out and disappears.

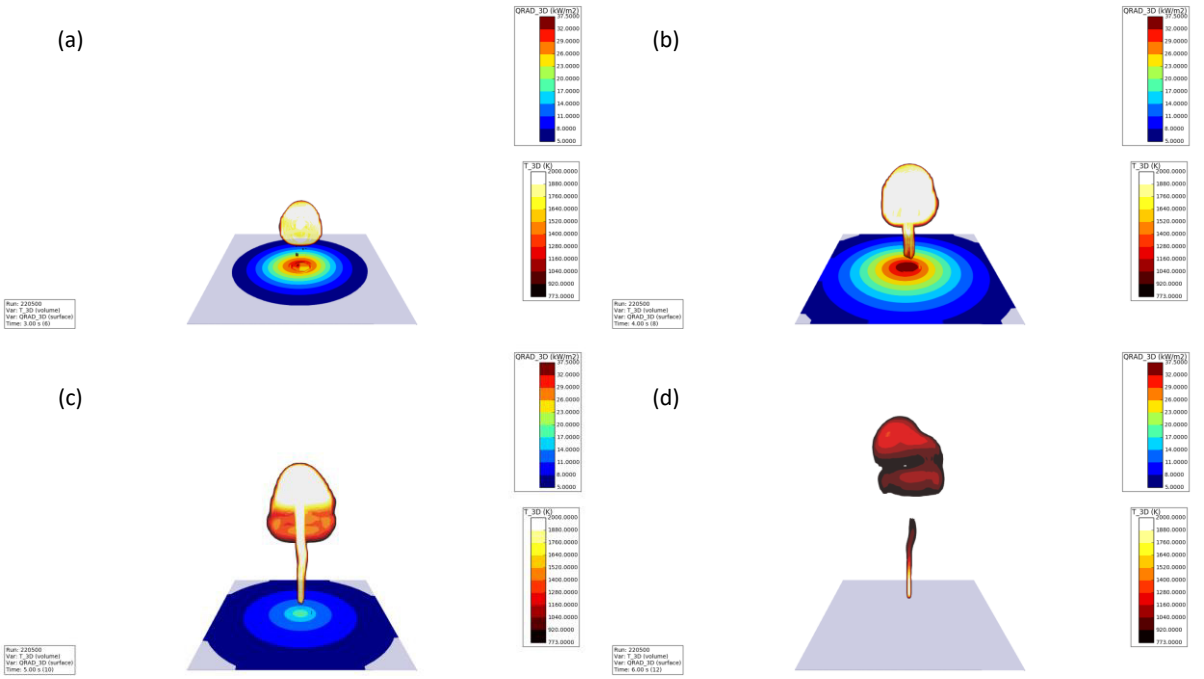

Fig. 7.13 – Evolution of the fireball produced for a 500 L LH_2 spill pool fire at different time intervals after ignition: (a) 2 s; (b) 3 s; (c) 4 s; (d) 5 s.

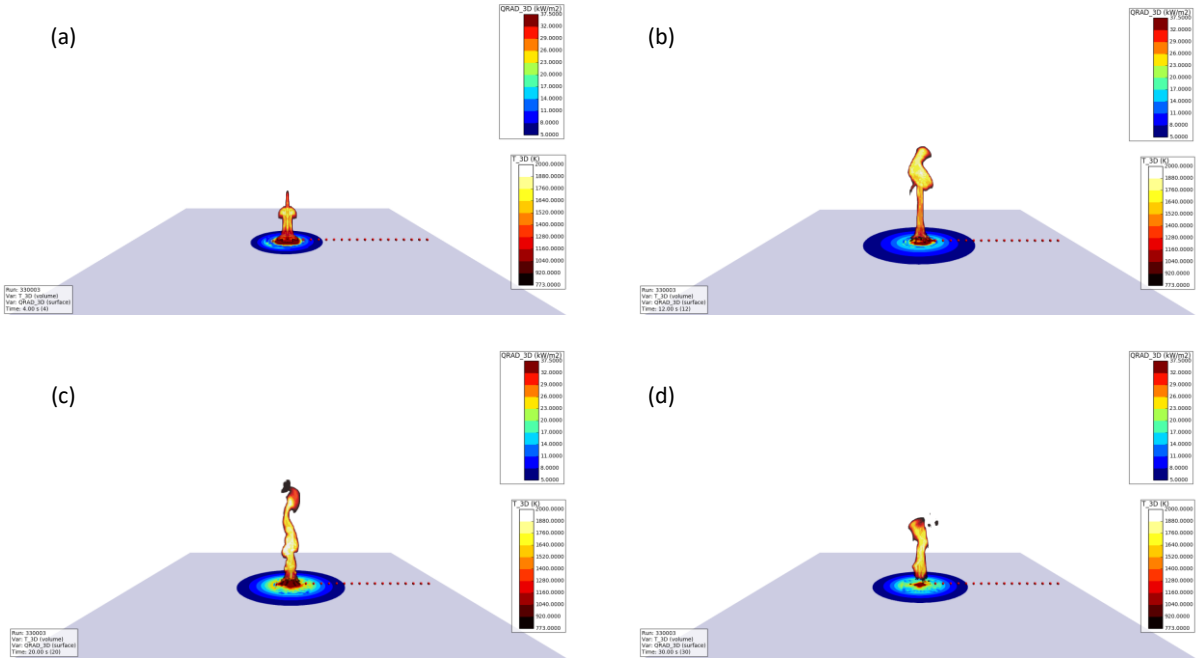

Fig. 7.14 - Evolution of the fire plume produced for a 500 L Jet A spill pool fire at different time intervals after ignition: (a) 3 s; (b) 11 s; (c) 19 s; (d) 29 s.

For comparison Fig 7.14(a-d) shows the development of the simulated pool fire obtained for a 500 L spill of Jet A. In contrast to the short duration, rising fireball found for LH_2 spills, the Jet A spill burns as a continuously fluctuating fire plume. The size of the radiation heat flux region produced on the ground also fluctuates accordingly.

Fig 7.15 compares the Heat Release Rate predicted for the 500 L LH_2 and Jet A pool fires (for the 30 s time period it is assumed that people would take to egress from the vicinity of a fire). The LH_2 spill produces a high intensity fire with a relatively high heat release rate peak over a short period of time (around 5 s) before consuming the available fuel and burning out. In contrast the Jet A pool fire has a flame that burns continuously with a lower level HRR but that which is sustained over a significantly longer period of time.

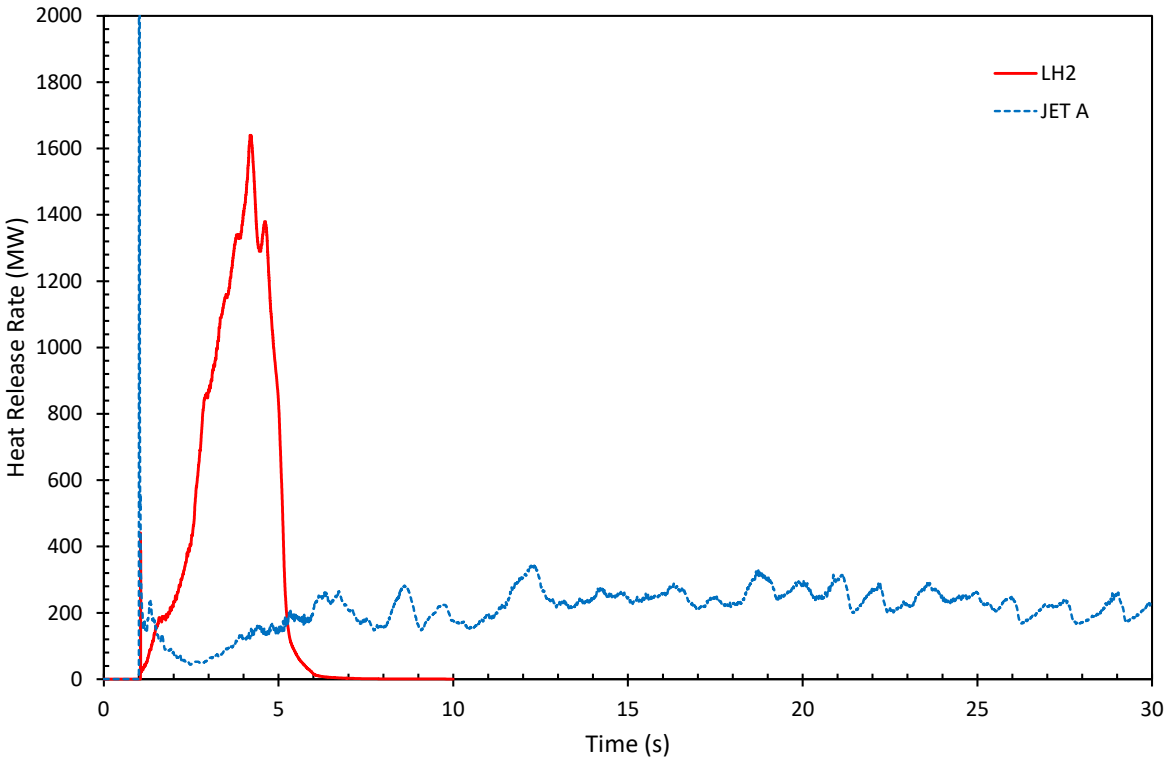

Fig. 7.15 – Comparison of the predicted heat release rate for LH_2 and Jet A 500 L fuel spill pool fires.

A comparison of radiation heat flux received at a monitor point located on the ground 15 m from the centre of the pool fire (for the 500 L LH_2 and Jet A spills) given in Fig 7.16 shows a short duration curve (around 6s) with a sharp peak flux (over 20 kW/m^2) produced for the LH_2 pool fire compared to the radiation flux fluctuating at a lower level (between 10 to 15 kW/m^2) over a longer period for the Jet A pool fire.

Fig 7.17 shows a comparison of the thermal dose received at a monitor point located on the ground 15 m from the centre of the 500 L LH_2 and Jet A pool fires. As a consequence of the short duration of the LH_2 fireball the total thermal dose delivered levels off (at around 150 (kW/m^2)$^{4/3}$ s) after 6 seconds whilst the dose delivered from the Jet A pool fire continues to increase to reach a total around 5 times that of the LH_2 pool fire after 30 s. Hence a significantly lower total thermal radiation dose is delivered by the LH_2 pool fire.

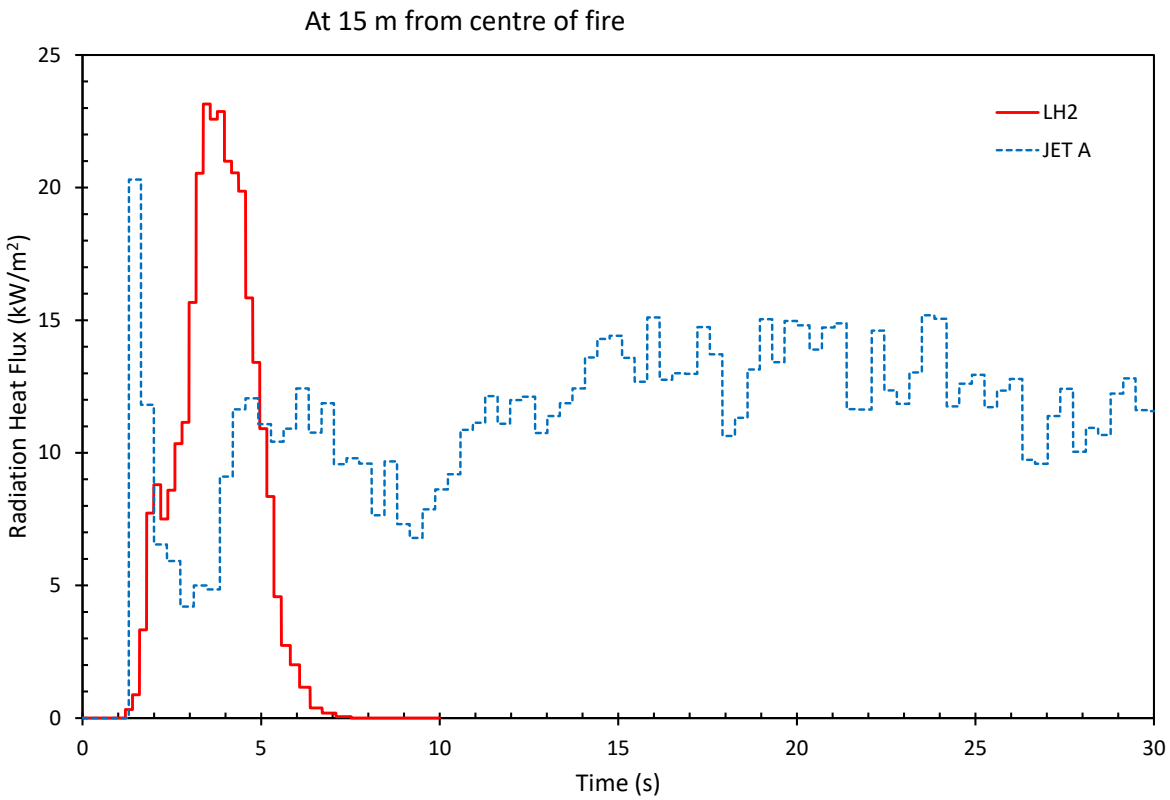

Fig. 7.16 – Comparison of the predicted radiation heat flux produced by LH_2 and Jet A 500 L fuel spill pool fires received at a monitor point 15 m from the origin of the fire.

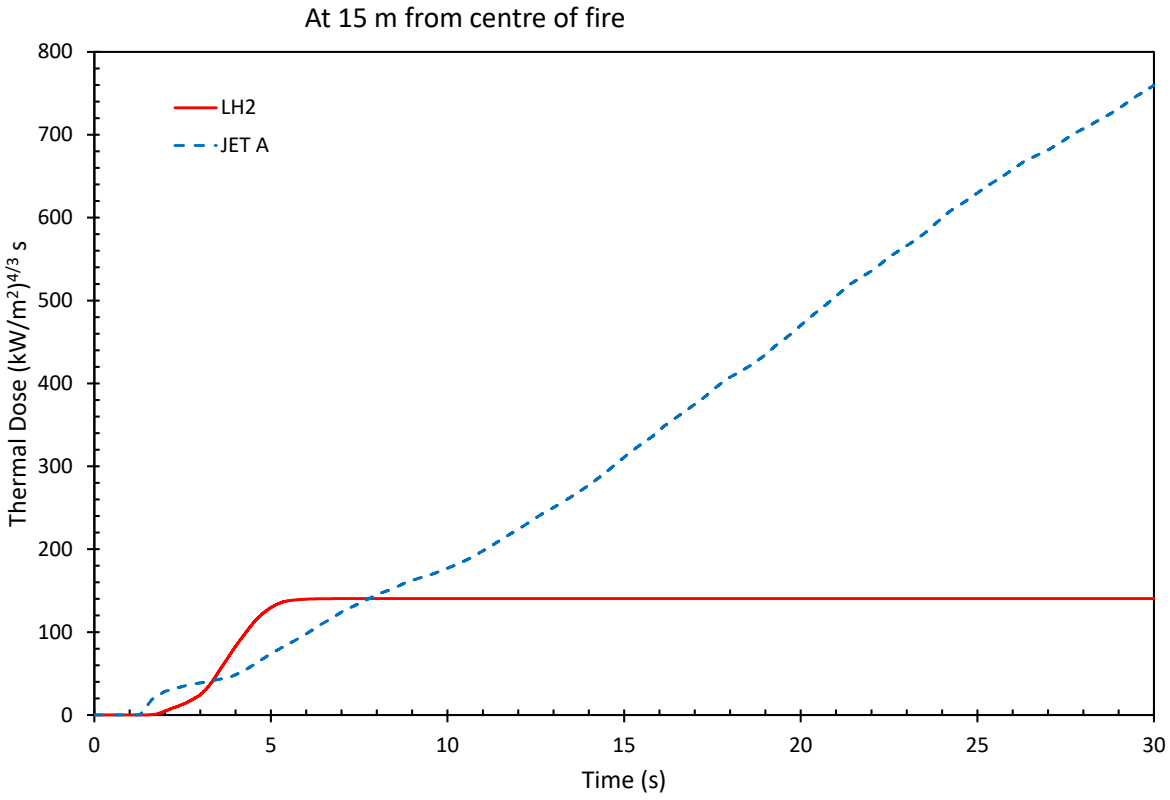

Fig. 7.17 – Comparison of the predicted thermal dose for 500 L LH_2 vs Jet A pool fires.

7.3.3 Hazardous distance for thermal radiation dose harm

By comparing the predicted thermal radiation dose produced at different distances from a pool fire with the specified thermal dose harm criteria the hazardous distance from the fire origin producing a given harm threshold can be determined for both LH_2 and Jet A spills. Table 7.3 summarises the results obtained for the different instantaneous fuel spill pool fire case scenarios that were examined.

Table 7.3 – Summary of the hazardous distance at different thermal dose levels predicted for the different instantaneous fuel spill pool fire case scenarios examined.

Case	Scenario	Fuel	Rmax	Hazardous Distance (m)			
			(m)	100 TDU	240 TDU	420 TDU	1050 TDU
IP-1	100 L Spill	LH_2	1.59	7.9	1.6*	1.6*	1.6*
	100 L Spill	Jet A	2.50	18.7	12.2	8.8	5.4
IP-2	500 L Spill	LH_2	3.20	19.8	8.6	3.2*	3.2*
	500 L Spill	Jet A	5.64	43.9	26.7	22.5	13.4
IP-3	1000 L Spill	LH_2	4.32	27	12.9	5.2	4.3*
	1000 L Spill	Jet A	7.98	> 56	44.2	33.0	19.5
IP-4	5000 L Spill	LH_2	8.77	> 50	27.2	14.5	8.8*
	5000 L Spill	Jet A	17.84	109	77.8	62.0	40.1
IP-5	318 L Spill	LH_2	2.62	17.1	6.1	2.6*	2.6*
	4.5 kg/s LH2 for 5 s	LH_2	2.15	11.7	4.8	2.2*	2.2*
IP-6	500 L Spill - 2 m/s Wind	LH_2	3.20	30.0	18.8	11.4	3.2*
	500 L Spill - 2 m/s Wind	Jet A	5.64	48.0	38.3	32.7	21.8
IP-7	1,250 kg Spill of Single Fuel Tank	LH_2	15.48	99.6	55.4	36.0	15.5*
	4,630 kg Spill of Tanks on One Side	Jet A	19.82	115.7	85.2	70.4	46.8
IP-8	5,000 kg Spill of Entire Fuel Load	LH_2	29.03	154.8	95.9	60.6	29.0*
	13,889 kg Spill of Entire Fuel Load	Jet A	34.34	163.3	118.6	93.6	64.4

*In cases where the thermal dose threshold has not been exceeded the hazardous distance has been set equal to the pool fire radius

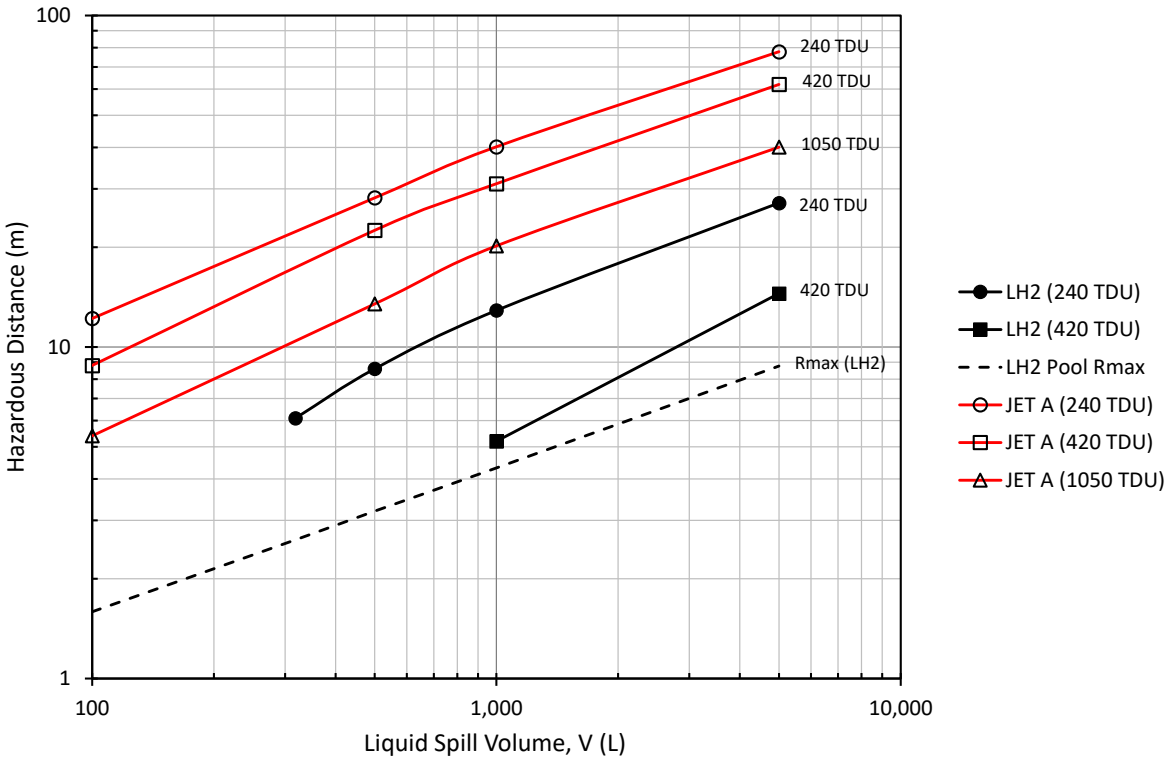

Fig. 7.18 – Comparison of hazardous distance vs. spill volume predicted for LH_2 and Jet A fuel spill pool fires, at different thermal dose thresholds.

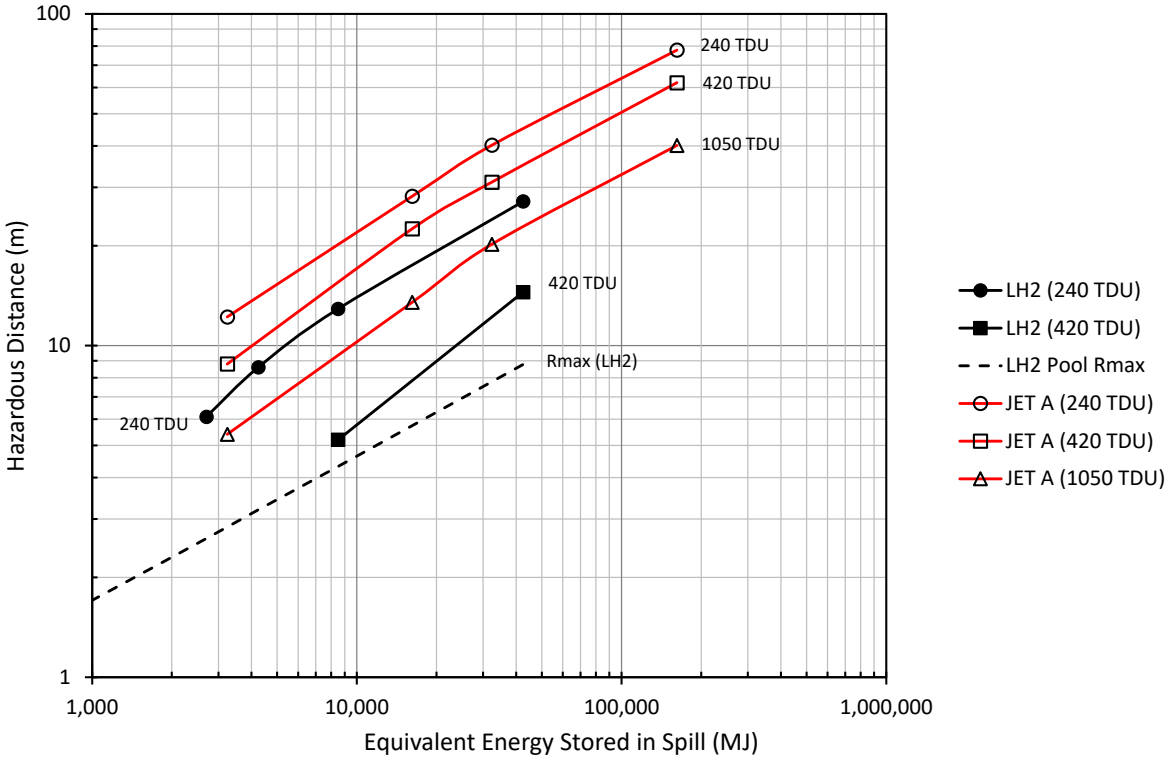

Fig. 7.19 - Comparison of hazardous distance vs. equivalent energy stored in fuel predicted for LH_2 and Jet A fuel spill pool fires, at different thermal dose thresholds.

Fig 7.18 compares the hazardous distance predicted by FLACS-Fire for the different thermal radiation dose harm thresholds as a function of the liquid spill volume for both LH_2 and Jet A pool fires. It is evident that, as a consequence of the short duration of the LH_2 fireball, the hazardous distance predicted for the LH_2 pool fires are significantly lower than those obtained for an equivalent spill volume of Jet A. In fact, not only is the hazardous distance to the 240 TDU (2nd degree burn) injury threshold predicted for LH_2 pool fires (for a given spill volume) to be much less than that found for Jet A (around a third the value), but it is also less than the distances to the 420 TDU (dangerous dose) and 1050 TDU (fatality) thresholds predicted for Jet A. In the case of the instantaneous LH_2 pool fires simulated, the 1050 TDU thermal dose threshold for a fatality was not exceeded. To provide a lower bound on the hazardous distance for these cases the maximum radius of the LH_2 spill/pool fire region has therefore also been plotted in Fig 7.18.

Upon combustion LH_2 releases around a quarter of the energy per unit volume as Jet A. Hence, a given spill volume of LH_2 contains significantly less stored energy than the same volume of Jet A. To adjust for this Fig 7.19 compares the predicted hazardous distance to the different thermal radiation dose harm thresholds, as a function of the equivalent energy stored in a spill, for both LH_2 and Jet A pool fires. Even in this case the results still suggest that the hazardous distance due to thermal radiation dose predicted for LH_2 pool fires (at a given stored energy level) is lower than that for a Jet A pool fire of an equivalent stored energy.

7.3.4 LH_2 pool fires - instantaneous vs finite rate/duration spills

In order to compare the effect on an LH_2 pool fire of an instantaneous versus finite rate/duration fuel spill some simulations were performed comparing the LH_2 pool fire produced for a 318 L instantaneous LH_2 spill with that produced for a 63.5 L/s release over 5 seconds (corresponding to an aircraft refuelling accident scenario where a fuel line supplying 4.5 kg/s to refuel a LH_2 aircraft, is severed and the supply cut after 5 s).

Fig 7.20 shows the evolution of the pool fire produced for an instantaneous spill of 318 L of LH_2. It can be shown to exhibit a similar pattern of behaviour to the previous LH_2 pool fires examined for instantaneous spills forming an expanding fireball which rises rapidly before burning out after a few seconds. In contrast Fig 7.21 shows the development of the LH_2 pool fire predicted for a 63.5 L/s release over 5 seconds. It initially resembles the fireball behaviour exhibited by instantaneous LH_2 spill pool fire, but then transitions into a tall continuous burning flame until the remaining LH_2 is consumed and it burns out. Similarly, the radiation heat flux incident to the ground transitions from a wide area region for the fireball to a small, localised region for the continuous tall flame phase.

Fig 7.22 compares the predicted radiation heat flux for the two cases incident at a monitor point located at a distance 15 m from the origin of the pool fire. The instantaneous 318 L spill produces a heat flux with a short duration sharp peak where-as the 63.5 L/s, 5 s spill produces a lower peak heat flux over a longer period of time.

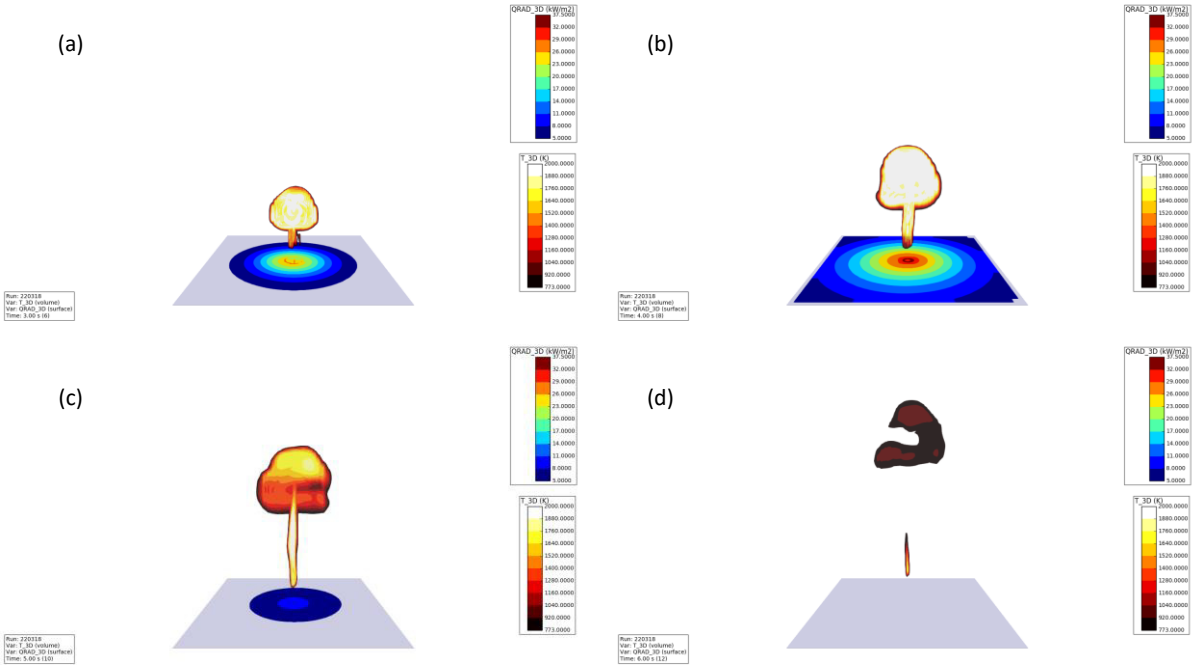

Fig. 7.20 - The evolution of the pool fire produced for an instantaneous spill of 318 L of LH_2 at different time intervals after ignition: (a) 2 s; (b) 3 s; (c) 4 s; (d) 5 s.

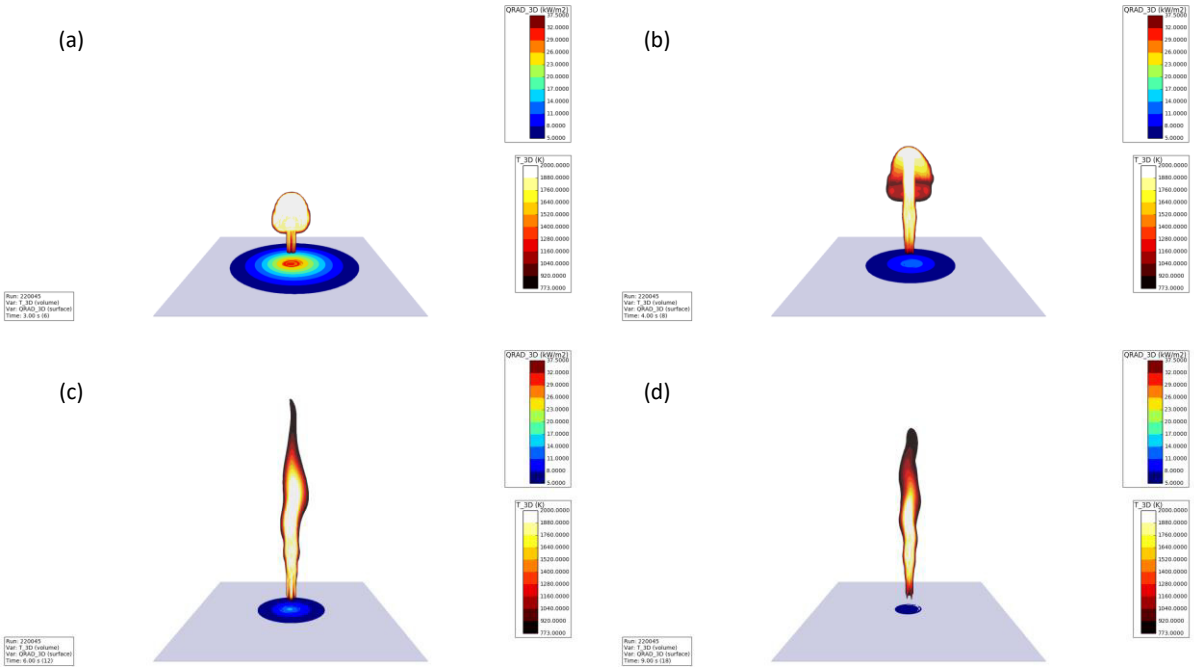

Fig. 7.21 - The evolution of the pool fire produced for an 63.5 l/s release of LH_2 over 5 s at different time intervals after ignition: (a) 2 s; (b) 3 s; (c) 5 s; (d) 8 s.

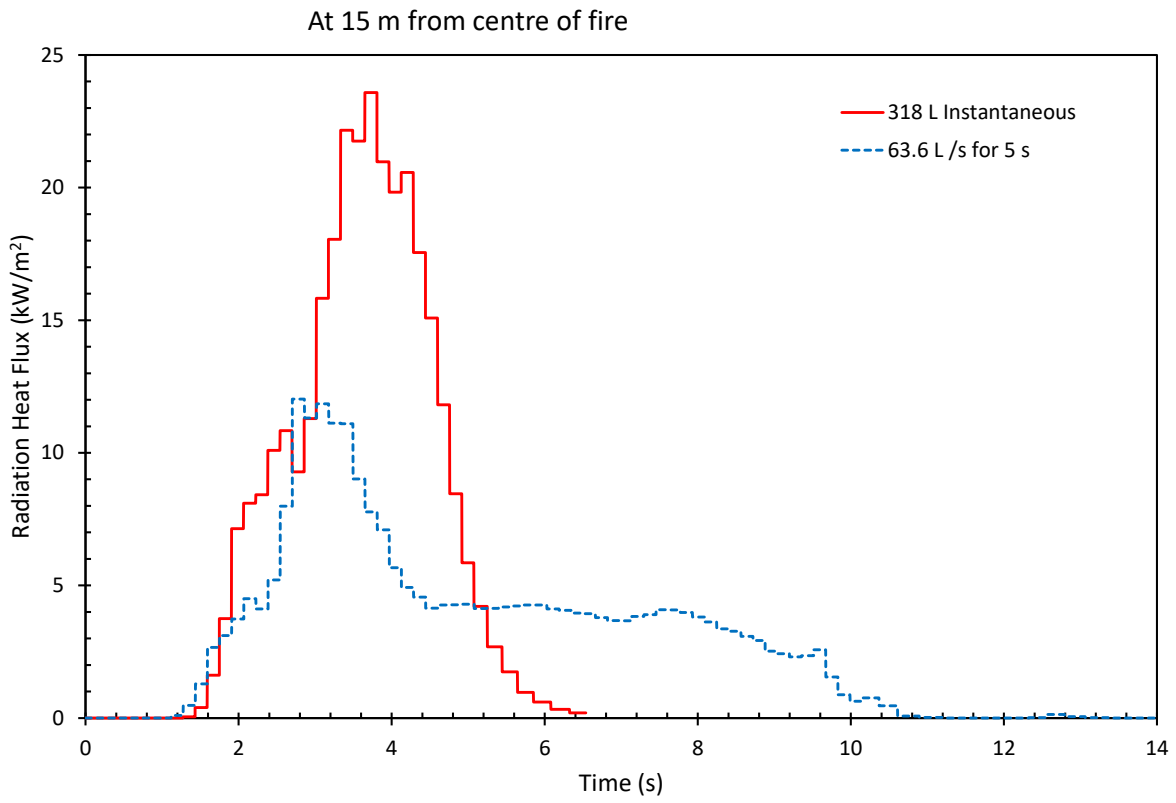

Fig. 7.22 – Comparison of pool fire radiation heat flux predicted for instantaneous 318 L LH_2 spill versus a 63.5 L/s LH_2 release over 5 s.

7.3.5 The effect of wind on pool fire behaviour

Fig 7.23 show the effect of a wind (flowing from left to right across the domain) on the development of an instantaneous spill 500 L LH_2 pool fire. Comparing with Fig 7.13 (without wind) it can be seen that its behaviour is still dominated by the buoyancy of the fireball, but that it is now deflected to the right of the domain by the wind as it ascends. The pattern of the radiation heat flux received on the ground beneath the fireball is also now shifted towards the right of the domain. The behaviour of the fire plume for the Jet A pool fire is also affected by the wind (Fig 7.24) with the fluctuating fire plume and associated radiation heat flux received on the ground being clearly deflected towards the right of the domain.

Comparing the predicted hazardous distance (due to thermal radiation) found for the 500 L instantaneous spill pool fire IP-2 (no wind) and IP-6 (2 m/s wind) cases, given in table 7.3, it can be seen that the (downwind) hazardous extent (in terms of burn injury and dangerous dose threshold) of the LH_2 pool fire has increased significantly with the wind present (by a factor of 2-4 times). The hazardous extent of the Jet A pool fire has also increased with the wind present by as much as 60% (in the case of the fatal threshold). Note however that the hazardous extent of the Jet A pool fire (for all the thermal radiation harm criteria) remains significantly higher than that found for LH_2 (by a factor of 2-3), even with the wind present, while the hazardous extent of the fatal threshold for the LH_2 pool fire with the wind remains limited to the maximum radius of the pool fire.

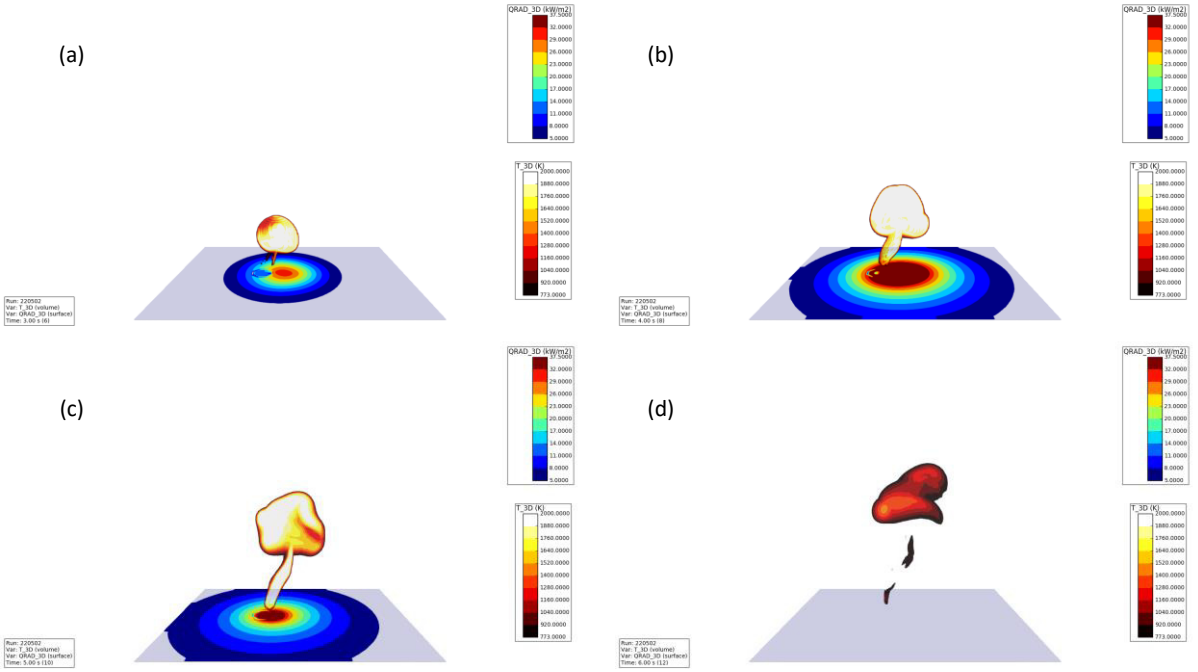

Fig. 7.23 – The predicted effect of 2 m/s wind profile (flowing left to right) on a 500 L LH_2 spill pool fire at different time intervals after ignition: (a) 2 s; (b) 3 s; (c) 4 s; (d) 5 s.

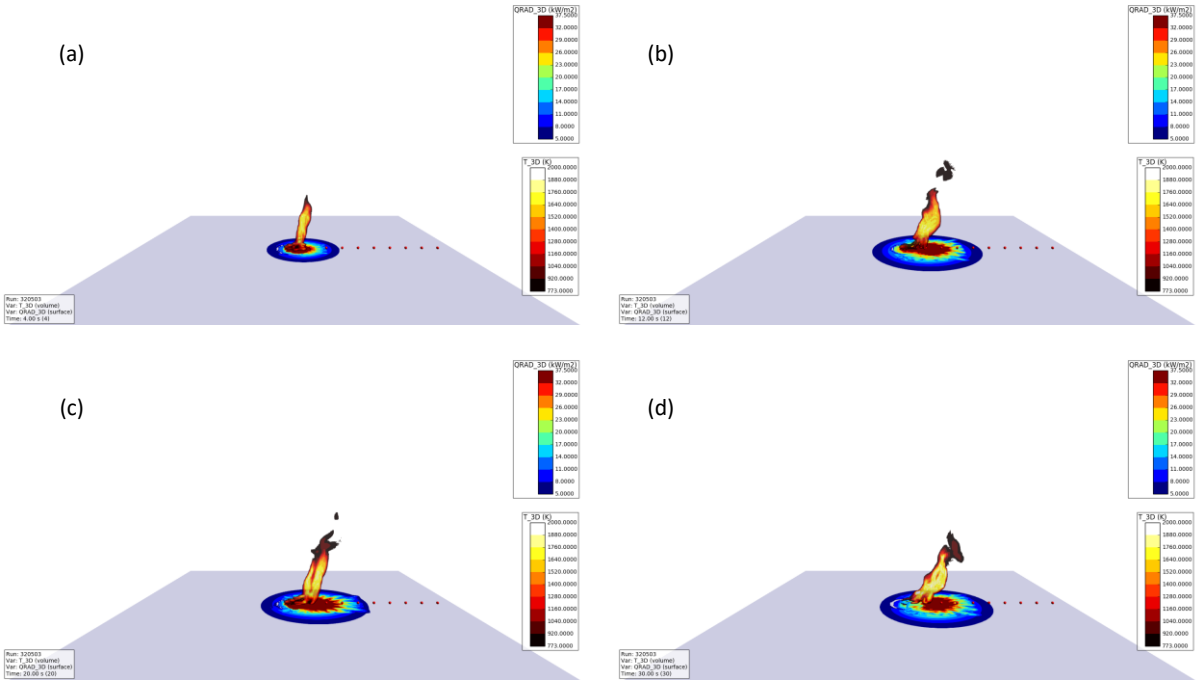

Fig. 7.24 – The predicted effect of 2 m/s wind profile (flowing left to right) on a 500 L Jet A spill pool fire at different time intervals after ignition: (a) 3 s; (b) 11 s; (c) 19 s; (d) 29 s.

7.4 Effect of pool fire on aircraft

Work has been carried out to examine the consequences of an instantaneous fuel spill and immediate ignition event resulting in a pool fire occurring during aircraft refuelling operations whilst also including the aircraft geometry as part of the simulation.

Aircraft geometries based upon both a conventional commercial short/medium range passenger aircraft design and a modified short/medium range 'tube and wing' LH_2 aircraft design developed for ENABLEH2, were digitised, and introduced as geometrical objects (comprised of boxes, cylinders and plates) into FLACS. Fig 7.25(a) shows the conventional aircraft geometry used, whilst Fig 7.25(b) shows the LH_2 aircraft geometry.

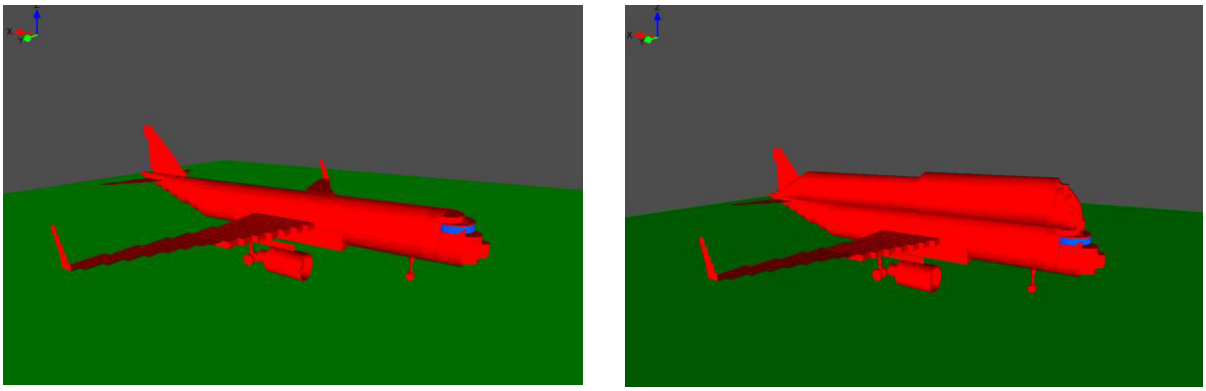

(a) (b)

Fig. 7.25 – The aircraft geometries introduced into FLACS: (a) conventional Jet A aircraft; (b) LH_2 short/medium range "tube and wing" aircraft.

FLACS-Fire simulations were performed to allow a comparison to be made between the pool fires resulting from a 500 L instantaneous spill of LH_2 and Jet A (kerosene). The Jet A spill/pool fire was located under the wing (corresponding to the location of the refuelling point used for a conventional Jet A aircraft). The LH_2 spill/pool fire was assumed to be located in one of two positions (Fig 7.26) – either on the right side of the aircraft fuselage towards the front of the aircraft ahead of the wing, or at the tail of the aircraft – corresponding to the refuelling position suggested for the LH_2 aircraft design developed by Brewer [1991]. The simulations carried out were used to compare pool fire behaviour, radiation heat flux and thermal radiation dose exhibited by the two fuels.

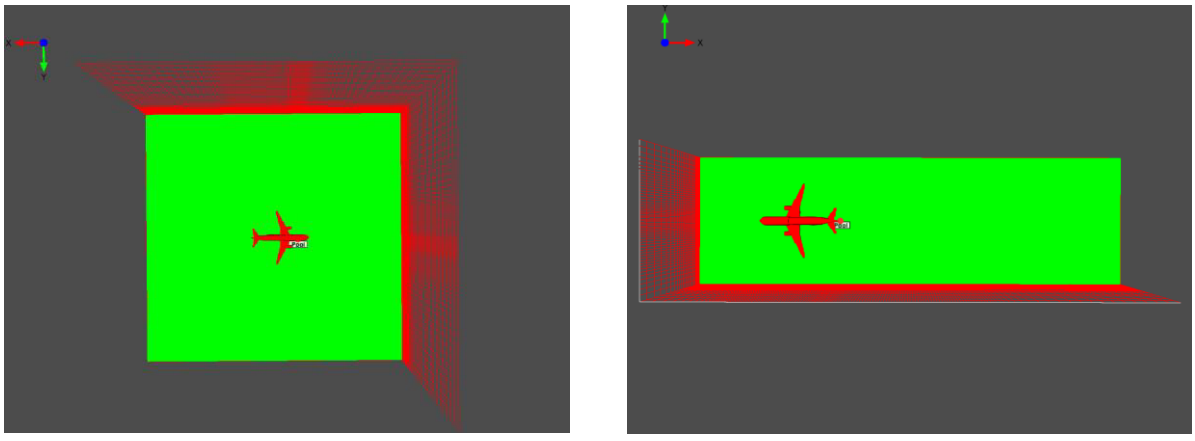

(a) (b)

Fig. 7.26 – Locations of LH_2 fuel spill pool fires used for the LH_2 aircraft: (a) side of aircraft; (b) tail of aircraft.

Fig 7.27 shows the development of a 500 L instantaneous spill LH_2 pool fire located on the front right side of the aircraft. The LH_2 spill vaporises rapidly and the ignited hydrogen gas forms a fireball - a rapidly rising expanding ball of flame. The resulting high intensity fire has a relatively high heat release rate over a short period of time before consuming the available fuel and burning out. The corresponding thermal radiation flux incident on the ground and aircraft surfaces is also shown. As the fireball rises the radiation flux incident on the aircraft shifts in intensity and position from the front right side to the top of the aircraft (toward the front) and the right wing. The size of the region with radiation incident on

the ground also expands, although the aircraft fuselage does provide some shielding of the radiation heat flux delivered to the area to the left of the aircraft.

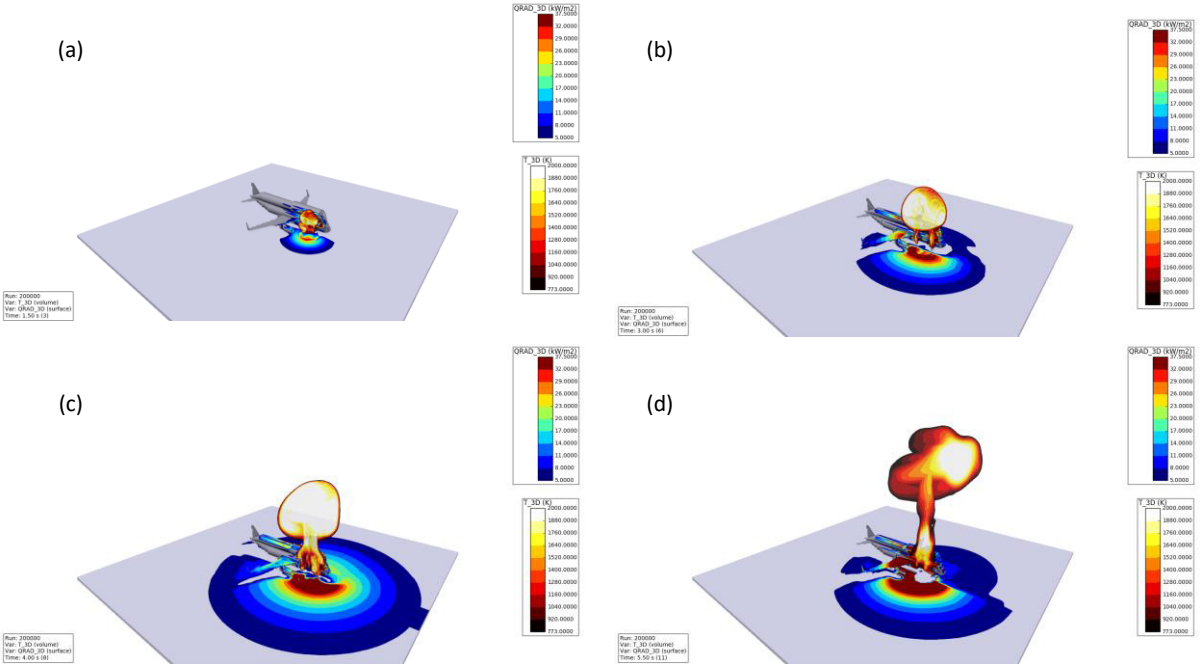

Fig. 7.27 - Development of a 500 L instantaneous spill LH_2 pool fire located on the front right side of the aircraft: (a) 1.5 s; (b) 3.0 s; (c) 4.0 s (d) 5.5 s.

Fig 7.28 shows a closer view (side and top) of the radiation heat flux incident on the ground and the aircraft surfaces at 4.0 s, when the fireball reaches its peak HRR, again illustrating the high thermal radiation levels delivered to the front, right side and top of the aircraft from the rising LH_2 fireball produced in this position.

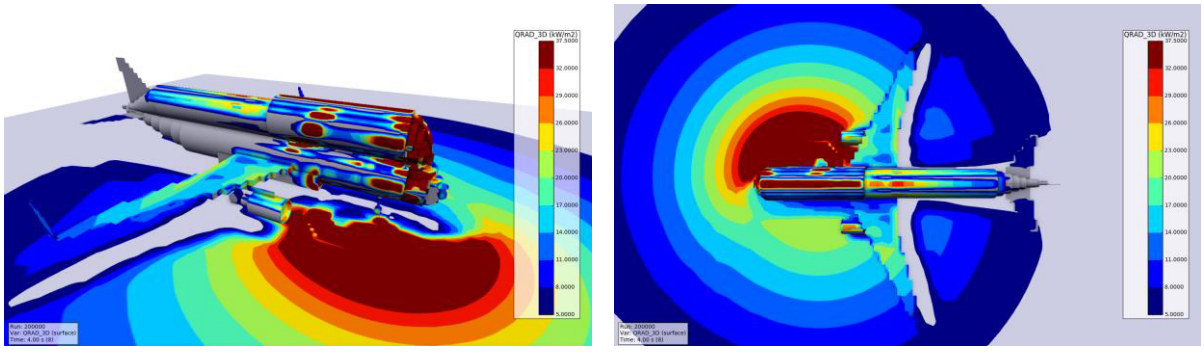

Fig. 7.28 - Radiation heat flux incident on the ground and the aircraft surfaces at 4.0 s. for the LH_2 pool fire located at front right side of the aircraft.

Fig 7.29 also shows the development of a 500 L instantaneous spill LH_2 pool fire but this time located at the tail of the aircraft, whilst Fig 7.30 provides a closer view (side and top) after 4.0 s. In this case the radiation heat flux released by the rising fireball falls mainly to the rear of the aircraft, with the highest intensities produced on the tail and top of the fuselage.

The development of the 500 L Jet A spill pool fire is shown in Fig 7.31 In comparison to the intense fireball produced for LH_2, the Jet A pool fire has a flame that burns continuously with a lower peak HRR, but that which is sustained over a significantly longer period of time. Fig 7.32 shows a closer view of the radiation heat flux incident of the aircraft after 30 s. The radiation flux from the Jet A pool fire is concentrated along the length of the right side and wing of the aircraft. The size and duration of the very

high thermal flux region (> 37.5 kW//m^2) produced by the Jet A fire (e.g. on the right wing and engine) is also predicted to be significantly greater than that for the LH_2 fire. However, the results also suggest that the fuselage of the aircraft does effectively shield the left-hand side of the aircraft from the radiation produced by the Jet A fire.

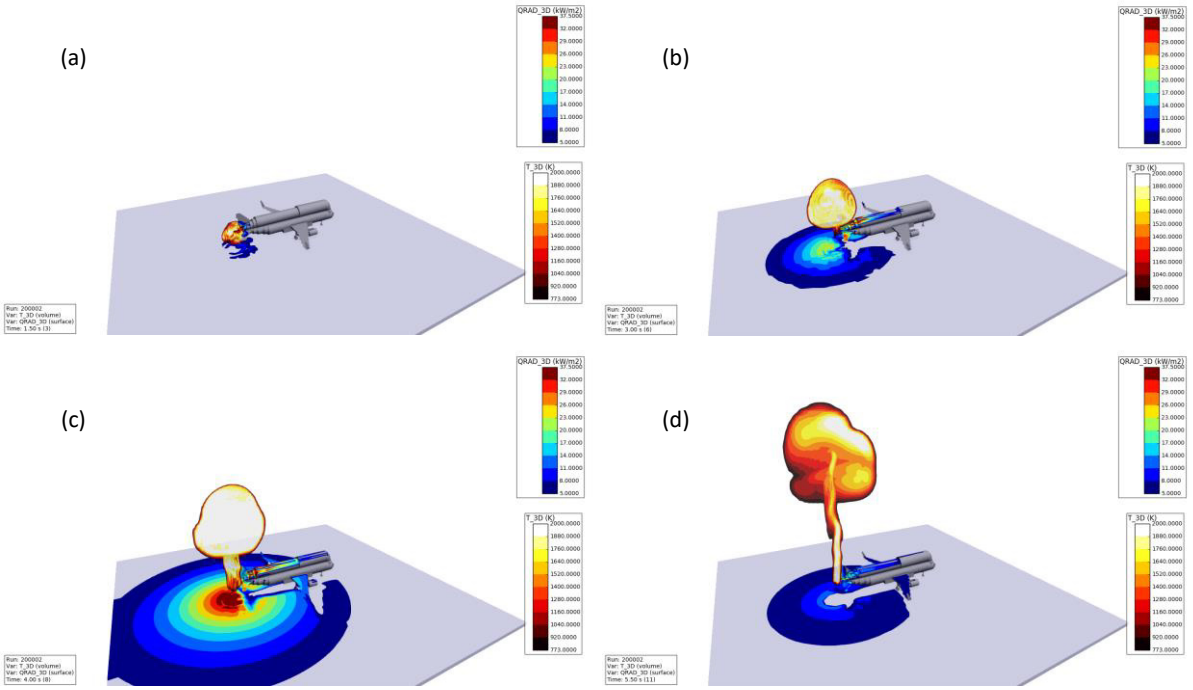

Fig. 7.29 - Development of a 500 L instantaneous spill LH_2 pool fire located at the tail of the aircraft: (a) 1.5 s; (b) 3.0 s; (c) 4.0 s (d) 5.5 s.

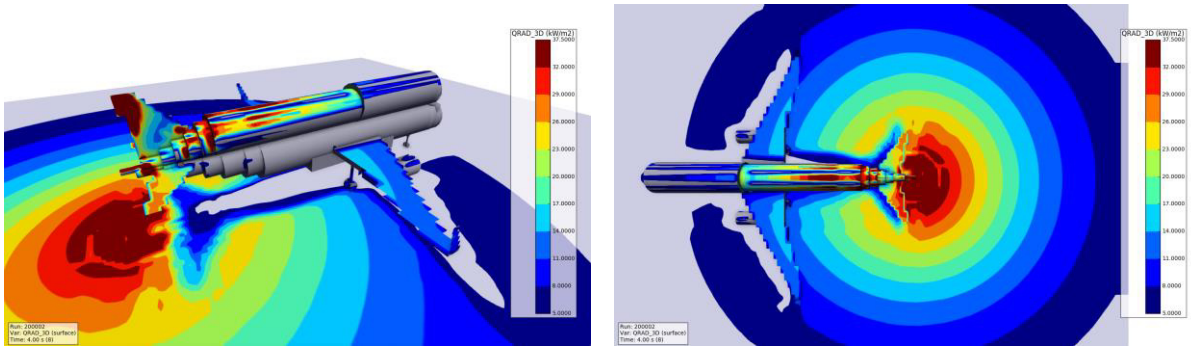

Fig. 7.30 - Radiation heat flux incident on the ground and the aircraft surfaces at 4.0 s. for the LH_2 pool fire located at the tail of the aircraft.

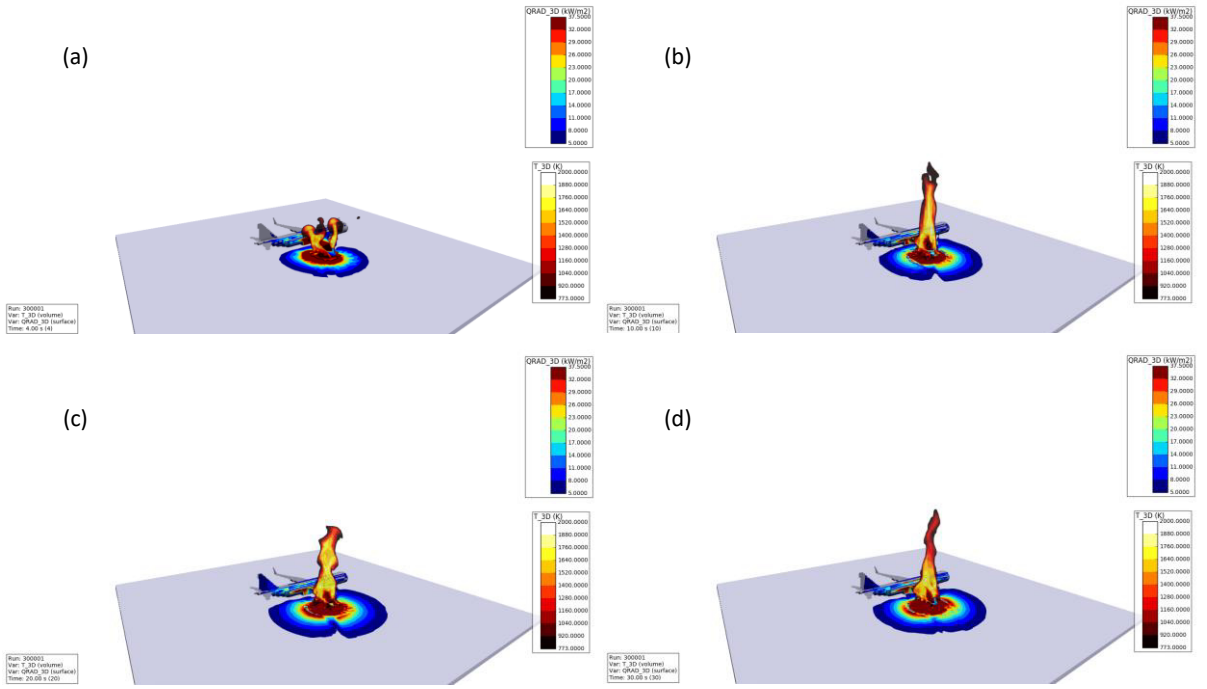

Fig. 7.31 - Development of a 500 L instantaneous spill Jet A pool fire located under the wing of the aircraft: (a) 4 s; (b) 10 s; (c) 20 s (d) 30 s.

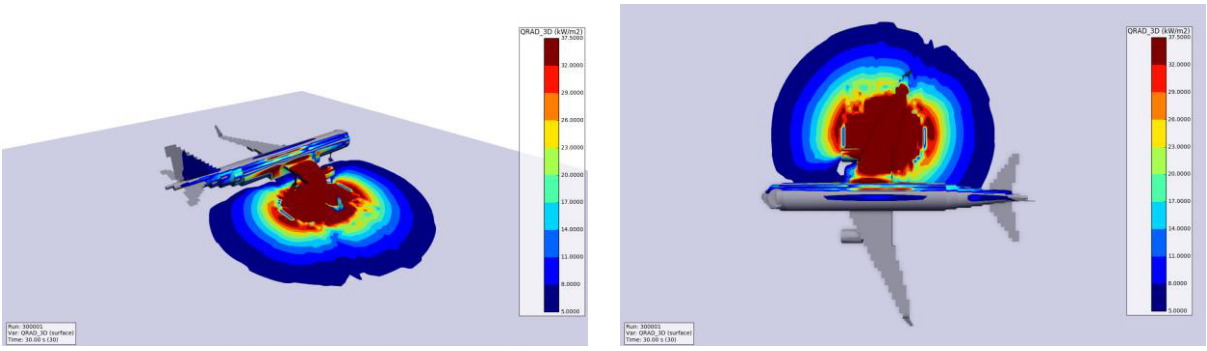

Fig. 7.32 - Radiation heat flux incident on the ground and the aircraft surfaces at 4.0 s. for the Jet A pool fire located under the wing of the aircraft.

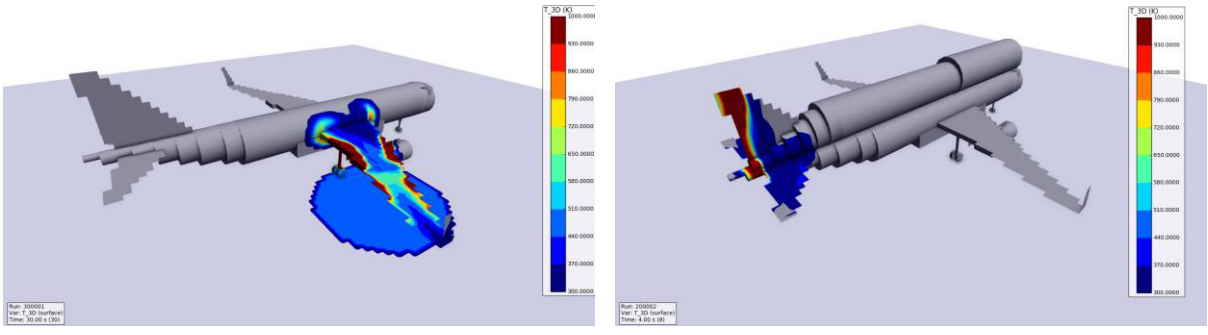

Fig. 7.33 - Comparison of the temperatures produced on the surface of the aircraft for: (a) 500 L Jet A pool fire; (b) LH_2 pool fire (located at the tail).

Fig 7.33 shows a comparison of the temperatures produced on the surface of the aircraft for the 500 L Jet A and LH_2 (located at the tail) pool fires. The Jet A pool fire produces high temperatures across the surface of the right wing, engine and fuselage with some very high temperature found at the wing edges. In comparison the LH_2 pool fire induces some high temperatures on the surface of the tail fin.

7.5 Characterisation of fireballs for instantaneous LH_2 spill pool fires

The FLACS-Fire simulation results obtained for pool fires resulting from instantaneous LH_2 spills ranging in size from 100 L to 5000 L, have been used to characterise the behaviour of the fireballs produced.

The maximum diameter of the fireball predicted for a given LH_2 spill mass, D_{fb} (m) was estimated from the 2D temperature contour plot data taken through the centre of the release (y = 0), around the time of the peak heat release rate. The horizontal and vertical distances between the sides and top and bottom of the simulated fireball were measured and used to find the volume of the ellipsoid formed and then the equivalent diameter of a sphere having the same volume.

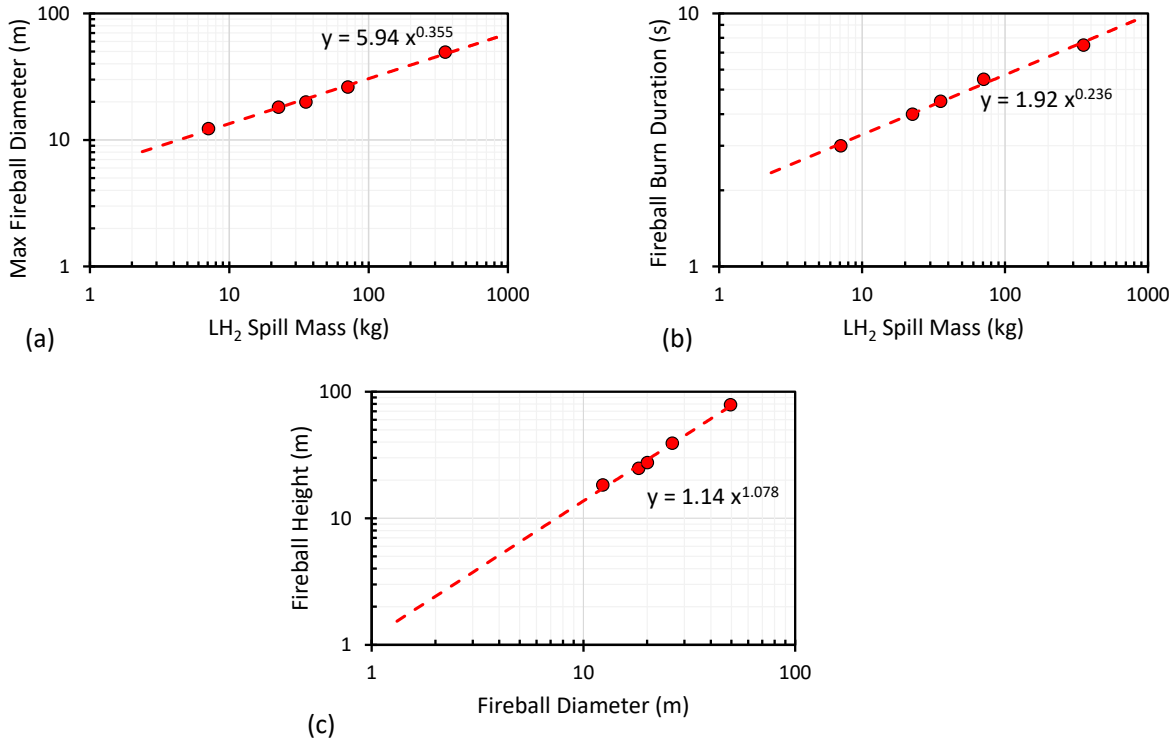

Fig. 7.34 – Characteristic fireball data and correlations obtained from FLACS-Fire simulations of instantaneous LH_2 spill pool fires: (a) max fireball diameter; (b) fireball burn duration; (c) fireball height.

Fig. 7.34(a) plots the maximum diameter of the fireball versus the mass of the instantaneous LH_2 spill found for FLACS pool fire simulation data. The maximum fireball diameter, D_{fb} (m) exhibits a power-law relationship with LH_2 spill mass, m (kg) which is fitted by:

$$D_{fb} = 5.94\, m^{0.355} \tag{7.9}$$

The power of 0.355 is reasonably close to the value of 1/3 which has been suggested theoretically for the scaling dependence of fireball diameter with mass of fuel [Fay and Lewis, 1977]. Eqn. (7.9) is similar

to a correlation for the maximum fireball diameter obtained by Roberts (for fireballs originating from a hydrocarbon BLEVE) [Beyler, 2016]:

$$D_{fb} = 5.8\, m^{1/3} \tag{7.10}$$

Hord [1978] also reported an expression which he suggested could be applied to predicting the maximum equivalent spherical diameter of the fireballs produced for a wide variety of rocket propellants and explosive including hydrogen-air:

$$D_{fb} = 7.93\, m^{1/3} \tag{7.11}$$

The smaller coefficient of 5.94 means that that the diameters predicted by Eqn. (7.9) will be slightly smaller than those predicted by the Hord correlation, although they will still exhibit a very similar scaling dependency.

The burning duration of the fireball was also estimated from the 2D temperature contour plot and heat release rate data based upon the times at which the fireball first formed and began to dissipate. The duration of the fireball versus the mass of the instantaneous LH_2 spill found for FLACS pool fire simulation data is shown in Fig. 7.34(b). The fireball duration, t_{fb} (s) also displays a power-law relationship with LH_2 spill mass, m (kg) which is fitted by:

$$t_{fb} = 1.92\, m^{0.236} \tag{7.12}$$

For hydrocarbon BLEVES the burning duration behaviour of the fireballs released are classified as being either momentum or buoyancy dominated [Beyler, 2016]. In the momentum dominated regime (such as those found for fuels undergoing flash vaporisation in pressurised BLEVE releases) the burning duration of the fireball is given by:

$$t_{fb} = 0.45\, m^{1/3} \tag{7.13}$$

On the other-hand in the buoyancy dominated regime (found for atmospheric releases) the fuel takes longer to rise and mix with the surrounding air and the burning duration of the fireball is given by:

$$t_{fb} = 2.6\, m^{1/6} \tag{7.14}$$

It can be seen that exponent of 0.236 obtained for Eqn. (7.12) falls somewhere between the values of 1/6 (0.167) and 1/3 (0.333) found respectively for the buoyancy and momentum dominated regimes, whilst the coefficient of 1.92 appears to be closer in magnitude to that found for the buoyancy dominated correlation. Overall the behaviour of the fireball burning duration predicted by Eqn. (7.12) for the LH_2 pool fire spills simulated using FLACS-Fire would appear to be closer to that found for the buoyancy dominated regime (i.e. extended duration).

The average height of the centre of the fireball was obtained from the vertical distance between the top and bottom of the simulated fireball. Fig 7.34(c) shows the relationship between the height of the centre of the fireball (when it reaches its maximum diameter) and the maximum diameter of the fireball based on the FLACS LH_2 pool fire simulation data. The relationship between the two quantities can be seen to be reasonably linear. In the analysis of hydrocarbon BLEVE fireballs it is typical to assume that the height of the fireball centre above the ground is equal to the maximum diameter ($H_{fb} = D_{max}$). Based upon the relationship shown in Fig. 7.34(c) this would also appear to be a reasonable approximation for the simulated fireballs found for instantaneous LH_2 spill pool fires.

The FLACS-Fire simulation results were also used to estimate the average surface emissive power (SEP) of the fireball and fraction of fireball's total the heat release rate that is radiated.

The incident radiation heat flux (kW/m^2) received at a target (outside the fireball) is given by:

$$q = SEP\ F\ \tau \tag{7.15}$$

Where SEP is the average surface emissive power of the fireball (kW/m^2), F is a geometrical view factor (-) and τ is the transmissivity of the atmosphere between the fireball and the target (-). For a fireball the view factor can be found using:

$$F = \left(\frac{R}{X}\right)^2 \tag{7.16}$$

Where R (= $D_{fb}/2$) is the radius of the (equivalent spherical) fireball (m), and X is the distance of the target from the centre of the fireball (m), which is given by:

$$X = \sqrt{H^2 + a^2} \tag{7.17}$$

Where H is the height of the centre of the fireball above the ground (m), and a is the horizontal distance between the target and the origin of the fireball on the ground (m).

Rearranging Eqn. (7.15) and assuming, as a conservative assumption, that the atmospheric transmissivity, $\tau = 1$, the SEP of the fireball can then be estimated from the radiation heat flux predicted by FLACS-Fire for a target at ground level using:

$$SEP = \frac{q}{F} \tag{7.18}$$

The SEP of the fireball can also be calculated from the predicted heat release rate of the fireball, $\dot{Q}$, (kW) the surface area of the equivalent sphere formed, and the radiation fraction, χ_R the fraction of the combustion heat released that is radiated from the flame surface (-):

$$SEP = \frac{\chi_R \dot{Q}}{4\pi R^2} \tag{7.19}$$

Hence, rearranging Eqn. (7.19) the fireball radiation fraction can be estimated using:

$$\chi_R = SEP / \frac{\dot{Q}}{4\pi R^2} \tag{7.20}$$

Table 7.4 shows the peak SEP and radiation fractions of the fireball (at the maximum diameter) obtained by applying this method to the instantaneous LH_2 spill pool fire data obtained using FLACS-Fire. The estimated peak SEP value calculated for the fireball varies ranges from 199 kW/m^2 to 268 kW/m^2 with an average value of 229 kW/m^2.

Table 7.4 – Peak SEP and radiation fractions of the LH_2 fireball (at the maximum diameter) obtained from instantaneous LH_2 spill pool fires FLACS-Fire simulations.

LH_2 Spill Size (L)	SEP (kW/m^2)	Radiative Fraction
100	199	0.27
318	223	0.21
500	233	0.21
1000	268	0.22
5000	223	0.20
Average	229	0.22

In comparison the study by Arthur D Little [1982] (Table 6.2) suggests that lower values be used for the emissive power of LH_2 spill pool fires, based on the steady turbulent diffusion flames generated by LH_2 pool fires in the range 75–144 kW/m^2 (versus 113 kW/m^2 for gasoline pool fires and 100-220 kW/m^2 for LCH_4 pool fires).

The radiative fraction of the fireball calculated varies from 0.20 to 0.27 with an average value of 0.22. This magnitude of radiative fraction is broadly similar to the upper range of values found in other studies of hydrogen-air flames (see section 2.3).

7.6 Summary

A series of simulations have been carried out using the FLACS-Fire model to simulate the pool fires resulting from instantaneous spills of LH_2 and Jet A, ranging in size from 100 L to 5000 L, to allow a comparison to be made between the behaviour and level of thermal hazard presented by the two different fuel types. The LH_2 spills vaporise rapidly and the ignited hydrogen gas forms a fireball. In comparison the pool fires produced from a Jet A spill burn as a continuously fluctuating fire plume with a lower peak HRR, but which is sustained over a significantly longer period of time. The results suggest that the thermal radiation dose hazardous distances predicted for the LH_2 pool fires are significantly lower than those obtained for an equivalent spill volume of Jet A. The effects of a finite duration and wind and aircraft geometry on pool fire behaviour have also been examined. Using the FLACS-Fire simulation results some correlations for the maximum diameter and burning duration of instantaneous LH_2 spill fireballs have been derived, along with estimates of the magnitude of the fireball's SEP and radiative fraction.

8 Aircraft Refuelling Spills (Delayed Ignition) – Flash Fire & Explosion

Work has been carried out to model the consequences of accidental LH_2 spills occurring during aircraft refuelling operations, in the case of delayed ignition of the resulting hydrogen gas cloud.

Depending upon the hydrogen concentration and the levels of confinement/ congestion the delayed ignition of the flammable gas cloud could result in either a flash fire or explosion:

- *Flash fire* – a relatively slow propagation of flame through the flammable gas cloud.
- *Explosion* – a rapid flame propagation through the flammable gas cloud and build-up of overpressure, enhanced by any confinement and turbulence generated by any congestion encountered by the travelling flame front.

8.1 Simulation details

In order to examine the effect of aircraft geometry on the hydrogen cloud dispersion and explosion behaviour of a LH_2 spill during refuelling operations a representative LH_2 aircraft geometry based upon a modified LH_2 "Tube and Wing" aircraft design (with a capacity of around 200 passengers), developed for ENABLEH2, were digitised and introduced as a series of primitive geometrical objects (comprised of boxes, cylinders and plates) into FLACS (see Fig 7.25(b)).

The FLACS pool model was used to simulate the dispersion behaviour of the vaporising LH_2 pool and resulting hydrogen cloud produced for a short duration LH_2 leak from an aircraft refuelling line. The baseline refuelling operations leak was characterised as 4.5 kg/s release of LH_2 for a duration of 5 s. As a limiting case to examine the effect of the largest possible LH_2 pool (i.e. a conservative assumption with regard to the formation of the liquid pool and the subsequent dispersion behaviour), it was assumed that all of the LH_2 release was deposited into the LH_2 pool and the effects of flash vaporisation were neglected. Such releases may approximate conditions where LH_2 is stored at low gauge pressures above atmospheric (such as may be the case with LH_2 tanks to be used in aircraft) and there is consequently expected to be a relatively low level of flashing.

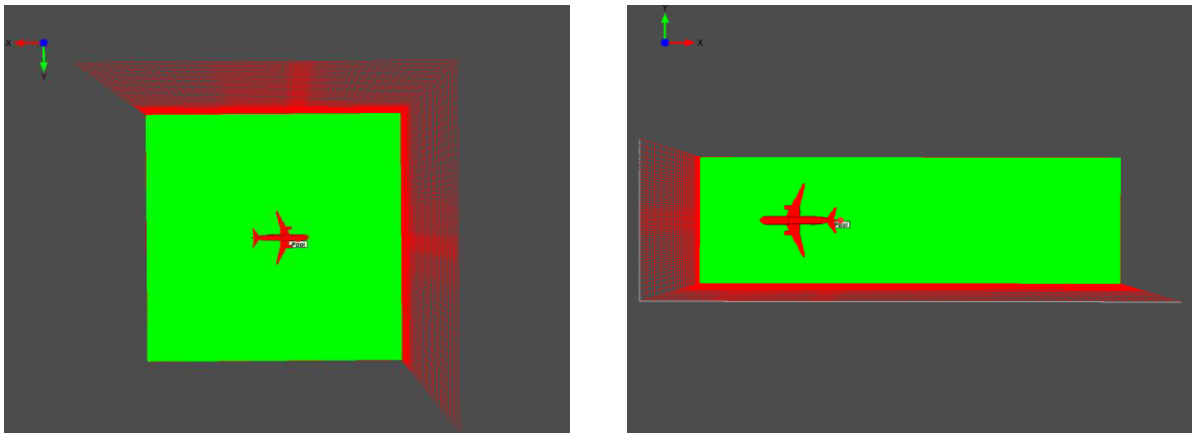

(a) (b)

Fig. 8.1 - Locations of LH_2 fuel spill pool fires used for the LH_2 aircraft: (a) side of aircraft; (b) tail of aircraft.

The effect of different leak locations, wind directions and leak duration upon the resulting flammable cloud was then examined. Two different LH_2 pool leak positions were considered (Fig 8.1). These were located (Fig 8,1(a)) on the right side of the aircraft fuselage towards the front of the aircraft ahead of the wing (X = 7, Y =2, Z = 1), or (Fig 8.1(b)) at the tail of the aircraft (X = 37, Y =0, Z = 1), corresponding to the refuelling position suggested for the LH_2 aircraft design developed by Brewer [1991].

The characteristic wind speed used was set to 2.0 m/s at a height of 10 m. Atmospheric stability was set to Pasquill class F (stable), with a ground surface roughness of 0.03 m. The wind direction used in the baseline simulations was aligned to run along the positive x-axis (wind direction 270°). Alternative wind directions coming from the north (wind direction 0°) moving in the -ve y direction and from the east (wind direction 90° degrees) moving in -ve x direction were also used in some simulations. The following cases were considered (the number in brackets refers to the FLACS run number):

Case A: (000009/001009) 4.5 kg/s LH_2 spill for 5 s located at forward side of aircraft (7,2,1) with 2 m/s wind from west (270 degrees) moving in +ve x direction.

Case B: (000010/001010) 4.5 kg/s LH_2 spill for 5 s located at forward side of aircraft (7,2,1) with 2 m/s wind from north (0 degrees) moving in -ve y direction.

Case C: (000012/001012) 4.5 kg/s LH_2 spill for 5 s located at rear of aircraft (37,0,1) with 2 m/s wind from east (90 degrees) moving in -ve x direction.

Case D: (000017) 4.5 kg/s LH_2 spill for 5 s located at rear of aircraft (37,0,1) with 2 m/s wind from west (270 degrees) moving in +ve x direction.

Leak durations of 5 s, 10s and 20 s were also examined (runs 000012, 000014, 000015).

The FLACS pool model dispersion simulations were performed on a domain 165 m × 160 m × 80 m in the X, Y and Z directions (-60 m to 105 m, -80 m to 80 m, 0 to 80 m). The grid used had a total of 346,752 cells (96 × 84 x 43 cells). In the pool region a grid cell size of 0.5 m was used in the X and Y directions and 0.25 m in the Z direction. Outside this region the grid cell size was increased, by using an expansion factor of 1.2, and setting a maximum grid cell size of 4 m. A modified domain 200 m × 60 m × 40 m in the X, Y and Z directions (-30 m to 170 m, -30 m to 30 m, 0 to 40 m) and grid with a total of 289,080 cells (146 x 60 x 33) was also employed in some simulations of the downwind dispersion of LH_2 released from the tail.

Figure 8.2 shows an example of the simulation domain, geometry and grid used in the LH_2 release dispersion FLACS simulations.

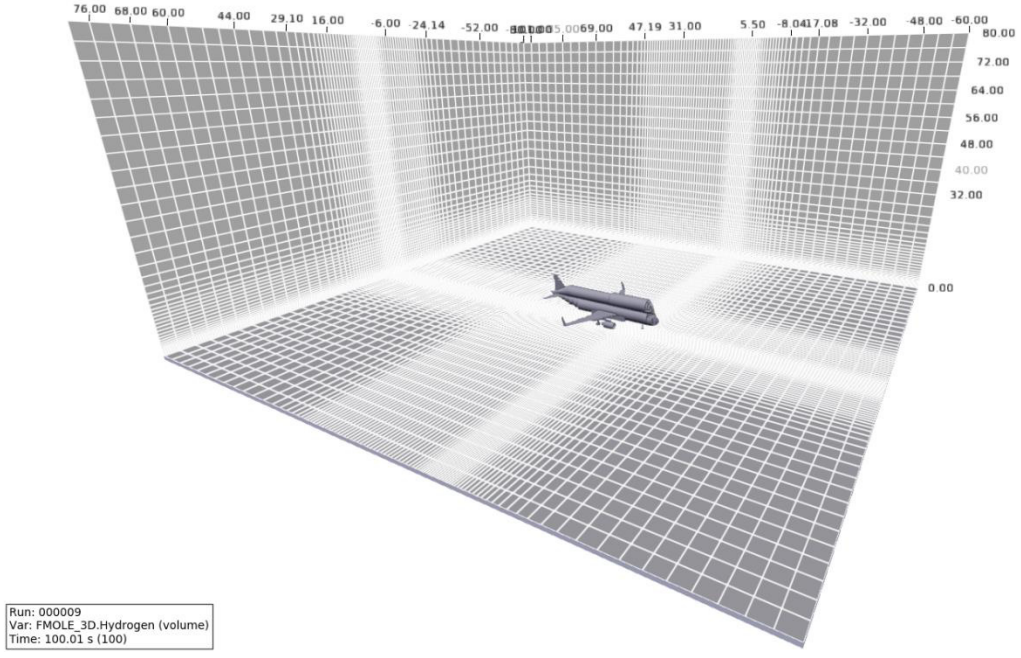

Fig. 8.2 - Example of the simulation domain, geometry and grid used in the LH_2 release dispersion FLACS simulations.

The hazard presented by a flash fire resulting from a delayed ignition of this cloud was characterised in terms of the area/region of the hydrogen cloud found in the dispersion simulations that was above the LFL of hydrogen (assumed to be 4% v/v although this may be different at cryogenic temperatures) or the maximum downwind distance from the spill origin to the LFL boundary of the simulated cloud.

An examination of the explosion hazard presented by different spill cases was also carried out. Two different approaches were used to characterise the explosion hazard represented by the delayed ignition of the flammable hydrogen gas clouds formed. In the first approach the results for the flammable hydrogen cloud obtained from the FLACS dispersion simulations at a suitable instant of time were dumped and converted onto a new grid suitable for explosion simulations. In this case the FLACS Q9 parameter was used as a guide to indicate a suitable time when flammable cloud hazard was at its peak. The FLACS Q9 parameter is a measure of the equivalent stoichiometric hydrogen-air volume representing a particular flammable gas cloud at a given instant of time. Hence it provides a metric for assessing the explosion hazard posed by different release scenarios. In the second approach the peak FLACS Q9 parameter obtained from the dispersion simulations were used to estimate the volume of the equivalent stoichiometric hydrogen-air volume to be used in the explosion simulation.

The FLACS explosion simulations were performed on a domain 165 m × 160 m × 80 m in the X, Y and Z directions (-60 m to 105 m, -80 m to 80 m, 0 to 80 m). A uniform cubical 0.5 m cell size was used in the core region encompassing the flammable cloud/aircraft region (-3 m to 45 m, -17 m to 17 m, 0 to 12 m) in accordance with FLACS user guidelines for an explosion simulation. Outside this region the grid cell size was increased, by using an expansion factor of 1.2, and setting a maximum grid cell size of 4 m, giving a total of 141 x 114 x 49 cells (787,626 cells).

8.2 Dispersion Simulation Results

Fig. 8.3 shows an example of the flammable cloud dispersion behaviour (4% LFL iso-surface) of a short duration 5s spill of LH_2 from a location on the right side of the aircraft parallel to the front wheel, with a wind of 2 m/s running nose to tail (Case A). The dense cryogenic hydrogen released by the vaporising LH_2 pool forms a discrete flammable cloud which is transported by the wind along the right side of the aircraft, moving around the wing and past the end of the tail before dispersing below the LFL.

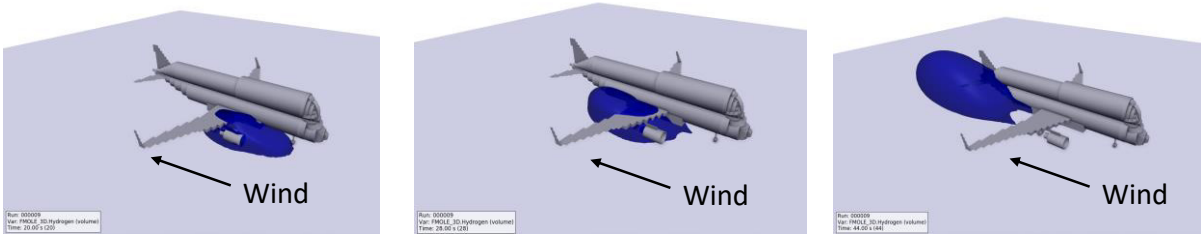

Fig. 8.3 - Dispersion of the hydrogen cloud (4% LFL iso-surface) formed following a 5 s LH_2 fuel spill with a wind 2 m/s running nose to tail (Case A) after: (a) 20 s; (b) 28 s; (c) 44 s.

Fig. 8.4 compares the maximum concentrations for the flammable cloud predicted for Cases A and B (both in 3D and along the X-Y plane at a height of 1 m) with the fuel spill located at the side of the aircraft. Note that these contour plots show the maximum hydrogen concentration produced in a given control volume over the duration of the simulation. Hence, they do not show the hydrogen gas concentration at a particular instant of time, but instead provide a composite of the maximum values over time – indicating any location where the concentration has been greater than 4% v/v. Hence, they demarcate the maximum flammable extent of the gas cloud over the course of the simulation.

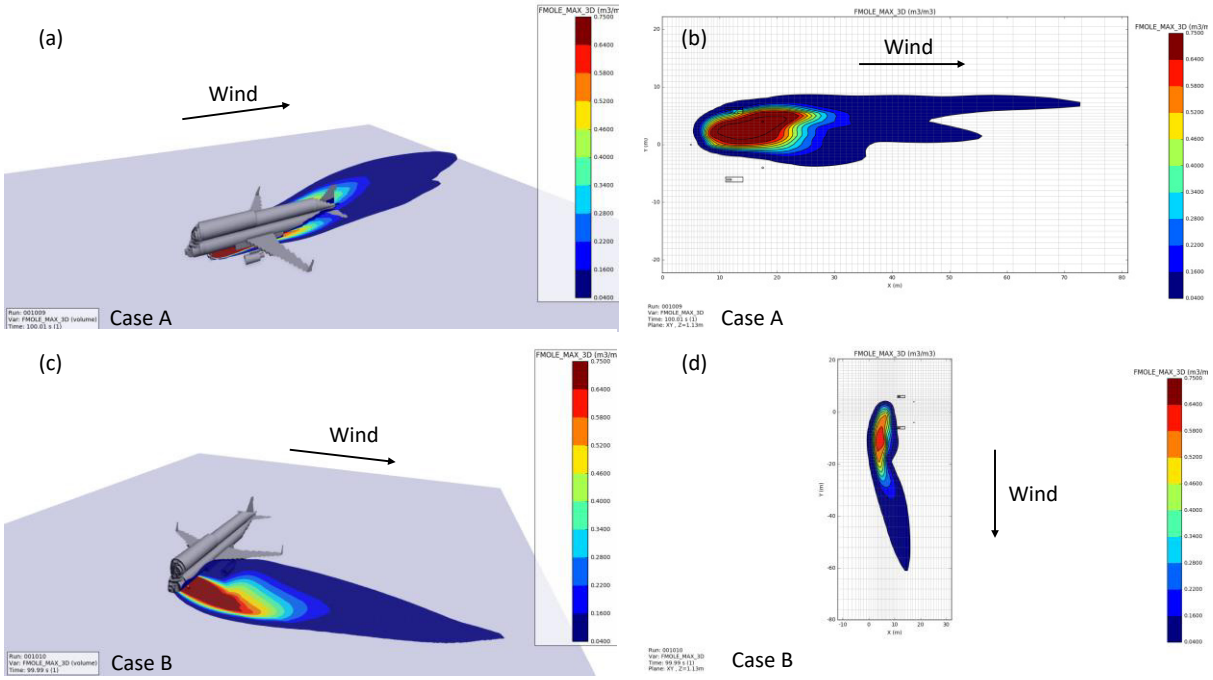

Fig. 8.4 – Maximum concentration of the flammable gas cloud predicted for Case A: (a) 3D; (b) x-y plane at 1 m; and Case B: (c) 3D iso; (d) x-y plane at 1 m.

In Case A, with the wind coming from the west, the max flammable cloud forms a region extending from the spill pool along the right side of the aircraft, beyond the tail, reaching a maximum downwind distance at x = 73 m (at a height of 1 m). In Case B, with the wind coming from the north, the max flammable cloud forms a region extending from the spill pool under the body of the aircraft (from right to left) to reach a maximum downwind distance at y = -61 m (at a height of 1 m).

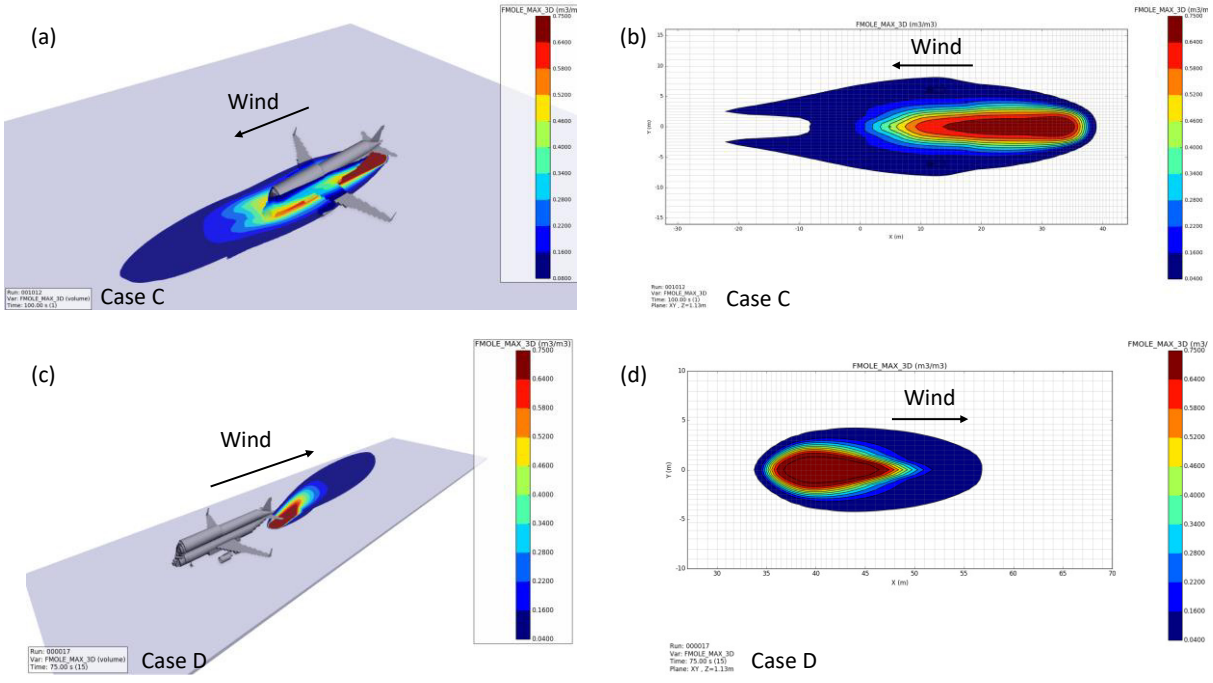

Fig. 8.5 - Maximum concentration of the flammable gas cloud predicted for Case C: (a) 3D; (b) x-y plane at 1 m; and Case D: (c) 3D iso; (d) x-y plane at 1 m.

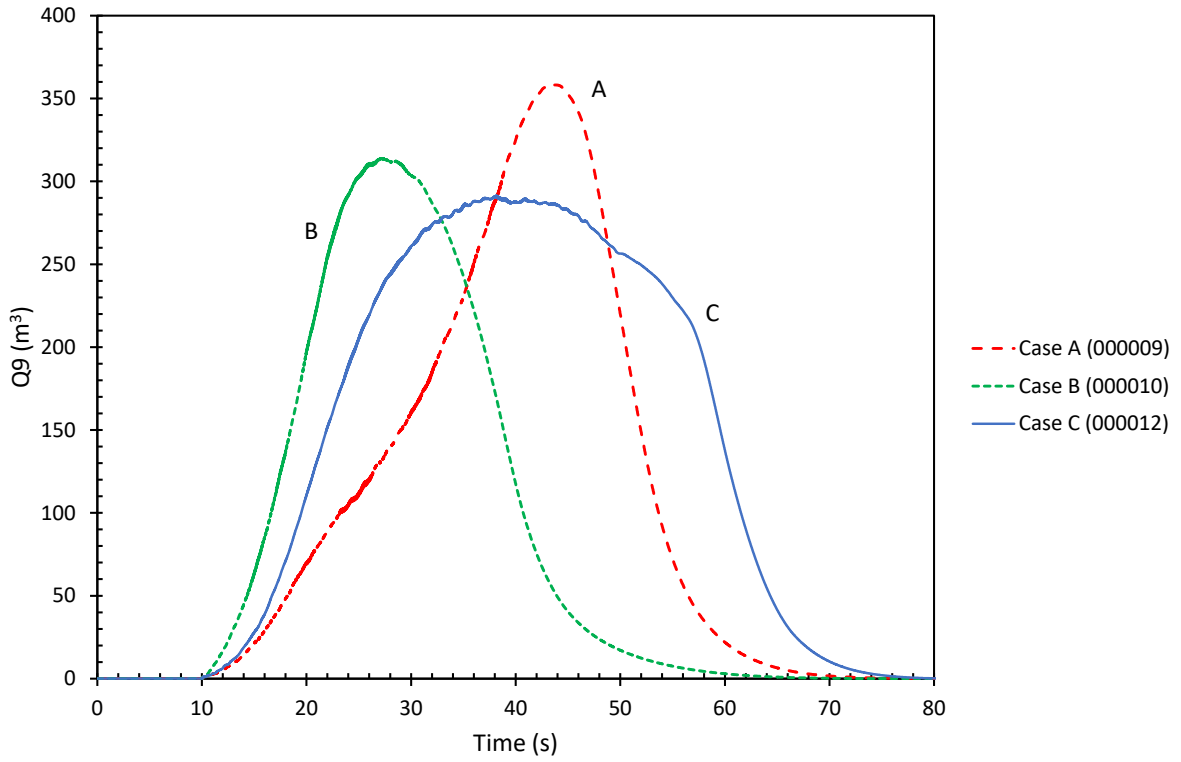

Fig. 8.6 – A comparison between the Q9 equivalent stoichiometric H_2-air volume versus time profiles predicted for Cases A, B and C.

Fig. 8.5 compares the maximum concentrations for the flammable cloud predicted for Cases C and D (both in 3D and along the X-Y plane at a height of 1 m), with the fuel spill located at the tail of the aircraft. In Case C, with the wind coming from the east, the max flammable cloud forms a region extending from the spill pool underneath the length of the aircraft, reaching a maximum downwind distance at x = -22 m (at a height of 1 m). In Case D, with the wind coming from the west, the max flammable cloud forms a region extending from the spill pool at the tail of the aircraft to reach a maximum downwind distance at x =57 m (at a height of 1 m).

A comparison between the Q9 versus time curves predicted for release cases A, B and C is shown in Fig 8.6. All three cases produce roughly similar peak Q9 values in the range 300 – 350 m^3, but take different lengths of time to reach the maximum value. Case A reaches its peak value after 44 s, whereas Case B reaches it maximum value after 28 s, and Case C after 40 s. Although it has a slightly lower peak value, the Q9 curve produced for Case C (with the cloud transported from the tail under the length of the aircraft) has a broader peak - around 30 s wide - than either Cases A or B (which have relatively sharp peaks which are around 10 s in width). This would suggest that Case C has a longer “time-at-risk” of producing a higher explosion overpressure.

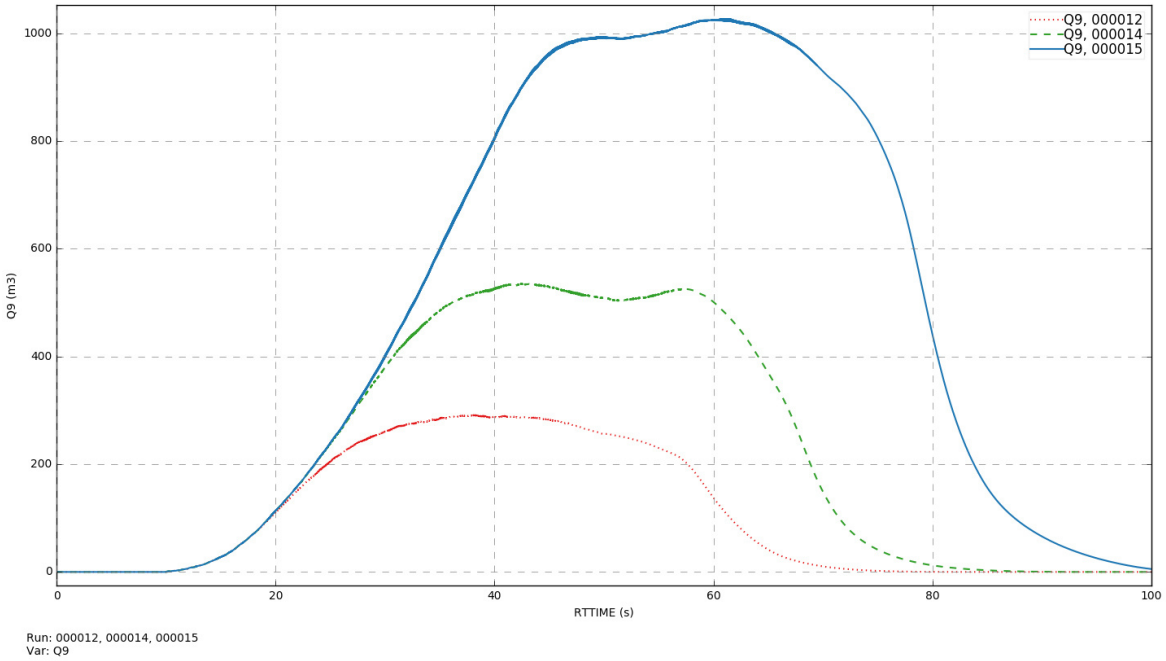

Fig. 8.7 – A comparison between the Q9 versus time profiles produced for different duration LH_2 spills: 5 s (000012); 10 s (000014) and 20 s (000015).

Additional FLACS dispersion simulations were also carried out for Case C, increasing the duration of the LH_2 spill from 5 s, to 10 s and 20 s. Fig 8.7 shows a comparison of the resulting Q9 versus time curves that are obtained. As would be expected the magnitude of the peak increases with the duration of the spill. For a release duration of 10 s the peak increases to around 500 m^3 and for 20 s to around 1000 m^3.

8.3 Explosion Simulation Results

Case Ex-A (Run 120009 - based on restart from 000009 @ 44 s) – ignition of cloud formed towards rear of aircraft

Fig 8.8 shows the results obtained for Case Ex-A, with contour plots (both 3D and X-Y plane at ground level) for the maximum explosion overpressure produced in a given control volume in the domain over the duration of the simulation, for the flammable gas cloud generated for Case A, ignited after 44 s. Ignition of the flammable cloud results in a relatively small explosion overpressure towards the tail of the aircraft. In this case no harmful overpressures (> 0.07 barg) are predicted to occur.

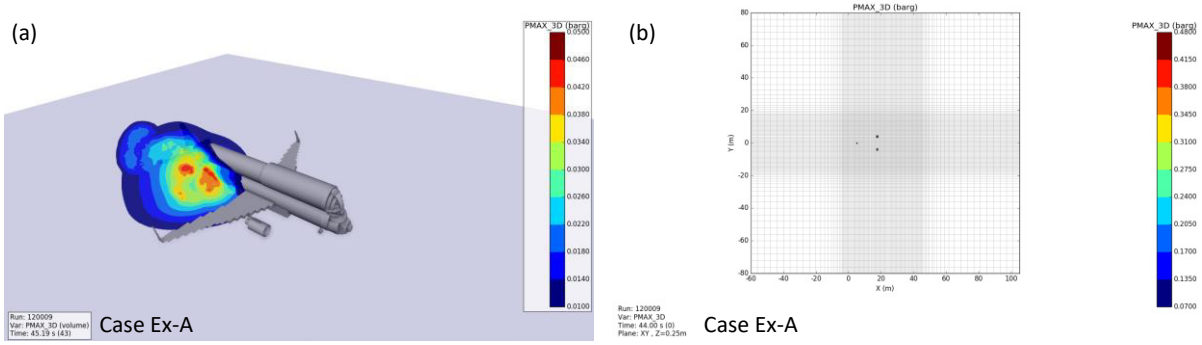

Fig. 8.8 - Maximum explosion overpressures obtained for Case Ex-A: (a) 3D; (b) x-y plane at ground level.

Case Ex-B (Run 110010 - based on restart from 000010 @ 28 s)

Fig 8.9 shows the maximum explosion overpressure results found for Case Ex-B, with the flammable gas cloud generated for Case B, ignited after 28 s. In this case a small region of harmful overpressures (> 0.07 barg) are predicted to occur in and around the left side of the aircraft, where the flammable gas cloud has travelled under the body of the aircraft.

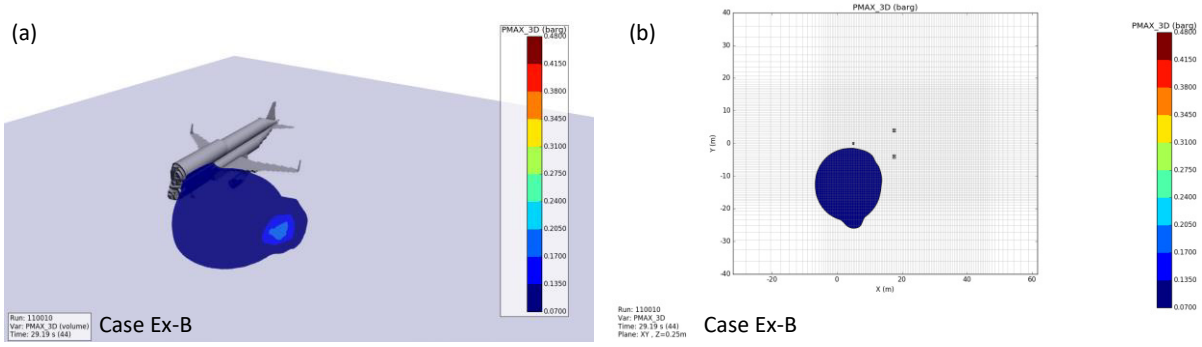

Fig. 8.9 - Maximum explosion overpressures obtained for Case Ex-B: (a) 3D; (b) x-y plane at ground level.

Case Ex-C (Run 100012 - based on restart from 000012 @ 40 s)

The maximum explosion overpressure results generated for Case Ex-C, with the flammable gas cloud found for Case C, ignited after 40 s, are shown in Fig 8.10. In this case a small region of harmful overpressures were also predicted to occur with some relatively high, damaging overpressures (~ 0.3 barg) located close to the body of the aircraft.

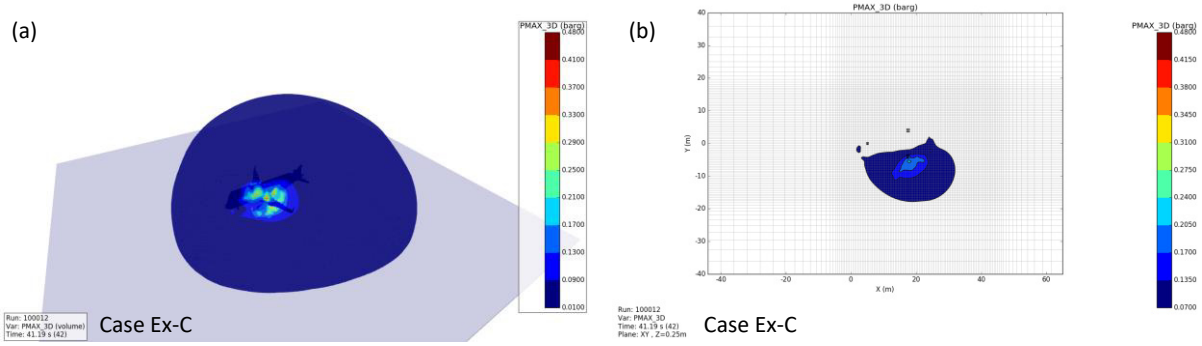

Fig. 8.10 - Maximum explosion overpressures obtained for Case Ex-C: (a) 3D; (b) x-y plane at ground level.

8.3.1 Examine effect of grid sensitivity

Based upon hydrogen cloud dispersion and Q9 results obtained for Case C (Run 000012) with a peak volume of 300 m^3 a stoichiometric hydrogen-air region (15 m x 10 m x 2 m) was introduced under the body of the aircraft, to represent the equivalent flammable cloud, with an ignition source located as shown in Fig 8.11.

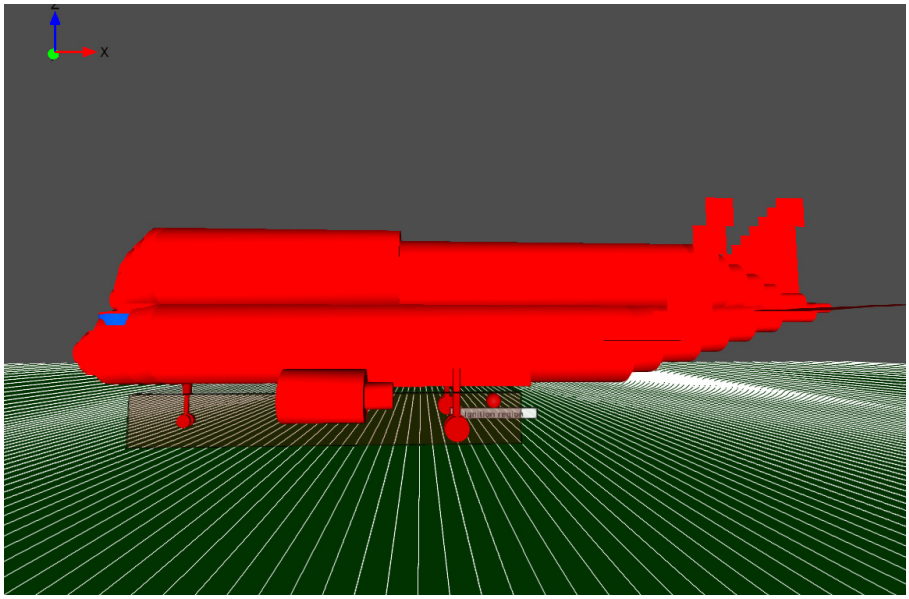

Fig. 8.11 – Location of the stoichiometric hydrogen-air region and ignition point introduced under the body of the aircraft.

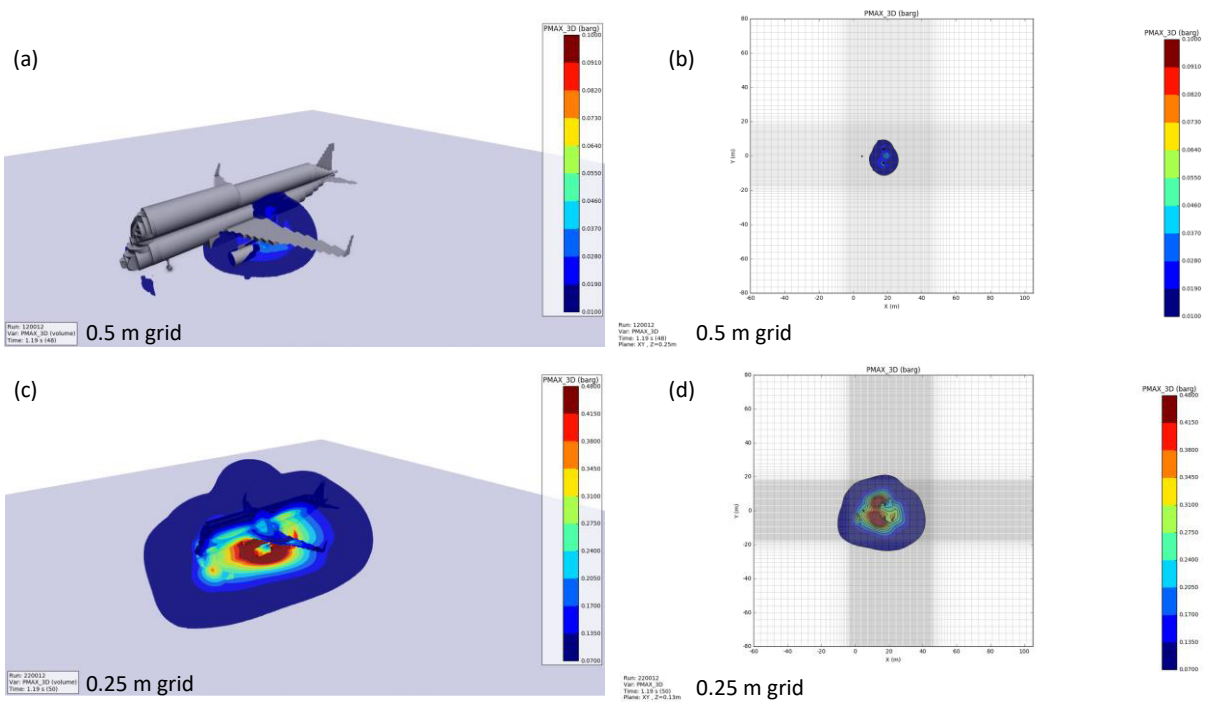

Fig. 8.12 - Comparison between the maximum explosion overpressure results obtained using the 0.5 m grid ((a) and (b)) and 0.25 m grid ((c) and (d)).

A grid sensitivity study was carried out to compare the results obtained using a 0.5 m grid (Run 120012) with a 0.25 m grid (Run 220012) in the core region around the aircraft.

Fig 8.12 shows a comparison between the maximum explosion overpressure results obtained using the two different grid resolutions. It is evident that the results found for the finer grid exhibit significantly higher overpressures over a wider area. A comparison of the overpressures predicted at monitor point MP-1 confirms the large difference in peak overpressures found for the two different grid cases.

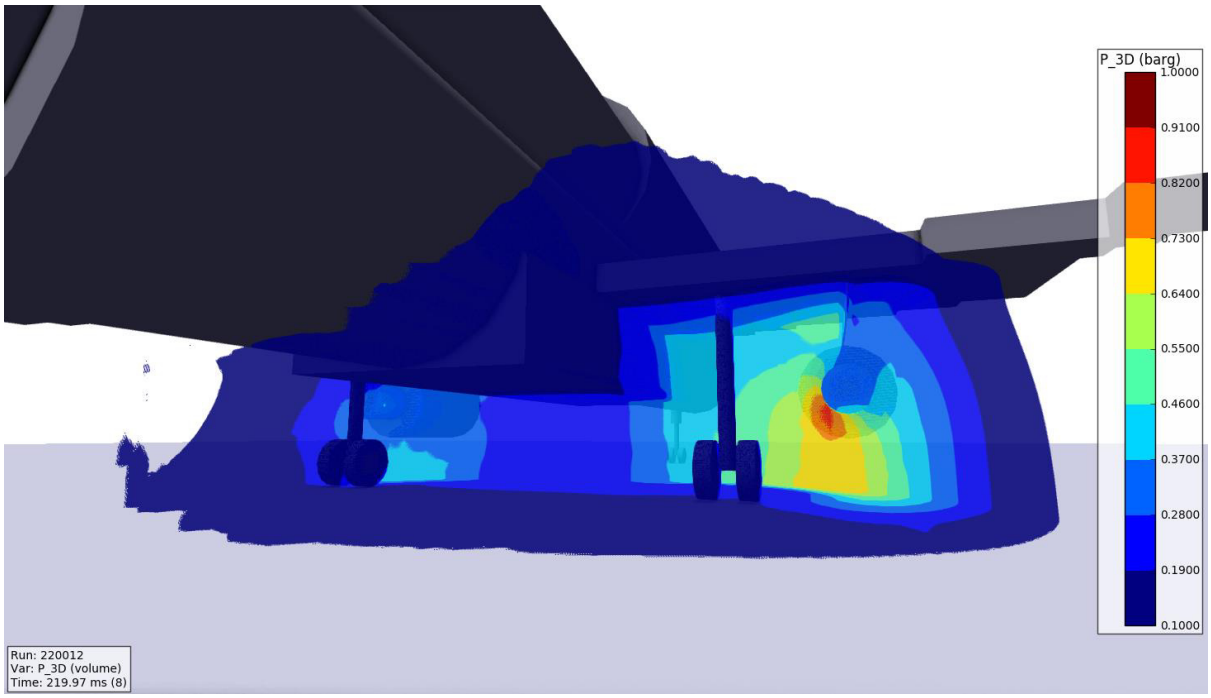

Fig. 8.13 - Explosion overpressure predicted for the 0.25 m cell grid case. A high overpressure region develops under the wing of the aircraft, between the undercarriage and engine.

An examination of the development of the explosion for the finer 0.25 m case (220012) shown Fig 8.13 reveals that, following an ignition, a very high overpressure develops under the wing of the aircraft, between the undercarriage and engine – which does not occur for the 0.5 m grid case.

The reason for this difference can be traced to variations in the representation of the right undercarriage wheel between the two grids and the effect this has on the development of the flame-front (visualised via the concentration of the combustion products). For the 0.5 m grid (120012) case shown in Fig 8.14 the wheel geometry is represented as a solid block within the grid, which does not have a significant effect upon the rate at which the flame front propagates. However, in the case of the finer 0.25 m grid (220012) shown in Fig 8.15 the wheel is represented as a cell porosity region. When the flame front encounters this porosity region it generates sub-grid scale turbulence, resulting in rapid acceleration of the flame (and producing a large change in position of the flame front in a short space of time). Consequently the 0.25 m refined grid (220012) exhibits much higher peak overpressures and over a larger area

The results suggest that for certain explosion simulation cases, involving ignition of hydrogen clouds formed under the body of the aircraft where the results indicated the potential for flame acceleration to occur, due to representation of undercarriage and engine as sub-grid scale porosities which could lead to significantly higher overpressures occurring over a wider area. Further work is required to validate this behaviour.

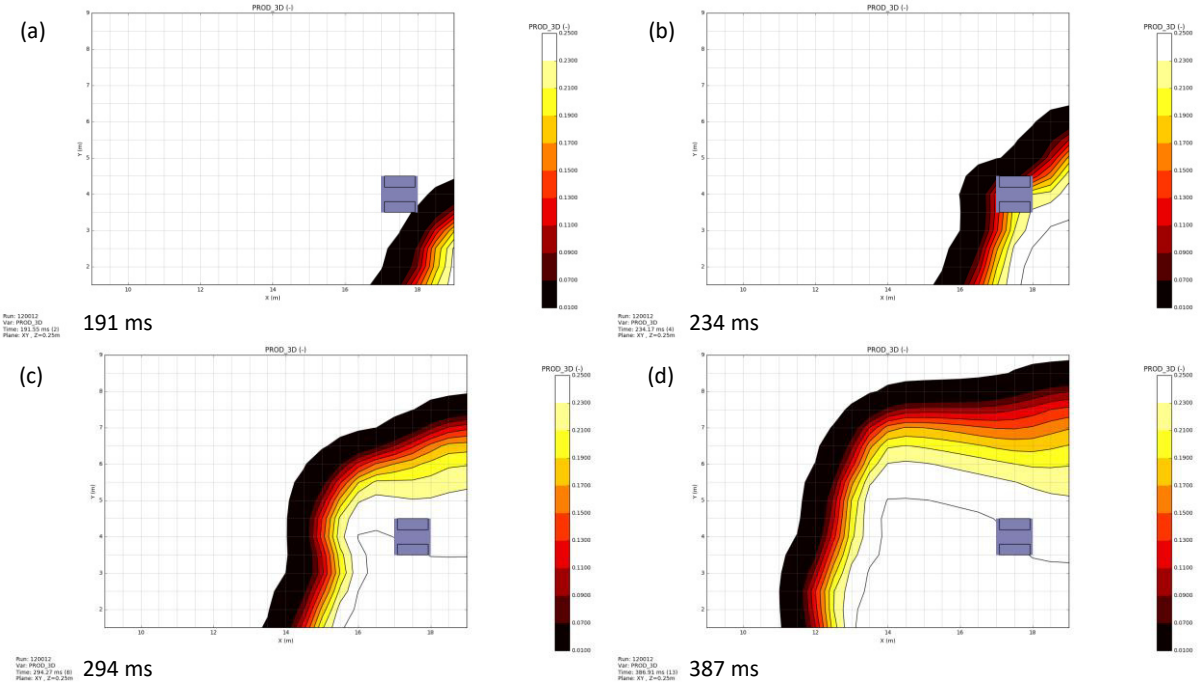

Fig. 8.14 - Development of the flame-front for 0.5 m grid case.

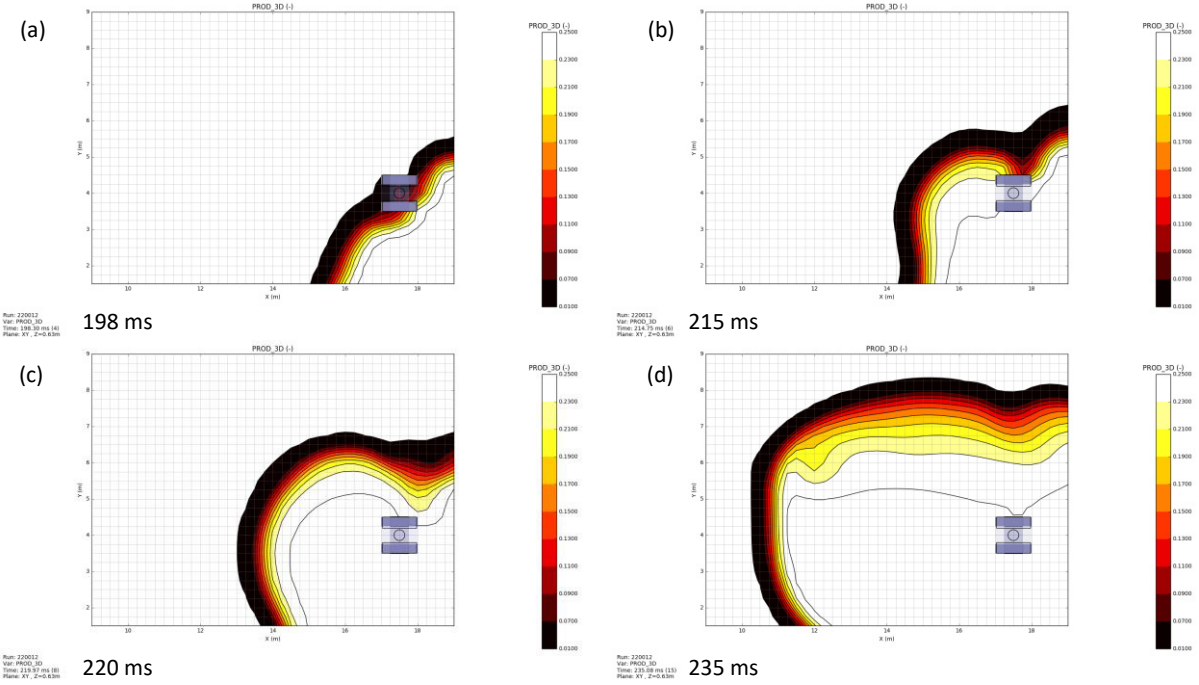

Fig. 8.15 - Development of the flame-front for 0.25 m grid case.

8.4 Summary

Work has been carried out to model the consequences of accidental LH_2 spills occurring during aircraft refuelling operations. In order to examine the effect of aircraft geometry on the flammable cloud dispersion and explosion behaviour of a short duration LH_2 leak during refuelling operations a representative LH_2 aircraft geometry based upon a modified LH_2 "Tube and Wing" short-medium range aircraft design developed for ENABLEH2 (with a capacity of around 200 passengers) was constructed

and introduced into FLACS. The effect of different leak locations, wind directions and leak duration upon the resulting flammable cloud were examined. A delayed ignition source was also introduced to allow the explosion overpressure resulting from ignition of the flammable clouds produced for different scenarios to be predicted.

The results suggest that use of LH_2 fuel and associated dense gas cloud dispersion behaviour will introduce additional hazards not found with Jet A that will need to be carefully managed and mitigated due to the extent of flammable gas cloud that can be formed and potential for associated flash fire and explosion hazards – particularly if wind direction could transport the cloud under the body of the aircraft where it could be partially confined or to the left side region of the aircraft where passengers typically de-plane from current Jet A fuelled aircraft.

The assumed LH_2 fuel leak rate of 4.5 kg/s for refuelling operations accident (based upon that required to fill the aircraft LH_2 tank in the same time as an equivalent energy Jet A aircraft) may also be highly conservative. Hansen [2020] observes that the release rate from the 1" (25 mm) fuel line supplied at 1 barg used in the HSL horizontal free jet release test (Test 7) [Royle and Willoughby, 2014] should theoretically be around 1.9 kg/s, but in practice was found to be only 1 l/s (0.07 kg/s). Friction pressure losses in the fuel supply line can account for only part of this reduction with the rest being attributed to flashing of LH_2 to vapour in the fuel line before it reaches the rupture outlet. Hence the actual LH_2 leak rate from a ruptured fuel line may be self-limited by flashing of LH_2 to vapour and be significantly lower than the (single-phase) flowrate of LH_2 that flows in an operational line.

9 Continuous Fuel Spill Pool Fires

9.1 Comparison between pool fires for continuous releases of LH_2 and Jet A

FLACS-Fire simulations were also performed for continuous releases of LH_2 and Jet A for several different fuel leak scenarios to allow the behaviour of the resulting pool fires to be compared.

The maximum radius of the spill pool formed for a continuous fuel leak was estimated by assuming it was approximately steady state and using:

$$R_{max} = \left(\frac{\dot{m}_{leak}}{\pi \, \dot{m}''_{vap}}\right)^{1/2} \tag{9.1}$$

For LH_2 an effective mass vaporisation rate per unit area value, $\dot{m}''_{vap}$, of 0.15 kg/m^2/s was assumed [Hankinson and Lowesmith, 2013], whilst an $\dot{m}''_{vap}$ of 0.063 kg/m^2/s (based upon test data for kerosene) was used for Jet A [Ahmadi, 2019]. In order to obtain the mass flow rate of the leak, $\dot{m}_{leak}$ (kg/s), the following fuel leak scenarios were considered:

9.1.1 Aircraft engine fuel leak (CP-1)

The aircraft engine fuel leaks examined were based upon the accident scenarios described in the report by Arthur D Little [1982]. For a loss of engine pod (severed fuel line at engine) aircraft accident scenario, continuous mass flow rates, $\dot{m}_{leak}$, of 0.6 kg/s (1.3 lb/s) and 9.0 kg/s (20 lb/s) were used for the LH_2 and Jet A leaks respectively. It was assumed that booster pumps deliver fuel from the tank to the engine and continue to run after the accident. For LH_2 it was assumed that the leak was driven by a fuel pump operating at 0.35 kg/s (0.77 lb/s) through a 2.54 cm (1 inch) diameter fuel line that had an effective length of 91 m (300 ft) between the fuel tank and the engine. For Jet A it was assumed that the fuel booster pump was located in the wing tank and connected to the engine via a 3.81 cm (1.5”) diameter fuel line.

9.1.2 50 mm and 100 mm hole in an aircraft fuel tank (CP-2 and CP-3)

In the case of LNG storage tanks Woodward and Pitblado [2010, pg. 55] suggest that 50 mm and 100 mm diameter holes would respectively represent “serious” and “very serious” fuel leak scenarios that could potentially occur during the lifetime of a plant. These hole sizes have also been adopted for the aircraft fuel leak scenarios considered here to examine the challenge that would be posed by the resulting continuous fuel spills and pool fires for LH_2 and Jet A.

To calculate the mass flow of liquid leaking through a hole in a vessel the following expression was used [Assael and Kakosimos, 2010, pg. 53]:

$$\dot{m}_{leak} = C_d \left(\frac{\pi d_h^2}{4}\right) \sqrt{2\rho_l (P_v + \rho_l g h - P_a)} \tag{9.2}$$

Where C_d is the discharge coefficient (-), assumed to be 0.6, d_h is the diameter of the hole (m), ρ_l is the density of the liquid (kg/m^3), P_v is the pressure exerted on the liquid’s surface inside the vessel (Pa), g

is gravitational acceleration (m/s^2), h is the height of the liquid above the hole (m), and P_a is the ambient atmospheric pressure (Pa).

For leaks from the aircraft fuel tank involving LH_2, a fuel tank operating pressure, P_v of 1.45 bara was assumed [Brewer, 1991] giving an associated LH_2 temperature of 21.65 K and liquid density of 69.33 kg/m^3 (calculated using NIST RefProp for hydrogen and assuming saturation conditions). In this case the leak rate is dominated by the tank pressure - the head of liquid makes only a very minor difference and so was neglected from calculation. However, in the case of Jet A aircraft the fuel tank (located in the wing) is at atmospheric pressure and the leak rate is determined by the head of liquid for which a height of 1 m was assumed.

9.1.3 100 mm hole in a ground fuel storage tank (CP-4)

For the ground storage tank accident scenario a 100 mm hole producing a “very serious” fuel leak has aslo been used. The LH_2 ground storage tank operating pressure is assumed to be 3.0 bara, giving an associated temperature of 24.68 K and liquid density of 65.19 kg/m^3 (from NIST RefProp). In the case of Jet A the tank is at atmospheric pressure. In both cases the hole is assumed to be located at the bottom of the storage tanks and the head of liquid is assumed to be 10 m. The respective flow rates are then calculated using Eqn. (9.2).

Table 9.1 summarises the leak mass flow rate and maximum pool radius used to characterise each of the continuous pool fire case scenarios examined. It is evident that the leak mass flow rates calculated are significantly lower for LH_2 than Jet A. As a consequence of this and the higher mass vaporisation rate per unit area, the continuous LH_2 pool fires have a higher maximum radius.

Table 9.1 – Summary of the continuous fuel leak pool fire scenario conditions examined.

Case	Scenario	Fuel	P_v (bara)	ρ_l (kg/m^3)	$\dot{m}_{leak}$ (kg/s)	$\dot{m}''_{vap}$ (kg/m^2/s)	R_{max} (m)
CP-1	Engine Fuel Leak (0.6 kg/s)	LH_2	n/a	70.8	0.6	0.150	1.13
	Engine Fuel Leak: (9.0 kg/s)	Jet A	n/a	750	9.0	0.063	6.74
CP-2	50 mm Hole Aircraft Tank	LH_2	1.45	69.3	2.90	0.150	2.48
	50 mm Hole Aircraft Tank	Jet A	1.00	750	3.91	0.063	4.44
CP-3	100 mm Hole Aircraft Tank	LH_2	1.45	69.3	11.60	0.150	4.96
	100 mm Hole Aircraft Tank	Jet A	1.00	750	15.65	0.063	8.89
CP-4	100 mm Hole Storage Tank	LH_2	3.00	65.2	24.37	0.150	7.19
	100 mm Hole Storage Tank	Jet A	1.00	750	49.50	0.063	15.82

Figure 9.1 shows a comparison of the continuous pool fire plumes predicted for the 50 mm hole aircraft leak tank scenarios for LH_2 and Jet A. The continuous LH_2 leak produces a taller fire plume than for Jet A, but the radiation heat flux level exceeding 5 kW/m^2 incident on the ground is restricted to a smaller region around the LH_2 fire.

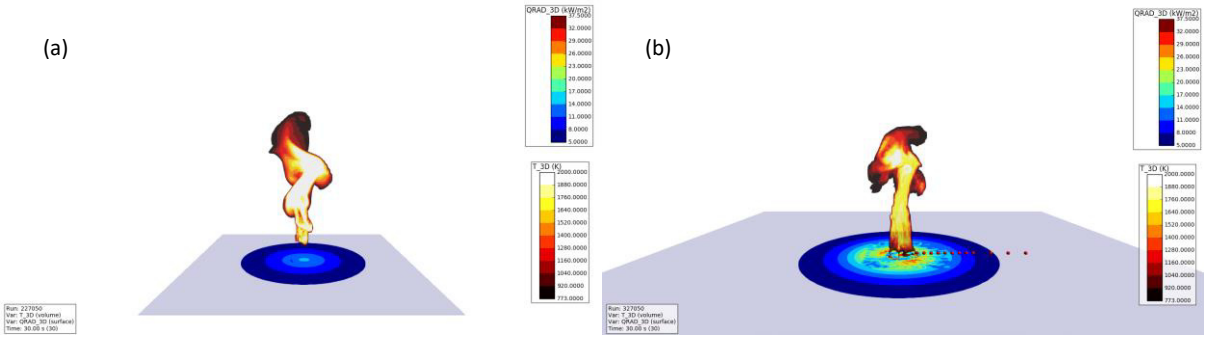

Fig. 9.1 - Comparison of the continuous pool fire plumes predicted for the 50 mm hole aircraft leak tank scenarios for: (a) LH_2; (b) Jet A.

Table 9.2 summarises the hazardous distance, based upon thermal radiation dose (over 30 seconds exposure time), predicted for each of the continuous pool fire leak scenarios (for both LH_2 and Jet A). In all of these cases the hazardous distance to the different thermal dose thresholds considered is predicted to be lower for LH_2 than it is for Jet A. In particular, the hazardous distance to the fatal threshold (1050 TDU) is predicted to be significantly less for the continuous leak scenario LH_2 pool fires considered.

Table 9.2 - Hazardous distance, for different thermal radiation dose levels, predicted for each of the continuous pool fire leak scenarios for both LH_2 and Jet A.

Case	Scenario	Fuel	Rmax	Hazardous Distance (m)			
			(m)	100 TDU	240 TDU	420 TDU	1050 TDU
CP-1	Engine Fuel Leak (0.6 kg/s)	LH_2	1.13	13.6	7.4	4.5	1.1*
	Engine Fuel Leak: (9.0 kg/s)	Jet A	6.74	47.4	32.7	25.4	16.0
CP-2	50 mm Hole Aircraft Tank	LH_2	2.48	> 20	18.3	12.7	4.7
	50 mm Hole Aircraft Tank	Jet A	4.44	28.4	19.7	14.7	8.6
CP-3	100 mm Hole Aircraft Tank	LH_2	4.96	> 40	33.7	23.7	10.6
	100 mm Hole Aircraft Tank	Jet A	8.89	> 56	43.1	33.5	21.4
CP-4	100 mm Hole Storage Tank	LH_2	7.19	> 50	39.7	29.5	10.8
	100 mm Hole Storage Tank	Jet A	15.82	100.9	69.9	54.9	35.5

*In cases where the thermal dose threshold has not been exceeded the hazardous distance has been set equal to the pool fire radius

9.2 Airport storage tank pool fire scenario

FLACS-FIRE simulations were carried out to model an airport fuel storage tank pool fire scenario – again comparing LH_2 with Jet A. An arrangement of three cylindrical fuel storage tanks was considered (each diameter 20 m, height 10 m). Each tank was surrounded by a 50 m x 50 m bund wall which was 2m high. In this scenario one of the storage tanks is assumed to have undergone a catastrophic

containment failure resulting in a release of its entire contents into the surrounding bund which is ignited to produce a constrained 50 m diameter pool fire.

The simulations were performed on a domain -100 m to 200 m, -100 m to 100 m and 0 to 500 m in the X, Y and Z directions. (Fig. 9.2) The "standard" grid employed had a total of 617,120 cells (70 x 58 x 152 cells). A 2.5 m uniform grid cell size was used in core the region (-35 m to 70 m, -50 m to 50m, 0 to 250 m) around the pool fire area which was centred on the origin. The size of the core region in the XY plane was chosen so that it would contain the pool formed in the bund of the first tank. Outside of the core region the grid cell size was stretched, by using an expansion factor of 1.2, and setting a maximum cell size of 10 m in the X and Y directions and 5 m in the Z direction.

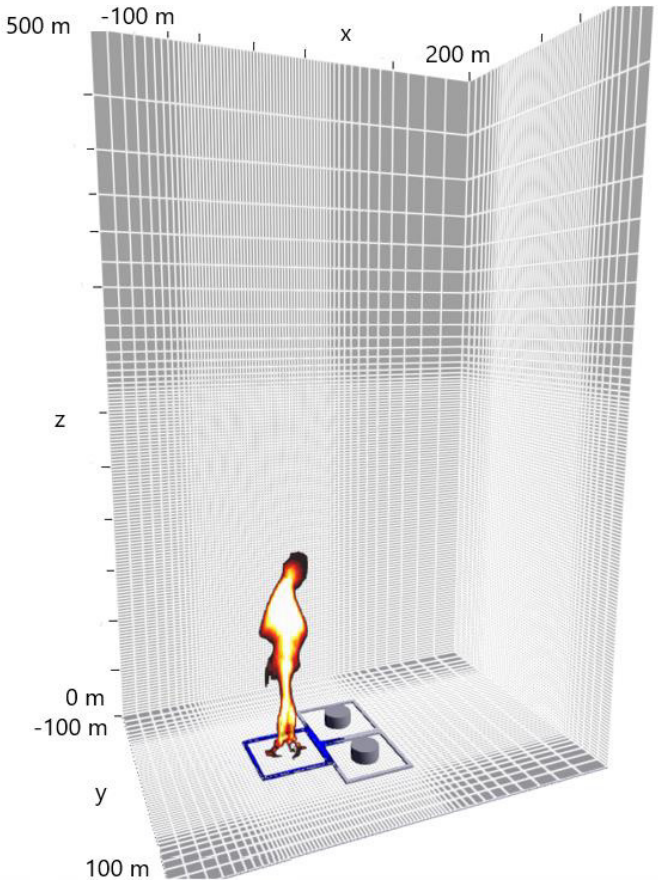

Fig. 9.2 – The domain and grid used in the FLACS-Fire airport fuel storage tank pool fire simulations.

9.2.1 Results

The LH_2 pool storage tank fire, shown in Fig. 9.3, initially produces a fireball (Fig 9.3(a-b)) with high radiation flux levels spread over a wide area, including the adjacent tanks, for a short period of time. It then transforms into a continuous, very tall flame height (~250m) burning fire (Fig 9.3(c-d)), with associated radiation flux delivered over a narrower ground area, broadly corresponding to the region of the failed tank's bund and with flux levels > 5 kW/m^2 no longer reaching to the adjacent storage tanks. In comparison, the Jet A pool fire, shown in Fig. 9.4, has a smaller flame height, burning with a continuously fluctuating plume, but delivers significant radiation levels > 5 kW/m^2 over the exposed surfaces of the adjacent storage tanks for the duration of the simulation.

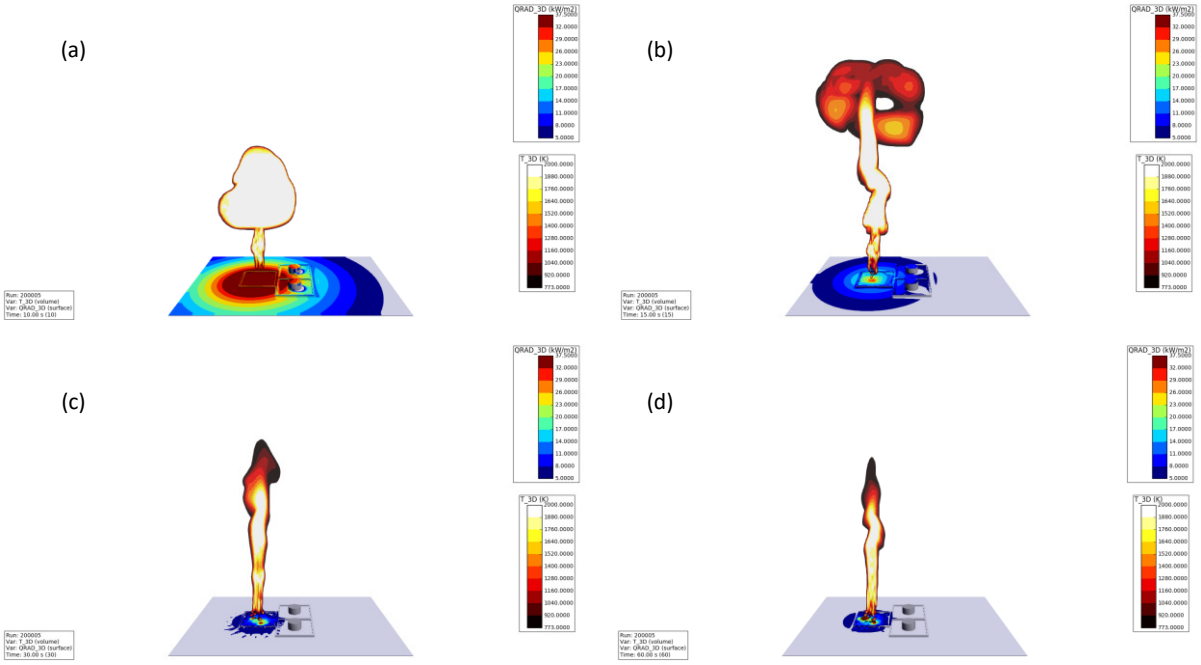

Fig. 9.3 - Development of the LH_2 airport storage tank pool fire: (a) 10 s; (b) 15 s; (c) 30 s (d) 60 s.

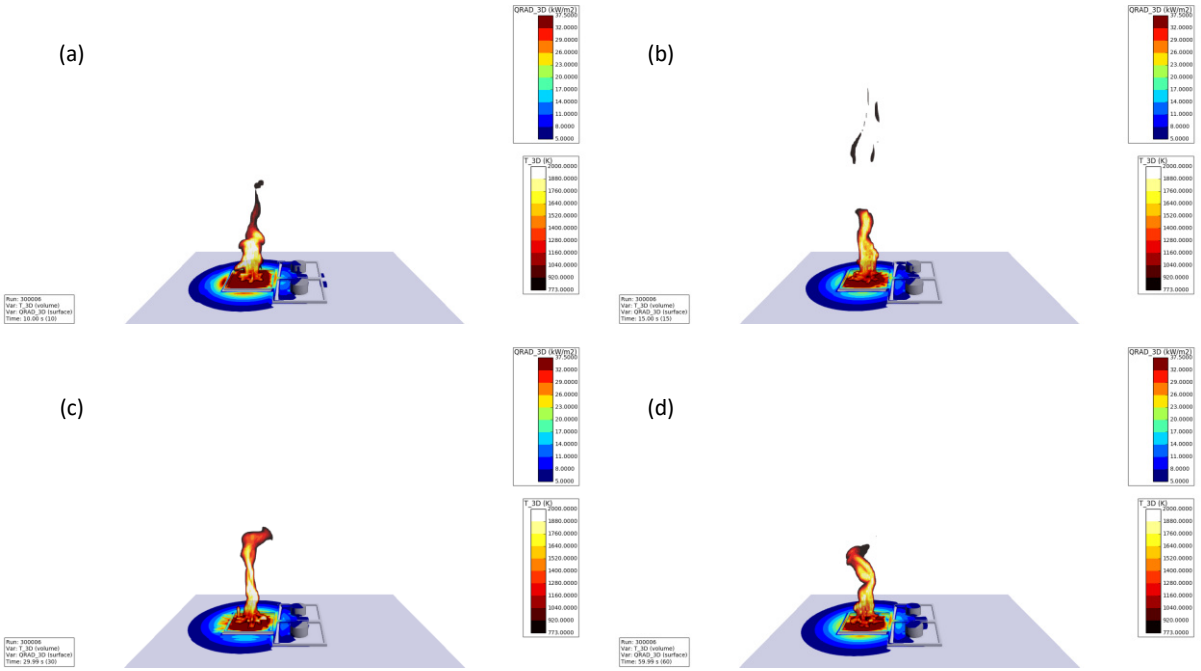

Fig. 9.4 - Development of the Jet A airport storage tank pool fire: (a) 10 s; (b) 15 s; (c) 30 s (d) 60 s.

9.3 Summary

FLACS-Fire simulations were performed for continuous releases of LH_2 and Jet A for several different fuel leak scenarios to allow the behaviour of the resulting pool fires to be compared. A continuous LH_2 leak produces a pool fire with a continuous burning flame plume that is taller than that predicted for an

equivalent size Jet A leak, but the size of the predicted hazardous thermal radiation distance and radiation heat flux level region exceeding 5 kW/m^2 incident on the ground is smaller.

Simulations were also carried out to model an airport fuel storage tank pool fire scenario with cylindrical fuel storage tanks (diameter 20 m, height 10 m) with each tank surrounded by a 50 m x 50 m bund wall which was 2 m high. The LH_2 pool fire was predicted to initially produce a fireball with high radiation flux levels spread over a wide area, before transforming into a continuous, very tall flame height (~250m) fire with flux levels > 5 kW/m^2 no longer reaching to the adjacent storage tanks. In comparison, the Jet A pool fire was predicted to produce a smaller flame height but delivered significant radiation levels > 5 kW/m^2 over the exposed surfaces of the adjacent storage tanks.

10 Discussion

10.1 Model validation

There is currently a lack of medium and large-scale experimental test data for LH_2 hazards with which to test and validate the performance of model predictions. This situation is particularly acute for LH_2 pool fires, where the available test data is extremely limited (not only at large-scale but also at medium and small scales). Since pool fires are regarded as one of the main hazard consequences of an LH_2 release from an aircraft or airport tank storage accident, large scale experimental LH_2 pool fire tests are urgently required to allow for model validation and to improve confidence in their predictions. Radiation flux measurements observed at different distances from a LH_2 pool fire (both instantaneous spills and continuous leaks) would be particularly valuable. Large-scale experimental test data is also required to further validate the dense flammable gas cloud behaviour predicted by the model.

10.2 Modelling limitations and uncertainties

There is at present significant uncertainty surrounding the modelling of LH_2 accident scenarios, particularly LH_2 pool fires, due to the lack of medium and large-scale experimental test data with which to validate the models with. The modelling predictions made in this study must therefore be treated with a degree of caution given these difficulties over validation - particularly with regard to the radiation heat flux from LH_2 pool fires.

In view of the challenges over validation, the FLACS-CFD modelling studies carried out here have a number of limitations which may call into question the fidelity of the predictions made for accidental LH_2 spills and hazards and which will act as additional sources of uncertainty to the results obtained:

Equation of State for Cryogenic Gases: FLACS currently employs the ideal gas law as the equation of state used for physical property calculations. However, in order to accurately represent the extremely cold, cryogenic, conditions associated with liquid hydrogen releases, a special equation of state (EoS) which can account for non-ideal gas behaviour exhibited at cryogenic temperatures, such as the one developed by Leachman et al. [2009] is required for physical property calculations.

Direct heating of cloud by the ground: The FLACS pool model does not include direct heating of the gas cloud by the ground – outside of the LH_2 pool region - which might be expected to increase the buoyancy of the cloud in contact with ground and hence reduce the hazardous distance of the cloud along the ground.

LFL for cold hydrogen mixtures: The 4% LFL Lower Flammability limit found at NTP has been assumed – but this may be modified for cold temperature hydrogen releases.

Two phase flow behaviour: The FLACS pool model does not directly represent the two-phase (liquid-gas) behaviour of liquid hydrogen releases. The FLACS HEM (Homogeneous Equilibrium Model) was developed to improve predictions of two-phase release behaviour but currently does not work for hydrogen.

Neglecting the effect of condensed water vapour fog, oxygen and nitrogen from the atmosphere: The gas cloud formed by the vaporising LH_2 is extremely cold (20K) upon release, causing water vapour in the atmosphere to condense into water vapour (at its dew point) when in come into contact with hydrogen cloud. The latent heat released during phase change from gas vapour to liquid, will heat the hydrogen gas cloud, increasing its temperature and reducing it density – hence enhancing its buoyancy and level of dispersion.

The effect of atmospheric water vapour on hydrogen flames: The far-field radiation model used in FLACS-Fire uses a radiation transmissivity model derived for a hydrocarbon flame (soot with black body/grey body radiation). This neglects the enhanced effect of atmospheric water vapour on reducing the radiation transmissivity for hydrogen flames. There is some evidence to suggest

that the far-field radiation flux received at a target predicted by FLACS-FIRE for a hydrogen flame will tend to be conservative. The comparison made with the experimental results of Zabetakis and Burgess presented 7.2 suggests that the incident radiation flux at a distant sensor is significantly overpredicted. However, the experimental data is extremely limited and so this result should be treated with caution.

Reduction in radiative heat fraction. FLACS-FIRE does not have a user setting for adjusting the radiative fraction of the flame being modelled. Studies of large hydrocarbon pool fires have shown that the radiation from a large pool fire flame can be very effectively shrouded by the cold soot at the edge of the fire region significantly reducing the fraction of heat that is radiated. Consequently it is expected that FLACS-FIRE will over-estimate the far-field radiation heat flux incident on targets for large Jet A pool fires.

10.3 Comparison of hazardous distance for different aircraft/airport accident scenarios

Table 10.1 presents a comparison of the hazardous distances estimated for different aircraft and airport accident scenarios involving releases of LH_2 or Jet A.

The accident scenarios considered are:

- An instantaneous spill of fuel during aircraft refuelling operations resulting in a pool fire (both LH_2 and Jet A), flammable gas cloud/flash fire/explosion or jet fire (LH_2 only)
- Venting of excess hydrogen from the aircraft tail resulting in a flammable jet plume or jet fire (LH_2 only)
- A serious aircraft crash resulting in an instantaneous spill of the entire fuel tank contents and pool fire (both LH_2 and Jet A)
- A severed engine fuel line (diameter 25 mm) resulting in a continuous fuel leak and pool fire (both LH_2 and Jet A), flammable jet plume or jet fire (LH_2 only)
- A serious (50 mm diameter hole) or very serious (100 mm diameter hole) continuous leak from an aircraft fuel tank or airport storage tank resulting in a pool fire (both LH_2 and Jet A), flammable gas cloud/plume or jet fire (LH_2 only)
- An aircraft fuel tank or airport storage tank BLEVE resulting in a fireball involving the entire fuel load (LH_2 only)

The results for LH_2 and Jet A pool fire hazards are taken from tables (Chapters 7 and 9). The hazardous distance values for flammable gas cloud/flash fire/explosion hazards occurring during aircraft refuelling operations are based on the results of Chapter 8. The hazardous distances for the flammable gas clouds generated for continuous fuel leaks was estimated using correlation Eqn. (4.1) The hazardous distances for the jet plume and jet fire hazards resulting from LH_2 leaks have been estimated using HyRAM (see Section 3.6). The tank BLEVE fireball hazard for a given release mass has been estimated using the fireball diameter and duration correlations derived in section 7.5 along with expressions for the view factor for a fireball, radiation heat flux and radiation heat dose and the value estimated for the SEP = 229 kW/m^2. Suitable harm criteria (also given in table 10.1) were applied for each type of hazard to determine the distance at which an injury might occur.

Given the difficulties with validation and associated level of uncertainty over the predicted results the aim of the analysis here is to observe general trends and make relative comparisons between the LH_2 hazards resulting from different accident scenarios and the behaviour of LH_2 versus Jet A.

It is evident from table 10.1 that the hazardous distance due to thermal radiation dose from a pool fire is predicted to be significantly less for LH_2 than is the case for Jet A. This is primarily due to the much shorter vaporization and burning time of the LH_2 pool fire, along with the lower radiation fraction. However, LH_2 spills also present additional safety hazards not exhibited by Jet A in the form of the flammable gas cloud formed and the potential for a flash fire, jet fire, explosion or BLEVE to occur. Jet A, being a relatively high flash point fuel, would not be expected to form a vapour cloud at all (a small cloud could conceivably form with Jet A due to break up of the fuel into a fine mist, but otherwise would require heating to well above its flash point). In this respect hydrogen will always be worse than Jet A.

Table 10.1 – A comparison of the hazardous distances estimated for different aircraft and airport accident release scenarios involving LH_2 or Jet A.

Case	Initiating event	Spill/leak scenario	Ignition type	Hazard type	Harm criteria	Hazardous distance (m)	
						LH_2	Jet A
IC-1	Aircraft refuelling spill 50 mm hose rupture	4.5 kg/s for 5 s pool	Delayed	Flammable cloud	4% LFL	73 m	n/a
			Delayed	Explosion o/p	0.07 barg	20 m	n/a
IP-1		100 L pool	Immediate	Pool fire	240 TDU	2 m	12 m
IP-2		500 L pool	Immediate	Pool fire	240 TDU	9 m	27 m
IP-3		1000 L pool	Immediate	Pool fire	240 TDU	13 m	44 m
IP-4		5000 L pool	Immediate	Pool fire	240 TDU	27 m	78 m
IP-5		4.5 kg/s for 5 s pool	Immediate	Pool fire	240 TDU	6 m	22 m
JP-1		50 mm hose: jet	Delayed	Jet plume	4% LFL	67 m	n/a
JF-1		50 mm hose: jet	Immediate	Jet fire	5 kW/m^2	30 m	n/a
JP-5	Venting aircraft tank 25 mm vent line	25 mm hole: jet	Delayed	Jet plume	4% LFL	30 m$^{(V)}$	n/a
JF-5		25 mm hole: jet	Immediate	Jet fire	5 kW/m^2	6 m	n/a
CP-1	Severed engine fuel line	0.6 kg/s LH_2 pool 9.0 kg/s Jet A pool	Immediate	Pool fire	240 TDU	7 m	33 m
JP-0		25 mm hole: jet	Delayed	Jet plume	4% LFL	35 m	n/a
JF-0		25 mm hole: jet	Immediate	Jet fire	5 kW/m^2	20 m	n/a
CP-3	Aircraft fuel tank leak	100 mm hole: pool	Immediate	Pool fire	240 TDU	34 m	43 m
CC-3		100 mm hole: pool	Delayed	Flammable cloud	4% LFL	244 m	n/a
JP-3		100 mm hole: jet	Delayed	Jet plume	4% LFL	100 m	n/a
JF-3		100 mm hole: jet	Immediate	Jet fire	5 kW/m^2	55 m	n/a
CP-4	Storage tank leak	100 mm hole: pool	Immediate	Pool fire	240 TDU	40 m	70 m
CC-4		100 mm hole: pool	Delayed	Flammable cloud	4% LFL	333 m	n/a
JP-4		100 mm hole: jet	Delayed	Jet plume	4% LFL	100 m	n/a
JF-4		100 mm hole: jet	Immediate	Jet fire	5 kW/m^2	75 m	n/a
BV-1	Aircraft tank BLEVE	5 t (Entire fuel load)	Immediate	Fireball	240 TDU	236 m	n/a
BV-2	Storage tank BLEVE	250 t	Immediate	Fireball	240 TDU	1208 m	n/a

$^{(V)}$ hazardous distance taken vertically rather than horizontally.

The largest hazardous distances in table 10.1 are associated with LH_2 tank BLEVE accident scenarios – particularly the airport storage tank BLEVE, which is predicted to have a hazardous distance of around 1.2 km. Ustolin at al. [2020] have suggested that a much higher SEP value of 1880 kW/m^2 (based upon theoretical radiation calculations) should be used when estimating the hazardous distance associated with an LH_2 tank BLEVE fireball. Using a higher value of the SEP would obviously produce an even greater value for the hazardous distances predicted for the aircraft/airport LH_2 tank BLEVEs than those shown in Table 10.1. Planned experimental LH_2 tank BLEVE tests being carried out as part of the SH2IFT project (Ustolin at al. [2020]) should hopefully help to clarify the magnitude of SEP that it is appropriate to use in such calculations.

Other studies of LH_2 hazards have also found that accident scenarios involving a tank BLEVE would produce the most severe consequences (Hankinson and Lowesmith [2013]). However, tank BLEVEs would also be expected to be highly unlikely events. Given the extremely hazardous consequences predicted for such events, in-depth safety measures (e.g. pressure relief devices, multiple redundant vents etc.) should be required to ensure that this is the indeed the case.

Whilst the hazardous explosion overpressure distance estimated for the refuelling spill scenario (IC-1) is estimated to be broadly similar to the thermal hazard distance predicted for a Jet A pool fire (IP-5), the hazardous distance for the flammable gas cloud/jet plume (4% LFL) and potential flash fire hazard is predicted to be significantly greater (around three times that distance). Hence the results would suggest that the overall hazardous distance for an LH_2 spill during refuelling operations, when also taking into account flammable gas cloud behaviour may be greater than that exhibited by a Jet A spill

and that separation distances (e.g., between re-fuelling aircraft and the terminal building) may need to be extended or the flammable gas cloud/jet plume hazard mitigated in other ways.

The accident scenarios involving serious and very serious continuous leaks of LH_2, from 50 mm and 100 mm holes from aircraft fuel tanks or airport storage tanks, are also estimated to be capable of producing flammable gas clouds with very large hazardous distances of up to several hundred metres. Such serious leaks would be expected to be highly unlikely events. However, if the risk is sufficiently high, measures may still be required to mitigate against their consequences.

It is possible that the greater hazardous distances predicted by FLACS for flammable gas cloud travel along the ground may be overly conservative and being overpredicted. This could reflect limitations in the modelling approach employed in the FLACS pool model (e.g. by using the Ideal Gas Equation as the Equation of State to model a cryogenic gas cloud and/or by neglecting the effect of heat transfer to the cloud from condensing atmospheric water vapour and the ground outside the pool region). However, in a recent research paper Hansen [2020] has also suggested that liquid hydrogen releases exhibit dense gas behaviour and found that the hazardous distance for an LH_2 release can be significantly longer than for other gases exhibiting dense gas behaviour, such as LNG. The NASA WSTF tests also suggested that the hydrogen gas clouds could travel significant distances along the ground under certain conditions.

The 4% LFL threshold adopted as a harm criterion here might also be overly onerous, for the hazardous distance and a higher limit threshold (e.g. 8% v/v hydrogen – the limit for flame propagation in all directions) might be more appropriate. In the case of the transient releases considered, it may also the case that the flammable volume/mass of the cloud at the maximum downwind extent is too small to pose a significant hazard if ignited and that it would be more representative to consider the cloud at an earlier time where it has a larger flammable volume/mass (and has a shorter hazardous extent). Additional model development and comparisons and validation against suitable experimental data are therefore required to further test and verify the ground travel behaviour of cold dense hydrogen clouds, to identify the conditions they can occur and to assess the level of hazard they present to airport refuelling operations more fully.

10.4 Refuelling with Passengers Onboard

The effect of a 500 L fuel spill pool fire during refuelling operations upon the aircraft fuselage has been examined, by introducing representative aircraft geometries into FLACS-Fire simulations. Assuming a refuelling position at the tail, for the LH_2 fuelled aircraft, the model predicts that the thermal radiation produced by the LH_2 pool fire radiates over a wider area than for the Jet A fire (located at a refuelling position under the wing), but for a shorter time. It falls mainly on the top of the aircraft fuselage, tail and both wings, whereas the radiation from a Jet A spill pool fire is concentrated along the side of the aircraft where refuelling takes place. In the case of the LH_2 pool fire the model predicts that high temperatures and levels of thermal radiation flux are restricted mainly to the tail region of the aircraft and would be of a relatively short duration. By contrast, for the Jet A pool fire the model predicts higher temperatures and thermal radiation flux levels across the wing and body of the aircraft. These preliminary results would seem to suggest that, at least for a relatively small LH_2 pool fire, it may be acceptable for the aircraft to be refuelled with passengers onboard, as they should be adequately protected from the effects of thermal radiation inside the aircraft. Indeed provided the LH_2 pool fire has a very short duration the best strategy might be for the passengers to stay put inside the aircraft until the fire has burnt out. However, there are also the consequences of a delayed ignition resulting in a flammable gas cloud and the potential for a flash fire or explosion to consider. In the case of a flash fire the passengers should also be adequately protected from the effects of thermal radiation for a short duration fire inside the aircraft. However, in the event of an explosion the outcome is less clear-cut and would be dependent upon the overpressures generated and the withstand of the aircraft. The model results from Section 8 suggested that there were some scenarios where significant local overpressures might be generated as a result of confinement and the representation of congestion under the body of the aircraft generating turbulence and flame acceleration. Further work is required to investigate and confirm this behaviour.

During current LH_2 industrial refuelling operations it is standard practice to vent any excess boil-off hydrogen gas generated directly to atmosphere. It seems likely that such routine venting of GH_2 to atmosphere next to an aircraft during normal refuelling operations would be deemed unacceptable in an airport setting – especially if passengers were still onboard. Instead the refuelling truck would need to be adapted to recover all the GH_2 vapour generated during the refuelling process, by introducing a re-cooling system inside refueller truck to re-condense all the GH_2 that comes back from the aircraft tank. The use of such GH_2 recovery systems during LH_2 aircraft refuelling at airports has also been advocated in previous studies [Brewer, 1991; Boeing, 1976]

It may well be having passengers on board is not such an issue as they are relatively well protected, from an explosion/fireball occurring outside the aircraft. However, existing fuelling arrangements where aircraft may be adjacent to terminal buildings, with other personnel such as baggage handlers in close proximity need to be re-assessed for the use of LH_2. An aircraft fuselage probably has a considerably better explosion withstand than a terminal building. That said hydrogen releases to the open air tend not to generate strong blast waves unless there are mechanisms to generate turbulence (e.g. obstacles or high velocity release) or a detonation wave propagates into the H_2/Air cloud from a duct or channel. A worst case, although unlikely, scenario could be a large spill dispersing and finding an ignition source inside a duct or channel within an aircraft or other machinery, resulting in a DDT which then propagates back into the unconfined cloud. These scenarios will need to be explored.

10.5 Delayed ignition of large hydrogen clouds

In the case of a large-scale release for an aircraft fuel tank or airport storage tank producing a very large LH_2 spill of a significant proportion of the tank contents (e.g. due to a crash or catastrophic tank failure) it has been assumed here that LH_2 spill would be ignited immediately resulting in a pool fire (i.e. a pool fire/fireball has been effectively treated as the worst case accident scenario). It would seem likely that such a crash or catastrophic tank failure would be accompanied by the generation of a reliable ignition source. Hence the possibility of an LH_2 spill produced from a very large release not being immediately ignited has been largely discounted in this study. The results would then suggest that the thermal radiation hazard presented by the resulting LH_2 pool fire should compare favourably with a corresponding Jet A accident scenario.

While the assumption may appear reasonable there is no hard evidence to back it up and it would probably be unwise to completely discount delayed ignition for large releases as a possibility. Immediate ignition has been claimed in the past as a reason why unconfined hydrogen vapour cloud explosions are not possible. However, as discussed by Thomas et al. [2015] this claim, at least with respect to industrial scenarios, is false and unconfined vapour cloud explosions can occur and hydrogen is susceptible to delayed ignition.

If there were scenarios for major releases where immediate ignition did not occur, then a very large flammable hydrogen gas cloud could potentially be formed. If this cloud were to subsequently become ignited, then the resulting consequences could be extremely serious resulting in a very large explosion or flash fire. The associated hazardous distance could be very large.

For example, in a risk assessment of the transportation of LH_2 by rail car, Moonis et al. [2010] tentatively suggested that the explosion or flash fire resulting from the catastrophic failure of a 200 t LH_2 tank could have an associated hazardous distance of around 30 to 40 km!

The credibility and potential consequences of delayed ignition of a hydrogen vapour cloud both require further study. It is conceivable that the vapour cloud explosion risk could affect other airport structures/building so the issue needs looking at even if the perceived likelihood of such an event is small.

10.6 Recommendations for Further Work

10.6.1 Further Development of LH_2 CFD modelling capability

Further work is required to develop, test and validate the prediction capability of CFD codes such as FLACS when applied to model LH_2 hazards relevant to aircraft and airport applications. Specific examples include, incorporating an Equation of State (EoS) which can account for non-ideal gas behaviour exhibited at cryogenic temperatures (such as the one developed by Leachman et al. [2009]) for physical property calculations and a radiation transmissivity model suitable for a hydrogen flame.

10.6.2 Develop simplified LH_2 spill consequence assessment models

Use information from ENABLEH2 and further analysis, to develop simpler engineering consequence models to be able to assess LH_2 hazards more quickly. These will comprise assessments of pool fire, jet fires, explosions and BLEVEs.

10.6.3 LH_2 system failure frequency data

In order to obtain a measure of the overall risk of different LH_2 accidental release scenarios occurring for aircraft and airports, it will also be necessary to take account of the frequency/likelihood with which such release scenarios will occur in addition to the consequences (hazardous distance) examined here. To do this frequency failure rate date for LH_2 systems will be required.

10.6.4 Definition of an experimental campaign to validate numerical models

There is currently significant uncertainty with the modelling of LH_2 accident scenarios, particularly LH_2 pool fires, due to a lack of medium and large-scale experimental test data to validate the models with. A campaign of experimental test work is required in order to obtain suitable experimental tests data to validate models against. This work will be needed in order to be able to assess LH_2 hazards in aircraft and airport storage more accurately and quantify the risk outcomes.

10.6.5 Development of design rules and operating protocols for LH_2 aircraft

Further work post ENABLEH2 will be needed to assess proposed modifications to airport facilities and assess the effectiveness of any mitigation measures proposed. The overall process should be captured, distilled and used as a template for safe LH_2 integration into airports guidance.

Consequence analysis needs to have been undertaken for credible accident scenarios for finalized airport geometries and performance of any mitigation measures demonstrated, with sufficient accuracy and resolution to enable prescriptive guidance to be underpinned and drafted. Design rules and operating protocols are required to allow:

- Assessment of risks from large scale LH_2 releases (dispersion, pool fire/fireball, blast wave) and examination of implications for aircraft/airport design and operation.
- Development of protocols for crash landing, release at airport LH_2 storage facility, and aircraft refuelling leaks.
- Development of fire-fighting requirements and procedures for LH_2 enabled airports (The procedures for Jet A and LH_2 are incompatible).

11 Conclusion

The aim of this work has been to study the large-scale hazards posed by the use of liquid hydrogen in civil aviation. Analytical studies have been carried out to examine liquid hydrogen release and dispersion behaviour for different airport LH_2 tank storage and aircraft tank failure/rupture accident scenarios. The FLACS CFD model has been used to simulate the potential hazard effects following an accidental LH_2 leak, including the extent of the flammable LH_2 clouds formed, magnitude of explosion overpressures and pool fire radiation hazards. A comparison has also been made between the relative hazard consequences of using LH_2 with conventional Jet A/A-1 fuel.

LH_2 Leaks and Flammable Cloud Dispersion Behaviour

The FLACS pool model has been used to predict the maximum downwind hazardous distances as a function of the LH_2 spill release rate for the 4%, 8% and 18% v/v hydrogen-air concentration limits, and the 200 K cryogenic temperature limit. These were found to exhibit a power law relationship. Original scaling correlations were obtained using the FLACS 4% lower flammable limit data allowing the hazardous distance for a given LH_2 release spill rate to be estimated. The dependence of the maximum pool radius upon LH_2 release rate predicted by FLACS was also examined and found to be in good agreement with an analytical expression for the equilibrium pool radius, with the steady-state evaporation rate of the LH_2 pool per unit area estimated to be 0.022 kg/m^2/s. The maximum downwind flammable distance predicted by FLACS for the 4% limit have also been compared with the method for estimating hazardous distance of a release used in EN 60079-10-1 for a heavy gas release. The results can be used to predict the hazardous distance for flammable clouds produced by accidental spills from both LH_2 aircraft and fixed tank storage at airports.

Leaks from a LH_2 Storage Tank at an Engine Test Facility

A case study has been carried out to examine the potential consequences of a large LH_2 leak occurring from an LH_2 storage tank at an engine test facility (based upon the Reaction Engines TF1 facility design). With a capacity of 4.5 tonnes the LH_2 storage tank examined is of a similar size to that which will be required for an LH_2 aircraft. The case study thus represents a natural stepping-stone for analysis on the way to the larger LH_2 storage tanks that will be required for airports operating LH_2 aircraft. Hence, it was regarded as providing a good case study for modelling LH_2 accident scenarios that will be relevant to the aims of the ENABLEH2 project. The FLACS CFD model has been used to represent the engine test facility geometry and simulate the consequences of large LH_2 leaks due to supply pipe rupture and catastrophic tank failure scenarios. The resulting behaviour has been characterised in terms of the variation with time of the LH_2 pool area and the size of the equivalent stoichiometric flammable clouds formed (FLACS Q9 parameter). The results suggest that the presence of a LH_2 storage tank bund significantly reduces both the maximum pool area and size of the equivalent stoichiometric gas clouds (Q9) formed for LH_2 tank leak scenarios (long duration pipe ruptures) and a catastrophic tank failure.

Aircraft Crash Scenario

A comparison has been made between LH_2, LNG and Jet A/A-1 fuelled aircraft for a serious aircraft crash scenario, resulting in an instantaneous spill of the entire fuel tank contents, which is immediately ignited to produce a large pool fire. The simulation results obtained with the FLACS-Fire CFD code, suggest that the spills of cryogenic fuels - LH_2 and LNG produce high intensity, short duration pool fires, behaving like a fireball. By comparison, the Jet A/A-1 spill is predicted to produce a pool fire with a lower peak heat release rate, but with sustained burning over a longer period of time. A comparison of the pool fires produced for each of the fuel types also suggests that the magnitude of the predicted peak radiation heat flux and thermal radiation dose is significantly lower for the LH_2 pool fire.

Aircraft Refuelling Spill (Immediate Ignition) – Pool Fire Simulations

A series of simulations were carried out using the FLACS-Fire model to simulate the pool fires resulting from instantaneous spills of LH_2 and Jet A/A-1, ranging in size from 100 L to 5000 L, to allow a comparison to be made between the behaviour and level of thermal hazard presented by the two different fuel types. The LH_2 spills vaporise rapidly and the ignited hydrogen gas forms a fireball - a rapidly rising expanding ball of flame. The resulting high intensity fire has a relatively high heat release rate over a short period of time before consuming the available fuel and burning out. In comparison to the intense fireball produced for LH_2, the pool fires produced from a Jet A spill have a flame that burns as a continuously fluctuating fire plume with a lower peak HRR, but which is sustained over a significantly longer period of time.

The predicted results of the pool fire resulting from the ignition of an instantaneous LH_2 spill of 100 L have been compared with those observed in one of the experimental tests described by Zabetakis and Burgess [1961]. The simulated LH_2 spill flame shows some broadly similar qualitative fireball behaviour to that observed in the test. However the magnitude of the predicted peak radiation heat flux at a distance of 33.5 m from the spill (4 kW/m^2) is significantly higher than was observed in the experimental test (0.5 kW/m^2). It is shown that the level of radiation transmissivity predicted by FLACS-FIRE in the far-field for a hydrogen flame would be expected to be highly conservative (over-predicted) in high humidity scenarios (where the effect of atmospheric humidity on radiation transmissivity is significant) as was the case in the experimental LH_2 spill/fire tests carried out by Zabetakis and Burgess.

A comparison of the hazardous distances predicted by FLACS-Fire for the different thermal radiation dose harm thresholds as a function of the liquid spill volume (and equivalent stored energy) for both LH_2 and Jet A/A-1 pool fires has been made. As a consequence of the short duration of the fireball produced by LH_2 releases, the thermal radiation dose hazardous distances predicted for the LH_2 pool fires are significantly lower than those obtained for an equivalent spill volume of Jet A/A-1. The hazardous distance to the 240 TDU (2nd degree burn) injury threshold predicted for LH_2 pool fires (for a given spill volume) is not only much less than that found for Jet A/A-1 (around a third the value), but it is also less than the distances to the 420 TDU (dangerous dose) and 1050 TDU (fatality) thresholds predicted for Jet A.

A finite duration LH_2 spill pool fire initially exhibits the fireball behaviour displayed by an instantaneous LH_2 spill pool fire, but then transitions into a tall continuous burning flame plume until the remaining LH_2 is consumed and it burns out.

A 2 m/s wind deflects the fireball produced by a 500 L instantaneous spill LH_2 pool fire at it ascends. The predicted (downwind) hazardous extent (in terms of burn injury and dangerous dose threshold) of the LH_2 pool fire is increased significantly (by a factor of 2-4 times) with a 2 m/s wind present. However, that the hazardous extent of the Jet A pool fire (for all the thermal radiation harm criteria) remains significantly higher than that found for LH_2 (by a factor of 2-3), even with a wind present.

The effect of a refuelling spill pool fire on the aircraft was also examined. Aircraft geometries based upon both a conventional commercial passenger aircraft design and a LH_2 “tube and wing” short/medium range aircraft design developed for ENABLEH2 (with a capacity of around 200 passengers), were constructed and introduced into FLACS. FLACS-Fire simulations were performed to allow a comparison to be made between the pool fires resulting from a 500 L instantaneous spill of LH_2 and Jet A/A-1 (kerosene). The thermal radiation produced by the LH_2 pool fire radiates over a wider area than for the Jet A/A-1 fire, but for a shorter time. It falls mainly on the top of the aircraft fuselage, tail and wings. The radiation flux from the Jet A/A-1 pool fire is concentrated along the length of the right side and wing of the aircraft. The size and duration of the high thermal flux region (> 37.5 kW//m^2) produced by the Jet A fire is also predicted to be significantly greater than that for the LH_2 fire. However, the results also suggest that the fuselage of the aircraft does effectively shield the left-hand side of the aircraft from the radiation produced by the Jet A/A-1 fire.

Aircraft Refuelling Leak (Delayed Ignition) – Flash Fire & Explosion

Work has been carried out to model the consequences of accidental LH_2 spills occurring during aircraft refuelling operations. In order to examine the effect of aircraft geometry on the flammable cloud dispersion and explosion behaviour of a short duration LH_2 leak during refuelling operations a representative LH_2 aircraft geometry based upon a LH_2 “tube and wing” short/medium range aircraft

design developed for ENABLEH2 (with a capacity of around 200 passengers) was constructed and introduced into FLACS. The effect of different leak locations, wind directions and leak duration upon the resulting flammable cloud were examined. A delayed ignition source was also introduced to allow the explosion overpressure resulting from ignition of the flammable clouds produced for different scenarios to be predicted.

The results suggest that use of LH_2 fuel and associated dense gas cloud dispersion behaviour will introduce additional hazards not found with Jet A/A-1 that will need to be carefully managed and mitigated due to the extent of flammable gas cloud that can be formed and potential for associated flash fire and explosion hazards – particularly if wind direction could transport the cloud under the body of the aircraft where it could be partially confined or to the left side region of the aircraft where passengers typically de-plane from current Jet A/A-1 fuelled aircraft.

For certain explosion simulation cases, involving ignition of hydrogen clouds formed under the body of the aircraft, performed using FLACS, the results also indicated the potential for flame acceleration to occur, due to representation of the undercarriage and engine as sub-grid scale porosities which could lead to signficantly higher overpressures occurring over a wider area. Further work is required to validate this behaviour.

Continuous Releases – Aircraft and Airport Storage Tank Pool Fires

FLACS-Fire simulations were also performed for continuous releases of LH_2 and Jet A/A-1 for several different fuel leak scenarios to allow the behaviour of the resulting pool fires to be compared. A continuous LH_2 leak produces a pool fire with a continuous burning flame plume that is taller than that predicted for an equivalent size Jet A/A-1 leak, but the size of the predicted hazardous thermal radiation distance and radiation heat flux level region exceeding 5 kW/m^2 incident on the ground is smaller.

FLACS-FIRE simulations were also carried out to model an airport fuel storage tank pool fire scenario - comparing LH_2 with Jet A/A-1. Three cylindrical fuel storage tanks were considered (each diameter 20 m, height 10 m). Each tank was surrounded by a 50 m x 50 m bund wall which was 2 m high. One of the storage tanks was assumed to have undergone a catastrophic containment failure resulting in a release of its entire contents into the surrounding bund which was ignited to produce a constrained 50 m diameter pool fire. The LH_2 pool fire was predicted to initially produce a fireball with high radiation flux levels spread over a wide area, including the adjacent storage tanks, for a short period of time. After this it then transformed into a continuous, very tall flame height (~250m) burning fire, with an associated radiation flux delivered over a narrower ground area, broadly corresponding to the region of the failed tank's bund, and with flux levels > 5 kW/m^2 no longer reaching to the adjacent storage tanks. In comparison, the Jet A/A-1 pool fire was predicted to produce a smaller flame height but delivered significant radiation levels > 5 kW/m^2 over the exposed surfaces of the adjacent storage tanks.

Implications of results for safety of LH_2 aircraft and airports

The results of the study indicate that, in the event of accidental fuel spill, LH_2 has some safety advantages over Jet A/A-1. Modelling of LH_2 pool fires suggests they will exhibit a smaller thermal radiation hazardous distance and deliver a lower thermal dose than those found for a comparable Jet A/A-1 pool fire. The rapid vaporisation of instantaneous LH_2 spills produces short duration fires such that the fuel spills will completely evaporate and burn-out rapidly. Hydrogen fires are also expected to emit a lower fraction of their heat as radiation and be clean burning such that no toxic smoke is produced (unless other materials become involved).

However, the use of LH_2 fuel will also introduce additional hazards not found with Jet A/A-1 that will need to be carefully managed and mitigated against. The largest hazardous distances are predicted to occur for LH_2 tank BLEVE accident scenarios – particularly airport storage tank BLEVEs. There are also additional hazards associated with LH_2 leaks and spills due to dense gas cloud dispersion behaviour that is predicted and the extent of flammable gas cloud that can be formed at ground level downwind of the spill and potential for accompanying flash fire/jet fire and explosion hazards. The hazard consequences produced may be accentuated if the prevailing wind could transport the cloud under the body of the aircraft where it could be partially confined, towards the airport terminal building, or to the side of the aircraft where passengers' egress.

There is significant uncertainty with current models and the limitations should be borne in mind when interpreting or making judgements based on the results. There is also an urgent requirement for more large-scale experimental test data for LH_2 releases and associated hazard behaviour in order to reduce uncertainty and allow models to be further developed and validated to improve confidence in their predictions.

ENABLEH2

This work forms part of a programme of work being carried out for the EU ENABLEH2 project, examining the feasibility of using LH_2 in commercial aviation. The usage of LH_2 in aviation will require the development of new types of aircraft and cryogenic fuel tank design, as well as the need for the provision of large-scale LH_2 storage facilities at airports. The results are intended to assist with assessing the safety of future LH_2 aircraft and large-scale airport LH_2 storage facilities, being considered as part of ENABLEH2.

12 References

Abdel-Gayed RG, Bradley D, Lawes M. [1987], Turbulent burning velocities: a general correlation in terms of straining rates. Proc R Soc A, 414:389-413.

Ahmadi O., Mortazavi S.B., Pasdarshahri H., Hassan, Mohabadi A. [2019], Consequence analysis of large-scale pool fire in oil storage terminal based on computational fluid dynamic (CFD). Process Safety and Environmental Protection, 123, 379-389.

ANSI [2017], Guide to Safety of Hydrogen and Hydrogen Systems, American Institute of Aeronautics and Astronautics, American National Standard, ANSI/AIAA G-095A-2017.

Arthur D. Little Inc. [1960], Final report on an investigation of hazards associated with the storage and handling of liquid hydrogen. Report to the U.S. Air Force, C-61092. 1960.

Arthur D. Little Inc.[1982], An assessment of the crash fire hazard of liquid hydrogen fueled aircraft. Final Report to the National Aeronautics and Space Administration, NASACR-165526.

Assael, M.J. and Kakosimos K.E. [2010], Fires, explosions and toxic gas dispersions: effects calculation and risk analysis, CRC Press, Taylor & Francis Group, Boca Raton, Florida.

Beyler C.L. [2016], Fire hazard calculations for large open hydrocarbon fires, in SFPE Handbook of Fire Protection Engineering, 5th Edition (Editor: Hurley M.J.), Society of Fire Protection Engineering, pp. 2591-2663.

Boeing [1976], An exploratory study to determine the integrated technological air transportation system ground requirements of liquid-hydrogen-fueled subsonic, long-haul civil air transports, NASA Contractor Report CR-2699, Washington, U.S.A.

Brewer, G. D. (Ed.), LH2, Airport Requirements Study, NASA Contractor Report CR-2700, October 1976, Washington, U.S.A.

Brewer G.D. [1991], Hydrogen Aircraft Technology, CRC Press, Boca Raton.

Brewer G.D., Wittlin G., Versaw E.F., Parmley R., Cima R. and Walther E.G. [1981], Assessment of crash fire hazard of LH2 – fueled aircraft, Final Report to the National Aeronautics and Space Administration. NASA CR-165525.

BS EN 60079-10-1 [2015], Explosive Atmospheres Part 10-1: Classification of areas —Explosive gas atmospheres, British Standards Institute, 2015.

Chirivella J.E. and Witcofski R.D. [1986], Experimental results from fast 1500 gallon LH2 spills. Cryog Prop Process Appl, AIChE Symp Ser, 251(82):120-40.

CRYOPLANE [2003], Liquid Hydrogen Fuelled Aircraft – System Analysis, Final Technical Report, Airbus Deutschland GmbH.

Drysdale D.D. [1998] An Introduction to Fire Dynamics. Second Edition, John Wiley & Sons, Chichester, UK.

Ekoto I.W., Ruggles A.J., Creitz L.W. and Li J.X. [2014], Updated jet flame radiation modelling with buoyancy corrections, Int J Hydrogen Energy, 39(35), 20570–20577.

ENABLEH2 [2021], https://www.enableh2.eu/ (accessed 18/03/2021).

Ehrhart, B.D. and Hecht E.S. [2020], Hydrogen Risk Assessment Models (HyRAM) Version 3.0 Technical Reference Manual. SAND2020-10600. September 2020.

Ehrhart B.D., Sims C., Hecht E., Muna A.B., Groth K.M., Reynolds J.T., Blaylock M.L., Carrier E., Ekoto I.W., and Walkup G.W. [2020], HyRAM (Hydrogen Risk Assessment Models), Version 3.0. Sandia National Laboratories; software available at http://hyram.sandia.gov.

Fay J.A., [2006], Model of Large Pool Fires. Journal of Hazardous Materials, 136: 219–32.

Fay J.A. [2007], Spread of large LNG pools on the sea. Journal of Hazardous Materials, 140, 541–551.

Fay, J.A. and Lewis, D.H. [1977], Unsteady burning of unconfined fuel vapor clouds. Symp. (Int.) Combust. 1977, 16, 1397–1405.

Fleming, G.G. and Ziegler, U. [2016], Environmental Trends in Aviation to 2050. ICAO (International Civil Aviation Organization) Environmental Report, 2016. https://www.icao.int/environmental-protection/Documents/EnvironmentalReports/2016/ENVReport2016_pg16-22.pdf

(accessed 03/02/2021).

Gallego E, Migoya E, Martin-Valdepenas JM, Crespo A, Garcia J, Venetsanos AG, et al. [2007], An inter-comparison exercise on the capabilities of CFD models to predict distribution and mixing of H2 in a closed vessel. Int J Hydrogen Energy, 32:2235-45.

Gexcon [2019], FLACS v10.9 User's Manual, Bergen, Norway.

Giannissi S.G. and Venetsanos A.G. [2018], Study of key parameters in liquid hydrogen release and dispersion in open environment. Int J Hydrogen Energy; 43(1), 455-467.

Giannissi S.G. and Venetsanos A.G. [2019], A comparative CFD assessment study of cryogenic hydrogen and LNG dispersion, Int J Hydrogen Energy, 44(17):9018-9030.

Giannissi S.G., Venetsanos A.G., Markatos N., Bartzis J.G. [2014], CFD modeling of hydrogen dispersion under cryogenic release conditions. Int J Hydrogen Energy, 39(28),15851-15863.

Golder D. [1972], Relations among stability parameters in the surface layer. Boundary-Layer Meteorol, 3: 47–58.

Haglind, F., Hasselrot, A. and Singh, R. [2006], Potential of reducing the environmental impact of aviation by using hydrogen Part III: Optimum cruising altitude and airport implications. The Aeronautical Journal, 110 (1110), August 2006, 553-565.

Hamdhan I. and Clarke B. [2010], Determination of Thermal Conductivity of Coarse and Fine Sand Soils. In Proceedings World Geothermal Congress 2010, Bali, Indonesia, 25-29 April 2010, 1-7.

Han J, Arya SP, Shen S, Lin YL. [2000], An estimation of turbulent kinetic energy and energy dissipation rate based on atmospheric boundary layer similarity theory. NASA/CR-2000-212298.

Hanna SR, Hansen OR, Dharmavaram S. [2004], FLACS air quality CFD model performance evaluation with Kit Fox, MUST, Prairie Grass, and EMU observations. Atmos Environ, 38, 4675-4687.

Hankinson G. and Lowesmith B.J. [2012], A consideration of methods of determining the radiative characteristics of jet fires, Combustion and Flame, 159(3), 1165–1177.

Hankinson G. and Lowesmith B.J. [2013], Qualitative Risk Assessment of Hydrogen Liquefaction, Storage and Transportation, - Integrated design for demonstration of efficient liquefaction of hydrogen (IDEALHY), Deliverable 3.11 Report, Grant Agreement Number 278177.

Hansen OR, Gavelli F, Davis, SG, Middha, P. [2013], Equivalent cloud methods used for explosion risk and consequence studies, J Loss Prev Process Ind 2013; 26: 511-27.

Hansen O. [2020], Liquid hydrogen releases show dense gas behaviour. Int J Hydrogen Energy, 45:1343-1358.

Hansen OR, Gavelli F, Ichard M, Davis S. [2010], Validation of FLACS against experimental data sets from the model evaluation database for LNG vapour dispersion. J Loss Prev Process Ind, 23(6), 857-877.

Hansen, O.R., Renoult, J., Sherman, M.P. and Tiezen, S.R. [2005], Validation of FLACS-HYDROGEN CFD consequence prediction model against large scale H_2 explosion experiments in the FLAME facility. First International Conference on Hydrogen Safety, Pisa, Italy.

Hord, J. [1978], Is hydrogen a safe fuel? Int J Hydrogen Energy, 3, 157-176.

Houf W. and Winters W. [2013], "Simulation of high-pressure liquid hydrogen releases" International J of Hydrogen Energy, 38(19), 8092–8099.

Ichard M., Hansen O.R., Middha P., Willoughby D. [2012], CFD computations of liquid hydrogen releases. Int J Hydrogen Energy, 37(22),17380-17389.

Ivings MJ, Gant SE, Jagger SF, Lea CJ, Stewart JR, Webber DM. [2016], Evaluating vapor dispersion models for safety analysis of LNG facilities, The Fire Protection Research Foundation, National Fire Protection Association, USA.

Jakel C., Kelm S., Verfondern K., Allelein H. [2019], Validation of a 3D multiphase-multicomponent CFD model for accidental liquid and gaseous hydrogen releases. Int J Hydrogen Energy; 44(17), 8807-8818.

Jin T., Wu M., Liu Y., Lei G., Chen H., and Lan Y. [2017a], CFD modeling and analysis of the influence factors of liquid hydrogen spills in open environment. Int J Hydrogen Energy, 42(1):732-739.

Jin T, Liu Y, Wei J, Wu M, Lei G, Chen H, et al. [2017b], Modeling and analysis of the flammable vapor cloud formed by liquid hydrogen spills. Int J Hydrogen Energy, 42(43), 26762-26770.

Jones C.R., Fewtrell P., Petrie A., Lines I., Cowell N., Livingston A. [2000], Quantified Risk Assessment of Aircraft Fuelling Operations. WS ATKINS Safety & Reliability Report AM5204 for Health and Safety Executive, UK, July 2000.

Jordan T, Garcia J, Hansen OR, Huser A, Ledin HS, Middha P, et al. [2007], Results of the HySafe CFD Validation Benchmark SBEPV5. In: 2nd Int. Conf. on Hydrogen Safety, San Sebastian, Spain; 2007.

Jordan, T., Jallais, S., Bernard, L., Venetsanos, A., Coldrick S., Kuznetsov, M. and Cirrone, D. [2019], Status of the pre-normative research project PRESLHY for the safe use of liquid hydrogen, Eighth International Conference on Hydrogen Safety (ICHS 2019), 24-26 September 2019, Adelaide, Australia.

Klebanoff LE, Pratt JW and LaFleur CB. [2017], Comparison of the safety-related physical and combustion properties of liquid hydrogen and liquid natural gas in the context of the SF-BREEZE high-speed fuel-cell ferry, Int J Hydrogen Energy, 42(1), 757-774.

LaChance J., Tchouvelev A. and Engebo A. [2011], Development of uniform harm criteria for use in quantitative risk analysis of the hydrogen infrastructure, Int J Hydrogen Energy, 36, 2381-2388.

Leachman J.W., Jacobsen R.T., Penoncello S.G., and Lemmon E.W. [2009], Fundamental equations of state for parahydrogen, normal hydrogen, and orthohydrogen, Journal of Physical and Chemical Reference Data, vol. 38, no. 3, 721–748.

Ledin, H.S. [2002], A review of the state-of-the-art in gas explosion modelling, HSL/2002/02. Buxton, UK: Health and Safety Laboratory.

Liu Y, Wei J, Lei G, Lan Y, Chen H, Jin T. [2018], Dilution of hazardous vapor cloud in liquid hydrogen spill process under different source conditions. Int J Hydrogen Energy, 43(15), 7643-7651.

Liu Y, Wei J, Lei G, Wang T, Lan Y, Chen H, et al. [2019a], Modeling the development of hydrogen vapour cloud considering the presence of air humidity. Int J Hydrogen Energy, 44(3), 2059-2068.

Liu Y, Wei J, Lei G, Lan Y, Chen H, Gao X et al. [2019b], Numerical investigation on the effects of dike around liquid hydrogen source on vapour cloud dispersion. Int J Hydrogen Energy, 44(10), 5063-5071.

Liu Y, Wei J, Lei G, Chen H, Lan Y, Gao X et al. [2019c] Spread of hydrogen vapor cloud during continuous liquid hydrogen spills. Cryogenics, 103, 102975.

Liu Y, Wei J, Liu Z, Lei G, Jin T. [2020], Dilution of flammable vapor cloud formed by liquid hydrogen spill. Int J Hydrogen Energy, 45, 5067-5072.

Lockwood, F.C. and Shah, N.G. [1981], A new radiation method for incorporation in general combustion prediction procedures. Proceedings, 18th Symposium (International) on Combustion, 1405-1414. The Combustion Institute, London.

Magnussen, B.F. and Hjertager, B.H. [1976], On mathematical modelling of turbulent combustion with special emphasis on soot formation and combustion. 16th Symp. (Int.) Combustion, 719–729. The Combustion Institute, Pittsburgh, PA.

Makarov D, Verbecke F, Molkov V, Roe O, Skotenne M, Kotchourko A, et al. [2009], An inter-comparison exercise on CFD model capabilities to predict a hydrogen explosion in a simulated vehicle refueling environment. Int J Hydrogen Energy, 34:2800-14.

McKinsey & Company [2020], Hydrogen-powered aviation – A fact-based study of hydrogen technology, economics and climate impact by 2050. Report for the Clean Sky 2 JU and Fuel Cells and Hydrogen 2 JU, May 2020.

Middha, P. [2010], Development, use and validation of the CFD tool FLACS for hydrogen safety studies. Ph.D. Thesis, University of Bergen, Norway.

Middha, P. and Hansen, O.R. [2008], Predicting deflagration to detonation transition in hydrogen explosions. Process Safety Progress, 27(3), 192-204.

Middha, P. and Hansen, O.R. [2009], Using computational fluid dynamics as a tool for hydrogen safety studies, J Loss Prev Process Indust, 22, 295-302.

Middha P, Hansen OR, Storvik IE. [2009b], Validation of CFD-model for hydrogen dispersion. J Loss Prev Process Indust, 22:1034-38.

Middha P., Ichard M., Arntzen B.J. [2011], Validation of CFD modelling of LH2 spread and evaporation against large-scale spill experiments. Int J Hydrogen Energy, 36, 2620-2627.

Moonis M., Wilday A.J., Wardman M.J. [2010], Semi-quantitative risk assessment of commercial scale supply chain of hydrogen fuel and implications for industry and society. Process Safety and Environmental Protection, 88, 97-108.

Moorhouse, J. and Pritchard, M. J. [1982], Thermal Radiation Hazards from Large Pool Fires and Fireballs: A Literature Review. IChemE Symposium Series, 71, 123.

Mumby, C. [2010], Predictions of explosions and fires of natural gas/hydrogen mixtures for hazard assessment, Doctoral Thesis, Loughborough University.

NFPA-2 [2016] Hydrogen Technologies Code. National Fire Protection Association, 2016.

NFPA-59A [2016], Standard for the Production, Storage and Handling of Liquefied Natural Gas (LNG), National Fire Protection Association, 2016.

Papanikolaou E, Venetsanos AG, Cerchiara GM, Carcassi M and Markatos N [2011], CFD simulations on small hydrogen releases inside a ventilated facility and assessment of ventilation efficiency. Int J Hydrogen Energy, 36:2597-2605.

Pasquill F. [1961], The estimation of the dispersion of windborn material, Meteorol Mag, 90(1063): 33-49.

Patankar S.V. [1980], Numerical Heat Transfer and Fluid Flow. Taylor & Francis.

Ponchaut N.F., Colella, F. and Marr K.C. [2016], Vapor Clouds, in SFPE Handbook of Fire Protection Engineering, 5th Edition (Editor: Hurley M.J.), Society of Fire Protection Engineering, pp. 2664-2704.

Popat NR, Catlin CA, Arntzen BJ, Lindstedt RP, Hjertager BH, Solberg T, Saeter O, Van den Berg AC [1996], Investigations to improve and assess the accuracy of computational fluid dynamic based explosion models. J Hazard Mater, 45:1-25.

PRESLHY [2021], https://preslhy.eu/ (accessed 24/03/21).

Raj P. [1981], Models for cryogenic liquid spill behavior on land and water, J Hazard Mater, 5, 111-130.

Rigas F. and Amyotte P. [2012], Hydrogen Safety (Green Chemistry and Chemical Engineering), 1st Edition, CRC Press, Boca Raton.

Royle M. and Willoughby D. [2014], Releases of unignited liquid hydrogen, Health and Safety Laboratory, HSE Report, RR986.

Schefer R.W., Kulatilaka W.D., Patterson B.D. and Settersten, T.B. [2009], Visible emission of hydrogen flames. Combustion and Flame, 156, 1234-1241.

Shao X., Pu L., Li Q., Li Y. [2018], Numerical investigation of flammable cloud on liquid hydrogen spill under various weather conditions. Int J Hydrogen Energy, 43, 5249-5260.

Statharas J.C., Venetsanos A.G., Bartzis J.G., Wurtz J. and Schmidtchen U. [2000], Analysis of data from spilling experiments performed with liquid hydrogen. J Hazard Mater, 7: 57-75.

Taylor, DW. [2007], The role of consequence modelling in LNG facility siting, J Hazard Mater 2007; 142: 776-85.

Tolias IC, Stewart JR, Newton A, Keenan J, Makarov D, Hoyes JR, et al. [2018], Numerical simulations of vented hydrogen deflagration in a medium-scale enclosure. J Loss Prev Process Ind, 52: 125-139.

Thomas J.K. Eastwood C. and Goodrich M. [2015], Are unconfined hydrogen vapor cloud explosions credible? Process Safety Progress, 34(1), 36-43.

Thomas P.H. [1963], The size of flames of natural fires. Proc. 9th Symp. on Combustion, Academic Press, New York, pp. 844-859.

Ustolin F., Paltrinieri N. and Landucci G. [2020], An innovative and comprehensive approach for the consequence analysis of liquid hydrogen vessel explosions, J Loss Prev Process Ind, 68, 104323.

van den Bosch C. J. H. and Weterings R.A.P.M., [2005] Methods for the Calculation of Physical Effects due to Releases of Hazardous Materials (Liquids and Gases) - CPR 14E (Yellow Book), TNO, The Hague.

Venetsanos A.G. and Bartzis J.G. [2007], CFD modeling of large-scale LH2 spills in open environment. Int J Hydrogen Energy, 32(13), 2171-2177.

Venetsanos AG., Papanikolaou E, Delichatsios M, Garcia J, Hansen OR, Heitsch M, et al. [2009], An inter-comparison exercise on the capabilities of CFD models to predict the short and long term distribution and mixing of hydrogen in a garage, Int J Hydrogen Energy, 34:5912-23.

Venetsanos AG, Papanikolaou E, Hansen OR, Middha P, Garcia J, Heitsch M, et al. [2010], HySafe standard benchmark Problem SBEP-V11: Predictions of hydrogen release and dispersion from a CGH2 bus in an underpass. Int J Hydrogen Energy, 35:3857-67.

Verfondern K. and Dienhart B. [1997], Experimental and theoretical investigation of liquid hydrogen pool spreading and vaporization. Int J Hydrogen Energy, 22(7), 649-660.

Verfondern K. and Dienhart B. [2007], Pool spreading and vaporization of liquid hydrogen. Int J Hydrogen Energy, 32, 2106-2117.

Vyazmina, E. and Jallais, S. [2016], Validation and recommendations for FLACS CFD and engineering approaches to model hydrogen vented explosions: Effects of concentration, obstruction, vent area and ignition position. Int J Hydrogen Energy, 41, 15101-15109.

Wayne, F.D. [1991], “An economical formula for calculating atmospheric infrared transmissivities, J Loss Prev Process Ind, 4(2), 86-92.

Witcofski, R.D. and Chirivella, J.E. [1984], Experimental and analytical analyses of the mechanisms governing the dispersion of flammable clouds formed by liquid hydrogen spills, Int J Hydrogen Energy, 9(5), 425-35.

Woodward, J.L and Pitblado, R.M. [2010], LNG Risk Based Safety – Modeling and Consequence Analysis, AIChE, John Wiley & Sons, USA.

Yin, C. [2013], Refined weighted sum of gray gases model for air-fuel combustion and its impacts. Energy and Fuels, 27: 6287–6294.

Zabetakis M.G., Burgess D.S. [1961], Research on the hazards associated with the production and handling of liquid hydrogen, U.S. Bureau of Mines Report of Investigations 5707, U.S. Department of the Interior.

ENABLEH2

Public Report

Test Report on Hydrogen Flammability, Ignition and Release

Authors

James Ingram, Paul Holborn, Claire Benson, Paul Battersby

London South Bank University

This project has received funding from the European Union's Horizon 2020 research and innovation programme under grant agreement no 769241